Metabolic control of hair follicle stem cell fate decisions

Inaugural-Dissertation

zur

Erlangung des Doktorgrades

der Mathematisch-Naturwissenschaftlichen Fakultät

der Universität zu Köln

vorgelegt von

Kira Allmeroth

aus Aachen

Köln, Dezember 2020

Gutachter: Dr. Martin Denzel
Prof. Dr. Mirka Uhlirova

Tag der mündlichen Prüfung: 24.02.2021

You never fail until you stop trying.

Albert Einstein

Table of contents

Acknowledgements

When I started my PhD, I didn't want to work with stem cells nor use the skin as a model. Today, I am grateful that I gained this experience and that I had the chance to meet incredible people, establish fruitful collaborations, and to grow scientifically, as well as personally, together with (and thanks to) this project. It has been a long journey and I am speechless when I think of all the help I received along the way. This project was difficult, since it was far away from the lab's expertise. I went through many ups and even more downs throughout the years. Luckily, I didn't have to travel alone: I was fortunate to meet very talented scientists and fantastic characters along the way. It is almost impossible to name everyone involved in this work, but I will try anyway.

First, I am very grateful to my supervisor Dr. Martin Denzel for giving me the opportunity to perform my PhD in his laboratory and for encouraging me to evolve both on a scientific and on a personal level during this time. Thank you for always believing in me and this project. Especially in the most difficult situations your positive attitude was essential. Thank you!

I want to thank the members of my advisory committee: I am grateful to Prof. Dr. Adam Antebi for his constant input during department meetings and TAC meetings. I owe gratitude to Prof. Dr. Carien Niessen for critical, but fair feedback during TAC meetings and SFB829 retreats, and for encouraging our application to join the SFB829. Additionally, I want to thank my thesis committee members Prof. Dr. Ulrich Baumann and Prof. Dr. Mirka Uhlirova for agreeing to evaluate my thesis and for participating in my defense. Thank you for taking the time!

I wish to extend my sincere gratitude to Sara Wickström for patiently explaining the hair cycle, hair follicle morphology, and the organoid culture to me. Thank you for answering all my questions, I really appreciate that. Your expertise was fundamental for my success! I owe thanks to Carlos Andrés Chacón-Martínez for helping me to establish the organoid culture in the lab. I am immensely grateful to Christine Kim for your tremendous help in various ways: thank you for discussions, for trouble shooting, for sharing your expertise and experience. Some experiments wouldn't have been possible without your advice! Many thanks also to Janis Koester for the efficient and mouse-life-saving collaboration across the street and for sharing depilated skin samples with me.

I address special thanks to Peter Tessarz for always being available, for your interest, for many fruitful discussions, and for taking the time to help me with the Metascape analysis.

Thanks to you, my manuscript not only got a new figure 1, but also a figure 4. I am still sorry that I did not appreciate the beauty of yeast as a model when we both started at the MPI (a long time ago, as you pointed out recently). I also sincerely thank Andromachi Pouikli for preparing the library for 3' RNA-sequencing, for constant input during meetings, and for your willingness to test my findings in MSCs. I was fortunate to have such great collaborators! Thank you both!

I am immensely grateful to Andrea Annibal for providing a *spark* of hope in the darkest time. Three years ago, your data encouraged me to proceed; they made me curious. Also, these data are the groundwork for my manuscript. Thank you! Many thanks also for your constant support and all the polyamine data you provided. Thanks to Christian Latza for your help with the metabolomics. I also owe sincere thanks to Christoph Geisen for insisting on proper controls. You changed this project, and you pushed me to become a better scientist. Thank you!

I was fortunate to be part of the Cologne Graduate School of Ageing. Thanks to the GCA for funding and for constant support. Special thanks to Daniela Morick for advice throughout the years and for her willingness to help with problems both big and small.

I gratefully acknowledge the SFB829 not only for funding, but also for enabling scientific exchange with this great community and for generating a stimulating research environment. Many thanks to project Z2, by name Sarah Loeck, Ruth Pofahl, and Marc Peskoller, for providing technical expertise and support, especially in the beginning of this project. I would like to express my sincere gratitude to my 'skin people': Noelle Ali, Mareike Damen, Anna Geueke, Annika Graband, Marta Gronzka, Christine Kim, Janis Koester, Soriba Letzian, Julian Nüchel, Matthias Rübsam, Hannah Schünke, Susi Vorhagen, and Emmi Wachsmuth. Thank you for accepting me as a member of your awesome group of people! Thanks for fun times at the ESDR in Munich, and at many retreats. I've had a blast! Thank you for your constant and critical feedback. You don't have a clue what your support meant to me! Thank you!

I am indebted to everyone working in the Comparative Biology Facility, but I owe special thanks to Patrick Wollek. Thank you for your excellent work throughout the years; I could not have asked for a better support! Thanks for handling last-minute requests, for accepting delays in genotyping, and for never complaining, although your room was totally packed most of the time.

I gratefully acknowledge the Bioinformatics Core Facility for their help with RNA-sequencing data analysis. I would like to thank especially Franziska Metge for patiently trying to explain the magic she did. Thank you!

Special thanks to the Metabolomics Core Facility, by name Patrick Giavalisco, Yvonne Hinze, and Silvina Perin. The µg of UDP-HexNAc that you have measured during this project probably add up to several kg. Thank you for your support!
I owe sincere thanks to the FACS & Imaging Core Facility. This was a flow cytometry-heavy project and I spent countless hours with you guys. I owe special gratitude to Kat Folz-Donahue and Lena Schumacher for introducing me to the world of colors, lasers, nozzles, events, peaks, and flow rates, for teaching me about compensation and all the other details, for discussing color combinations and gating strategies, for sorting millions of cells (fusion + svea - 100 µm nozzle - chillers on - mouse skin stem cells), for Free-Access-Candy-Supply, for fun and laughter, and for forgiving me for always being 5 minutes late. You enabled me to successfully finish this work! Thank you! Also, thanks to good old Canto for being the most reliable instrument in the institute, for never complaining without reason, and for spending endless nights with me.

I am sincerely grateful to my former lab in Münster, especially to Oliver Sendscheid: you guys paved the way for my scientific and personal development. Today, I understand many things better. Still, I am grateful that I started this endeavor.
I gratefully acknowledge Gabriel Guerrero, Matías Hartman, Moritz Horn, Christine Kim, Virginia Kroef, Felix Mayr, and Laura Wester for proof reading parts of my thesis (or my book/chronicles as they called it) and for their constructive comments and suggestions. I was fortunate to have such talented and supportive colleagues.

Sincere thanks are extended to all past and present members of the Denzel lab and the Antebi lab. Thank you for the supportive and friendly atmosphere, for your interest both scientifically and especially personally. You are a fantastic group of people, I loved working with you. Thank you for suffering with me and for sharing my happiness. Thereby, you made even the most frustrating times bearable and the success more pleasant. Thanks for countless coffee breaks and (too) many Feierabendbier! Thanks to Sarah Denzel, Julia Noack, Isabelle Schiffer, and Jule Vesting for cake and/or salad supply in good and in bad times. I owe thanks to Sabine Ruegenberg, who had a part in me working on this project. Thanks to Max and Moritz. Mo, I am sorry that I didn't always present myself in the best light. The enterprise 'hexosamine pathway' developed differently than expected, but I guess we made the best of it. Thanks for 4+2 years! I am grateful to Dr. Gabi G. and Felix A.M.C. Mayr for being there from week 7 on. It was good to have someone around, who understands. SDD to Matías Hartman for reminding me how fortunate I was to work in such a great environment and for being the amazing character that you are. You made this lab a better place! I address sincere thanks to my lunch crew, which was rather a

support group consisting of friends: Ruth Baddi, Virginia Kroef, Stephan Miethe, and Laura Wester. Thank you for sharing emotions (the good ones and the ‘Quank’ ones), problems (big and small), and solutions (serious ones and not so serious ones) with me! Thanks to all of you, I enjoyed coming to work, which rather felt like a second home. I had a great time!

Zum Schluss möchte ich meinen Freunden, Pascals Familie und meiner Familie meine tiefste Dankbarkeit aussprechen: danke, dass ihr akzeptiert habt, dass diese Arbeit eher eine Leidenschaft als ein Job war und dass ihr mir verziehen habt, wenn ich mal wieder eine Gelegenheit euch zu sehen verpasst habe. Wann ich fertig bin? Jetzt!

Kleines Caro, danke, dass du in meinem Kopf wohnst und meine Gedanken und Emotionen ohne viele Worte verstehst. Deine Freundschaft bedeutet mir sehr viel!

Oma Johanna und Opa Gustav, es tut mir leid, dass ich es nicht rechtzeitig geschafft habe. Ich weiß wie stolz ihr auf mich wart! Oma Thea und Opa Heinz, danke für euer unbändiges Interesse, den Versuch meine Arbeit zu verstehen, euer Verständnis und eure Unterstützung! Ich bin sehr froh diesen Moment mit euch teilen zu können.

Pascal, ich finde nicht die passenden Worte, um auszudrücken, was du für mich und diese Arbeit bedeutest. Das kannst du eindeutig besser als ich. Du hast all die Höhen und Tiefen der letzten Jahre und die damit verbundenen Emotionen miterlebt und viel zu oft ausbaden müssen. Du warst für mich da, auch wenn ich es dir nicht immer leicht gemacht habe. Danke, für deine kontinuierliche Unterstützung. Danke, dass du mich getröstet hast, wenn es nötig war, und mich zum Lachen gebracht hast, wann immer es möglich war. Danke, dass du deine Schulter und deine Ohren zur Verfügung gestellt hast. Danke, dass du mein Ruhepol, mein bester Freund und mein Teampartner bist! Dein Anteil an dieser Arbeit ist größer als du glaubst! Du hast die Schnaction möglich gemacht!

Mama, danke, dass du mich zu dem Menschen (v)erzogen hast, der ich heute bin. Danke für deine grenzenlose Liebe und Unterstützung. Danke, dass du mir in den Hintern getreten hast, wenn es nötig war. Danke, dass du immer an mich geglaubt und für mich gekämpft hast! Ohne dich wäre diese Arbeit nicht möglich gewesen. Ich kann das und ich habe es geschafft!

List of abbreviations

α-MeSpd	α-methylspermidine
α6	integrin α6
%	percent
°C	degree Celsius
3-AAP	3-acetamidopropanal
3D-3C	3 dimension, 3 compounds
4-MU	4-methylumbelliferone
4E-BP	eIF4E-binding protein
7AAD	7-aminoactinomycin D
A-site	aminoacyl-site
ABCE1	ATP-binding cassette sub-family E member 1
acetyl-CoA	acetyl-coenzyme A
ADP	adenosine 5'-diphophate
AF488	Alexa Fluor™ 488
AMD1	adenosylmethionine decarboxylase 1
AMPK	AMP-activated protein kinase
Asn	asparagine
ATF4	activating transcription factor 4
ATF6	activating transcription factor 6
ATP	adenosine 5'-triphophate
BMP	bone morphogenic protein
bp	base pair
BSA	bovine serum albumin
C. elegans	*Caenorhabditis elegans*
$CaCl_2$	calcium chloride
CaMKII	calcium/calmodulin-dependent protein kinase II
CD34	cluster of differentiation 34
cKO	conditional knock-out
CO_2	carbon dioxide
COL17A1	type XVII collagen
CS	chondroitin sulfate
Da	dalton
dcSAM	decarboxylated *S*-adenosylmethionine
ddH_2O	deionized water
DENSpm	*N*1,*N*11-diethlynorspermine
DFMO	2-difluoromethylornithine
Dkk3	Dickkopf 3
DNA	deoxyribonucleic acid
dNTPs	deoxynucleosidetriphosphate
Dol-P-Man	dolichol-phosphate-mannose
DP	dermal papilla
DS	dermatan sulfate
E	glutamic acid
E-site	exit-site
E. coli	*Escherichia coli*
ECL	enhanced luminol-based chemiluminescent substrate
ECM	extracellular matrix
EDTA	ethylenediaminetetraacetic acid
EdU	5-ethynyl-2'-deoxyuridine
eEF	eukaryotic elongation factor

EGF	epidermal growth factor
EGFR	EGF receptor
eIF	eukaryotic initiation factor
eIF2α	eukaryotic initiation factor 2α
ELISA	enzyme-linked immunosorbent assay
ER	endoplasmic reticulum
ERAD	ER-associated degradation
eRF	eukaryotic release factor
ESC	embryonic stem cell
ETC	electron transport chain
F	forward
FACE	Fluorophore-Assisted-Carbohydrate-Electrophoresis
FACS	fluorescence-activated cell sorting
$FADH_2$	reduced flavin adenine dinucleotide
FBS	fetal bovine serum
FC	fold change
FGF	fibroblast growth factor
Foxc1	forkhead box c1
FPKM	fragments per kilobase million
Frc1,6P	fructose-1,6-biphosphate
Frc6P	fructose-6-phosphate
fwd	forward
G	glycine
g	gram
GAG	glycosaminoglycan
GALE	UDP-galactose-4'-epimerase
GCN2	general control non-derepressible 2
GDP	guanosine 5'-diphophate
GDP-Man	GDP-mannose
GEF	guanine nucleotide exchange factor
GFAT	glutamine fructose-6-phosphate amidotransferase
Glc	D-glucose
Glc6P	D-glucose-6-phosphate
GlcN	D-glucosamine
GlcN6P	D-glucosamine-6-phosphate
GlcNAc	*N*-acetyl-D-glucosamine
GlcNAc1P	*N*-acetyl-D-glucosamine-1-phosphate
GlcNAc6P	*N*-acetyl-D-glucosamine-6-phosphate
Gln	L-glutamine
Glu	L-glutamate
GNA1	D-glucosamine-6-phosphate-*N*-acetyltransferase 1
GNPDA	D-glucosamine-6-phosphate deaminase
GO	gene ontology
gof	gain-of-function
GPI	glycophosphotidylinositol
GTP	guanosine 5'-triphophate
H	heparin
H	histidine
h	hour
HA	hemagglutinin
HA	hyaluronic acid
haESCs	haploid mouse embryonic stem cells
HAS	hyaluronic acid synthase

HAT	histone acetyltransferase
HDAC	histone deacetylase
HESI	heated electrospray ionization
HF	hair follicle
HFSC	hair follicle stem cell
HG	hair germ
HK	hexokinase
HP	hexosamine pathway
hr	hairless
HRI	heme regulated inhibitor
HRP	horseradish peroxidase
HS	hair shaft
HS	heparan sulfate
HSC	hematopoietic stem cell
HSP	heat shock protein
hu	human
HYAL	hyaluronidase
Id2	inhibitor of DNA binding 2
IFD	infundibulum
IFE	interfollicular epidermis
IIS	insulin/IGF-1 signaling
iPSC	induced pluripotent stem cell
IRE1α	inositol requiring enzyme 1α
IRS	inner root sheath
ISC	intestinal stem cell
ISR	integrated stress response
K	lysine
kDa	kilodalton
KGM	keratinocyte growth medium
ki	knock-in
ko	knock-out
Krt	keratin
KS	keratan sulfate
l	liter
LC	liquid chromatography
LDH	lactate dehydrogenase
Lhx2	LIM homeobox 2
LIF	leukemia inhibitory factor
LSD1	lysine-specific demethylase 1
m^7G	7-methyl-GTP
Man	D-mannose
Man1P	D-mannose-1-phosphate
Man6P	D-mannose-6-phosphate
Met-$tRNA_i^{Met}$	methionine-loaded initiator tRNA
mFAO	mitochondrial fatty acid oxidation
min	minute
ml	milliliter
mM	millimolar
MPC	mitochondrial pyruvate carrier
MPI	phosphomannose isomerase
MRM	multi reaction monitoring
mRNA	messenger RNA
MS	mass spectrometry

ms	mouse
MSC	mesenchymal stem cell
MT	metallothionein I
MTA	5'-methylthioadenosine
mTOR	mammalian target of rapamycin
*N*1-AcSpd	*N*1-acetylspermidine
*N*1-Acspm	*N*1-acetylspermine
NAD^+	oxidized nicotinamide adenine dinucleotide
NADH	reduced nicotinamide adenine dinucleotide
NAGK	*N*-acetyl-D-glucosamine kinase
Nfatc1	nuclear factor of activated T-cells, cytoplasmic 1
ng	nanogram
nm	nanomolar
NSUN2	NOP2/Sun RNA methyltransferase family member 2
nt	nucleotide
OAZ	ODC antizyme
ODC	ornithine decarboxylase
OE	overexpression
OGA	*O*-GlcNAcase
OGT	*O*-GlcNAc transferase
ORF	open reading frame
ORS	outer root sheath
OXPHOS	oxidative phosphorylation
P	postnatal day
P-eIF2α	phosphorylated eIF2α
P-site	peptidyl-site
P/S	penicillin-streptavidin
PAGE	polyacrylamidegelelectrophoresis
PAOX	polyamine oxidase
PBS	phosphate-buffered saline
PCR	polymerase chain reaction
PDK	pyruvate dehydrogenase kinase
PDPK1	3'-phosphoinositide-dependent kinase 1
PERK	PKR-like endoplasmic reticulum kinase
PFA	paraformaldehyde
PFK	phosphofructokinase
PG	proteoglycan
PGI	phosphoglucoisomerase
PGM3	phosphoglucomutase
PI	propidium iodide
PKA	cAMP-dependent protein kinase
PKR	protein kinase R
PMM2	phosphomannomutase 2
PPARδ	peroxisome proliferator-activated receptor δ
PQC	protein quality control
PSMD	proteasome non-ATPase regulatory subunit
R	reverse
R26	Rosa26
rev	reverse
RNA	ribonucleic acid
rpm	rounds per minute
rRNA	ribosomal RNA
RT	room temperature

RT-PCR	real-time PCR
RTK	receptor tyrosine kinase
s	second
SAM	*S*-adenosylmethionine
Sca1	stem cell antigen 1
SD	standard deviation
SDS	sodium dodecyl sulfate
SEM	standard error of the mean
Ser	serine
Shh	sonic hedgehog
siRNA	small interfering RNA
SMOX	spermine oxidase
SMS	spermine synthase
Sox9	SRY-box 9
SRM	spermidine synthase
SSAT	spermidine/spermine *N*1-acetyltransferase
T_A	annealing temperature
TAC	transient-amplifying cell
TBS	Tris-buffered saline
TC	ternary complex
TCA	tricarboxylic acid
Tcf3	transcription factor 3
tg	transgene
TGF	transforming growth factor
Thr	threonine
tRNA	transfer RNA
U	units
UAP1	UDP-*N*-acetylglucosamine pyrophosphorylase
UDP	uridine 5'-diphosphate
UDP-GalNAc	uridine 5'-diphospho-*N*-acetyl-D-galactosamine
UDP-GlcNAc	uridine 5'-diphospho-*N*-acetyl-D-glucosamine
UDP-GlcUA	UDP-glucuronic acid
UDP-HexNAc	uridine 5'-diphospho-*N*-acetyl-D-hexosamine
UDP-IdoUA	UDP-iduronic acid
UGT	UDP-glucuronosyltransferase
UMI	unique molecular identifier
uORF	upstream open reading frame
UPR	unfolded protein response
UPS	ubiquitin-proteasome system
UTP	uridine-5'-triphosphate
UV	ultraviolet
V	volt
v/v	volume/volume
VEGF	vascular endothelial growth factor
Wnt	Wingless-related integration site
wt	wildtype
WT	wildtype
Xbp1	X-box binding protein 1
Xbp1s	spliced X-box binding protein 1
µg	microgram
µl	microliter
µM	micromolar

Abstract

Aging is the main risk factor for the manifestation of numerous serious diseases, including cancer, cardiovascular diseases and neurodegeneration. Thus, the growing proportion of elderly people in the population poses a major challenge to the health care systems worldwide.

Tissue homeostasis declines with age and its maintenance late in life has been intimately linked to prolonged healthspan. Stem cells act as drivers of tissue homeostasis through the interplay of self-renewal and differentiation. Therefore, it is of utmost importance to identify stem cell fate determinants to be able to delay stem cell exhaustion in the elderly. Of note, metabolic changes have been described to influence function and maintenance of stem cell populations. However, whether manipulation of metabolism affects cell fate decisions and stem cell maintenance remains poorly understood.

Here, I focus on three metabolic pathways that have been described to become dysregulated with age, and to affect stemness: the hexosamine pathway (HP), aerobic sugar metabolism, and the polyamine metabolism. I assess their influence on cell fate decisions in an *in vitro* organoid culture system, which allows for the manipulation of hair follicle stem cells (HFSCs) and their direct progeny. First, I activate the HP by GlcNAc supplementation and through genetic manipulation of the rate-limiting enzyme GFAT1. While pathway flux and downstream metabolites increase, HFSC fate is not affected by these interventions. Second, I investigate the effect of sugar supplementation on cell fate decisions. Both, D-glucose and D-mannose, enhance stemness. While D-glucose supplementation boosts glycolysis, D-mannose addition specifically increases the acetylated polyamines *N*1-acetylspermidine (*N*1-AcSpd) and *N*1-acetylspermine without elevating glycolytic flux. Third, I elucidate how polyamine levels influence cell fate decisions. I confirm that low translation rates mark the stem cell state and that a forced decrease in translation is sufficient to elevate stemness. Surprisingly, I demonstrate that reducing translation by changes in polyamine availability does not correlate with increased stemness in the organoids. I identify *N*1-AcSpd as novel regulator of HFSC fate decisions, accelerating cell cycle progression. Finally, I demonstrate that HFSC activation by depilation results in an elevation of the acetylated polyamines, suggesting a functional role of *N*1-AcSpd in cell fate decisions *in vivo*. Overall, my results suggest that manipulation of metabolism is an effective means to control cell fate decisions, delay stem cell exhaustion, and improve tissue homeostasis in the elderly.

Zusammenfassung

Das Altern ist der größte Risikofaktor für das Auftreten vieler ernsthafter Erkrankungen wie Krebs, Herz-Kreislauf-, sowie neurodegenerativer Erkrankungen. Deshalb stellt der wachsende Anteil der älteren Menschen in der Bevölkerung eine große Herausforderung für die Gesundheitssysteme weltweit dar.

Die Homöostase der einzelnen Gewebe wird im Alter schlechter und ihre Erhaltung ist eng mit der Verlängerung der gesunden Lebenszeit verknüpft. Stammzellen erhalten die Homöostase durch das Wechselspiel von Erneuerung und Differenzierung. Deshalb ist es von höchster Wichtigkeit, Faktoren, die das Verhalten der Stammzellen bestimmen, zu identifizieren, um letztendlich die Erschöpfung der Stammzellfunktion bei älteren Menschen zu verlangsamen. Es ist bekannt, dass metabolische Veränderungen die Funktion und die Erhaltung von Stammzellpopulationen beeinflussen können. Ob die Manipulation des Metabolismus aber kausal das Verhalten der Stammzellen bestimmen kann, ist noch nicht vollständig verstanden.

In dieser Arbeit fokussiere ich mich auf drei Stoffwechselwege, deren Regulation im Alter verloren geht und die bereits mit verbesserter Stammzellfunktion in Verbindung gebracht wurden: der Hexosamin-Syntheseweg (HSW), der aerobische Zuckermetabolimus, und der Polyamin-Syntheseweg (PSW). Ich teste den Einfluss dieser Stoffwechselwege auf das Verhalten von Stammzellen des Haarfollikels in einem Organoid-Kultursystem, das die einfache Manipulation dieser Stammzellen ermöglicht. Zuerst aktiviere ich den HSW durch GlcNAc Gabe oder durch genetische Veränderung des Reaktionsgeschwindigkeits-bestimmenden Enzyms GFAT1. Obwohl die Menge der Endprodukte des HSW erhöht ist, wird das Verhalten der Stammzellen nicht verändert. Zweitens beobachte ich den Einfluss von Zuckerzugabe auf das Verhalten der Stammzellen. Glukose und Mannose erhöhen die Anzahl der Stammzellen. Während Glukose Glykolyse steigert, führt Zugabe von Mannose zu einer spezifischen Anreicherung der acetylierten Polyamine *N*1-Acetylspermidin (*N*1-AcSpd) und *N*1-Acetylspermin. Drittens kläre ich auf, wie der PSW das Verhalten der Stammzellen beeinflusst. Ich bestätige, dass Stammzellen geringe Translation zeigen und dass eine erzwungene Minderung der Proteinsynthese ausreicht, um die Stammzellfunktion zu erhöhen. Überraschenderweise zeige ich, dass eine Reduktion der Translation durch eine Veränderung in der Verfügbarkeit der Polyamine nicht mit erhöhter Stammzellfunktion in dem Organoid-Kultursystem korreliert. Ich identifiziere *N*1-AcSpd als neuen Regulator, der das Verhalten von Stammzellen durch erhöhtes Fortschreiten des Zellzyklus beeinflusst. Abschließend zeige ich, dass die Aktivierung von Stammzellen des Haarfollikels durch Depilation zu einer Erhöhung der

acetylierten Polyamine führt, was eine funktionale Rolle von *N*1-AcSpd in der Regulation des Verhaltens der Stammzellen *in vivo* suggeriert. Insgesamt deuten meine Ergebnisse darauf hin, dass die Manipulation verschiedener Stoffwechselwege das Verhalten von Stammzellen beeinflussen, die Erschöpfung der Stammzellfunktion verlangsamen und die Homöostase der verschiedenen Gewebe bei älteren Menschen verbessern kann.

1 Introduction

1.1 The aging process

Aging is an inevitable consequence of life (Foo et al. 2019). It is a complex process that is defined as the time-dependent, gradual decline in tissue function. With advanced chronological age, the ability to perform everyday physical and cognitive tasks is diminished, while the susceptibility to many common diseases rises (Melzer et al. 2020). Aging has a genetic basis: it is regulated by evolutionarily conserved pathways since single-gene mutations in energy metabolism, nutrition sensing, or reproduction can extend lifespan (Kenyon 2005; Vijg and Campisi 2008). Simultaneously, single-gene mutations can result in the manifestation of premature aging syndromes, which are characterized by aging-like pathologies arising early in life (Ashapkin et al. 2019). Although the accumulation of cellular damage is widely considered to contribute to the aging process, its cause remains poorly understood. Thus, unraveling the molecular basis of aging is one of the greatest remaining challenges for science (Gems and Partridge 2013).

1.1.1 Our aging society

The increase in the proportion of elderly people in the population is one of the most remarkable sociodemographic phenomena of the twenty-first century (Nomura et al. 2018). Today, the number of senior citizens accounts for about a fifth of the global population (Mitrečić et al. 2020). Worldwide human life expectancy more than doubled over the past two centuries: it increased from about 25 years to around 65 years for men and 70 years for women (Oeppen and Vaupel 2002). Although the limit of human life expectancy is still under debate, general projections predict that survival rates will continue to increase (Dong et al. 2016; Kontis et al. 2017). Consequently, the current proportion of the global population above 60 years (17%) will double in only thirty to forty years (Mitrečić et al. 2020). However, the healthy, disease-free lifespan (healthspan) has not increased as much as lifespan, resulting in 16-20% of life spent in late-life morbidity (Partridge et al. 2018). Aging is the leading risk factor for diseases like cancer, neurodegeneration, type 2 diabetes mellitus, chronic kidney disease, and coronary artery disease, which are also referred to as age-associated diseases (Melzer et al. 2020). The increased number of morbid patients represents a common challenge for the health care systems around the world. Therefore, it is of utmost importance to understand the fundamentals of aging to

tackle age-associated diseases and increase healthspan of the growing proportion of elderly people.

1.1.2 Hallmarks of aging

López-Otín et al. (2013) identified and categorized the cellular and molecular hallmarks of aging. The following nine hallmarks generally to contribute to the aging process and determine the aging phenotype: genomic instability, telomere attrition, epigenetic alterations, loss of protein homeostasis (proteostasis), deregulated nutrient sensing, mitochondrial dysfunction, cellular senescence, stem cell exhaustion, and altered intercellular communication (Figure 1A). All hallmarks manifest during normal aging and their manipulation can accelerate or retard the aging process, depending on the experimental set-up. The hallmarks can be grouped into three main categories (Figure 1B). First, primary hallmarks that cause cellular damage. Second, antagonistic hallmarks that respond to the damage and become detrimental if exacerbated. Third, integrative hallmarks that arise when the damage cannot be compensated further and are responsible for the functional decline associated with aging. These hallmarks are not mutually exclusive, and thus can co-occur during aging.

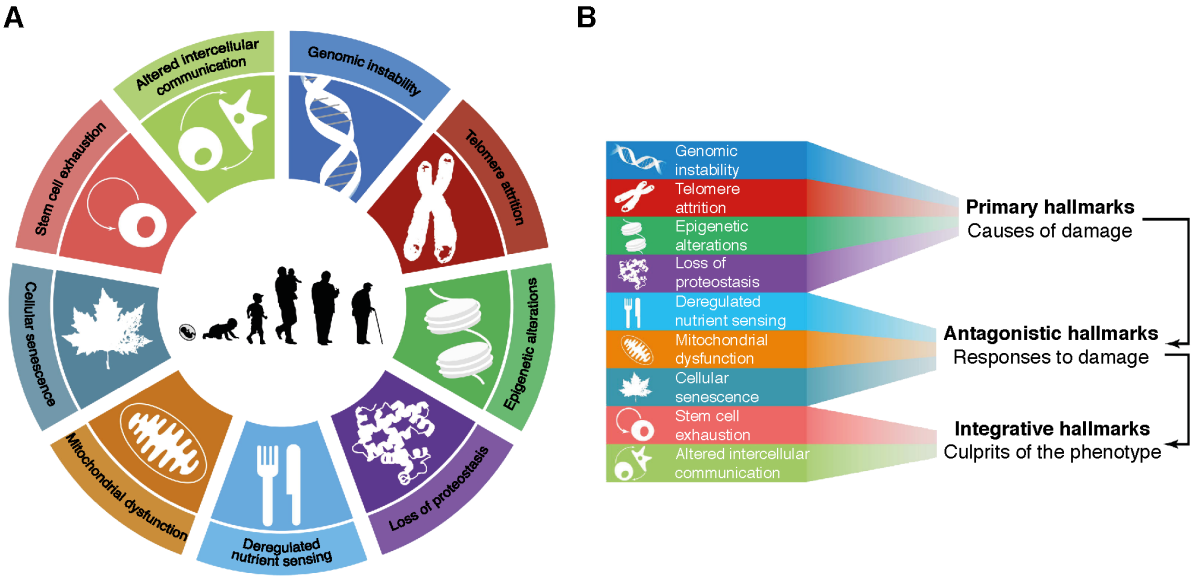

Figure 1: The molecular hallmarks of aging. (**A**) The nine hallmarks are depicted: genomic instability, telomere attrition, epigenetic alterations, loss of proteostasis, deregulated nutrient sensing, mitochondrial dysfunction, cellular senescence, stem cell exhaustion, and altered intercellular communication. (**B**) The hallmarks can be divided into three groups: primary hallmarks, antagonistic hallmarks, and integrative hallmarks. Modified from López-Otín et al. 2013.

The sum of these molecular hallmarks of aging manifests in the clinical picture of the elderly patient: frailty, sarcopenia, anemia, poor nutrition, and a blunted immune system

(Aunan et al. 2016). Therefore, deciphering the underlying mechanisms that contribute to the manifestation of the molecular hallmarks will help to slow the decline in tissue function.

1.2 Tissue homeostasis

Long-term maintenance of tissue homeostasis relies on adult somatic stem cell function. The latter are characterized by their ability to self-renew and to differentiate into multiple cell types within a tissue. These processes are tightly controlled to ensure tissue growth and regeneration during normal physiology or in response to injury (Schultz and Sinclair 2016). However, if this control goes awry, increased stem cell self-renewal can result in tumorigenesis, whereas aberrant differentiation causes stem cell depletion and thereby tissue aging.

Stem cell function, and subsequently tissue homeostasis, depends on many different determinants. In this study, I focused on three different metabolic pathways that show decreased activity during the aging process: hexosamine biosynthesis, aerobic sugar metabolism, and the polyamine metabolism (Denzel et al. 2014; Goyal et al. 2017; Ravera et al. 2019; Vivó et al. 2001; Nishimura et al. 2006). In the following sections, I will highlight their function and dissect their influence on protein homeostasis, and the surrounding stem cell niche. Furthermore, I will discuss how the manipulation of these metabolic pathways affects cell fate decisions and might ultimately improve stem cell maintenance and tissue homeostasis.

1.2.1 Adult somatic stem cell fate decisions

During cell division, stem cells continuously undergo fate decisions, which directly impact tissue homeostasis. Three different division modes of stem cells are conceivable: symmetric division yields two stem cells; asymmetric division results in one stem cell and one differentiated progenitor cell; symmetric commitment leads to two differentiated daughter cells (Ito and Ito 2016). These division modes cause stem cell expansion, stem cell maintenance, stem cell exhaustion, respectively. Furthermore, cell fate can be determined after a symmetric division with an asymmetric distribution of aged mitochondria, or damaged proteins to the daughter cells (Katajisto et al. 2015; Moore et al. 2015). Aged mitochondria and damaged proteins are asymmetrically inherited by one daughter cell which is poised to differentiate. Thereby, stem cells retain a healthy state. However, aged stem cells are less able to exclude damaged proteins, which contributes to their functional decline, and ultimately to stem cell exhaustion (Moore et al. 2015).

1.2.2 Stem cell exhaustion

Adult somatic stem cell function declines during the aging process in numerous tissues, including the brain, blood, bone, skeletal muscle, and skin (Kuhn et al. 1996; Morrison et al. 1996; Gruber et al. 2006; Conboy et al. 2005; Nishimura et al. 2005). This effect correlates with the accumulation of DNA damage, a decrease in cell cycle activity, and telomere shortening, for example (Rossi et al. 2007; Janzen et al. 2006; Flores et al. 2005). Stem cell exhaustion can also be caused by excessive proliferation due to loss of quiescence as described for *Drosophila* intestinal stem cells, hematopoietic stem cells (HSCs), and neural stem cells, resulting in their premature loss (Rera et al. 2011; Cheng et al. 2000; Kippin et al. 2005).

The functional decline of adult somatic stem cells causes deterioration of tissue homeostasis and regeneration, which is one of the most apparent manifestations of the aging process and the basis for many age-associated diseases (López-Otín et al. 2013; Signer and Morrison 2013). Therefore, maintaining stem cell function is pivotal to slow the aging process in general and to tackle age-associated diseases in particular (Chandel et al. 2016). Accordingly, Rando and Chang (2012) suggest that many of the secrets to organismal longevity might be linked to stem cell quiescence and self-renewal. In fact, ensuring proliferative homeostasis of intestinal stem cells in *Drosophila* extends lifespan (Biteau et al. 2010). Thus, the identification of cell fate determinants is key to delay stem cell exhaustion, and ultimately, to improve tissue function late in life.

1.3 The skin

The skin is a multi-layered organ that forms a protective barrier against environmental impact. It is the largest organ of the body, accounting for about 15 % of the total body weight (Kanitakis 2002). The skin is arranged in three main layers: the epidermis, the dermis, and the hypodermis (Figure 2). The structural or pilosebaceous unit of a hair follicle (HF) consists of the HF itself, the arrector pili muscle, and the sebaceous gland (Figure 2) (Martel et al. 2020). The HF begins at the surface of the epidermis and extends deep in the dermal layer of the skin.

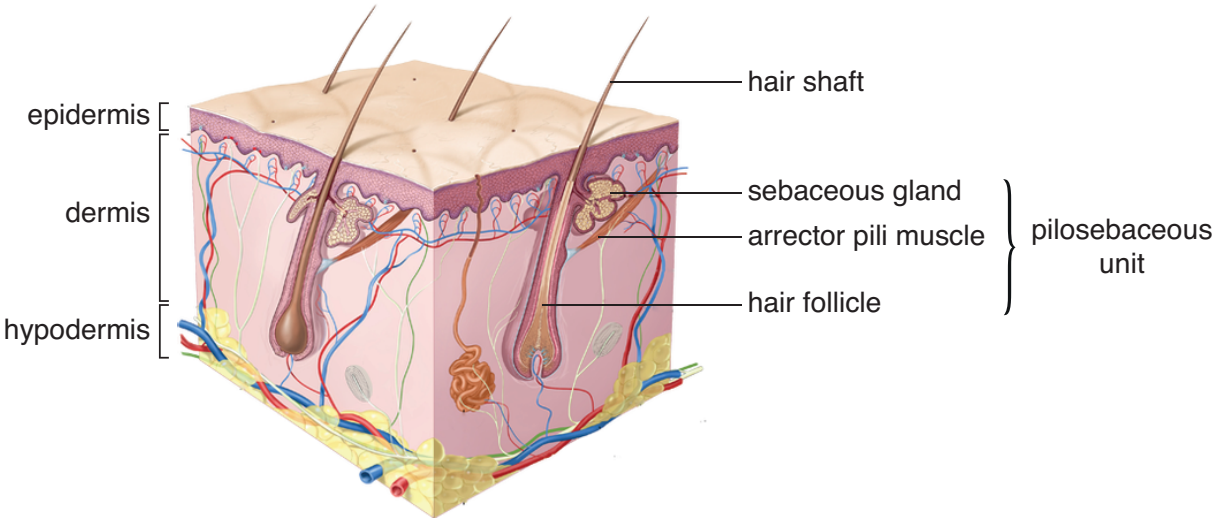

Figure 2: Schematic representation of the skin. The three layers of the skin are shown: epidermis, dermis, and hypodermis. A pilosebaceous unit comprises the hair follicle, the sebaceous gland, and the arrector pili muscle. Modified from PDQ Adult Treatment Editorial Board, PDQ Cancer Information Summaries, National Cancer Institute (US), 2020.

In this study, I use the skin, more precisely the stem cells in the hair follicle, as a model to study adult somatic stem cell fate. These stem cells fuel the cyclical growth of hair follicles, and thus, undergo constant fate decisions *in vivo*. In the following sections, I will introduce the skin in general and hair follicle stem cells (HFSCs) in particular. Also, I will outline the advantages of HFSCs as a model in more detail.

1.3.1 Skin aging

Skin aging is the most apparent aging phenotype and serves as an age estimate. Thus, there exists a vast cosmetic need attempting to prevent or reverse skin aging (Zhang and Duan 2018). Aging of the skin is caused by intrinsic and extrinsic factors, such as reduced hydration and ultraviolet (UV) irradiation, respectively (Shah and Kennedy 2018). While intrinsically aged skin is characterized by fine wrinkles, loss of underlying fat, reduced elasticity, and dryness, extrinsic skin aging manifests in deep wrinkles, roughness, and mottled discoloration (Nikolakis et al. 2013).

Epidermal aging is associated with thinning, loss of melanocytes, and decreased barrier function due to the changed composition of the outermost layer, the cornified layer (Rinnerthaler et al. 2015; Choi 2019). These changes are likely caused by loss of the epidermal calcium gradient, which is required for proper differentiation of keratinocytes and the expression of terminal differentiation makers like filaggrin and loricrin (Rinnerthaler et al. 2013). Furthermore, aged epidermis displays reduced lipid levels in the cornified layer and abnormal cholesterol synthesis (Elias and Ghadially 2002). Accordingly, loss of

ceramide synthase 4 disrupts epidermal barrier function independent of other age-associated changes (Peters et al. 2020). Histologically, aged skin displays a flat epidermal-dermal interface (El-Domyati et al. 2002). This is caused by the loss of cytoplasmic projections of the basal cells into the dermis compared to young basal cells (Waller and Maibach 2005). Dermal aging is accompanied by the gradual reduction of collagen fibers (El-Domyati et al. 2002) resulting from diminished collagen synthesis (Uitto 1989).

Skin hydration highly depends on glycosaminoglycans (GAGs) in general, and on hyaluronic acid (HA) in particular. Of note, GAGs can bind up to 1000 times their volume in water (Bernstein et al. 1996). In intrinsically aged skin, epidermal HA and dermal GAG content are reduced (Lee et al. 2016), which is in accordance with the observed dryness. However, photo-aged dermis displays increased GAG content with aberrant localization on the elastotic material, which is characteristic for UV-damaged skin (Bernstein et al. 1996).

Aging of the hair follicle is associated with thin, dull, and brittle hair (Goodier and Hordinsky 2015). Hair graying is caused by the loss of melanin production and the reduction of melanocytes in hair follicles (Fernandez-Flores et al. 2019). Also, hair loss is a common characteristic of skin aging and imbalanced stem cell differentiation as well as altered stem cell activity have been identified as important factors (Ji et al. 2017). Aged hair follicles display prolonged resting phases and impaired entry of the growth phase (Courtois et al. 1995). In androgenetic alopecia, HFSCs are maintained, but their activation into a more proliferative state is impaired, resulting in greatly diminished numbers of early progenitors (Garza et al. 2011).

1.3.2 Epidermal homeostasis

In this section, I will focus on the epidermis, which is the outermost layer of the skin. It comprises a multi-layered epithelium, the interfollicular epidermis (IFE), and associated appendages like the hair follicle (HF) and the sebaceous gland (Watt and Jensen 2009). The IFE undergoes regular renewal, since the top layer, the cornified layer, is continuously shed from the surface of the skin. Cornified cells are terminally differentiated keratinocytes that form a mesh of cross-linked proteins conferring impermeability and barrier protection (Solanas and Benitah 2013). They are substituted through differentiating stem cells from the basal layer (Jensen et al. 2009). Strikingly, differentiation of a stem cell from the basal layer triggers the self-renewal of the neighboring stem cell to ensure epidermal homeostasis (Mesa et al. 2018).

In contrast to the IFE, which is constantly renewed, the HF undergoes cyclical rounds of growth (anagen), apoptosis-mediated regression (catagen) and rest (telogen), called the hair cycle (Fuchs et al. 2001; Niemann and Watt 2002).

1.3.3 The hair cycle

The HF consists of an upper, permanent portion, and a lower, cycling portion that produces the hair (Figure 3) (Alonso and Fuchs 2003). In its mature form, the HF comprises a relatively undifferentiated outer root sheath (ORS), which is contiguous with the basal layer of the IFE, and an inner root sheath (IRS), which serves as the channel from which the hair shaft (HS) exits the skin surface (Figure 3A) (Fuchs et al. 2001). Hair regeneration is fueled by HFSCs, which reside in the bulge region of the HF, and cells located beneath the bulge in the secondary hair germ (HG) (Morris et al. 2004; Rompolas et al. 2013). At the onset of anagen, cells in the HG become activated and respond to signals from a mesenchymal structure, the dermal papilla (DP), which is located at the base of the HF (Greco et al. 2009). Proliferating cells from the HG establish a population of matrix cells, which differentiate to give rise to IRS and HS. Matrix cells are also described as transient-amplifying cells (TACs) since they undergo a limited number of divisions before they differentiate (Alonso and Fuchs 2006). Thus, TACs represent a transition state between stem cells and terminally differentiated cells (Hsu et al. 2014b). Strikingly, TACs can stimulate the proliferation of quiescent HFSC in the bulge region through sonic hedgehog (Shh) signaling (Hsu et al. 2014b). A subset of HFSCs contributes to the ORS, while all differentiated lineages originate from cells of the HG (Rompolas et al. 2013). After the anagen growth phase, some bulge-derived ORS cells, which underwent only a few divisions, return to the bulge region, where they resume quiescence and CD34 expression, a key marker of HFSCs. These cells become the primary stem cells for the initiation of the next hair cycle (Hsu et al. 2011). Other ORS cells, which underwent more divisions, become activated stem cells of the HG and give rise to differentiated cells in the next hair cycle (Greco et al. 2009; Hsu et al. 2011; Rompolas et al. 2013). When the supply of TACs declines, the HF enters the destructive phase catagen. The anagen-catagen transition is supported by FGF5, EGF and TGFβ1 signaling (Hebert et al. 1994; Hansen et al. 1997; Foitzik et al. 2000). During catagen, the entire lower portion of the HF, besides the DP, undergoes apoptosis-mediated regression (Lindner et al. 1997). The HS seals off into a rounded structure called club, which moves upward until it reaches the non-cycling, permanent bulge region of the upper follicle, where it remains anchored during telogen (Alonso and Fuchs 2006). Due to its contact with the basement membrane, the DP is

drawn up to the base of the permanent part of the HF (Figure 3B) (Fuchs et al. 2001). Subsequently, the HF enters the resting phase telogen. During telogen, HFSCs rely on bone morphogenic protein (BMP) signaling to maintain a quiescent state (Genander et al. 2014). Initiation of the next hair cycle requires Wnt (Huelsken et al. 2001; Van Mater et al. 2003) and Shh signaling (St-Jacques et al. 1998; Hsu et al. 2014b).

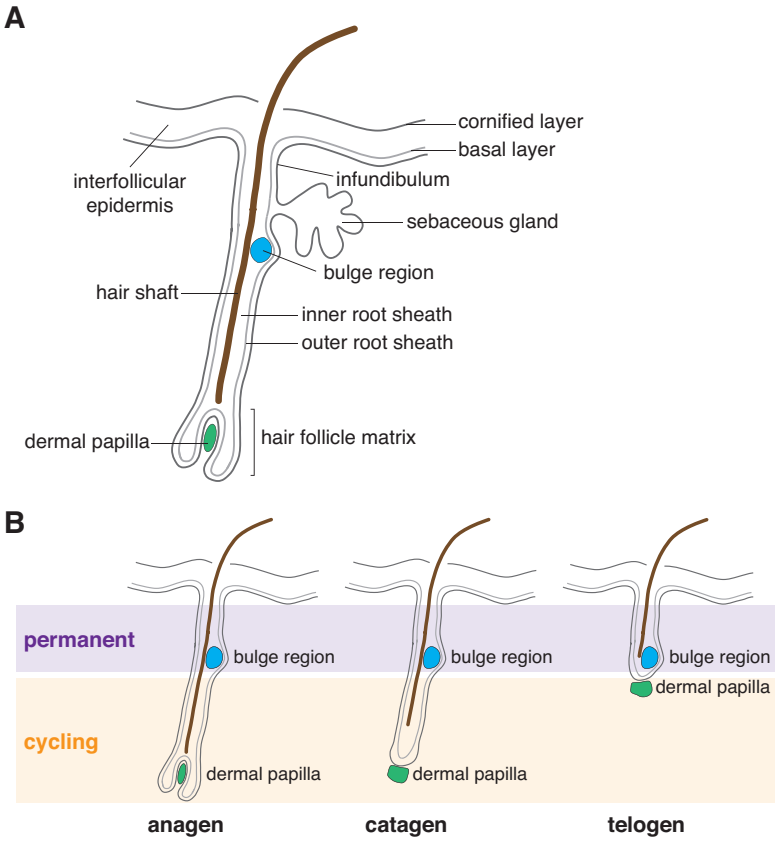

Figure 3: Hair follicle morphology and hair cycle progression. (**A**) Schematic representation of HF morphology. Adapted from Alonso and Fuchs 2003. (**B**) Schematic representation of the HF in the different phases of the hair cycle. The permanent portion of the HF is marked in violet; the cycling portion is depicted in orange. Adapted from Waters et al. 2007. (**A**-**B**) blue: bulge region, green: dermal papilla.

1.3.3.1 Hair follicle stem cells

Since the hair follicle is a self-contained mini-organ that undergoes constant renewal, HFSCs play a crucial role in skin homeostasis and represent an excellent paradigm to study adult somatic stem cell fate decisions (Fuchs 2007; Blanpain and Fuchs 2009). In general, the stem cells in the hair follicle bulge region are slow cycling, label-retaining cells (Cotsarelis et al. 1990; Morris and Potten 1999; Tumbar et al. 2004). However, their activity and gene expression markedly vary during the hair cycle (Blanpain et al. 2004; Fuchs 2009). These temporal differences hinder the study of HFSC cell fate decisions *in vivo*.

Quiescent bulge HFSCs generate all epithelial cell types within the intact HF during regular HF cycling (Morris et al. 2004). Upon activation, bulge-derived stem cells proliferate and trail down to the HG. Primed stem cells in the HG establish and expand the pool of TACs, thereby contributing to IRS and HS (Greco et al. 2009; Hsu et al. 2014b). Furthermore, HFSCs differentiate to form the ORS (Rompolas et al. 2013). Also, HFSCs can contribute to the IFE in response to wounding, demonstrating the fate plasticity of HFSCs (Taylor et al. 2000). Intriguingly, lineage-tracing and laser ablation studies showed that HFSCs are dispensable for HF regeneration and that early HFSC descendants, like activated stem cells in the HG, can return to the bulge, where they resume quiescence (Hsu et al. 2011; Rompolas et al. 2013). Moreover, upon genetic ablation of quiescent keratin 19-expressing HFSCs, HF morphology remains normal and the wound healing process is unaltered, further supporting that quiescent bulge stem cells are dispensable for HF regeneration (Driskell et al. 2015).

1.3.3.2 3D-3C organoid culture of HFSCs

Chacón-Martínez et al. (2017) established an *ex vivo* organoid culture system (3D-3C culture) allowing for the long-term culture and manipulation of HFSCs in the absence of heterologous cell types. Importantly, the cells maintain self-renewing capacity and multipotency and still respond to the same signals as they would *in vivo*. The addition of the BMP pathway inhibitor dorsomorphin to the 3D-3C organoids triggers HFSCs to become progenitor cells, since BMP signaling is important for stem cell quiescence (Genander et al. 2014). Cyclopamine, an inhibitor of Shh signaling, induces a shift from the progenitor cells back to the stem cell state, since Shh signaling is required for stem cell activation (Hsu et al. 2014b).

In the 3D-3C organoids, a balance between α6+/CD34+ HFSCs and α6+/CD34- progenitor cells is formed in a self-driven process. Based on their transcriptome and marker expression analysis, these progenitor cells represent hair follicle ORS cells and inner bulge cells (Kim et al. 2020), both of which represent HFSC progeny and act as niche cells for HFSCs *in vivo* (Hsu et al. 2014a). Chacón-Martínez et al. (2017) have described the self-organizing plasticity in the 3D-3C organoids, which results not only in the differentiation of stem cells to progenitor cells, but also in the de-differentiation of progenitor cells to the stem cell state. Overall, this self-organizing 3D-3C organoid culture system allows for easy manipulation of the niche, as well as the HFSCs and their immediate progenitors retained in it, and subsequently the investigation of HFSC fate decisions.

1.4 The stem cell niche

The term ‘stem cell niche’ was first introduced by Schofield (1978). It describes the *in vivo* microenvironment where stem cells reside in association with other cells and the surrounding extracellular matrix (ECM). The niche is responsible for the maintenance of stem cell populations, their controlled proliferation, and the differentiation of their progeny (Rojas-Ríos and González-Reyes 2014). Extrinsic stimuli play a pivotal role in these processes and ensure stem cell homeostasis. These stimuli include cell-to-cell and cell-matrix interactions and signals that can activate or repress genes or transcriptional programs (Ferraro et al. 2010). The importance of the stem cell niche is best described by Fuchs et al. (2004), who use embryonic stem cells (ESCs) as an example: ESCs can divide indefinitely in tissue culture while maintaining their pluripotent potential. When injected into nude mice, these cells form teratomas, which contain differentiated cells of all lineages. However, when injected into a recipient blastocyst, the ESCs contribute to the development of a healthy chimeric mouse. Thus, the properties and the potential of stem cells are defined by the microenvironment.

1.4.1 The extracellular matrix

The ECM is an essential three-dimensional, non-cellular structure present in all tissues (Bonnans et al. 2014). ECM components are not only a scaffold surrounding cells, but also a key regulator of cellular events such as cell adhesion, migration, proliferation, differentiation and survival (Hynes 2009). As such, the ECM is an important contributor to the stem cell niche, thereby regulating epidermal stem cell fate, for example (Chermnykh et al. 2018). In mammals, the core matrisome, which includes all components constituting the ECM, consists of around 300 different proteins, corresponding to approximately 1% of the proteome (Naba et al. 2012). Collagen, glycoproteins and proteoglycans are major building blocks of the ECM (Hynes and Naba 2012). Collagens are the most abundant proteins in mammals. They form supramolecular assemblies of different types which are incorporated in the ECM and important for proper tissue function (Gordon and Hahn 2010). Glycoproteins are the biggest class in the mammalian matrisome, comprising around 200 proteins. They confer different functions including interactions allowing ECM assembly, cell adhesion and signaling (Hynes and Naba 2012). Proteoglycans (PGs) are composed of a core glycoprotein substituted with covalently linked glycosaminoglycan (GAG) chains. The number of chains and their length can vary, as well as their pattern of sulfation, resulting in an enormous diversity of PGs (Hardingham and Fosang 1992). In addition to being structural molecules, proteoglycans play a pivotal role in signal transduction and are

capable of affecting different intracellular signaling cascades and phosphorylation events (Schaefer and Schaefer 2010).

GAGs are long, linear, negatively charged, repetitive disaccharide chains that contain acetylated aminosugars (UDP-GlcNAc or UDP-GalNAc) and mainly uronic acid (D-glucuronic acid or L-iduronic acid). The lumen of the Golgi apparatus is the main site for GAG synthesis (Prydz and Dalen 2000). They can be divided into two classes: (1) the sulfated GAGs comprising chondroitin sulfate (CS), dermatan sulfate (DS), keratan sulfate (KS), heparin (H), and heparan sulfate (HS), and (2) the non-sulfated GAGs such as hyaluronic acid (HA) (Schaefer and Schaefer 2010). The sulfated GAGs H, HS, DS, and CS bind to their respective core proteins via serine residues (Figure 4). Depending on the oligosaccharide linking KS to the core protein, two different types of KS can be distinguished (Figure 4): KSI is attached to asparagine residues, while KSII is linked to serine or threonine residues (Funderburgh 2002).

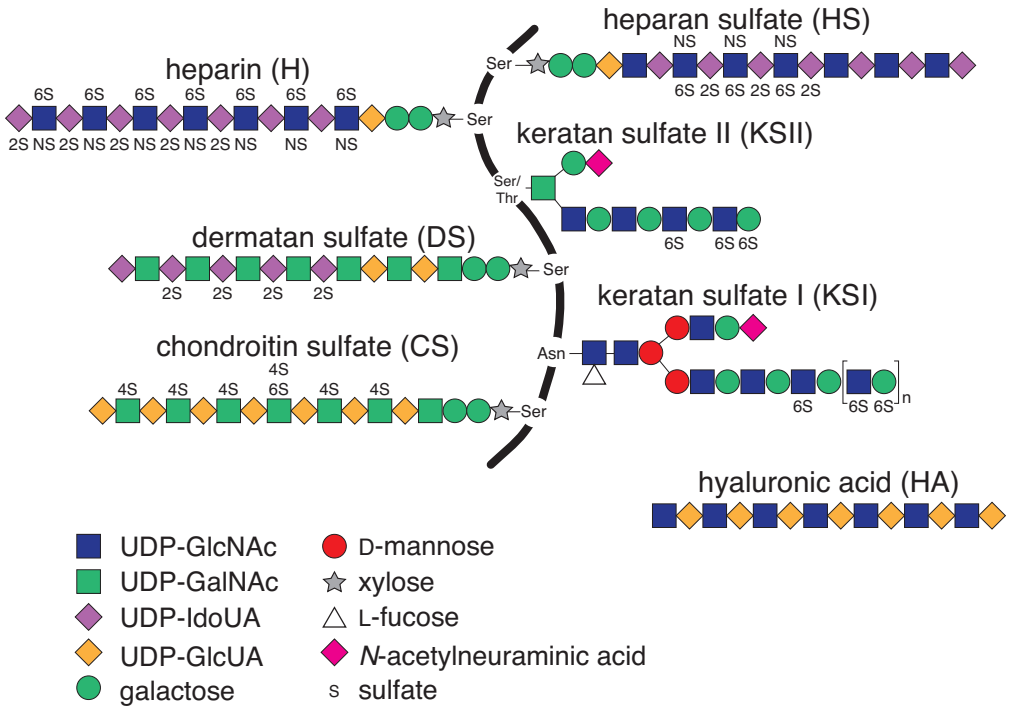

Figure 4: Composition of different glycosaminoglycans and their linkage to core proteins. All GAGs contain either UDP-GlcNAc (blue squares) or UDP-GalNAc (green squares). While the sulfated GAGs H, HS, DS, CS are linked to the protein core via serine residues (Ser), KSI is attached to asparagine residues (Asn) and KSII is linked to serine or threonine residues (Ser/Thr). HA is not linked to a protein core. Adapted from Merida-de-Barros et al. 2018.

In contrast to the other GAGs, HA is synthesized by plasma membrane-bound hyaluronic acid synthases (HAS) -1, -2, and -3, that release HA directly to the extracellular space (Itano and Kimata 2002). HAS use the UDP-sugars UDP-glucuronic acid (UDP-GlcUA)

and uridine 5'-diphospho-*N*-acetyl-D-glucosamine (UDP-GlcNAc) as substrates (Vigetti et al. 2006). HA is the only GAG that is not linked to a protein core (Figure 4), but it can bind to a variety of proteins and PGs, called hyalectans (HA- and lectin-binding PGs) (Day and Prestwich 2002). HA catabolism is mediated by hyaluronidases (HYALs). HYALs specifically hydrolyze HA at hexosaminidic β (1-4) linkages, therefore reducing the amount of extracellular high molecular weight HA (Buhren et al. 2016). The main cell surface receptor for HA is CD44 (Aruffo et al. 1990). Binding of HA to CD44 influences intracellular signaling events, and ultimately, can regulate cellular behavior directly or indirectly.

1.4.2 The stem cell niche influences cell fate

HFSCs undergo cycles of activation and regression that are regulated by the surrounding niche (Fuchs et al. 2004). Periodic expression of BMP2 and BMP4 in the dermis was shown to regulate the regeneration of hair follicles (Plikus et al. 2008; Plikus et al. 2011). These results highlight the importance of extrinsic stimuli in stem cell homeostasis, which can also be provided by the inter-organ macroenvironment. During hair follicle growth, early HFSC progenitor-derived Shh signaling promotes HFSC activation for as long as the progenitor cells are in close proximity to the stem cell niche (Hsu et al. 2014b). This self-organizing feedback loop ensures precise scaling of HFSC activation and hair follicle growth (Chacón-Martínez et al. 2018). Also, the ECM exerts a key role in regulating stem cell fate decisions, especially via its biomechanical properties (d'Angelo et al. 2019). In mesenchymal stem cells (MSCs), lineage commitment is sensitive to tissue-level elasticity: soft matrices that mimic brain are neurogenic, while stiff matrices that mimic muscle are myogenic (Engler et al. 2006). Moreover, a stiff environment, established by ECM deposition, improves the maintenance of skeletal muscle stem cells since it enhances symmetric divisions (Moyle et al. 2020).

The stem cell niche is directly affected by aging. Remarkably, HFSCs within their aged niche were recently shown to maintain lineage identity (Ge et al. 2020). However, the same study found that aging skin is severely compromised in its ability to regenerate hair follicles upon injury. The authors could show that regeneration was improved by young dermal cells during *in vivo* transplantation experiments. In contrast, aged dermal cells failed to support young HFSCs, which suggests that the extrinsic stimuli from the niche override intrinsic stem cell function. Also, proteolysis of type XVII collagen (COL17A1) triggers HFSC aging, resulting in their elimination through terminal differentiation, which can be rescued by forced maintenance of COL17A1 (Matsumura et al. 2016; Liu et al. 2019). In sum, improved maintenance of the stem cell niche might improve stem cell function, slow

down stem cell exhaustion, and delay the subsequent decline in tissue homeostasis upon aging.

1.5 Protein homeostasis and its role in stem cells

Tissue homeostasis depends on functional protein homeostasis, which comprises tight regulation of protein synthesis, folding, and degradation. In this paragraph, I will describe these processes in general and highlight their role in stem cells and cell fate decisions in particular.

1.5.1 Protein synthesis

Translation of messenger RNAs (mRNAs) is one of the most complex and energy-consuming processes in the cell (Roux and Topisirovic 2018). It involves initiation, elongation, and termination, as well as ribosome recycling. Translational control and fidelity play a key role in gene expression regulation (Hershey et al. 2019). Here, I will focus on cap-dependent translation. Translation initiation is a dynamic process (reviewed in Preiss and Hentze 2003), which ultimately results in pairing of the initiator tRNA anti-codon with the start codon of the mRNA. It the requires the formation of a ternary complex (TC) composed of a methionine-loaded initiator tRNA (Met-tRNA$_i^{Met}$) and eukaryotic initiation factor (eIF) 2 bound to GTP. The TC assembles with the 40S ribosomal subunit and other initiation factors to produce the 43S pre-initiation complex. Binding of this complex to the mRNA is dependent on eIF4E, which recognizes the 7-methyl-GTP (m^7G) cap at the 5'-end of the mRNA. Recognition of the initiation codon (AUG) and joining of the large ribosomal subunit trigger GTP hydrolysis on eIF2 (Gebauer and Hentze 2004). In the resulting 80S initiation complex, the Met-tRNA$_i^{Met}$ is bound in the P- (peptidyl) site of the ribosome and its anticodon is base-paired with the start codon of the mRNA. The first step of translation elongation (reviewed in Dever et al. 2018) is the delivery of the cognate elongating aminoacyl-tRNA to the A- (aminoacyl) site of the ribosome, in which the second codon of the open reading frame (ORF) is located. Next, the translation factor eIF5A locates to the E- (exit) site to promote substrate positioning for peptide bond formation. Afterwards, the binding of eEF2-GTP to the A-site promotes the translocation of the tRNAs to the P- and E-sites. The deacetylated tRNA is released from the E-site and the next elongation cycle starts. Translation termination is mediated by the eukaryotic release factors (eRF) 1 and 3 and occurs when a stop codon enters the A-site of the ribosome (Hellen 2018). Ribosome recycling requires splitting of the 80S ribosome by the

ATP-binding cassette protein ABCE1 to release the 60S subunit (Hellen 2018). Overall, cap-dependent translation involves a plethora of different players, of which I only named a few. In the cell, it requires strict regulation to avoid dispensable energy-consumption.

1.5.1.1 Regulation of protein synthesis

The rate of protein synthesis is tightly controlled by signaling pathways that sense various internal and external signals (Roux and Topisirovic 2018). Two different control modes are conceivable: global control, in which the translation of most mRNAs in the cell is regulated, and mRNA-specific control, which results in modulation of translation of a subset of mRNAs, while global protein synthesis rates remain unaffected (Gebauer and Hentze 2004). Global mRNA translation needs to be adjusted during acute stress situations like starvation, for example. General control is achieved by changes in the phosphorylation status of initiation factors or their regulators (Gebauer and Hentze 2004). As mentioned above, eIF4E recognizes the m^7G cap at the 5'-end of the mRNA and is therefore required for the recruitment of ribosomes to the mRNA. eIF4E function can be inhibited by eIF4E-binding proteins (4E-BPs) (Pause et al. 1994). Extracellular cues, such as insulin, trigger phosphorylation of 4E-BPs, which results in release from eIF4E (Pause et al. 1994). The serine/threonine protein kinase mammalian target of rapamycin (mTOR), which is the central nutrient sensor, is responsible for the phosphorylation of 4E-BPs (Wang et al. 2000; Dobashi et al. 2011). Therefore, the availability of eIF4E can be adjusted according to nutrient availability to regulate global translation rates. Additionally, global control of protein synthesis can be achieved by phosphorylation of the α subunit of eIF2 at serine 51. GTP-bound eIF2 is part of the TC, which is required for translation initiation. Upon start codon recognition, GTP is hydrolyzed and eIF2-GDP is released from the TC. The guanine nucleotide exchange factor (GEF) eIF2B catalyzes the exchange of GDP for GTP on eIF2 (Sonenberg and Hinnebusch 2009). Various stress conditions are sensed by four eIF2α kinases, namely heme-regulated inhibitor (HRI), protein kinase R (PKR), PKR-like endoplasmic reticulum kinase (PERK), and general control non-derepressible 2 (GCN2) (Taniuchi et al. 2016). Their activation results in phosphorylation of eIF2α (P-eIF2α) and thereby initiates the integrated stress response (ISR): while global translation initiation is reduced, translation of specific mRNAs, which contain upstream open reading frames (uORFs) in their 5' untranslated region, like the activating transcription factor 4 (ATF4), is increased (Harding et al. 2000). Under normal conditions, uORFs inhibit translation of the respective mRNAs through ribosome dissociation and release. Upon stress, P-eIF2α competitively inhibits its GEF eIF2B, since the affinity of eIF2B to P-eIF2α is higher than

that to eIF2α-GDP (Rowlands et al. 1988). Thereby, P-eIF2α blocks GDP-GTP exchange and decreases the amount of active TC. Consequently, global translation initiation is reduced, whereas the likeliness of the scanning 40S ribosomal subunit to reach the ORF of uORF-containing mRNAs is increased (Hinnebusch 1993). Activation of ATF4 translation optimizes the cellular response to stress and thereby promotes survival under unfavorable conditions (Harding et al. 2003; Pakos-Zebrucka et al. 2016).

1.5.1.2 Translational control of cell fate decisions

Translational control is fundamental for normal development. During the transition of mouse embryos from the one-cell to the two-cell stage, for example, the abundance of most proteins is changed at least 2-fold (Latham et al. 1991). Of note, deregulation of translation can manifest in a variety of diseases, including neurodegeneration and cancer (Tahmasebi et al. 2018). For example, cancer progression in B cell lymphoma has been linked to increased cap-dependent mRNA translation caused by elevated levels of the proto-oncogene MYC. Strikingly, reduction of translation rates by decreased levels of the 60S ribosomal protein L24 suppressed MYC oncogenic activity and improved survival (Barna et al. 2008).

Moreover, the regulation of mRNA translation has previously been implicated in early cell fate transitions (Ingolia et al. 2011; Lu et al. 2009; Kristensen et al. 2013). Several studies in both embryonic and somatic stem cells demonstrate that global translation is suppressed in stem cells to retain an undifferentiated state and increased in progenitor cells (Sampath et al. 2008; Signer et al. 2014; Zismanov et al. 2016). HSCs display lower protein synthesis rates than restricted hematopoietic progenitors independent of the cell cycle status. Also, forcing HSCs to undergo self-renewing divisions does not increase protein synthesis (Signer et al. 2014). Blanco et al. (2016) showed that the activation of HFSCs during the transition from the resting phase telogen to differentiation in anagen during the hair cycle also coincides with an increase of translation. Further, this study confirms that protein synthesis rates do not correlate with proliferation. Strikingly, inhibition of translation by loss of NOP2/Sun RNA methyltransferase family member 2 (NSUN2) in the mouse blocks the differentiation of HFSCs to committed progenitor cells, resulting in cyclic alopecia due to a delay in the initiation of the growth phase anagen (Blanco et al. 2011). Also, in skeletal muscle stem cells global repression of translation by phosphorylation of eIF2α is required to maintain quiescence (Zismanov et al. 2016). The authors show that reduced phosphorylation results in differentiation, while pharmacological inhibition of eIF2α dephosphorylation enhances skeletal muscle stem cell

self-renewal. Overall, these data demonstrate a functional role of translation upregulation during differentiation and suggest that manipulation of translation influences cell fate decisions.

1.5.2 Protein quality control

Preserving protein homeostasis not only requires translational control, but also different protein quality control (PQC) mechanisms that ensure folding of nascent polypeptides and degradation of misfolded and unfolded proteins. In the following section I will highlight how protein folding is regulated and which control mechanisms become activated when protein folding goes awry.

Proper protein folding is achieved by a complex network of molecular chaperones. A molecular chaperone is defined as any protein that interacts with or stabilizes a non-native protein to acquire its final conformation but is not present in the functional structure (Hartl and Hayer-Hartl 2009). Some chaperones are also referred to as heat-shock proteins (HSPs), since they are upregulated upon heat stress, which increases the abundance of aggregation-prone folding intermediates (Hartl et al. 2011). During protein synthesis, HSP70 and HSP40 interact with the growing polypeptide, to allow co-translational formation of protein domains (Frydman et al. 1994). Subsequently, HSP60 mediates the folding of proteins to its native state (Langer et al. 1992). Of note, all proteins destined for the secretory pathway are directed to the endoplasmic reticulum (ER) for folding (Schröder and Kaufman 2005). Protein folding in the ER is based on the same principles as cytosolic protein folding; however, it additionally involves post-translational modifications like N-linked glycosylation, which is outlined in detail below (for further information see 1.6.2 The hexosamine pathway).

If the influx of nascent polypeptides exceeds the folding capacity of the ER, the accumulation of unfolded or misfolded proteins in the ER lumen activates the unfolded protein response (UPR) (Schröder and Kaufman 2005). Activation of the UPR, in turn, results in inhibition of protein synthesis and upregulation of chaperones (García-Prat et al. 2017). UPR signaling is mediated by three different branches: IRE1α (inositol requiring enzyme 1α), PERK, and ATF6 (activating transcription factor 6) (Walter and Ron 2011). IRE1α cleaves the mRNA encoding the transcription factor X-box binding protein 1 (Xbp1), generating spliced Xbp1 (Xbp1s), which enhances expression of chaperones and components involved in ER-associated degradation (ERAD) (Hetz et al. 2011). Upon activation of ERAD, terminally misfolded proteins are dislocated from the ER to the cytosol, where they are degraded by the ubiquitin-proteasome system (UPS) (Smith et al. 2011).

ATF6 is proteolytically processed to release its amino-terminal transcriptional activator domain, which translocates to the nucleus to activate transcription of UPR target genes (Gardner et al. 2013). PERK undergoes activating autophosphorylation and subsequently phosphorylates eIF2α on serine 51, which results in the reduction of general protein synthesis and enhanced translation of uORF containing mRNAs like ATF4 (Harding et al. 1999). Thus, PERK activation downstream of the UPR results in the initiation of the ISR (see also 1.5.1.1 Regulation of protein synthesis).

Degradation of misfolded proteins is mediated by the UPS or through autophagy (Vilchez et al. 2014b). The eukaryotic 26S proteasome is a large multi-subunit complex that degrades the majority of cellular proteins, which are marked for proteasomal degradation by the addition of one or more ubiquitin moieties (Budenholzer et al. 2017). Autophagy is a catabolic process, where intracellular components like fractions of the cytosol, organelles, or macromolecules are delivered to the lysosome for degradation (Vilchez et al. 2014a). The UPS and autophagy also play a pivotal role under physiological conditions, since these processes modulate protein levels during the cell cycle, for example, and recycle amino acids for protein synthesis.

1.5.2.1 Protein quality control in cell fate decisions

Importantly, all PQC mechanisms outlined in the previous section have been implicated in stem cell maintenance. Several studies suggest that stem cells display an elevated protein folding capacity: the levels of the HSP70 family members HSPA1A and HSPA1B are increased in ESCs compared to their more differentiated counterparts (Saretzki et al. 2004; Saretzki et al. 2008). Furthermore, HSCs have fewer misfolded and unfolded proteins than more differentiated progenitors (Hidalgo San Jose et al. 2020). Consistently, inhibition of HSP90 results in differentiation of ESCs, suggesting that protein folding is required for stem cell maintenance (Bradley et al. 2012). Moreover, ESCs exhibit elevated levels of the proteasome subunit PSMD11, enhanced assembly of the proteasome, and, correspondingly, increased proteasome activity compared to their more differentiated counterparts (Vilchez et al. 2012). Additionally, the proteasome subunit PSMD14 is required for ESC self-renewal and cellular reprogramming (Buckley et al. 2012). Also, enhancing proteasome activity in MSCs results in the maintenance of self-renewing capacity (Kapetanou et al. 2017). These data implicate the UPS and elevated proteasome activity in stem cell maintenance. Of note, the basal level of autophagy is upregulated upon early differentiation of ESCs (Tra et al. 2011). In adult somatic stem cells, however, autophagy is a key regulator of stem cell function (Chang 2020). Loss of autophagy in

HSCs results in accelerated differentiation and impaired self-renewal (Ho et al. 2017). Also, epidermal and dermal stem cells display high autophagic activity under physiological conditions (Salemi et al. 2012). Thus, autophagy might not be required for self-renewal in all types of stem cells but could mediate protection against cellular stress. When damaged proteins cannot be cleared by the UPS or through autophagy, they can be asymmetrically distributed during cell division: while one daughter cell inherits a healthy proteome and maintains stemness, the other daughter cell inherits the damaged proteins and is poised to differentiate (Moore et al. 2015). Overall, the maintenance of a healthy proteome is fundamental for stem cell function and tissue homeostasis. It is achieved by regulation of protein homeostasis at the levels of protein synthesis, folding, and degradation, or through the asymmetric distribution of damaged proteins to the daughter cells.

1.6 Cellular metabolism

Metabolic changes drive organismal aging and interventions that affect cellular metabolism, like dietary restriction, can extend lifespan in several model organisms (Chandel et al. 2016). Changes in nutritional conditions also significantly influence function and maintenance of stem cell populations (Jasper and Jones 2010). Here, I will focus on three different metabolic pathways: glycolysis, the hexosamine pathway, and the polyamine metabolism. These pathways, that have been described to become dysregulated with age, have been implicated in stemness before.

1.6.1 Glycolysis

Glycolysis is the first step in glucose metabolism (Figure 5). It occurs in the cytosol of all cells and involves the conversion of glucose to pyruvate, generating reduced nicotinamide adenine dinucleotide (NADH) and two molecules of adenosine 5'-triphosphate (ATP) per molecule glucose (Naifeh et al. 2020). Under aerobic conditions, pyruvate and NADH are shunted to the mitochondria, where pyruvate enters the tricarboxylic acid (TCA) cycle and generates more NADH and reduced flavin adenine dinucleotide ($FADH_2$) (Melkonian and Schury 2020). These reducing equivalents are oxidized by the electron transport chain (ETC), which uses oxygen as final electron acceptor to form water and generates a proton gradient across the inner mitochondrial membrane. Finally, this proton gradient is used to produce ATP in a process called oxidative phosphorylation (OXPHOS) (Montoya et al. 2009). Instead, under anaerobic conditions, lactate dehydrogenase (LDH) converts

pyruvate to lactate and regenerates NAD^+ from NADH, since OXPHOS, which requires oxygen as a final electron acceptor, is unavailable (Melkonian and Schury 2020).

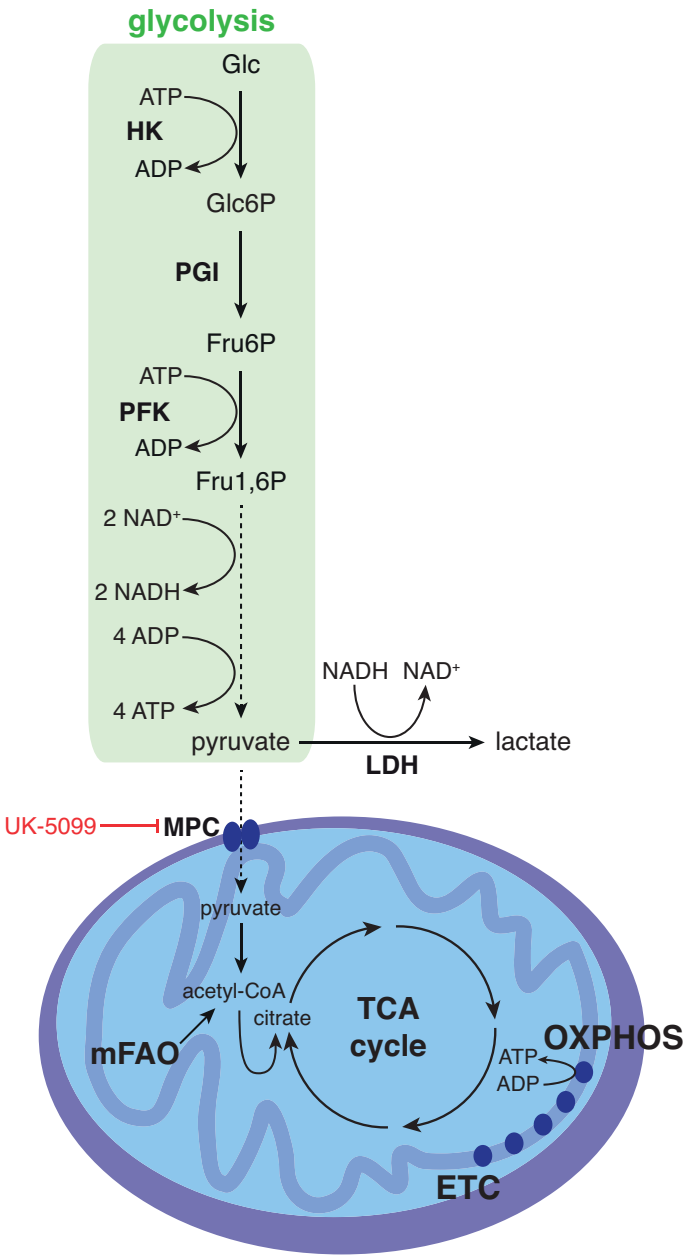

Figure 5: Schematic representation of glycolysis, TCA cycle, and OXPHOS. The conversion of glucose (Glc) to pyruvate generates 2 ATP and 2 NADH per molecule glucose. Under aerobic conditions, pyruvate is transported into mitochondria via mitochondrial pyruvate carrier (MPC), which can be inhibited by UK-5099. The tricarboxylic acid (TCA) cycle generates more reducing equivalents, which are oxidized by the electron transport chain (ETC). The proton gradient, which is established by the ETC, is used to generate ATP during oxidative phosphorylation (OXPHOS). Under anaerobic conditions, lactate dehydrogenase (LDH) produces lactate from pyruvate and recovers NAD^+. HK: hexokinase, PGI: phosphoglucoisomerase, PFK: phosphofructokinase, Glc6P: glucose-6-phophate, Frc6P: fructose-6-phophate, Frc1,6P: fructose-1,6-bisphosphate.

In the 1950s, Otto Warburg observed that cancer cells use glycolysis for energy production, even when there was sufficient oxygen present to perform OXPHOS. This

became known as the Warburg effect (Warburg 1956). Thus, the Warburg effect, or aerobic glycolysis, refers to a condition in which glucose is converted to lactate in the presence of oxygen (Naifeh et al. 2020). Although its efficiency of energy production is relatively low, glycolysis can produce sufficient ATP for rapid cell proliferation (Ishida et al. 2020). Moreover, it is essential for the biosynthesis of nucleotides, amino acids, and lipids in proliferating cells (Vander Heiden et al. 2009). Thus, it is not surprising that numerous studies demonstrate that not only cancer cells, but also stem cells and induced pluripotent stem cells (iPSCs) have an elevated dependence on aerobic glycolysis compared to differentiated cell types (Zhang et al. 2012b). Especially HSCs in their hypoxic niche have been well described to rely on glycolysis for energy production, while OXPHOS is activated upon differentiation (Simsek et al. 2010). This glycolytic phenotype is also characteristic of ESCs (Kondoh et al. 2007), MSCs (Chen et al. 2008), and hepatic stem cells (Turner et al. 2008). Recently, metabolomic analysis of HFSCs relative to the entire epidermis revealed that also HFSCs have higher levels of glycolysis intermediates, suggesting the dependence of HFSCs on glycolytic metabolism (Flores et al. 2017). Strikingly, glycolytic ESCs have spherical and cristae-poor mitochondria, which are randomly distributed in the cell and do not form a mitochondrial network (Chung et al. 2007). Such mitochondrial infrastructure is also characteristic of HSCs (Piccoli et al. 2005) and MSCs (Chen et al. 2008) and may represent a marker of stemness (Folmes et al. 2012). At the onset of differentiation, ESCs and MSCs increase mtDNA replication to ensure mitochondrial biogenesis (Cho et al. 2006; Chen et al. 2008).

Besides glucose, mannose has also been described to readily enter glycolysis and the TCA cycle (Slade et al. 2016). Mannose is an important precursor for N-linked glycosylation, which is one of the most common protein modifications and is required for glycoprotein folding and function (Cherepanova et al. 2016). Upon entry of the cell via hexose transporters, mannose (Man) is phosphorylated by hexokinase (HK) to produce mannose-6-phosphate (Man6P), which serves as a substrate for two major enzymes (Figure 6): phosphomannomutase 2 (PMM2) and phosphomannose isomerase (MPI) (Sharma et al. 2014). PMM2 converts Man6P to mannose-1-phosphate (Man1P), which is needed to produce the glycosylation intermediates GDP-mannose (GDP-Man) and dolichol-phosphate-mannose (Dol-P-Man) (Andreotti et al. 2013). These intermediates contribute to N-linked glycosylation, *O*-mannosylation, *C*-mannosylation, and glycophosphotidylinositol (GPI) anchors (Sharma et al. 2014). MPI isomerizes Man6P to fructose-6-phosphate (Frc6P) (Gracy and Noltmann 1968). Thereby, MPI effectively connects N-linked glycosylation with energy metabolism (Shtraizent et al. 2017). Also,

Frc6P is used in the hexosamine pathway (HP), which is described in detail below (for further information see 1.6.2 The hexosamine pathway).

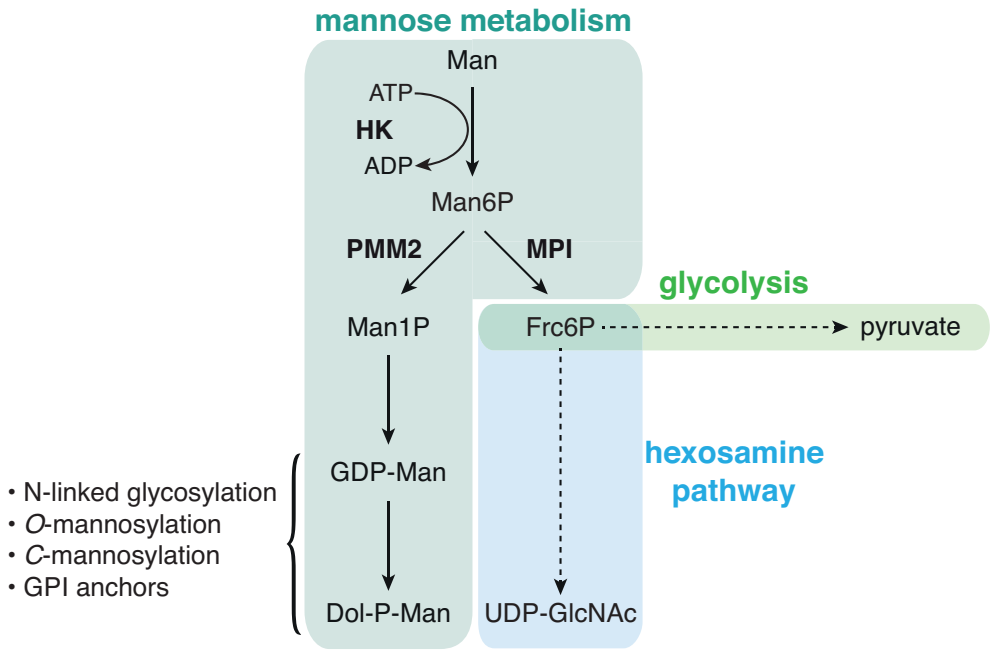

Figure 6: Schematic representation of mannose metabolism. Mannose (Man) is phosphorylated by hexokinase (HK) to form mannose-6-phosphate (Man6P), which is either converted to mannose-1-phophate (Man1P) by phosphomannomutase 2 (PMM2) or to fructose-6-phosphate (Frc6P) by phosphomannose isomerase (MPI). Mannose metabolism is shown in teal. Frc6P fuels glycolysis (green) and the hexosamine pathway (light blue).

1.6.1.1 Sweet control of cell fate decisions

Glucose metabolism has been related to stem cell fate decisions previously. Stemness of pluripotent stem cells can be enhanced by elevation of glycolysis through hypoxia (Ezashi et al. 2005), or inhibition of the mitochondrial respiratory chain (Varum et al. 2009). A study in intestinal stem cells (ISCs) has shown that the limitation of mitochondrial pyruvate metabolism is necessary and sufficient to maintain the ISC compartment (Schell et al. 2017). Folmes et al. (2011) demonstrated that reprogramming of somatic cells to iPSCs caused mitochondrial regression, electron transport chain downregulation, and upregulation of glycolytic enzymes. Moreover, the authors found that inhibiting glycolysis or enhancing pyruvate entry in the TCA cycle reduced reprogramming efficiency (Folmes et al. 2011). Consistently, enhancing glycolytic flux improves reprogramming efficiency: small molecule-mediated activation of 3'-phosphoinositide-dependent kinase 1 (PDPK1), which results in the elevated expression of glycolytic genes, as well as hypoxia, increase reprogramming efficiency (Zhu et al. 2010; Yoshida et al. 2009). Furthermore, treatment of HSCs with a pyruvate dehydrogenase kinase (PDK) mimetic, which leads to

suppression of the influx of glycolytic metabolites into mitochondria, enhanced stem cell capacity, whereas loss of PDK2 and PDK4 attenuates HSC quiescence (Takubo et al. 2013).

Apart from ATP synthesis, glycolysis also ensures a steady supply with acetyl-coenzyme A (acetyl-CoA), which is a cofactor for histone acetylation. Strikingly, inhibition of glycolysis in ESCs causes histone deacetylation and subsequently loss of pluripotency (Moussaieff et al. 2015). Consistently, another study demonstrates that inhibition of histone deacetylases (HDACs) promotes ESC self-renewal (Ware et al. 2009). In addition to glycolysis, mitochondrial fatty acid oxidation (mFAO) generates acetyl-CoA through the breakdown of fatty acid molecules in the mitochondrial matrix (Figure 5) (Ito and Ito 2016). Peroxisome proliferator-activated receptor δ (PPAR-δ) positively regulates the rate-limiting enzyme of mFAO. Of note, loss of PPAR-δ or inhibition of mFAO induces reduction of the HSC pool by the symmetric commitment of daughter cells (Ito et al. 2012). Thus, HSCs, like ESCs, might require high acetyl-CoA levels to ensure histone acetylation and self-renewal. These studies demonstrate that metabolism, epigenetics, and cell fate are tightly connected. Overall, there is evidence that metabolic changes are not only a consequence of the stem cell state but can influence cell fate decisions (Wei et al. 2018).

1.6.2 The hexosamine pathway

The hexosamine pathway (HP) is an anabolic pathway that converts the glycolysis intermediate fructose-6-phosphate (Frc6P) to uridine 5'-diphospho-*N*-acetyl-D-glucosamine (UDP-GlcNAc) in four consecutive enzymatic reactions (Figure 7), using around 2-3 % of intracellular glucose (Marshall et al. 1991). The first and rate-limiting step is catalyzed by glutamine fructose-6-phosphate amidotransferase (GFAT), which uses L-glutamine (Gln) as nitrogen donor to convert Frc6P to D-glucosamine-6-phosphate (GlcN6P) (Ghosh et al. 1960). In the second reaction, D-glucosamine-6-phosphate-*N*-acetyltransferase (GNA1) converts GlcN6P to *N*-acetyl-D-glucosamine-6-phosphate (GlcNAc6P) in an acetyl-CoA dependent reaction (Wang et al. 2008). Subsequently, GlcNAc6P is isomerized to *N*-acetyl-D-glucosamine-1-phosphate (GlcNAc1P) by phosphoglucomutase (PGM3) (Ricciardiello et al. 2018). In the last enzymatic step, UDP-*N*-acetylglucosamine pyrophosphorylase (UAP1) uses uridine-5'-triphosphate (UTP) to form UDP-GlcNAc from GlcNAc1P (Mio et al. 1998). Overall, the HP is well-positioned to function as a nutrient sensor, since its end-product UDP-GlcNAc is a high energy compound that requires carbohydrate, amino acid, lipid, and nucleotide donors for its synthesis (Wells et al. 2003).

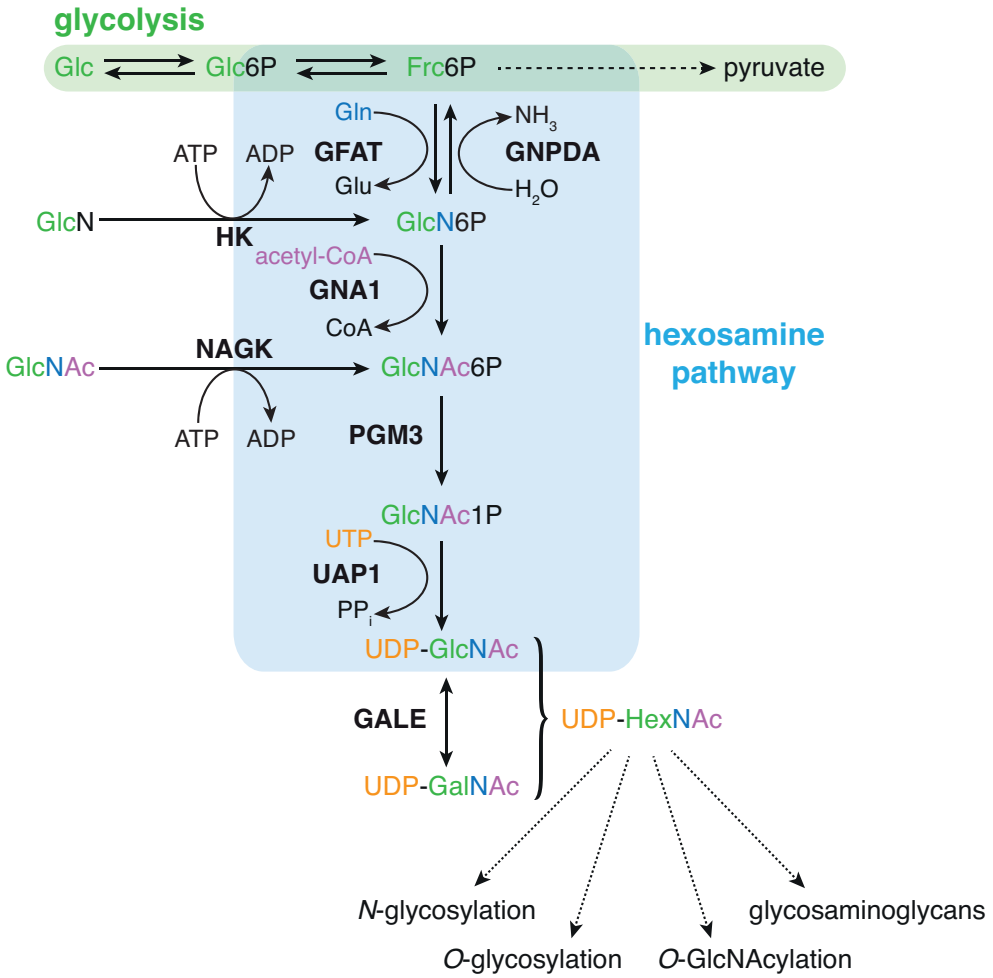

Figure 7: Schematic representation of the hexosamine pathway and its versatile outputs. Synthesis of UDP-GlcNAc requires carbohydrate (green), amino acid (blue), lipid (purple), and nucleotide (orange) donors for its synthesis. Glycolysis is depicted in green, the hexosamine pathway is shown in light blue. The combination of UDP-GlcNAc and UDP-GalNAc is referred to as UDP-HexNAc. GFAT: glutamine fructose-6-phosphate amidotransferase, GNPDA: D-glucosamine-6-phosphate deaminase, HK: hexokinase, GNA1: D-glucosamine-6-phosphate-*N*-acetyltransferase, NAGK: *N*-acetyl-D-glucosamine kinase, PGM3: phosphoglucomutase, UAP1: UDP-*N*-acetylglucosamine pyrophosphorylase, GALE: UDP-galactose-4'-epimerase.

UDP-GlcNAc can be converted to its epimer uridine 5'-diphospho-*N*-acetyl-D-galactosamine (UDP-GalNAc) by UDP-galactose-4'-epimerase (GALE) in a reversible reaction (Thoden et al. 2001; Schulz et al. 2004). Both acetylated aminosugars are essential precursors for biopolymer synthesis and for at least three types of glycosylation reactions (Figure 7). First, N-linked glycosylation is one of the most common protein modifications in eukaryotic cells and occurs on secreted or membrane-associated proteins in the ER (Cherepanova et al. 2016). It can be divided in two distinct processes: the assembly of a lipid-linked oligosaccharide at the ER membrane and the transfer of this core oligosaccharide from the lipid anchor to selected asparagine residues of nascent proteins (Burda and Aebi 1999). UDP-GlcNAc is required for the first two reactions in the assembly of the core oligosaccharide (Yoo et al. 2018; Bickel et al. 2005). After addition

to nascent proteins, the core oligosaccharide undergoes extensive modifications, which reflect different functions in glycoprotein folding, quality control, degradation, and secretion (Helenius and Aebi 2004). Also, N-linked glycosylation is pivotal for glycoprotein function. Second, mucin-type *O*-glycosylation of proteins occurs in the Golgi apparatus in a stepwise manner. In the initial step, the GalNAc moiety from UDP-GalNAc is α-linked to the hydroxyl group of serine or threonine residues (Julenius et al. 2005). Mucin-type *O*-glycosylation influences protein conformation and is involved in cell adhesion, cell-cell and cell-matrix interactions (Hanisch 2001). Additionally, this modification protects proteins against proteolytic cleavage and thereby increases protein stability (Kozarsky et al. 1988). Third, *O*-GlcNAcylation is the attachment of a single GlcNAc moiety to the hydroxyl group of serine or threonine residues. *O*-GlcNAc transferase (OGT) is the sole enzyme that catalyzes the β-linkage of GlcNAc derived from UDP-GlcNAc to target proteins and only *O*-GlcNAcase (OGA) can remove the *O*-GlcNAc modification (Haltiwanger et al. 1992; Dong and Hart 1994). *O*-GlcNAcylation is often reciprocal to phosphorylation, which also occurs on serine or threonine residues (van der Laarse et al. 2018). Modification by *O*-GlcNAc plays a role in a plethora of cellular functions, such as chromatin remodeling, gene transcription, proliferation, apoptosis, and proteasomal degradation, and can regulate the function, localization, and stability of target proteins (Love and Hanover 2005; Boyce et al. 2011). In addition to glycosylation reactions, UDP-GlcNAc and UDP-GalNAc are required for the synthesis of glycosaminoglycans (GAGs), which are described in detail above (for further information see 1.4.1 The extracellular matrix).

1.6.2.1 Glutamine fructose-6-phosphate amidotransferase

As mentioned above, GFAT catalyzes the first and rate-limiting step of the HP (Figure 7). GFAT consists of two domains: the glutaminase domain hydrolyzes Gln to L-glutamate (Glu) and releases ammonia, and the isomerase/transferase domain, which first converts Frc6P to glucose-6-phosphate (Glc6P) and subsequently transfers ammonia to Glc6P, resulting in the formation of GlcN6P (Denisot et al. 1991; Ruegenberg et al. 2020). Ammonia is transferred via an ammonia channel, which is formed upon substrate binding and connects the two active sites (Mouilleron et al. 2006). In mice and human, two paralogs of GFAT are expressed: GFAT1 and GFAT2. They share around 75 % identity at the amino acid level; however, their tissue distribution differs (Oki et al. 1999). Since GFAT2 was found to be mainly expressed in the nervous system and thus, might exert tissue-specific functions, I will focus on GFAT1, which is described to be expressed ubiquitously (Oki et al. 1999). GFAT1 is essential since a full body knockout in mice results

in embryonic lethality (Issop et al. 2018). Two splice-variants of GFAT1 are expressed: a short (GFAT1) and a long isoform (GFAT1-L). Human GFAT1-L contains a 54 bp insertion at amino acid position 299 and is predominantly expressed in skeletal muscle and heart (DeHaven et al. 2001; Niimi et al. 2001). GFAT1 can be feedback inhibited by its product GlcN6P, as well as the end-product of the HP UDP-GlcNAc (Kornfeld 1967; Broschat et al. 2002; Assrir et al. 2014). Remarkably, the UDP-GlcNAc epimer UDP-GalNAc, which differs only in the orientation of the hydroxyl group at C4 of the sugar ring, inhibits GFAT1 at much higher doses compared to UDP-GlcNAc, and thus, is only a weak inhibitor (Broschat et al. 2002; Ruegenberg et al. 2020). The activity of GFAT1 can also be modulated by phosphorylation through AMP-activated protein kinase (AMPK) and calcium/calmodulin-dependent protein kinase II (CaMKII) at serine 243 and cAMP-dependent protein kinase (PKA) at serine 205 and serine 235 (Li et al. 2007; Eguchi et al. 2009; Zhou et al. 1998; Chang et al. 2000). However, the consequences of phosphorylation on GFAT1 activity are poorly understood and appear to depend on the cellular context, as well as isoform expression.

1.6.2.2 Hexosamine pathway activation

Activation of the HP results in elevated UDP-GlcNAc levels and can be achieved by different means. As mentioned above, the HP uses 2-3 % of cellular glucose (Marshall et al. 1991). Changing intracellular glucose concentration affects the flux through the HP: while glucose deprivation reduces UDP-GlcNAc levels, the addition of extracellular glucose is sufficient to increase HP activity (Nakajima et al. 2010; Abdel Rahman et al. 2013; Marshall et al. 2004). Interestingly, D-glucosamine (GlcN) has been described to activate the HP more potently than glucose (Marshall et al. 2004). GlcN is phosphorylated by hexokinase (HK) and enters the HP as GlcN6P (Figure 7). Hence, GlcN bypasses the rate-limiting step catalyzed by GFAT1, which is also sensitive to UDP-GlcNAc feedback inhibition, and thus, can be converted to UDP-GlcNAc more efficiently. Also, *N*-acetyl-D-glucosamine (GlcNAc) addition has been shown to activate the HP in cells, worms, and mice (Sasai et al. 2002; Abdel Rahman et al. 2013; Denzel et al. 2014; Ryczko et al. 2016; Horn et al. 2020). GlcNAc is converted to GlcNAc6P by *N*-acetyl-D-glucosamine kinase (NAGK), which requires ATP (Figure 7) (Weihofen et al. 2006). Additionally, NAGK catalyzes GlcNAc salvage from lysosomally degraded glycoconjugates or upon OGA-mediated removal of the *O*-linked GlcNAc moiety from proteins (Weihofen et al. 2006; Gloster et al. 2011). In contrast to GlcN addition, GlcNAc supplementation does not affect intracellular acetyl-CoA levels, however, both require ATP to enter the HP (Marshall

et al. 2004; Abdel Rahman et al. 2013). In this study, I will use GlcNAc supplementation, since GlcNAc has been suggested to activate the HP more efficiently than GlcN (Grigorian et al. 2007).

As mentioned above, GFAT1 is the rate-limiting enzyme of the HP. Consistently, several studies have shown that GFAT1 overexpression (OE) elevates HP flux. In cells, GFAT1 OE enhances UDP-GlcNAc production (Crook et al. 2000; Weigert et al. 2001). Also, OE in skeletal muscle and adipose tissue, in the liver, or in the heart of transgenic mice increases GFAT1 activity, UDP-GlcNAc level, and *O*-GlcNAcylation, respectively (Hebert et al. 1996; Veerababu et al. 2000; Tran et al. 2020). In this study, I use transgenic mice, which ubiquitously overexpress human GFAT1 (Horn et al. 2020). Finally, HP flux can be increased by point mutations in *GFAT1*. Denzel et al. (2014) identified three different gain-of-function mutations using a forward genetic approach in *Caenorhabditis elegans* (*C. elegans*). In this study, I will focus on the G451E substitution (dh785 in *C. elegans*), which has been recently shown to drastically reduce the sensitivity of GFAT1 to UDP-GlcNAc feedback inhibition (Ruegenberg et al. 2020). Consistently, UDP-GlcNAc levels are increased in a mouse neuroblastoma cell line (N2a cells) carrying this gain-of-function mutation (Horn et al. 2020; Ruegenberg et al. 2020). Here, I will use mice, which ubiquitously overexpress human GFAT1 G451E. Taken together, HP flux can be modulated by precursor availability, as well as GFAT1 abundance and activity.

1.6.2.3 Effects of hexosamine pathway activation

HP activation has been shown to confer resistance to aggregation-prone proteins by improving PQC mechanisms and to extend lifespan in the nematode *C. elegans* (Denzel et al. 2014). Also, GlcN feeding to aged mice increases their life expectancy (Weimer et al. 2014). Furthermore, HP activation ameliorates proteotoxicity in mammalian cells through modulation of the ISR (Horn et al. 2020). Thus, HP activation increases PQC pathways in different model organisms, likely by inducing the ISR downstream of PERK-mediated eIF2α phosphorylation. Strikingly, Wang et al. (2014) demonstrated that UPR induction upon ischemia/reperfusion triggers *GFAT1* expression and, as a consequence, elevates *O*-GlcNAcylation in the heart, conferring cardioprotection. Furthermore, the authors suggested HP activation as a general response to UPR induction, since it was observed using a variety of different stressors. Thus, ER stress can activate the HP to ensure cell survival via increased glycosylation reactions. Taken together, these findings suggest that the HP and PQC pathways are tightly connected. The HP functions as a nutrient sensor, and thus, is optimally positioned to regulate protein

turnover according to nutrient availability. As mentioned above, stem cells rely on proper protein folding and degradation to maintain self-renewal. Therefore, HP activation might have beneficial effects on stem cell maintenance by improving PQC mechanisms.
Additionally, HP activation has been shown to modulate HA content. HA synthesis is controlled by substrate availability: limiting UDP-GlcUA or UDP-GlcNAc reduces HA synthesis and an increase in one UDP-sugar is sufficient to elevate HA synthesis (Kultti et al. 2009; Vigetti et al. 2006; Jokela et al. 2008). Accordingly, several studies showed increased HA content upon GlcN supplementation (Jokela et al. 2008; Jokela et al. 2011; Vigetti et al. 2012). Interestingly, HAS2 is *O*-GlcNAcylated on serine 221, which increases its activity and stability (Vigetti et al. 2012). Hence, HP activation modulates HA content by increased UDP-GlcNAc availability and *O*-GlcNAc-mediated stabilization of HAS2. Elevated HA synthesis, in turn, changes ECM composition. Thus, HP activation might improve stem cell maintenance through effects on the stem cell niche.

1.6.2.4 The hexosamine pathway in cell fate decisions

The HP has been suggested to mediate the crosstalk between the metabolic state, cellular signaling, and epigenetic regulation of cell fate (Sun et al. 2016). Furthermore, the activity of the pluripotency factors Oct4 and Sox2 depends on their *O*-GlcNAc modification, which clearly demonstrates that the HP is important for stem cell self-renewal (Jang et al. 2012). Accordingly, the elevation of *O*-GlcNAcylation improves stem cell maintenance. For example, HP activation through GlcN supplementation favors mouse ESC self-renewal (Jang et al. 2012; Jeon et al. 2014). Also, inhibition of OGA impairs differentiation of mouse ESCs into neuronal progenitors and during embryonic body formation, as well as differentiation of human ESCs into cardiomyocyte precursors (Speakman et al. 2014; Jang et al. 2012; Kim et al. 2009). In turn, reduction of global *O*-GlcNAc levels favors a more differentiated state: knockdown of OGT, inhibition of OGT, or inhibition of GFAT1 impairs self-renewal, accelerates the differentiation of human ESCs along the neuronal lineage, or elevates differentiation of human ESCs into cardiomyocyte precursors, respectively (Jang et al. 2012; Andres et al. 2017; Kim et al. 2009). Moreover, reprogramming of mouse embryonic fibroblasts into iPSCs is modulated by *O*-GlcNAcylation levels: overexpression of OGT enhances reprogramming efficiency, while low-glucose culture medium dampens cellular reprogramming (Jang et al. 2012). Thus, activation of the hexosamine pathway favors the stem cell fate through elevated *O*-GlcNAcylation. However, whether HP activation affects cell fate by improved protein quality control or by changes in ECM composition remains elusive.

1.6.3 The polyamine metabolism

Polyamines are polycations that are essential for cell growth and can bind to a variety of negatively charged cellular molecules, including nucleic acids (Dever and Ivanov 2018). Polyamine homeostasis is critical to cell survival and is achieved by regulation at different levels of their synthesis, degradation, uptake and excretion (Wallace et al. 2003).

The first and rate-limiting step in the polyamine metabolism (Figure 8) is the synthesis of putrescine from ornithine, which is catalyzed by ornithine decarboxylase (ODC). Subsequently, spermidine is synthesized from putrescine, and spermine from spermidine, by transfer of the aminopropyl moiety of decarboxylated *S*-adenosylmethionine (dcSAM), which is generated from SAM by adenosylmethionine decarboxylase (AMD1) (Igarashi and Kashiwagi 2010). During polyamine catabolism, spermidine/spermine *N*1-acetyltransferase (SSAT) acetylates spermidine and spermine using acetyl-CoA to form *N*1-acetylspermidine (*N*1-AcSpd) and *N*1-acetylspermine (*N*1-AcSpm), respectively (Figure 8). These acetylated intermediate products are the major polyamines exported from the cell (Seiler and Dezeure 1990). *N*1-AcSpd and *N*1-AcSpm can be converted back to putrescine and spermidine, respectively, by the FAD-dependent polyamine oxidase (PAOX) (Wallace et al. 2003). The control of polyamine biosynthesis is mainly achieved via control of ODC levels through a feedback mechanism. High polyamine levels enhance synthesis and stability of ODC antizyme (OAZ), which targets ODC for ubiquitin-independent proteasomal degradation (Fong et al. 1976; Heller et al. 1976; Palanimurugan et al. 2004).

Interestingly, up to 15 % of polyamines are stably associated with ribosomes in *Escherichia coli* (*E. coli*), which established their importance for protein synthesis (Cohen and Lichtenstein 1960). Polyamines were also described to be associated with the tRNA of *E. coli* (Cohen et al. 1969). The fidelity of polypeptide synthesis in a cell-free system is increased by polyamines via enhanced binding of aminoacyl-tRNAs to the ribosome (Igarashi et al. 1982). Furthermore, the assembly of the 30S ribosomal subunits is stimulated by polyamines through enhanced methylation of two adjacent adenine residues near the 3'-end of 16S rRNA (Echandi and Algranati 1975; Igarashi et al. 1980). Additionally, the polyamine spermidine is converted to the amino acid hypusine (Park et al. 1981), which is used to post-translationally modify the elongation factor eIF5A (Cooper et al. 1983). This modification occurs on lysine 50 of eIF5A in a two-step process: deoxyhypusine synthase transfers the aminobutyl moiety of spermidine to the lysine residue, forming deoxyhypusine, which can then be hydrolyzed by deoxyhypusine hydroxylase to form hypusine (Park et al. 1982; Abbruzzese et al. 1986). Hypusination of

eIF5A is critical for translation elongation, especially for difficult substrates like polyproline stretches (Saini et al. 2009; Gutierrez et al. 2013).

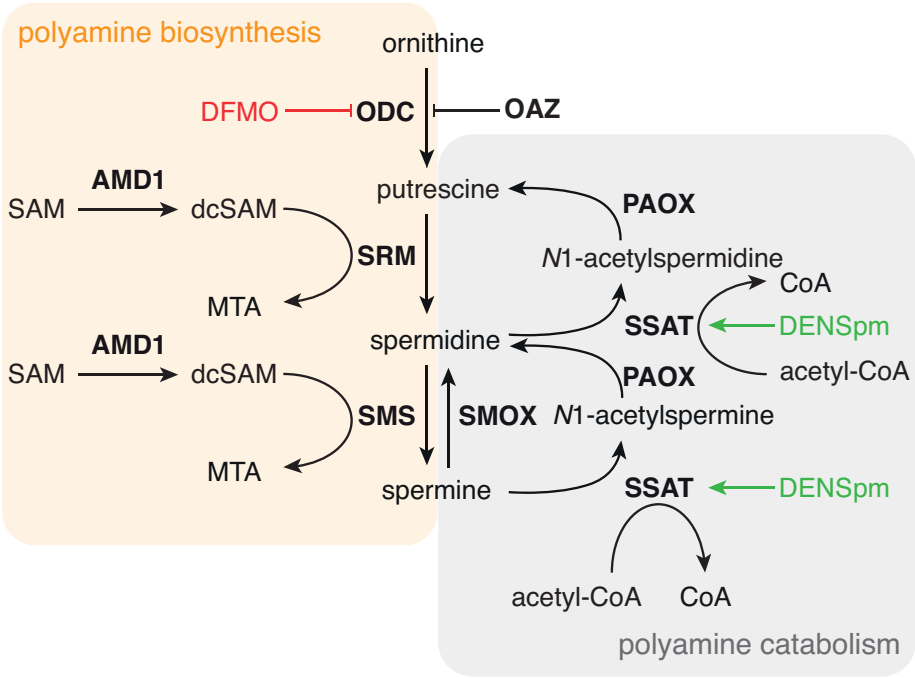

Figure 8: Schematic representation of the polyamine metabolism. The natural polyamines putrescine, spermidine, and spermine are required for protein synthesis. Polyamine biosynthesis (orange) can be inhibited using 2-difluoromethylornithine (DFMO), while polyamine catabolism (gray) can be activated by *N*1,*N*11-diethylnorspermine (DENSpm). dcSAM: decarboxylated SAM, MTA: 5'-mehylthioadenosine, SAM: *S*-adenosylmethionine, AMD1: adenosylmethionine decarboxylase 1, OAZ: ODC antizyme, ODC: ornithine decarboxylase, PAOX: polyamine oxidase, SMS: spermine synthase, SMOX: spermine oxidase, SRM: spermidine synthase, SSAT: spermidine/spermine *N*1-acetyltransferase.

Apart from their function in translation, polyamines have also been implicated in the regulation of ion channels. Inward rectifier potassium channels, for example, play a pivotal role in the maintenance of the resting potential of cell membranes and potassium homeostasis (Williams 1997). Spermine and spermidine act as high-affinity blockers being effective at nanomolar concentrations (Ficker et al. 1994). Furthermore, polyamines influence cell-cell interactions through the regulation of E-cadherin (Liu et al. 2009) and Toll-like receptor 2 (Chen et al. 2007). Cytoskeleton dynamics are controlled by polyamines via the activation of the small RhoGTPases RhoA and Rac1 (Bueb et al. 1992; Ray et al. 2003; Mäkitie et al. 2009) and alterations in the microtubule network (Mechulam et al. 2009). Polyamines promote gap junction communication between proliferating cells by promoting dynamical microtubule plus ends at the cell periphery, and thus, allow polyamine exchange between cells (Desforges et al. 2013). Intercellular polyamine exchange can thereby regulate proliferation in a multicellular system (Hamon et al. 2016).

Importantly, the polyamine spermidine is described to alleviate aging and aging-associated diseases. Spermidine supplementation induces autophagy and promotes longevity (Eisenberg et al. 2009; Morselli et al. 2009). Additionally, increased autophagy by spermidine addition is also sufficient to reverse immune cell senescence (Zhang et al. 2019). Cardiovascular dysfunction can also be attenuated by spermidine treatment through the activation of mitochondrial biogenesis (Wang et al. 2020). Furthermore, increased spermidine levels are required for IIS-mediated longevity in the fly (Tain et al. 2019).

1.6.3.1 Targeting the polyamine metabolism

Since polyamines are required for cell growth, targeting polyamine biosynthesis is an attractive cancer therapy. Additionally, ODC is a transcriptional target of the MYC oncogene (Bello-Fernandez et al. 1993). Therefore, overexpression of MYC, which is often described in cancer, can promote dysregulation of the polyamine metabolism as seen in many cancer types like leukemia, neuroblastoma and breast cancer (Funakoshi-Tago et al. 2013; Koomoa et al. 2013; Ozfiliz et al. 2015). ODC activity can be potently inhibited by 2-difluoromethylornithine (DFMO), which is enzyme-activated and irreversibly binding (Metcalf et al. 1978). Consequently, DFMO was used in clinical trials; however, there was no significant clinical response observed (Abeloff et al. 1984; Horn et al. 1987). Due to the poor success of DFMO, polyamine analogs, which should interrupt polyamine biosynthesis and compete for uptake, were synthesized (Damiani and Wallace 2018). These analogs increase polyamine catabolism by activation of SSAT, and thereby deplete intracellular polyamine pools and inhibit growth (Porter et al. 1991). Clinical trials were conducted using the spermine analog *N*1,*N*11-diethylnorspermine (DENSpm). However, no evidence for disease response was detected (Hahm et al. 2002; Wolff et al. 2003).

1.6.3.2 The polyamine metabolism in cell fate decisions

Given that increased polyamine levels positively regulate translation and that high translation rates promote stem cell differentiation, it is surprising that previous studies have implicated high polyamine levels in stem cell maintenance. For example, polyamines positively influence the expression of MINDY1, a deubiquitinating enzyme, which promotes ESC self-renewal (James et al. 2018). Additionally, forced overexpression of AMD1 or ODC in ESCs results in a delay in differentiation upon removal of LIF and can also improve cellular reprogramming (Zhang et al. 2012a; Zhao et al. 2012). Strikingly, reduced polyamine levels were described to cause uterine quiescence, which was shown by the

entry of blastocysts into embryonic diapause (Fenelon and Murphy 2017). This finding clearly highlights the importance of high polyamine levels in stem cell function. Consistently, the differentiation of human bone marrow-derived MSCs coincides with decreased polyamine levels (Tsai et al. 2015). Overall, these data suggest that changes in polyamine levels can affect cell fate decisions. However, the mechanism underlying polyamine-mediated changes in cell fate decisions are poorly understood. Also, the link between polyamines and translation in the regulation of cell fate decisions remains obscure.

1.7 Aims of this study

Aging is the main risk factor for the manifestation of numerous serious diseases, including cancer, cardiovascular diseases and neurodegenerative disorders. Thus, the growing proportion of elderly people in the global population poses a major challenge to the health care systems around the world. Maintaining tissue homeostasis with age is key to prolong healthspan and requires retention of adult somatic stem cell function. Therefore, it is of utmost importance to identify stem cell fate determinants to be able to delay stem cell exhaustion in the elderly. Hair follicle stem cells (HFSCs) represent an ideal model to study adult somatic stem cell fate, since they fuel cyclical rounds of hair follicle growth *in vivo*, and thus, continuously undergo fate decisions. Furthermore, the 3D-3C organoid culture system allows for easy manipulation of HFSCs and investigation of the resulting cell fate changes.

It has been well described that changes in nutritional conditions drive organismal aging and that interventions that affect cellular metabolism, like dietary restriction, can extend lifespan. Importantly, metabolic changes also significantly influence function and maintenance of stem cell populations. However, whether manipulation of metabolism can influence cell fate decisions and thereby improve stem cell maintenance remains poorly understood. Here, I will focus on three different metabolic pathways that have been described to become dysregulated with age and have been linked to the regulation of stemness before: hexosamine biosynthesis, aerobic sugar metabolism, and the polyamine metabolism. I aim to understand on a molecular level, how these three pathways and their versatile outputs modulate stem cell fate. Therefore, I manipulate HFSC metabolism by different approaches and investigate the resulting cell fate decisions to address three specific research questions:

Aim 1: Does hexosamine pathway activation affect hair follicle stem cell fate, potentially via modulation of the extracellular matrix?

Aim 2: Does the modulation of intracellular sugar levels improve hair follicle stem cell maintenance?

Aim 3: Does polyamine availability regulate hair follicle stem cell fate through mRNA translation or other mechanisms?

2 Results

The decline of adult somatic stem cell function leads to deterioration of tissue homeostasis and regeneration, which is one of the most obvious characteristics of the aging process and the basis for many age-associated diseases (López-Otín et al. 2013; Signer and Morrison 2013). Thus, the identification of cell fate determinants is of utmost importance to delay stem cell exhaustion, thereby to improve tissue function, and ultimately, to prolong healthspan (Figure 9). In my study, I focus on three different metabolic pathways that show decreased activity during the aging process and have been linked to stemness previously: the hexosamine pathway (HP), aerobic sugar metabolism, and polyamine metabolism (Denzel et al. 2014; Goyal et al. 2017; Ravera et al. 2019; Vivó et al. 2001; Nishimura et al. 2006). As shown in the project outline, I asked whether manipulation of these pathways can influence cell fate decisions (Figure 9):

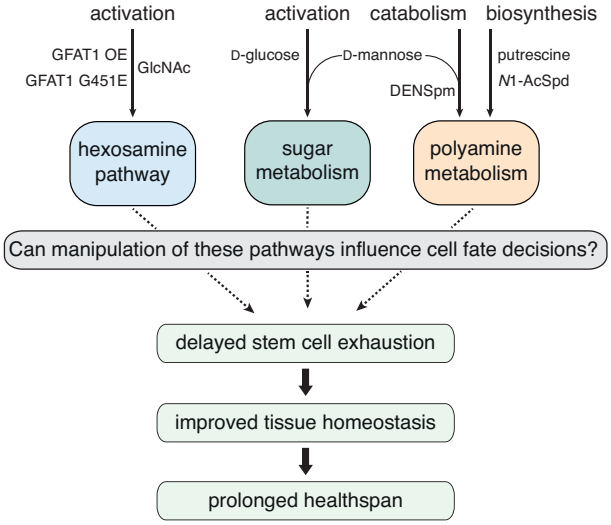

Figure 9: Project outline. Different metabolic pathways that are dysregulated during the aging process were manipulated with the aim to identify determinants of adult somatic stem cell fate that might ultimately help to delay stem cell exhaustion, to improve tissue homeostasis, and to prolong healthspan in the growing population of elderly people.

Hair follicle stem cells (HFSCs) represent an excellent paradigm to study adult somatic stem cell fate decisions, since they fuel cyclical rounds of hair follicle regeneration during the natural hair cycle (Fuchs et al. 2001; Blanpain and Fuchs 2009). Therefore, I use an *ex vivo* organoid culture of HFSCs as a tool to investigate adult somatic stem cell fate decisions. In the following sections, I will dissect whether the manipulation of the different metabolic pathways affects cell fate decisions in the HFSC organoids and which interventions might ultimately improve stem cell maintenance in the growing population of elderly people.

2.1 Deciphering the role of hexosamine pathway activation in hair follicle stem cell fate decisions

The HP is well positioned to function as nutrient sensor, since its end-product UDP-GlcNAc is a high energy compound that requires carbohydrate, amino acid, lipid, and nucleotide donors for its synthesis (Wells et al. 2003). UDP-GlcNAc and its epimer UDP-GalNAc are essential precursors for at least three types of glycosylation reactions (Figure 7). Protein glycosylation is important for folding, function, and stability of target proteins, and thereby it is tightly connected to protein homeostasis. Interestingly, HP activation leads to elevated UDP-GlcNAc levels and improved protein quality control in different model organisms (Denzel et al. 2014; Horn et al. 2020). Elevated protein homeostasis, in turn, is pivotal for ESC function and identity (Vilchez et al. 2012). Moreover, UDP-GlcNAc and UDP-GalNAc are required for synthesis of glycosaminoglycans (GAGs), such as hyaluronic acid (HA). GAGs are major constituents of the ECM, which is an important contributor to the stem cell niche. Thereby, changes in the ECM can influence cell fate decisions. Importantly, HA synthesis is controlled by substrate availability. Thus, an increase in UDP-GlcNAc levels is sufficient to elevate HA content in the ECM (Jokela et al. 2008). Hence, the HP might be linked to stem cell maintenance in two ways: First, its effect on protein homeostasis could improve or maintain cellular functions. Second, activation of the HP might modulate ECM composition, and thereby affect the stem cell niche. Therefore, in the first part of this work, I focus on the effect of HP activation on cell fate decisions.

2.1.1 GlcNAc supplementation potently activates the hexosamine pathway in mammalian cells

It has been shown previously that HP activation can be achieved by different means: increasing glucose concentration, D-glucosamine (GlcN) or *N*-acetyl-D-glucosamine (GlcNAc) supplementation, overexpression of the first and rate-limiting enzyme of the HP, glutamine fructose-6-phosphate amidotransferase 1 (GFAT1), as well as introducing gain-of-function mutations in GFAT1 cause elevation of UDP-GlcNAc levels in different model organisms (Marshall et al. 2004; Denzel et al. 2014; Ryczko et al. 2016; Horn et al. 2020). To test HP activation in different mammalian cells, I first used GlcNAc supplementation. GlcNAc can enter the HP upon NAGK-mediated phosphorylation (Figure 7), which requires ATP (Weihofen et al. 2006). GlcNAc has been suggested to activate the HP more efficiently than GlcN, and its addition does not affect intracellular acetyl-CoA levels (Grigorian et al. 2007). Here, I treated different human cell lines with 10 mM GlcNAc for 24 h and analyzed UDP-GlcNAc levels, the end product of the HP. Importantly,

UDP-GlcNAc can be reversibly converted to its epimer UDP-GalNAc by UDP-galactose-4'-epimerase (GALE) (Thoden et al. 2001; Schulz et al. 2004). The combination of the two epimers will be referred to as UDP-*N*-acetyl-D-hexosamines (UDP-HexNAc). Of note, GlcNAc treatment significantly increased UDP-HexNAc levels in HeLa, HEK293T, and HaCaT cells (Figure 10A-C), suggesting successful activation of the HP. Apart from various types of glycosylation reactions, UDP-GlcNAc is also one of the two building blocks for HA synthesis: HA is composed of repeating disaccharides of UDP-glucuronic acid (UDP-GlcUA) and UDP-GlcNAc (Toole 2004). It is synthesized by plasma membrane-bound hyaluronic acid synthases that release HA directly into the extracellular space (Itano and Kimata 2002). Therefore, I investigated the HA amount in the culture medium in the same cell lines used before. HeLa cells displayed slightly elevated HA secretion; however, this effect was not significant (Figure 10D). In contrast, HA secretion was significantly increased upon GlcNAc supplementation in HEK293T and HaCaT cells (Figure 10E-F). Strikingly, HaCaT cells showed the lowest intracellular UDP-GlcNAc concentration, while HA secretion in the medium was 5 times higher than in HeLa cells and approximately 50 times higher than in HEK293T cells. HaCaT cells are spontaneously transformed, immortal epidermal keratinocytes isolated from adult human skin (Boukamp et al. 1988). HA is very abundant in the skin, making up half of the total body HA (Stern 2003). Therefore, I focused on HaCaT cells for the analysis of GAG levels in the ECM deposited by the cell layer. The content of HA and chondroitin sulfate (CS), another GAG containing UDP-GalNAc, was determined via fluorophore-assisted carbohydrate electrophoresis (FACE). FACE analysis revealed that HA deposition in the ECM was significantly increased and CS levels tended to be elevated (Figure 10G-H). Overall, these data suggest that the HP can be activated by GlcNAc treatment in mammalian cells. GlcNAc addition did not only increase UDP-HexNAc levels, but also HA secretion. Thus, HP activation shows great promise for improved stem cell maintenance by modulating the stem cell niche.

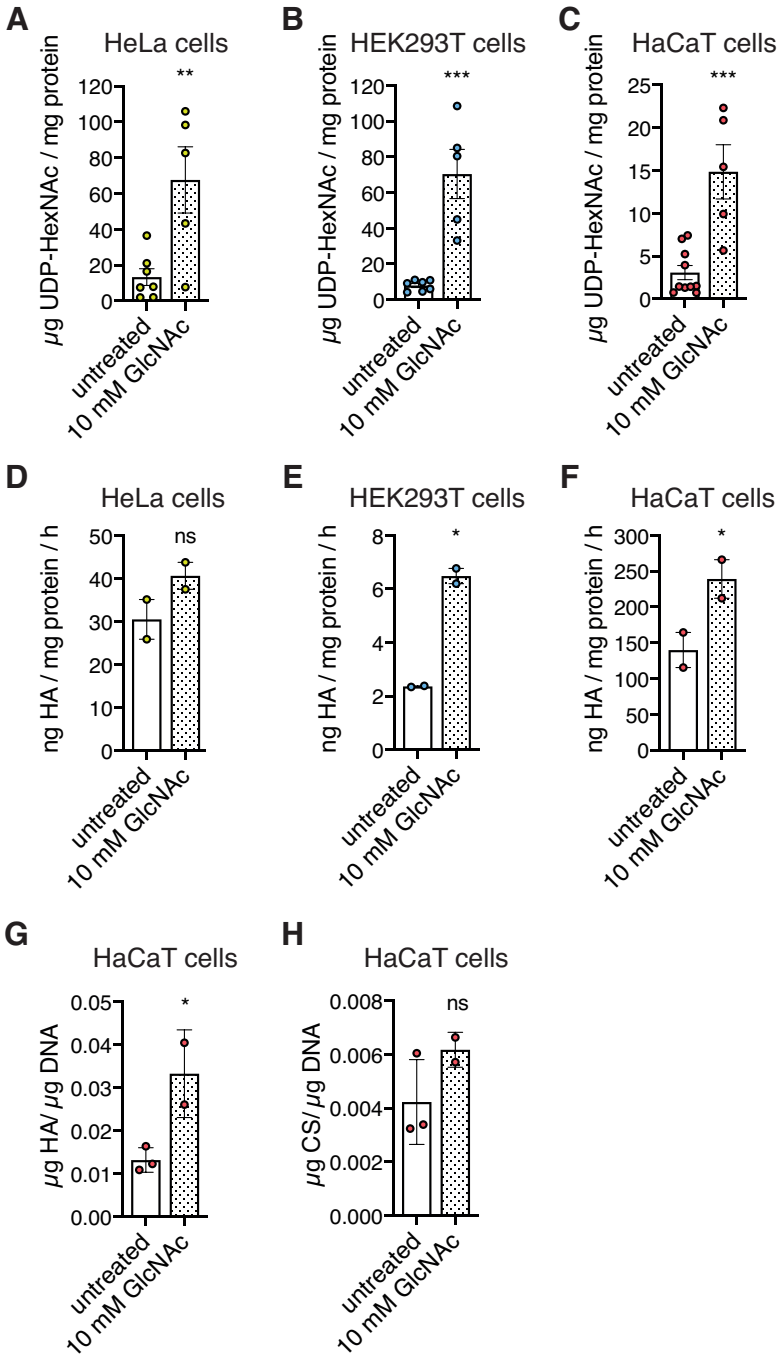

Figure 10: GlcNAc supplementation activates the hexosamine pathway in human cell lines. (**A**) UDP-HexNAc levels in HeLa cells with or without 10 mM GlcNAc treatment for 24 h (n≥5). (**B**) UDP-HexNAc levels in HEK293T cells with or without 10 mM GlcNAc treatment for 24 h (n≥5). (**C**) UDP-HexNAc levels in HaCaT cells with or without 10 mM GlcNAc treatment for 24 h (n≥5). (**D**) HA secretion into the medium using HeLa cells with or without 10 mM GlcNAc treatment for 24 h (n=2). (**E**) HA secretion into the medium using HEK293T cells with or without 10 mM GlcNAc treatment for 24 h (n=2). (**F**) HA secretion into the medium using HaCaT cells with or without 10 mM GlcNAc treatment for 24 h (n=2). (**G**) HA content in the cell layer using HaCaT cells with or without 10 mM GlcNAc treatment for 24 h (n≥2). (**H**) CS content in the cell layer using HaCaT cells with or without 10 mM GlcNAc treatment for 24 h (n≥2). (**A**-**F**) Data are presented as mean ± SEM. (**G**-**H**) Data are presented as mean ± SD. (**A**-**H**) Statistical significance was calculated by unpaired t-test. Two-tailed p-values: *** p<0.001, ** p<0.01, * p<0.05, ns: not significant.

2.1.2 Establishing the 3D-3C organoid culture as a tool to study adult somatic stem cell fate decisions

To study cell fate decisions, I used an *ex vivo* organoid culture system (3D-3C culture), which allows for the long-term culture and manipulation of hair follicle stem cells (HFSCs) (Chacón-Martínez et al. 2017). Analysis of the 3D-3C organoid culture is based on two different markers (Figure 11A): integrin α6 (α6) is expressed in all progenitors both in the interfollicular epidermis (IFE) and the hair follicle (HF) (Sonnenberg et al. 1991; Li et al. 1998); the hematopoietic stem cell marker CD34 marks the bulge stem cells of the HF (Trempus et al. 2003). I confirmed that freshly isolated epidermal cells, which contain around 5 % of α6+/CD34+ HFSCs (Figure 11B), form a 50:50 balance between α6+/CD34+ HFSCs and α6+/CD34- progenitor cells in the 3D-3C organoids after two weeks of culture (Figure 11C). Based on their transcriptome and marker expression analysis, these progenitor cells represent HF outer root sheath (ORS) cells and inner bulge cells (Kim et al. 2020a), both of which represent HFSC progeny and act as niche cells for HFSCs *in vivo* (Hsu et al. 2014a). To confirm cell identity of α6+/CD34+ HFSCs and α6+/CD34- progenitors, I sorted cells after two weeks of 3D-3C culture and gene expression was analyzed by quantitative RT-PCR or 3' RNA-sequencing (Figure 11D). First, I investigated expression of some HFSC maker genes, that have been described to be upregulated in α6+/CD34+ HFSCs previously (Chacón-Martínez et al. 2017), by quantitative RT-PCR. As expected, the expression of most stem cell marker genes was higher in HFSCs compared to progenitor cells (Figure 11E). Comparing global gene expression in the two populations by 3' RNA-sequencing, the most enriched GO term was skin development (Figure 11F). Thus, α6+/CD34- progenitors and α6+/CD34+ HFSCs are clearly distinguishable at the gene expression level and represent distinct cellular states. Moreover, I validated the organoid culture by comparing my 3' RNA-sequencing data to a previously published dataset obtained by Chacón-Martínez et al. (2017) (Figure 11G). Expression of selected HFSC identity markers as well as markers for lineage progression was similar in HFSCs compared to progenitors in both datasets. In sum, these data confirm cell identity of α6+/CD34- progenitors and α6+/CD34+ HFSCs. Thus, the 3D-3C organoids represent a good model to study cell fate decisions of HFSCs and their early progenitors.

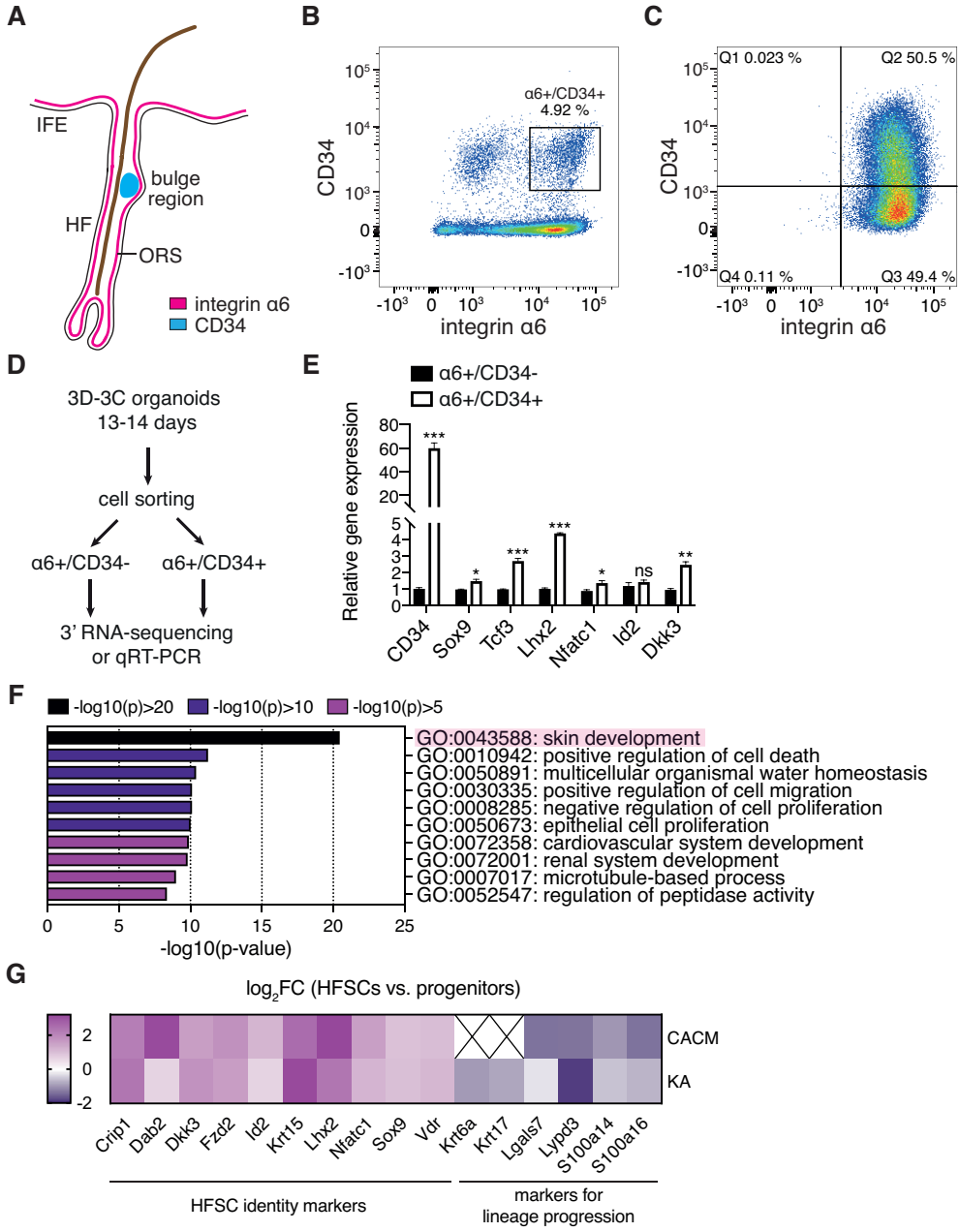

Figure 11: Characterization of the 3D-3C organoid culture system. (**A**) Schematic of marker expression in the hair follicle (HF). Integrin α6 is expressed in the basal layer of the interfollicular epidermis (IFE) and the HF. CD34 expression is restricted to the bulge region of the HF. ORS: outer root sheath. (**B**) Representative dot plot showing the distribution of the different populations of freshly isolated epidermis cells using integrin α6 and CD34 as markers. (**C**) Representative dot plot showing the distribution of the different populations after two weeks of 3D-3C organoid culture using integrin α6 and CD34 as markers. (**D**) Schematic representation of the workflow for quantitative RT-PCR (qRT-PCR) and 3' RNA-sequencing sample collection. (**E**) Stem cell marker gene expression in sorted α6+/CD34- and α6+/CD34+ cells determined by qRT-PCR. Mean + SEM (n=3). Statistical significance was calculated by unpaired t-test. p-values: *** p<0.001, ** p<0.01, * p<0.05, ns: not significant. Data are also shown in Figure 12J. (**F**) GO term analysis of differentially expressed genes (p-value < 0.05, $log_2FC > \pm 0.5$) from 3' RNA-sequencing experiment comparing α6+/CD34- progenitor cells with α6+/CD34+ stem cells (biological process, metascape.org). (**G**) Heatmap showing mean values of log_2FC of different HFSC identity markers (left) and markers for lineage progression (right) based on published RNA-sequencing data from Chacón-Martínez et al. (2017) (top; CACM), compared to the 3' RNA-sequencing results obtained in this project (bottom, KA). The ratio of the log_2FC in HFSCs vs. progenitor cells is displayed.

2.1.2.1 HA secretion is required but not sufficient to influence hair follicle stem cell fate decisions in the 3D-3C organoids

Having established the 3D-3C organoid cultures as a tool, I aimed to investigate the effect of HP activation on HFSC fate decisions. Given that HP activation has been described to improve protein quality control, I first tested whether autophagy was required for stem cell maintenance. I focused on autophagy, since autophagy maintains stemness of HSCs by repressing an activated metabolic state through clearance of active mitochondria (Ho et al. 2017). However, autophagy is dysregulated with age, resulting in the loss of HSC quiescence. Here, I used chloroquine and bafilomycin A1 which inhibit autophagic flux by blocking lysosomal function. While bafilomycin A1 increases lysosomal pH by inhibiting the lysosomal proton pump and thereby changes protease activity, chloroquine decreases autophagosome-lysosome fusion (Vinod et al. 2014; Mauthe et al. 2018). Both treatments reduced the number of α6+/CD34+ cells slightly, but not significantly (Figure 12A-B). This result suggests that autophagy might be partially required for HFSC maintenance.

Next, I asked whether HA deposition in the extracellular matrix is required for HFSC maintenance and interfered with HA synthesis, degradation, and receptor binding. First, I treated cells with 4-methylumbelliferone (4-MU), which reduces the synthesis of HA (Nakamura et al. 1995). Under normal conditions, UDP-glucuronosyltransferase (UGT) transfers an UDP-residue to the HA building block glucuronic acid (Nagy et al. 2015). 4-MU functions as a competitive substrate for UGT and binds to glucuronic acid through its hydroxyl group (Kakizaki et al. 2004). Thereby, the concentration of UDP-GlcUA declines and HA synthesis is reduced. Strikingly, 4-MU treatment in the 3D-3C organoids reduced the number of α6+/CD34+ stem cells (Figure 12C). Second, I tested hyaluronidase (HYAL) treatment. HYALs specifically hydrolyze HA at hexosaminidic β (1-4) linkages, thereby reducing the amount of extracellular high molecular weight HA (Buhren et al. 2016). Here, I used HYAL from bovine testis, which randomly cleaves HA, resulting in HA fragments of different sizes. The number of stem cells was slightly, but not significantly decreased upon HYAL treatment (Figure 12D). Third, the binding of HA to its main cell surface receptor CD44 was blocked, using an anti-CD44 antibody. The binding of HA to the extracellular domain of CD44 promotes activation of RhoGTPases, resulting in the initiation of intracellular signaling cascades (Bourguignon 2014). Therefore, anti-CD44 treatment inhibits HA-mediated intracellular signaling, mimicking the loss of extracellular HA. Interestingly, anti-CD44 treatment significantly lowered the number of stem cells after two weeks of 3D-3C culture (Figure 12E). Overall, these treatments indicated that extracellular

HA and the subsequent intracellular signaling were partially required for stem cell maintenance in the 3D-3C organoid culture.

Since autophagy and HA signaling were partially required for stem cell maintenance, I speculated that HP activation would be beneficial in the organoid culture. First, I tested HP activation by GlcNAc supplementation: I treated the 3D-3C organoids with different concentrations of GlcNAc and saw a dose-dependent increase in the number of α6+/CD34+ cells (Figure 12F). This elevation was significant and highly reproducible using 50 mM GlcNAc (data not shown). UDP-HexNAc levels and HA secretion were determined upon treatment with 50 mM GlcNAc. Both were strongly increased, confirming successful HP activation by addition of GlcNAc in the 3D-3C organoids (Figure 12G-H). To confirm that GlcNAc supplementation affected HFSC fate, I analyzed the expression of different stem cell marker genes. To this end, I sorted cells from untreated and GlcNAc-treated cultures, isolated RNA, and performed quantitative RT-PCR (Figure 12I). CD34 expression was strongly induced in α6+/CD34+ stem cells compared to α6+/CD34- committed progenitor cells. Strikingly, GlcNAc addition resulted in a further induction of CD34 expression in α6+/CD34+ cells by 3-fold compared to untreated α6+/CD34+ HFSCs (Figure 12J). However, expression of the other stem cell marker genes in GlcNAc-treated α6+/CD34+ cells was more comparable to untreated α6+/CD34- committed progenitor cells than to untreated α6+/CD34+ HFSCs (Figure 12J). Collectively, these data demonstrate that GlcNAc supplementation potently activated the HP in the 3D-3C organoids. However, it specifically elevated the expression of CD34 and did not affect cell fate, according to the unchanged expression of other stem cell marker genes.

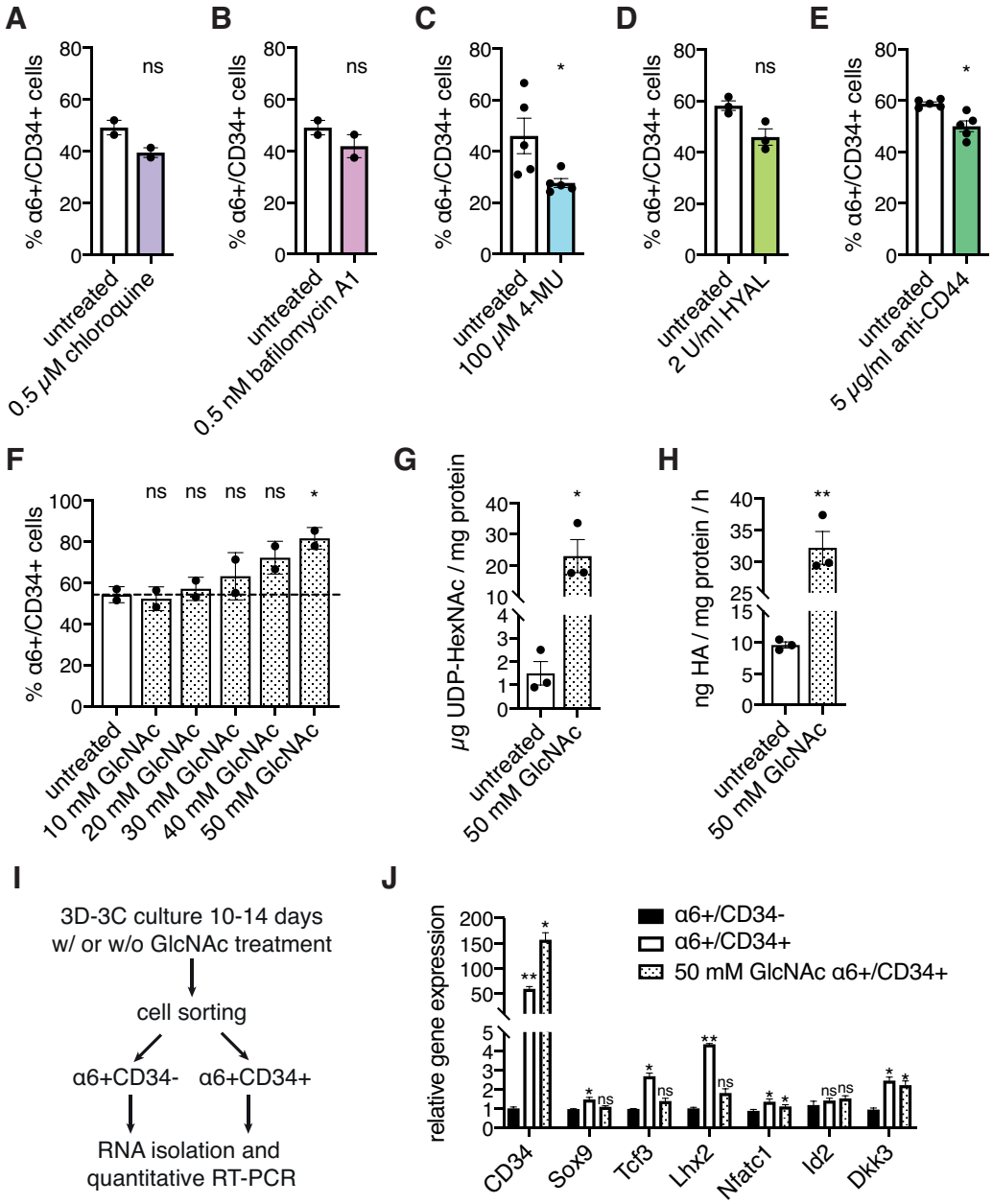

Figure 12: HA secretion is required but not sufficient for HFSC maintenance. (**A**) Ratio of α6+/CD34+ cells after two weeks of 3D-3C culture with or without chloroquine treatment. Mean ± SEM (n=2). (**B**) Ratio of α6+/CD34+ cells after two weeks of 3D-3C culture with or without bafilomycin A1 treatment. Mean ± SEM (n=2). (**C**) Ratio of α6+/CD34+ cells after two weeks of 3D-3C culture with or without 4-MU treatment. Mean ± SEM (n=5). (**D**) Ratio of α6+/CD34+ cells after two weeks of 3D-3C culture with or without HYAL treatment. Mean ± SEM (n=3). (**E**) Ratio of α6+/CD34+ cells after two weeks of 3D-3C culture with or without anti-CD44 treatment. Mean ± SEM (n=5). (**F**) Ratio of α6+/CD34+ cells after two weeks of 3D-3C culture with or without GlcNAc treatment. Mean ± SD (n=1). Statistical significance was calculated by One-way ANOVA Dunnett post-test. p-values: * p<0.05, ns: not significant. (**G**) UDP-HexNAc levels in 3D-3C organoids with or without 50 mM GlcNAc treatment. Mean ± SEM (n=3). (**H**) HA secretion in the medium using 3D-3C organoids with or without 50 mM GlcNAc treatment. Mean ± SEM (n=3). (**I**) Schematic representation of the workflow for quantitative RT-PCR using sorted cells. (**J**) Stem cell marker gene expression in sorted α6+/CD34- and α6+/CD34+ cells (Data are also shown in Figure 11E) and α6+/CD34+ cells with 50 mM GlcNAc treatment. Mean + SEM (n=3). Statistical significance was calculated by unpaired t-test. p-values: ** p<0.01, * p<0.05, ns: not significant. (**A**-**E**, **G**-**H**) Statistical significance was calculated by paired t-test. Two-tailed p-values: ** p<0.01, * p<0.05, ns: not significant.

2.1.3 Genetic manipulation of GFAT1 mildly activates the hexosamine pathway *in vivo*

Given the specific effect of GlcNAc supplementation on CD34 expression, I next tested genetic HP activation. GlcNAc exerts its effects once it is added to the culture medium. In stark contrast, genetic manipulation of HP activity can influence cell fate decisions from early embryogenesis. Additionally, cell and tissue non-autonomous effects might be mediated upon genetic manipulation of GFAT1. Transgenic mice overexpressing N-terminally tagged human GFAT1 (huGFAT1) were generated by Taconic Biosciences (Cologne, Germany) using recombination-mediated cassette exchange targeting the *Rosa26* locus. The used gene trap cassette encoded a loxP-flanked transcription termination cassette upstream of the huGFAT1 open reading frame (conditional knock-in allele, Figure 13A). Upon cre-mediated excision of the transcription termination cassette, huGFAT1 was expressed under the control of the chicken β-actin promoter, resulting in its overexpression (constitutive knock-in allele, Figure 13A). Either wildtype huGFAT1 (OE) or huGFAT1 carrying the G451E gain-of-function mutation (G451E) was overexpressed. Here, mice expressing the cre recombinase under the control of the CMV promoter were used to induce ubiquitous overexpression of huGFAT1. To assess HP activity, UDP-GlcNAc and UDP-GalNAc levels were analyzed in brains of 3-months old mice. Importantly, ubiquitous expression of the cre recombinase did not influence UDP-sugar levels compared to wildtype mice (Figure 13B-E). Heterozygous overexpression of huGFAT1 ($Rosa26^{OE/wt}$) resulted in a 1.5- to 2-fold increase of UDP-GlcNAc and UDP-GalNAc levels in both females (Figure 13B-C) and males (Figure 13D-E). Homozygous overexpression ($Rosa26^{OE/OE}$) elevated UDP-sugar levels slightly more than heterozygous overexpression in both sexes (Figure 13B-E). Recently, the G451E substitution has been shown to decrease the sensitivity of GFAT1 to UDP-GlcNAc feedback inhibition (Ruegenberg et al. 2020), suggesting a more potent HP activation compared to overexpression of wildtype GFAT1. Surprisingly, heterozygous ($Rosa26^{G451E/wt}$), as well as homozygous overexpression of huGFAT1 G451E ($Rosa26^{G451E/G451E}$) did not enhance UDP-sugar levels further than overexpression of wildtype huGFAT1 in both sexes (Figure 13B-E). In sum, the difference between heterozygous and homozygous overexpression was negligible. Nevertheless, overexpressing wildtype huGFAT1 or huGFAT1 G451E elevated UDP-sugar levels in the brains of 3-months old mice, suggesting successful genetic HP activation.

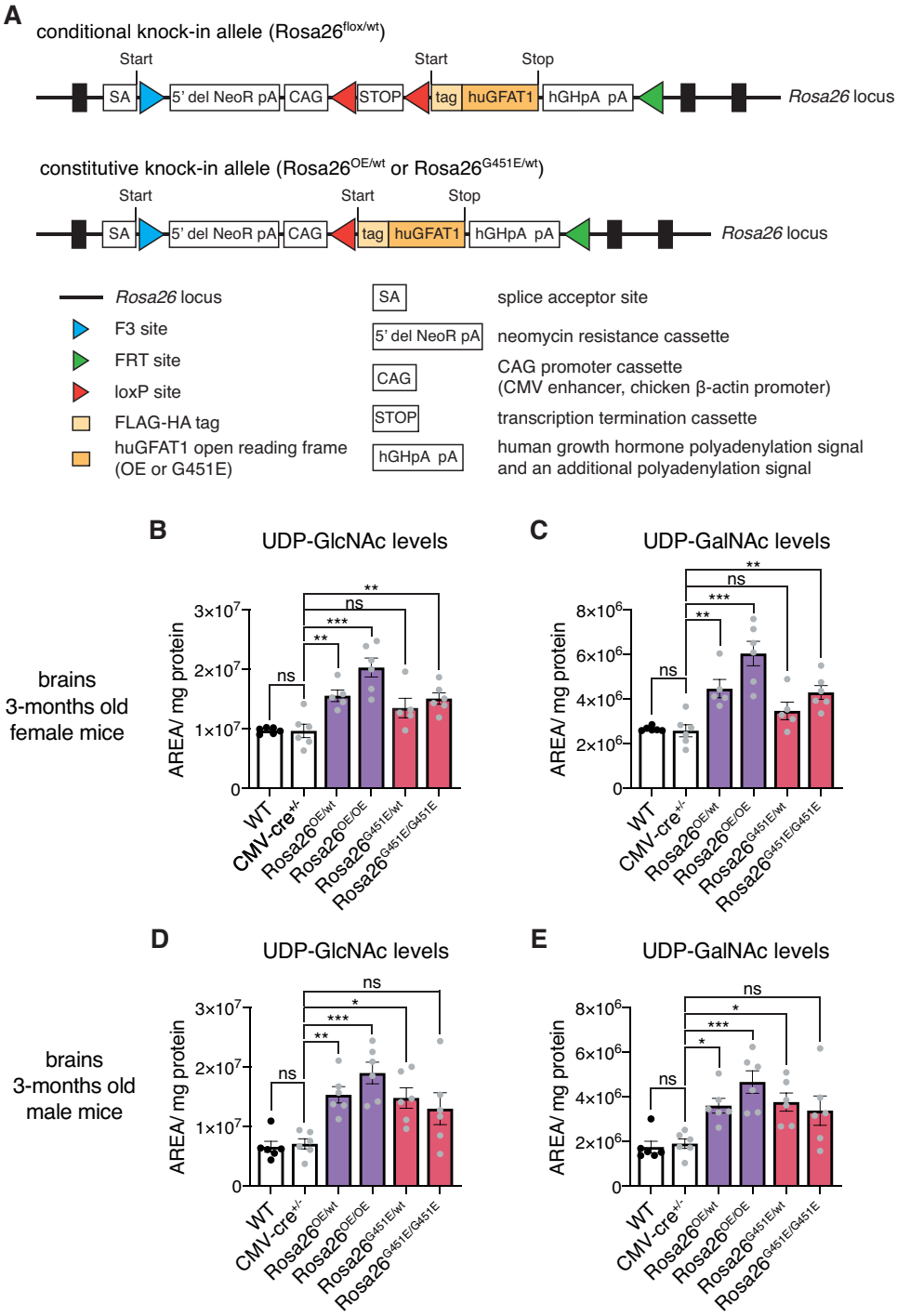

Figure 13: Genetic manipulation of GFAT1 slightly elevates hexosamine pathway activity *in vivo*. (**A**) Schematic representation of the targeted *Rosa26* locus. Conditional knock-in allele: no expression of huGFAT1 due to the loxP-flanked transcription termination cassette (Rosa26$^{flox/wt}$). Constitutive knock-in allele: cre-mediated deletion of the transcription termination cassette results in huGFAT1 overexpression (wildtype huGFAT1: Rosa26$^{OE/wt}$, huGFAT1 G451E: Rosa26$^{G451E/wt}$). huGFAT1 is N-terminally tagged with FLAG-HA. (**B**) UDP-GlcNAc levels in brains isolated from 3-months old female mice. Mean ± SEM (n≥5). (**C**) UDP-GalNAc levels in brains isolated from 3-months old female mice. Mean ± SEM (n≥5). (**D**) UDP-GlcNAc levels in brains isolated from 3-months old male mice. Mean ± SEM (n=6). (**E**) UDP-GalNAc levels in brains isolated from 3-months old male mice. Mean ± SEM (n=6). (**B**-**E**) Statistical significance was calculated by One-way ANOVA Dunnett post-test. p-values: *** p<0.001, ** p<0.01, * p<0.05, ns: not significant. Heterozygous expression of cre recombinase is indicated by gray dots. WT: wildtype mice, wt: wildtype *Rosa26* locus, OE: overexpression of wildtype huGFAT1, G451E: overexpression of huGFAT1 G451E.

2.1.3.1 Overexpression of human GFAT1 activates the hexosamine pathway in primary skin cells

To investigate the effect of huGFAT1 overexpression in the skin, primary fibroblasts and keratinocytes were isolated from newborn mice. GFAT1 expression was analyzed by Western blot using protein extracts from primary fibroblasts. While fibroblasts from WT, Rosa26$^{flox/wt}$ and CMV-cre$^{+/-}$ mice displayed similar GFAT1 levels, GFAT1 expression was strongly induced in Rosa26$^{OE/wt}$ fibroblasts. Since the GFAT1 antibody recognizes mouse and human GFAT1, I also used an anti-HA antibody to specifically detect the transgene, which was only present in Rosa26$^{OE/wt}$ fibroblasts. Loading was comparable according to β-actin levels (Figure 14A). Overall, this western blot confirmed GFAT1 overexpression in fibroblasts isolated from Rosa26$^{OE/wt}$ mice. Importantly, transgene expression was not detectable in cells isolated from mice carrying the conditional allele (Rosa26$^{flox/wt}$); thus, the transcription termination cassette upstream of the huGFAT1 ORF efficiently prohibits huGFAT1 expression. Next, UDP-HexNAc levels were analyzed. GlcNAc treatment served as positive control, since I could show that it potently activated the HP in different human cell lines (Figure 10A-C). Fibroblasts isolated from WT, Rosa26$^{flox/wt}$ and CMV-cre$^{+/-}$ mice displayed similar UDP-HexNAc levels, while UDP-sugar levels were 2-fold higher in Rosa26$^{OE/wt}$ fibroblasts and upon GlcNAc supplementation (Figure 14B). UDP-HexNAc levels were comparable to HeLa and HEK293T cells, but higher than in HaCaT cells (Figure 10A-C). Although UDP-HexNAc levels were 2-fold increased by GlcNAc supplementation and huGFAT1 overexpression, HA secretion was not affected by HP activation in primary fibroblasts (Figure 14C). Remarkably, HA levels secreted into the culture medium were around 10-fold higher than in HaCaT cells (Figure 10F). In primary keratinocytes, GlcNAc supplementation and heterozygous overexpression of huGFAT1 elevated UDP-HexNAc levels by 3-fold and 2-fold, respectively (Figure 14D). UDP-HexNAc levels from WT, Rosa26$^{flox/wt}$ and CMV-cre$^{+/-}$ keratinocytes were similar and comparable to the levels measured in HaCaT cells (Figure 10C; Figure 14D). Noticeably, HA secretion was increased by HP activation in primary keratinocytes (Figure 14E). Primary WT keratinocytes secreted 100-fold less HA than WT fibroblasts. Taken together, these data show that genetic HP activation elevated UDP-HexNAc levels in primary fibroblasts and keratinocytes. Of note, HA secretion was increased only in keratinocytes.

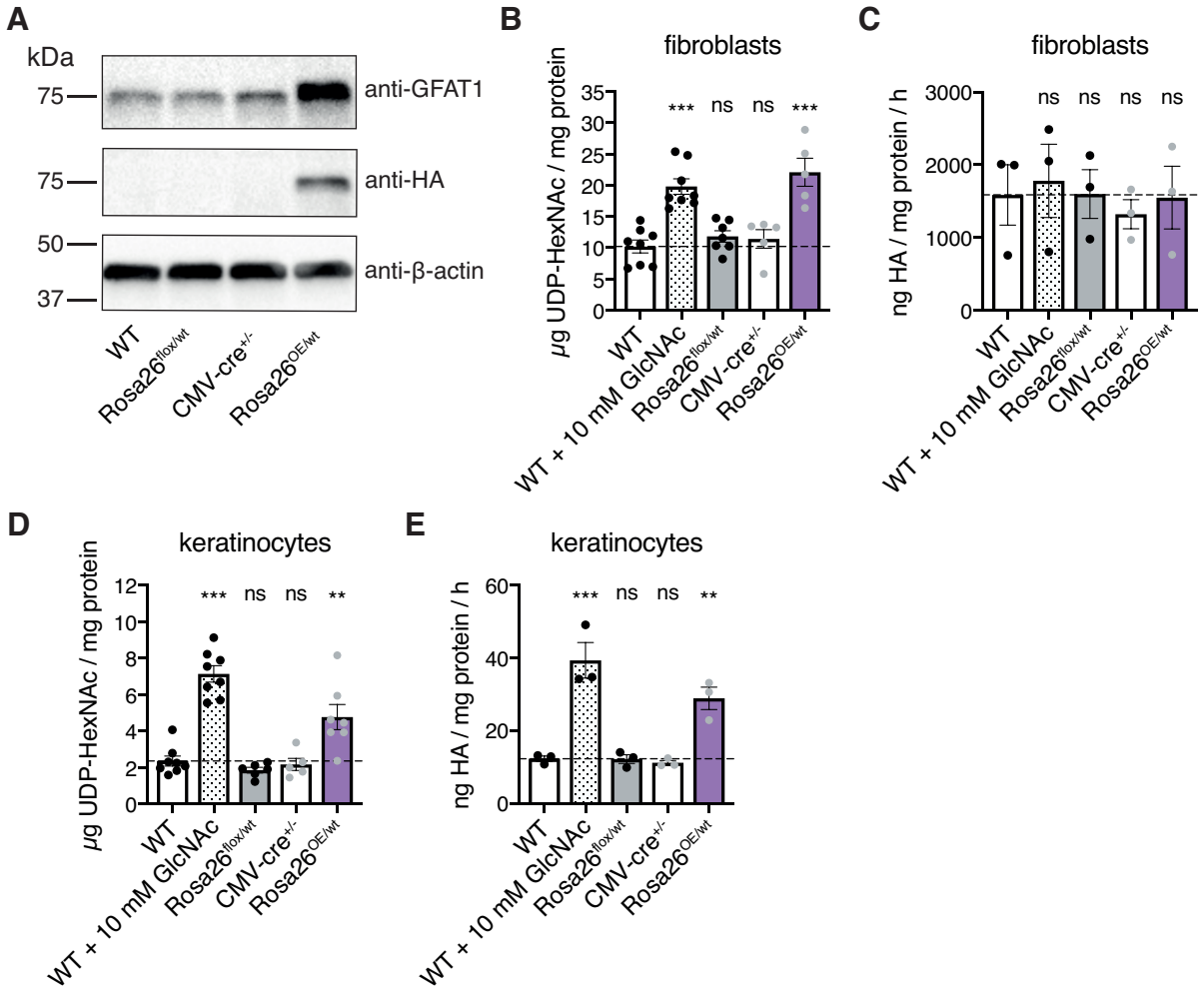

Figure 14: Overexpression of human GFAT1 activates the hexosamine pathway in primary skin cells. (**A**) Western blot analysis of GFAT1 and HA expression in primary fibroblasts isolated from newborn mice. β-actin was used as loading control. (**B**) UDP-HexNAc levels in primary fibroblasts. Mean ± SEM (n≥5). (**C**) HA secretion into the medium using primary fibroblasts. Mean ± SEM (n=3). (**D**) UDP-HexNAc levels in primary keratinocytes. Mean ± SEM (n≥5). (**E**) HA secretion into the medium using primary keratinocytes. Mean ± SEM (n=3). (**B**-**E**) GlcNAc treatment was performed for 24 h. Heterozygous expression of the cre recombinase is indicated by gray dots. Statistical significance was calculated by One-way ANOVA Dunnett post-test. p-values: *** p<0.001, ** p<0.01, ns: not significant.

2.1.3.2 Genetic hexosamine pathway activation does not affect hair follicle stem cell fate decisions

Analysis of primary keratinocytes from newborn mice demonstrated that the HP can not only be activated by GlcNAc supplementation, but also genetically by heterozygous overexpression of huGFAT1. Thus, I tested the effect of genetic HP activation on cell fate in the skin. Since I demonstrated that cells isolated from WT, Rosa26$^{flox/wt}$, and CMV-cre$^{+/-}$ mice do not express the transgene and display comparable UDP-HexNAc levels and HA secretion, all genotypes were used as control. In stark contrast to GlcNAc supplementation, genetic manipulation of GFAT1 can influence cell fate decisions from

early embryogenesis and might mediate cell and tissue non-autonomous effects. Therefore, I first evaluated the distribution of the different cell types in the epidermis of control and Rosa26$^{OE/wt}$ mice, using integrin α6 and CD34 expression as readout. Surprisingly, heterozygous overexpression of huGFAT1 did not affect cell type distribution in the epidermis (Figure 15A). Moreover, the number of α6+/CD34+ HFSCs in the organoids was unchanged (Figure 15B). GlcNAc treatment served as control, although it did not affect cell fate, but specifically CD34 expression (Figure 12J). Next, UDP-HexNAc levels and HA secretion was analyzed to confirm HP activation in this system. While GlcNAc treatment resulted in a strong increase of UDP-HexNAc levels, overexpression of huGFAT1 elevated UDP-sugars around 2-fold without reaching significance (Figure 15C). GlcNAc treatment in huGFAT1 overexpressing cells did not further increase UDP-HexNAc levels compared to GlcNAc treatment alone (Figure 15C). HA secretion was elevated 4-fold by GlcNAc treatment (Figure 15D); however, this effect was not significant due to high variation between the biological replicates. Overexpression of huGFAT1 resulted in slightly increased HA secretion (Figure 15D). GlcNAc supplementation in the huGFAT1 overexpressing cells did not further elevate HA secretion compared to GlcNAc treatment alone (Figure 15D). Next, I tested cells isolated from heterozygous huGFAT1 G451E mice. In these mice, huGFAT1 carries the G451E substitution, resulting in loss of feedback inhibition (Ruegenberg et al. 2020), and is overexpressed at the same time. Therefore, the HP should be strongly induced in these cells. Strikingly, also huGFAT1 G451E did not affect cell type distribution in the epidermis (Figure 15E) or cell fate in the 3D-3C organoids (Figure 15F). UDP-HexNAc levels and HA secretion were slightly elevated, but not significantly changed, compared to control cells (Figure 15G-H). Additional GlcNAc supplementation in huGFAT1 G451E cells did not further increase UDP-HexNAc levels or HA secretion compared to GlcNAc treatment alone (Figure 15G-H). Collectively, these data suggest that HP activation by genetic manipulation of GFAT1 was not sufficient to affect cell fate. Remarkably, heterozygous huGFAT1 overexpression had only minor effects on UDP-HexNAc levels and HA secretion compared to GlcNAc treatment, which potently activated the HP in the 3D-3C organoids.

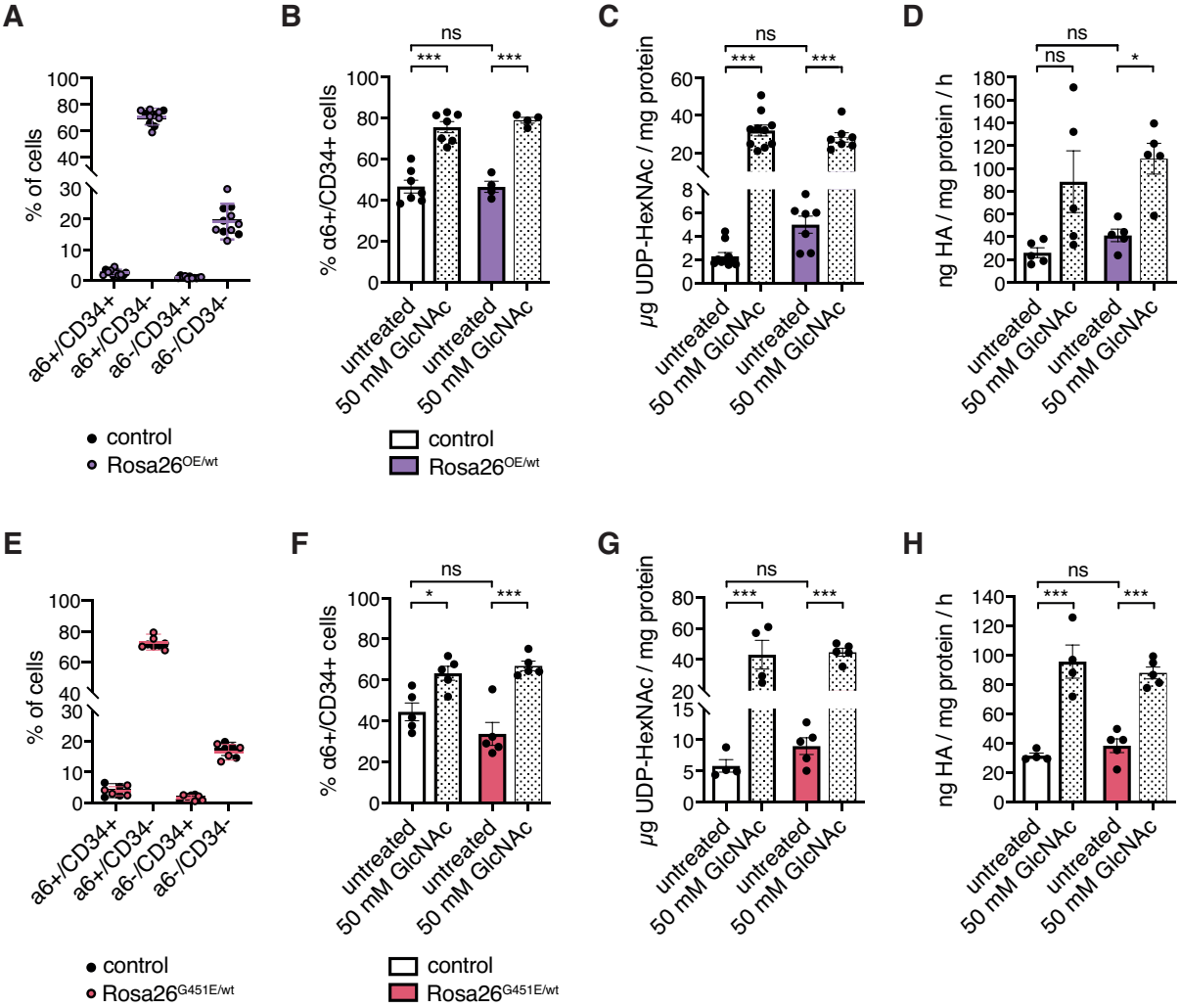

Figure 15: Heterozygous overexpression of huGFAT1 does not affect cell fate. (**A**) Analysis of freshly isolated epidermis cells from control mice and mice with heterozygous overexpression of huGFAT1 regarding integrin α6 and CD34 expression. Mean ± SD (n≥5). (**B**) Ratio of α6+/CD34+ cells after two weeks of 3D-3C culture comparing cells overexpressing huGFAT1 to control cells with or without 50 mM GlcNAc treatment. Mean ± SEM (n≥4). (**C**) UDP-HexNAc levels in 3D-3C organoids comparing cells overexpressing huGFAT1 to control cells with or without 50 mM GlcNAc treatment. Mean ± SEM (n≥7). (**D**) HA secretion in the medium using 3D-3C organoids comparing cells overexpressing huGFAT1 to control cells with or without 50 mM GlcNAc treatment. Mean ± SEM (n=5). (**E**) Analysis of freshly isolated epidermis cells from control mice and mice with heterozygous overexpression of huGFAT1 G45E regarding integrin α6 and CD34 expression. Mean ± SD (n=4). (**F**) Ratio of α6+/CD34+ cells after two weeks of 3D-3C culture comparing cells overexpressing huGFAT1 G451E to control cells with or without 50 mM GlcNAc treatment. Mean ± SEM (n=5). (**G**) UDP-HexNAc levels in 3D-3C organoids comparing cells overexpressing huGFAT1 G451E to control cells with or without 50 mM GlcNAc treatment. Mean ± SEM (n≥4). (**H**) HA secretion in the medium using 3D-3C organoids comparing cells overexpressing huGFAT1 G451E to control cells with or without 50 mM GlcNAc treatment. Mean ± SEM (n≥4). (**A-H**) Control cells were isolated from WT, huGFAT1$^{flox/wt}$, or CMV-cre$^{+/-}$ mice. (**B-D**, **F-H**) Statistical significance was calculated by One-way ANOVA Tukey post-test. p-values: *** p<0.001, * p<0.05, ns: not significant.

Since heterozygous overexpression of huGFAT1 only slightly increased UDP-HexNAc levels and HA secretion, I tested the effects of homozygous overexpression of huGFAT1 G451E (Rosa26$^{G451E/G451E}$) in the skin. First, I evaluated the distribution of the different cell

types in the epidermis of control and Rosa26$^{G451E/G451E}$ mice using integrin α6 and CD34 expression as readout. There was no change in the distribution detectable, suggesting a normal composition of the epidermis in transgenic animals (Figure 16A). Noticeably, homozygous overexpression of huGFAT1 G451E did not affect cell fate in the 3D-3C organoids (Figure 16B), although UDP-GlcNAc and UDP-GalNAc levels were significantly increased compared to control cells (Figure 16C-D). Again, heterozygous overexpression of huGFAT1 G451E elevated UDP-sugar levels compared to control; however, this effect was not significant (Figure 16C-D). GlcNAc treatment served as positive control, strongly increasing both UDP-sugars (Figure 16C-D). Taken together, these data suggest that homozygous overexpression of huGFAT1 G451E activated the HP more efficiently than heterozygous overexpression. However, also this level of HP activation was not sufficient to influence HFSC fate in the 3D-3C organoids.

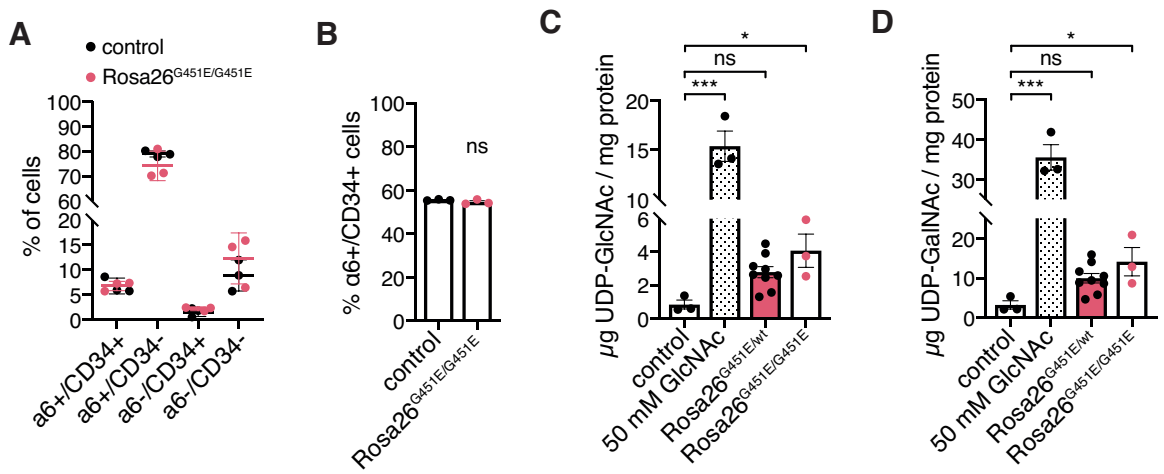

Figure 16: Homozygous overexpression of huGFAT1 G451E does not affect cell fate. (**A**) Analysis of freshly isolated epidermis cells from control mice and mice with homozygous overexpression of huGFAT1 G451E regarding integrin α6 and CD34 expression. Mean ± SD (n=3). (**B**) Ratio of α6+/CD34+ cells after two weeks of 3D-3C culture comparing cells with homozygous overexpression of huGFAT1 G451E to control cells. Mean ± SEM (n=3). Statistical significance was calculated by unpaired t-test. p-value: ns: not significant. (**C**) UDP-GlcNAc levels in 3D-3C cultured cells from mice with heterozygous or homozygous overexpression of huGFAT1 G451E to control cells with or without 50 mM GlcNAc treatment. Mean ± SEM (n≥3). (**D**) UDP-GalNAc levels in 3D-3C cultured cells from mice with heterozygous or homozygous overexpression of huGFAT1 G451E to control cells with or without 50 mM GlcNAc treatment. Mean ± SEM (n≥3). (**C-D**) Statistical significance was calculated by One-way ANOVA Dunnett post-test. p-values: *** p<0.001, * p<0.05, ns: not significant.

Overall, I confirmed HP activation by GlcNAc supplementation in different cell lines, as well as primary cells. Furthermore, I validated genetic HP activation in our transgenic mice. However, I found that HP activation does not improve stem cell maintenance in the 3D-3C organoid culture. While GlcNAc supplementation efficiently increased UDP-HexNAc levels and HA secretion, it specifically affected CD34 expression instead of HFSC fate. Genetic

HP activation increased UDP-HexNAc levels and HA secretion around 2-fold compared to control cells; however, this level of activation was not sufficient to influence HFSC fate *in vivo* or in the 3D-3C organoids.

2.2 Investigating the role of sugar metabolism in hair follicle stem cell fate decisions

Especially HSCs in their hypoxic niche have been well described to rely on glycolysis for energy production, while oxidative phosphorylation (OXPHOS) is activated upon differentiation (Simsek et al. 2010). Recently, metabolomic analysis of HFSCs relative to total epidermis revealed that also HFSCs have higher levels of glycolysis intermediates, suggesting a glycolytic metabolism (Flores et al. 2017). The limitation of mitochondrial pyruvate metabolism is necessary and sufficient to maintain the intestinal stem cell (ISC) compartment (Schell et al. 2017). Consistently, elevating glycolytic flux improves reprogramming efficiency and enhances stem cell capacity of HSCs (Yoshida et al. 2009; Zhu et al. 2010; Takubo et al. 2013). Thus, there is evidence that metabolic changes are not only a consequence of the stem cell state, but can influence cell fate decisions (Wei et al. 2018).

2.2.1 A forced increase in glycolysis is sufficient to improve hair follicle stem cell maintenance

Aerobic sugar metabolism has been described to decline during the aging process (Goyal et al. 2017; Ravera et al. 2019). Thus, stem cell exhaustion might be linked to reduced glycolytic capacity, which has been shown to attenuate HSC quiescence (Takubo et al. 2013). Here, I tested whether sugar supplementation can elevate stem cell maintenance in the 3D-3C organoids. I used different sugars, which can fuel glycolysis, or are closely connected to glucose metabolism: D-glucose, D-mannose, and D-sorbitol (Figure 17A). In addition to D-glucose, which is converted to pyruvate during glycolysis (Naifeh et al. 2020), D-mannose has been described to contribute to glycolytic flux (Slade et al. 2016). D-sorbitol is formed from D-glucose and further metabolized to fructose in the polyol pathway (Chung et al. 2003). L-glucose served as osmolarity control, since it cannot be metabolized by mammalian cells (Livesey and Brown 1995). Remarkably, treatment with D-glucose and D-mannose significantly increased the number of α6+/CD34+ stem cells, while D-sorbitol and L-glucose did not affect cell fate (Figure 17B). Importantly, D-glucose and D-mannose supplementation elevated the expression of stem cell marker genes in

mixed cultures (Figure 17C). This result suggested that these treatments, in contrast to GlcNAc supplementation, affected cell fate and not CD34 expression. As mentioned above, D-glucose and D-mannose are likely to fuel glycolysis. Since stem cells display an elevated dependence on aerobic glycolysis, NAD^+ has to be recovered by conversion of pyruvate to lactate (Zhang et al. 2012b). Therefore, I tested lactate concentration in the medium after supplementation with D-glucose and D-mannose to monitor aerobic glycolysis. As expected, D-glucose treatment significantly increased the amount of lactate secretion after two weeks of 3D-3C culture, suggesting that an increase in glycolysis was sufficient to affect HFSC fate (Figure 17D). However, D-mannose supplementation rather decreased lactate secretion but this effect was not significant (Figure 17D). Thus, D-mannose treatment affected cell fate via a different mechanism.

Interestingly, a study in ISCs has shown that the limitation of mitochondrial pyruvate metabolism is necessary and sufficient to maintain the ISC compartment (Schell et al 2017). To test, whether this was also true in HFSCs, I treated the cells with UK-5099, which blocks the mitochondrial pyruvate carrier (see also Figure 5). It has been previously described that inhibiting pyruvate transport into mitochondria attenuates OXPHOS, while glycolysis is increased (Zhong et al. 2015). Noticeably, UK-5099 supplementation elevated the number of α6+/CD34+ stem cells in the 3D-3C organoids (Figure 17E), suggesting that limitation of mitochondrial pyruvate metabolism was sufficient to better maintain HFSCs. Overall, these data suggest that a forced increase of aerobic glycolysis either by D-glucose supplementation or by blockage of pyruvate transport into mitochondria influenced HFSC fate. However, D-mannose treatment elevated the number of α6+/CD34+ stem cells without affecting glycolysis.

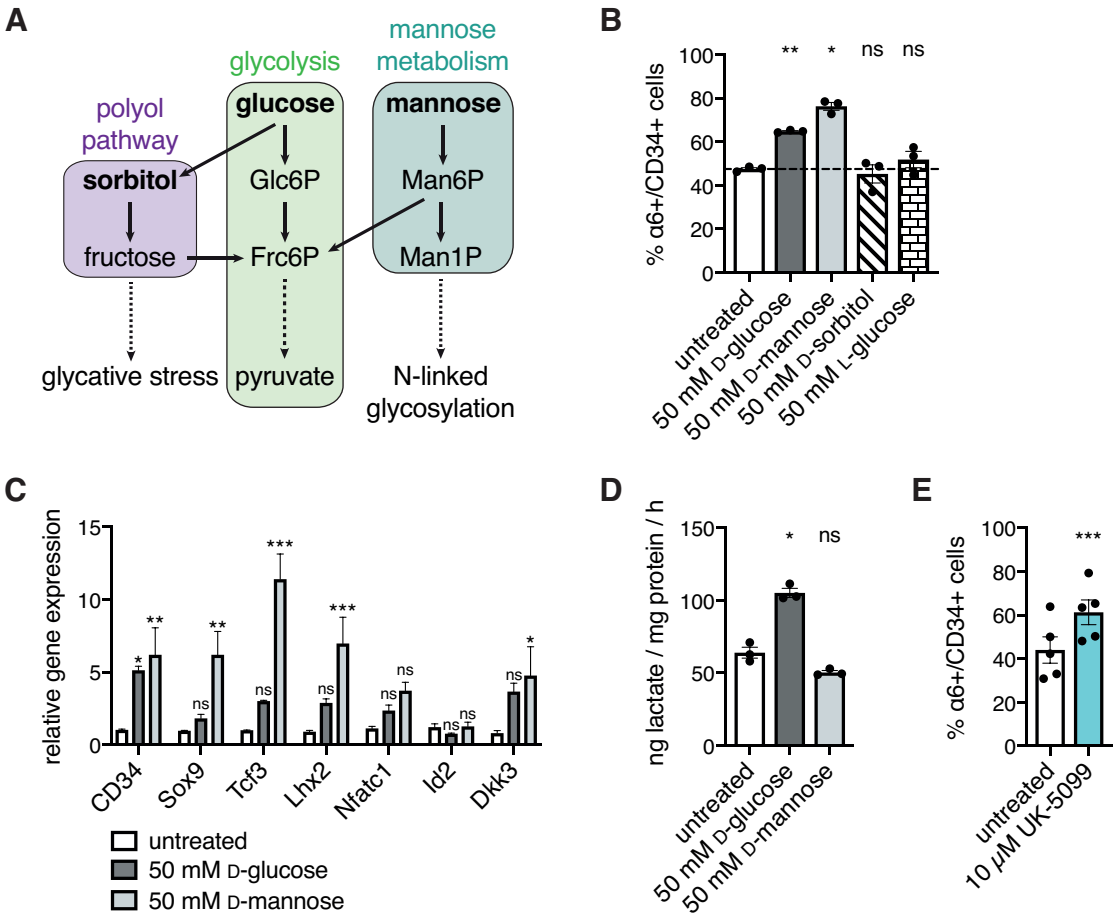

Figure 17: A forced increase in glycolysis is sufficient to increase HFSC maintenance. (**A**) Schematic representation of D-sorbitol (purple), D-glucose (green), and D-mannose (teal) metabolism. (**B**) Ratio of α6+/CD34+ cells after two weeks of 3D-3C culture with or without supplementation of different sugars. Mean ± SEM (n=3). (**C**) Stem cell marker gene expression in 3D-3C cultured cells with or without 50 mM D-glucose or D-mannose treatment. Mean + SEM (n≥2). Two-way ANOVA Tukey post-test. *** p<0.001, ** p<0.01, * p<0.05, ns: not significant. (**D**) Lactate secretion in the medium of 3D-3C cultured cells with or without 50 mM D-glucose or D-mannose treatment. Mean ± SEM (n=3). (**B**, **D**) Statistical significance was calculated by One-way ANOVA Dunnett post-test. p-values: ** p<0.01, * p<0.05, ns: not significant. (**E**) Ratio of α6+/CD34+ cells after two weeks of 3D-3C culture with or without 10 µM UK-5099 treatment. Mean ± SEM (n=5). Statistical significance was calculated by paired t-test. two-tailed p-value: *** p<0.001.

2.2.2 D-mannose supplementation reduces proliferation

To identify the downstream regulator upon D-mannose treatment, I performed RNA-sequencing. Cells were cultures for two weeks in the 3D-3C organoids and treated with D-mannose for the entire period of the experiment (14 d) or for the last 24 h only (Figure 18A). While 14 d treatment robustly elevated the number of α6+/CD34+ stem cells, 24 h treatment increased the stem cell ratio mildly, but not significantly (Figure 18B-C). Thus, the RNA-sequencing results might help to dissect the early effects that drive the observed cell fate decisions, as well as the long-term changes that are required to maintain

the stem cell state. Untreated and D-mannose treated cells were compared for the two treatment durations to identify differentially expressed genes (Figure 18D). The two groups of differentially expressed genes were subjected to further analysis. GO term analysis of the around 2.500 genes affected by 24 h D-mannose supplementation compared to untreated cells revealed ‘mitotic cell cycle progression’ as most significant GO term (Figure 18E). Strikingly, most of the 177 differentially expressed genes that belong to this GO term were downregulated upon D-mannose treatment, suggesting reduced proliferation (Figure 18G; Supplementary Table 1). This hypothesis was further supported, since also the GO term ‘negative regulation of cell proliferation’ was significantly enriched upon 24 h D-mannose supplementation (Figure 18E). Importantly, GO term analysis of the around 2.400 genes differentially expressed upon 14 d D-mannose treatment showed ‘skin development’ as most significant GO term (Figure 18F). Consistent with the stem cell ratio (Figure 18B-C), expression of the stem cell marker genes CD34, Sox9, Nfatc1, Id2, and Dkk3 was elevated upon 14 d D-mannose supplementation, whereas 24 h treatment was not sufficient to increase expression of Nfatc1, Id2, and Dkk3 (Figure 18H). Expression of the differentiation markers Krt1 and Krt10 was reduced in both conditions (Figure 18H). Apart from skin development, also cell migration and adhesion were affected upon long-term D-mannose treatment (Figure 18F). These processes might be regulated by receptor tyrosine kinase (RTK) signaling, which was also significantly changed (Figure 18F). Moreover, the GO term ‘negative regulation of cell proliferation’ was significantly enriched (Figure 18F), further supporting the hypothesis that D-mannose supplementation reduced proliferation.

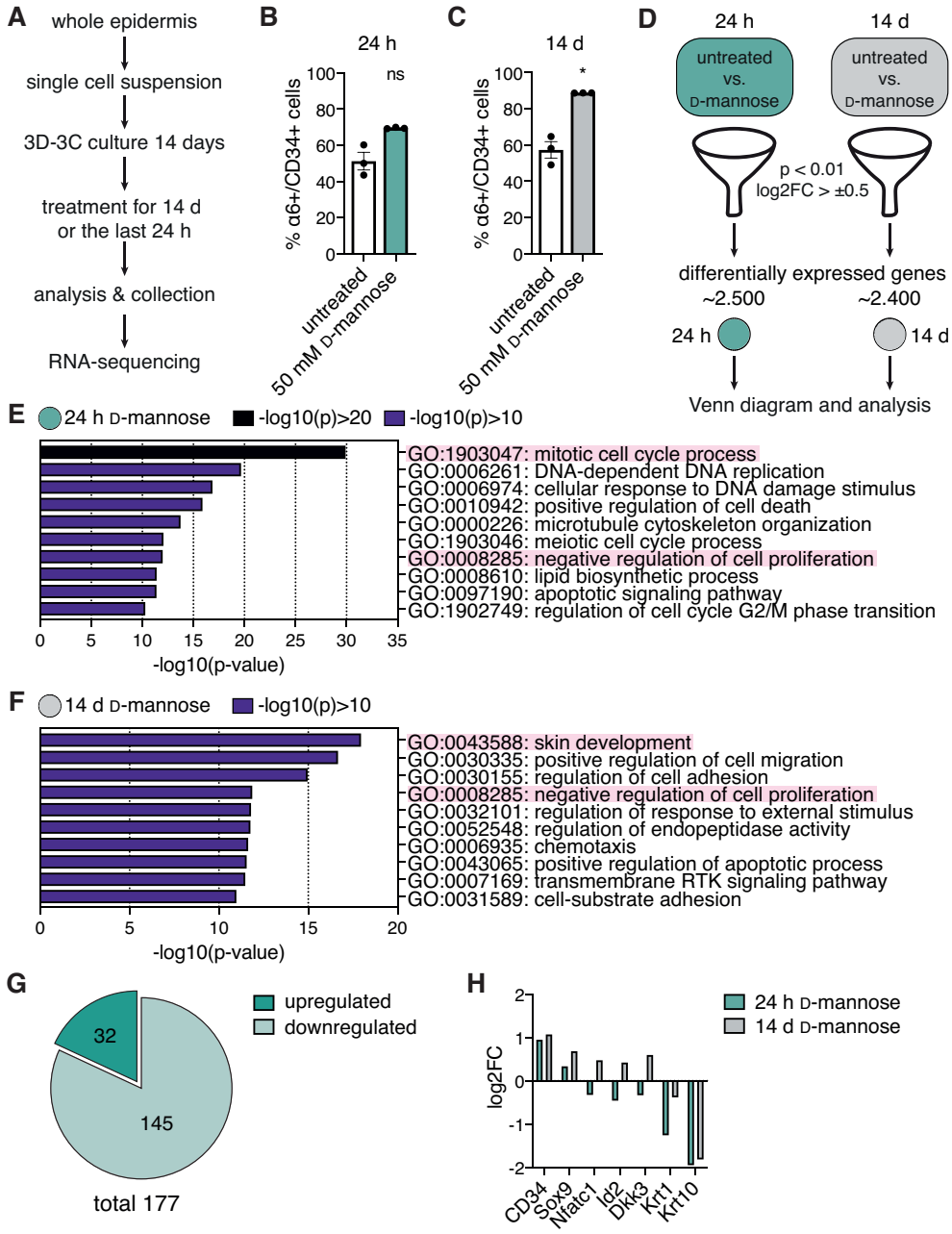

Figure 18: RNA-sequencing confirms cell fate changes upon long-term D-mannose treatment. (**A**) Schematic representation of the workflow for RNA-sequencing sample collection upon short- and long-term D-mannose supplementation. (**B**) Ratio of α6+/CD34+ cells after two weeks of 3D-3C culture with or without 50 mM D-mannose supplementation for the last 24 h. (**C**) Ratio of α6+/CD34+ cells after two weeks of 3D-3C culture with or without 50 mM D-mannose supplementation for 14 d. (**B**-**C**) Statistical significance was calculated by paired t-test. two-tailed p-values: * p<0.05, ns: not significant. (**D**) Schematic representation of the bioinformatic workflow for RNA-sequencing analysis. Untreated and D-mannose treated cells were compared. Genes were filtered (p-value < 0.01, log2FC > ±0.5) and the resulting lists were used for further analysis. 24 h treatment is shown in teal; 14 d treatment is depicted in gray. (**E**) GO term analysis of differentially expressed genes upon 24 h D-mannose supplementation compared to untreated cells (biological process, metascape.org). (**F**) GO term analysis of differentially expressed genes upon 14 d D-mannose supplementation compared to untreated cells (biological process, metascape.org). RTK: receptor tyrosine kinase. (**G**) 177 genes, which belong to the GO term 'mitotic cell cycle process' highlighted in (**E**) were differentially expressed upon 24 h D-mannose treatment. 32 genes were upregulated (dark teal), 145 genes were downregulated (light teal) upon D-mannose treatment. (**H**) log2FC of stem cell marker genes and differentiation markers. The ratio of the log2FC in 24 h (teal) or 14 d (gray) D-mannose treated cells vs. untreated cells is shown.

To further narrow down the possible candidates, I analyzed the overlap of differentially expressed genes upon 24 h and 14 d D-mannose treatment (Figure 19A). Expression of around 1.000 genes was affected by short- and long-term treatment (Figure 19A). GO term analysis of these 1.000 genes revealed ‘positive regulation of cell migration’ as most enriched GO term (Figure 19B), which might also affect ‘extracellular structure organization’, since cell migration requires constant assembly and disassembly of the cell-ECM contacts (Brunton et al. 2004). Additionally, RTK signaling might be linked to changes in cell migration. However, RTK signaling is also involved in keratinocyte proliferation (Peus et al. 1997) and the GO term ‘negative regulation of cell proliferation’ was significantly enriched in this comparison as well (Figure 19B). Therefore, I investigated the live cell number after two weeks 3D-3C culture. Long-term D-mannose treatment significantly reduced the live cell number (Figure 19C). Moreover, EdU incorporation was significantly decreased upon D-mannose supplementation in both cell types (Figure 19D). The effect was more pronounced in α6+/CD34- progenitor cells compared to α6+/CD34+ stem cells, which might contribute to the changed stem cell ratio upon D-mannose supplementation (Figure 19D). Importantly, also ‘positive regulation of apoptotic process’ was significantly changed, suggesting that elevated apoptosis might add to the reduced live cell number upon D-mannose addition. In sum, the RNA-sequencing data confirmed that D-mannose supplementation affected cell fate decisions in HFSCs. However, cell proliferation is significantly reduced upon D-mannose treatment, which might contribute to the observed changes in the stem cell ratio after long-term treatment. Furthermore, the GO term analysis suggests that cell migration and adhesion are affected. RTK signaling might be involved in these processes, since it was described to play a role in cell adhesion, migration, proliferation, and also differentiation (Andl and Rustgi 2005; Lemmon and Schlessinger 2010). Nevertheless, a specific downstream effect of D-mannose on cell fate remains elusive.

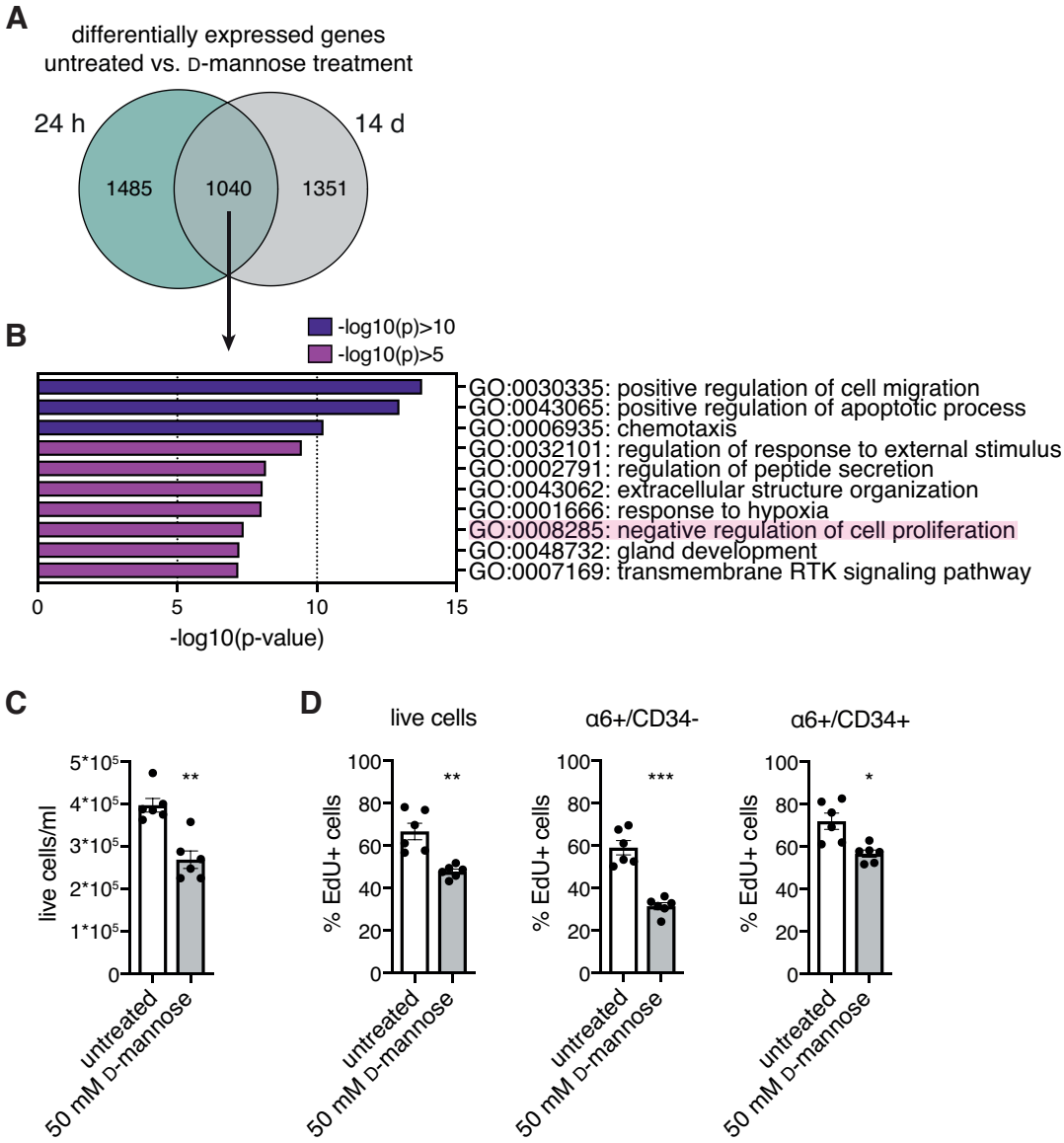

Figure 19: D-mannose supplementation reduces cell proliferation. (**A**) Venn diagram of differentially expressed genes upon short-term (24 h) D-mannose treatment (teal) compared to differentially expressed genes upon long-term (14 d) D-mannose treatment (gray). (**B**) GO term analysis of the overlap shown in (**A**). biological process, metascape.org. RTK: receptor tyrosine kinase. (**C**) Live cell number after two weeks of 3D-3C culture with or without long-term 50 mM D-mannose supplementation. Mean ± SEM (n=6). (**D**) Ratio of EdU+ cells with or without long-term 50 mM D-mannose treatment. EdU was incorporated for 24 h. Mean ± SEM (n=6). (**C**-**D**) Statistical significance was calculated by paired t-test. two-tailed p-values: *** p<0.001, ** p<0.01, * p<0.05.

2.2.3 D-mannose supplementation increases the intracellular levels of the acetylated polyamines

Since D-mannose supplementation is likely to directly affect cellular metabolism, I next aimed to investigate changes in metabolite abundance. Therefore, Andrea Annibal from Adam Antebi's laboratory (Max Planck Institute for Biology of Ageing, Cologne, Germany) performed untargeted metabolomics. Due to the limited amount of material that can be

generated from 3D-3C cultured cells, I isolated primary keratinocytes from newborn wildtype mice and treated them with D-mannose for 24 h (Figure 20A). Andrea determined the intracellular levels of around 100 metabolites (Supplementary Table 2). Seven metabolites were significantly changed comparing untreated and D-mannose treated cells: formyl-L-methionine, L-acetylcarnithine, and inosinic acid were depleted, while the levels of *N*1-acetylspermidine, UDP-glucose, UDP, and homocysteine were elevated upon mannose supplementation (Figure 20B). The most significant hit was *N*1-acetylspermidine (*N*1-AcSpd), an acetylated polyamine, which was approximately 2-fold increased upon D-mannose supplementation (Figure 20B). Polyamines are polycations, that can bind to a variety of negatively charged cellular molecules, including nucleic acids (Dever and Ivanov 2018). Of note, the other polyamines identified by this approach, spermidine and spermine, were not changed (Figure 20C). Additionally, the precursor for polyamine synthesis, L-arginine, was not affected by D-mannose treatment (Figure 20C). To investigate the effect of D-mannose supplementation on intracellular polyamine levels more thoroughly, Andrea performed targeted metabolomics using 3D-3C cultured cells, which were treated with D-mannose for two weeks. Importantly, this approach confirmed the increase in *N*1-AcSpd upon D-mannose treatment (Figure 20D). Moreover, also *N*1-acetylspermine (*N*1-AcSpm) levels were increased, while ornithine and putrescine levels were reduced by D-mannose supplementation (Figure 20D). The acetyl-CoA-dependent acetylation of spermidine and spermine to form *N*1-AcSpd and *N*1-AcSpm, respectively, is catalyzed by spermidine/spermine *N*1-acetyltransferase (SSAT) (Figure 8). The specific increase in the levels of acetylated polyamines upon D-mannose treatment suggested, that SSAT expression would be affected. Thus, I investigated SSAT expression in 3D-3C cultured cells upon short- (24 h) and long-term (12 d) D-mannose treatment. SSAT expression was elevated after 24 h treatment, however, it was not changed after 12 d of D-mannose supplementation (Figure 20E). Thus, not only SSAT expression, but also its stability might affect polyamine levels in the 3D-3C organoids. In sum, these data demonstrate that the effect of D-mannose supplementation on cellular metabolism was surprisingly low: less than 10 % of the identified metabolites were significantly affected. Also, glycolysis intermediates were not identified or not significantly changed, further supporting that D-mannose treatment did not affect glycolysis. Of note, D-mannose supplementation specifically elevated the levels of the acetylated polyamines *N*1-AcSpd and *N*1-AcSpm.

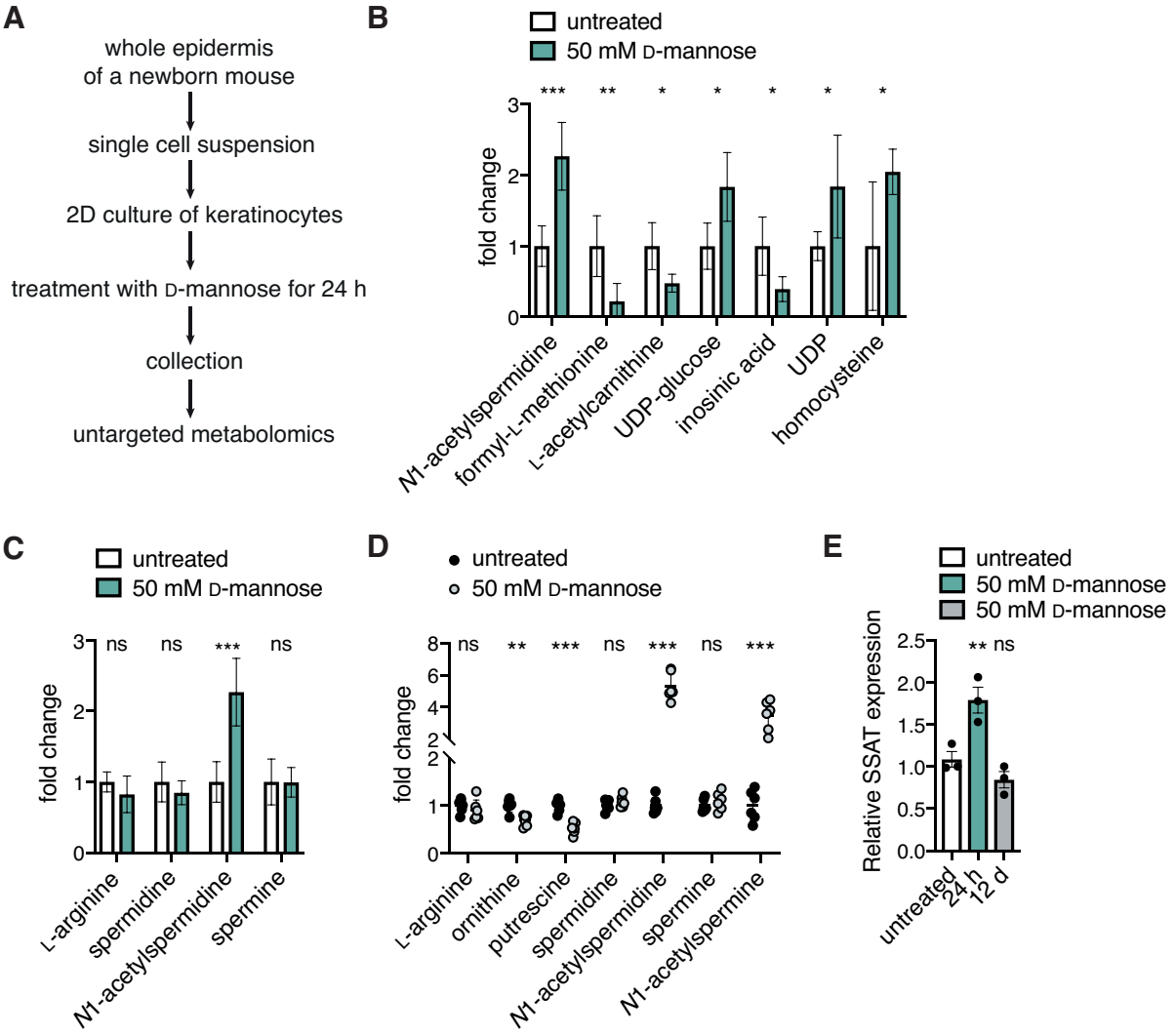

Figure 20: D-mannose supplementation increases the levels of acetylated polyamines. (**A**) Schematic representation of the workflow for untargeted metabolomics using primary keratinocytes isolated from newborn mice. (**B**) Significantly changed metabolites identified by untargeted metabolomics with or without 50 mM D-mannose treatment for 24 h. Mean ± SEM (n=5). (**C**) Levels of polyamines identified by untargeted metabolomics with or without 50 mM D-mannose treatment for 24 h. Mean ± SEM (n=5). (**D**) Polyamine levels in 3D-3C cultured cells with or without 50 mM D-mannose treatment for 14 days. Mean ± SEM (n=6). (**B**-**D**) Statistical significance was calculated by unpaired t-test. p-values: *** p<0.001, ** p<0.01, * p<0.05, ns: not significant. (**E**) Relative SSAT expression in 3D-3C cultured cells with or without D-mannose treatment for 24 h (teal) or 12 d (gray). Mean ± SEM (n=3). Statistical significance was calculated by One-way ANOVA Dunnett post-test. p-values: ** p<0.01, ns: not significant.

2.3 Elucidating the role of polyamine availability in hair follicle stem cell fate decisions

Since D-mannose supplementation clearly elevated the levels of the acetylated polyamines *N*1-AcSpd and *N*1-AcSpm, I aimed to elucidate the role of polyamine metabolism in stem cell maintenance in the last part of this work. Polyamines have been linked to stemness previously. For example, polyamines positively influence expression of MINDY1, a deubiquitinating enzyme, which promotes ESC self-renewal (James et al. 2018). Thus, I asked whether HFSCs in the 3D-3C organoids displayed higher levels of intracellular polyamines compared to progenitor cells. I sorted 3D-3C cultured cells and Andrea Annibal performed targeted analysis of polyamines by LC-MS. Surprisingly, he found that the levels of putrescine, spermidine, spermine, and *N*1-AcSpd, were decreased in α6+/CD34+ HFSCs compared to α6+/CD34- progenitor cells (Figure 21A). This result suggests that, depending on the cellular context, high polyamine levels, but also low polyamine availability can be beneficial for stem cell maintenance. Of note, reduction of the natural polyamines putrescine, spermidine, and spermine has been implicated in reduced translation previously (Pegg 2016; Dever and Ivanov 2018). Moreover, it has been described that various types of stem cells display lower translation rates than their differentiated counterparts (Sampath et al. 2008; Signer et al. 2014; Blanco et al. 2016; Zismanov et al. 2016). Therefore, I hypothesized that low availability of the natural polyamines reduced translation and thereby favored the stem cell state in the organoid culture.

2.3.1 Low translation rates mark the hair follicle stem cell state and decreasing translation enhances stemness in the organoids

To test whether α6+/CD34+ HFSCs display lower mRNA translation than α6+/CD34- progenitor cells, I established a puromycin incorporation assay: the antibiotic puromycin is a structural analog of aminoacyl-tRNAs, consisting of a nucleoside and an amino acid moiety (Figure 21B). Puromycin can enter the A-site of the ribosome, where its free amino group accepts the nascent polypeptide chain from the P-site peptidyl-tRNA; however, extension of the nascent chain is prevented, since the peptide bond of puromycin cannot be cleaved, resulting in premature termination of translation (Aviner 2020). Once incorporated in the nascent polypeptide chain, puromycin can be detected by immunoblotting (Schmidt et al. 2009). In HaCaT cells, pre-treatment with the translation inhibitor cycloheximide (CHX) potently reduced the anti-puromycin signal compared to

puromycin treatment alone (Figure 21C). Thus, puromycin incorporation is a good tool to investigate translation rates.

Blanco et al. (2016) showed that the activation of HFSCs during the transition from the resting phase, telogen, to proliferation in anagen during the hair cycle coincides with elevated protein synthesis. These data demonstrate a functional role for increased translation during differentiation in the epidermis. However, the mechanisms that regulate translation in stem cells in general and upon differentiation remain elusive. Here, I aimed to better understand the mechanisms and functional consequences of this difference in translation. First, I tested whether translation rates were also reduced in freshly isolated HFSCs compared to more differentiated counterparts. Besides CD34 and integrin α6, I also used stem cell antigen-1 (Sca1) as marker (Figure 21D): Sca1 expression can be detected in the infundibulum (IFD) region of the HF and the basal layer of the epidermis (Jensen et al. 2008). By gating for Sca1-negative cells, IFE and IFD progenitors can be separated from HF progenitors (Figure 21E). Thus, I compared HF bulge stem cells (Sca1-/α6+/CD34+) to HF outer root sheath cells (ORS; Sca1-/α6+/CD34-). After cell sorting, I performed puromycin incorporation (Figure 21F). Western blot analysis revealed a significant reduction of puromycin incorporation in Sca1-/α6+/CD34+ HFSCs compared to Sca1-/α6+/CD34- ORS cells (Figure 21G-H), thereby confirming reduced translation rates described for HFSCs *in vivo* (Blanco et al. 2016). Next, I asked whether this difference in translation is maintained during the *in vitro* culture in the 3D-3C organoids. I sorted cells after two weeks of 3D-3C culture (Figure 21I) and found reduced translation in α6+/CD34+ stem cells compared to α6+/CD34- progenitors by puromycin incorporation (Figure 21J-K). Thus, the 3D-3C organoids maintain this key *in vivo* property of HFSCs, making them a suitable model to study the influence of translation on cell fate decisions. Taken together, these data demonstrate that both freshly isolated and 3D-3C cultured HFSCs display lower translation rates compared to their more differentiated counterparts, which are likely required to maintain stemness. Further, my data suggest that low polyamine levels in HFSCs endogenously reduce translation.

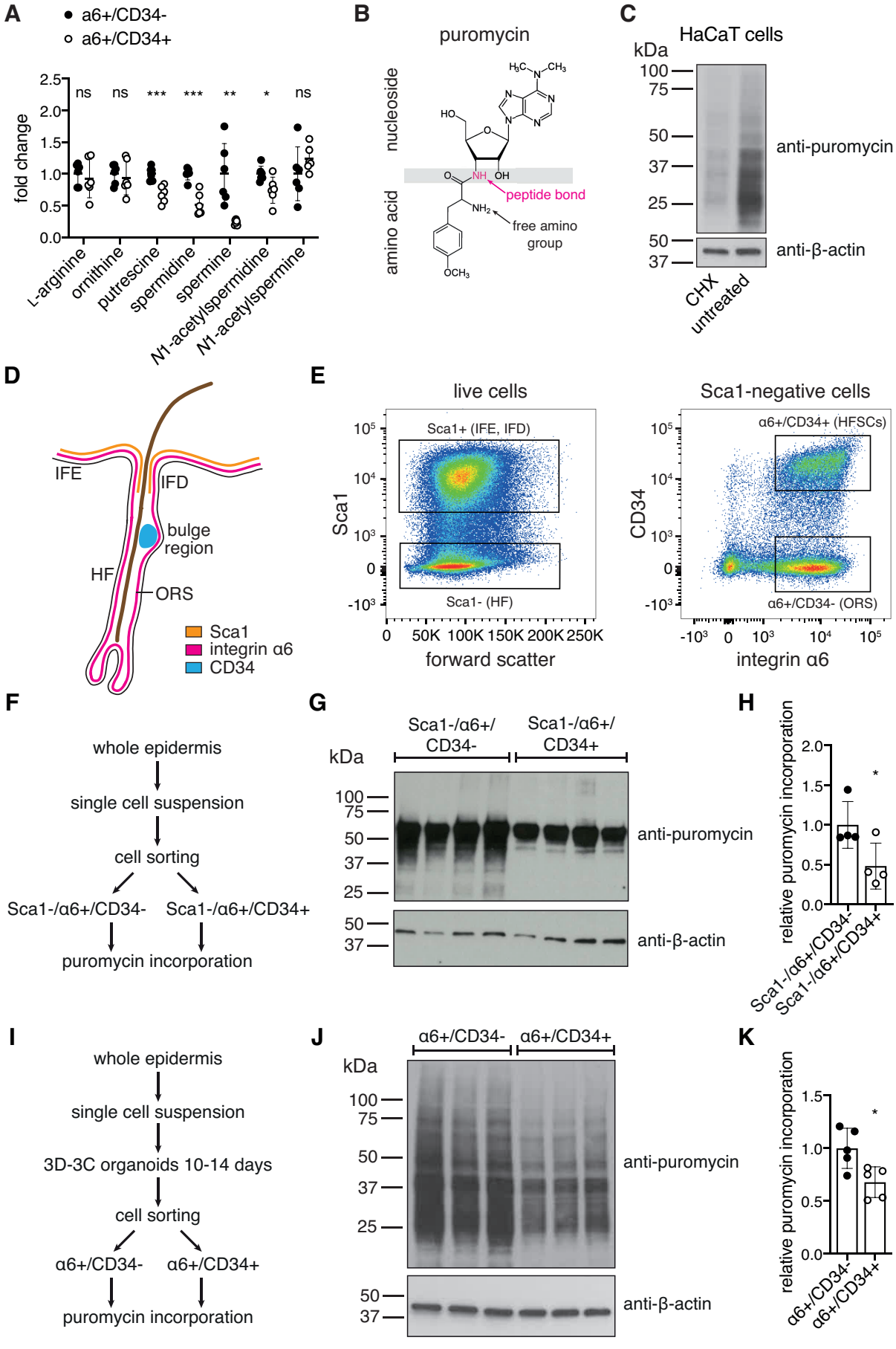

(Figure 21: legend on next page)

Having established that HFSCs displayed lower translation rates than their progenitors in the 3D-3C organoids, I aimed to validate that reduction of translation is sufficient to drive cell fate decisions. To this end, I manipulated translation in the 3D-3C organoids by addition of low doses of G418, a well described inhibitor of translation elongation (Bar-Nun et al. 1983). I confirmed reduced translation after 4 h of G418 treatment in the 3D-3C organoids by measuring puromycin incorporation (Figure 22A-B). Strikingly, a forced decrease in translation resulted in a significant increase of α6+/CD34+ stem cells after two weeks of 3D-3C culture (Figure 22C). Of note, the self-organizing plasticity of the 3D-3C organoids results in a balance between α6+/CD34- progenitors and α6+/CD34+ HFSCs, which is first established around day 9 (Chacón-Martínez et al. 2017). To exclude that G418 increased the ratio of HFSC due to their specific selection from the mixed starting population (Figure 11B), I started the treatment on day 9, when the 50:50 ratio was established (data not shown). Importantly, G418 elevated the number of α6+/CD34+ stem cells also when supplemented for the last five days of culture only (Figure 22D). To unravel whether the increase in the stem cell ratio upon G418 treatment in the organoids culture had a functional consequence, I analyzed the proliferative potential of the cells after 3D-3C culture in a colony formation assay. Importantly, α6+/CD34+ HFSCs display higher proliferative potential than α6+/CD34-progenitors when freshly isolated, but also after 3D-3C organoid culture (Trempus et al. 2003; Kim et al. 2020a). Thus, this assay is a suitable read-out to confirm cell fate changes. For the colony formation assay, 3D-3C cultured cells were seeded in clonal density on a feeder layer and cultured for 2 to 3 weeks without treatment before emerging colonies were fixed and stained (Figure 22E). Quantification of total colony number revealed a significant increase upon G418 treatment

Figure 21: Reduced translation is a consequence of the stem cell state. (**A**) Polyamine levels in sorted α6+/CD34- and α6+/CD34+ cells after 3D-3C culture. Mean ± SEM (n=6). (**B**) Structure of puromycin. Modified from Aviner 2020. (**C**) Representative Western blot analysis after puromycin incorporation in HaCaT cells with or without cycloheximide (CHX) treatment. (**D**) Schematic of marker expression in the hair follicle (HF). The interfollicular epidermis (IFE) and the infundibulum (IFD) region of the HF are marked by Sca1 expression. Integrin α6 is expressed in the basal layer of the IFE and the HF. CD34 expression is restricted to the bulge region. ORS: outer root sheath. (**E**) Dot plot showing the gating strategy for sorting of freshly isolated epidermis cells. Live cells were gated according to Sca1-expression. Sca1-negative cells were separated into HFSCs and ORS cells. (**F**) Schematic representation of the workflow for puromycin incorporation using freshly isolated cells. (**G**) Western blot analysis after puromycin incorporation in Sca1-/α6+/CD34- progenitor cells compared to Sca1-/α6+/CD34+ HFSCs. (**H**) Quantification of the Western blot in (**G**). Mean ± SD (n=4). (**I**) Schematic representation of the workflow for puromycin incorporation using 3D-3C cultured cells. (**J**) Representative Western blot analysis after puromycin incorporation in α6+/CD34- progenitor cells compared to α6+/CD34+ HFSCs. (**K**) Quantification of the Western blot in (**J**). Mean ± SD (n=5). (**A**, **H**, **K**) Statistical significance was calculated by unpaired t-test. p-values: *** p<0.001, ** p<0.01, * p<0.05, ns: not significant.

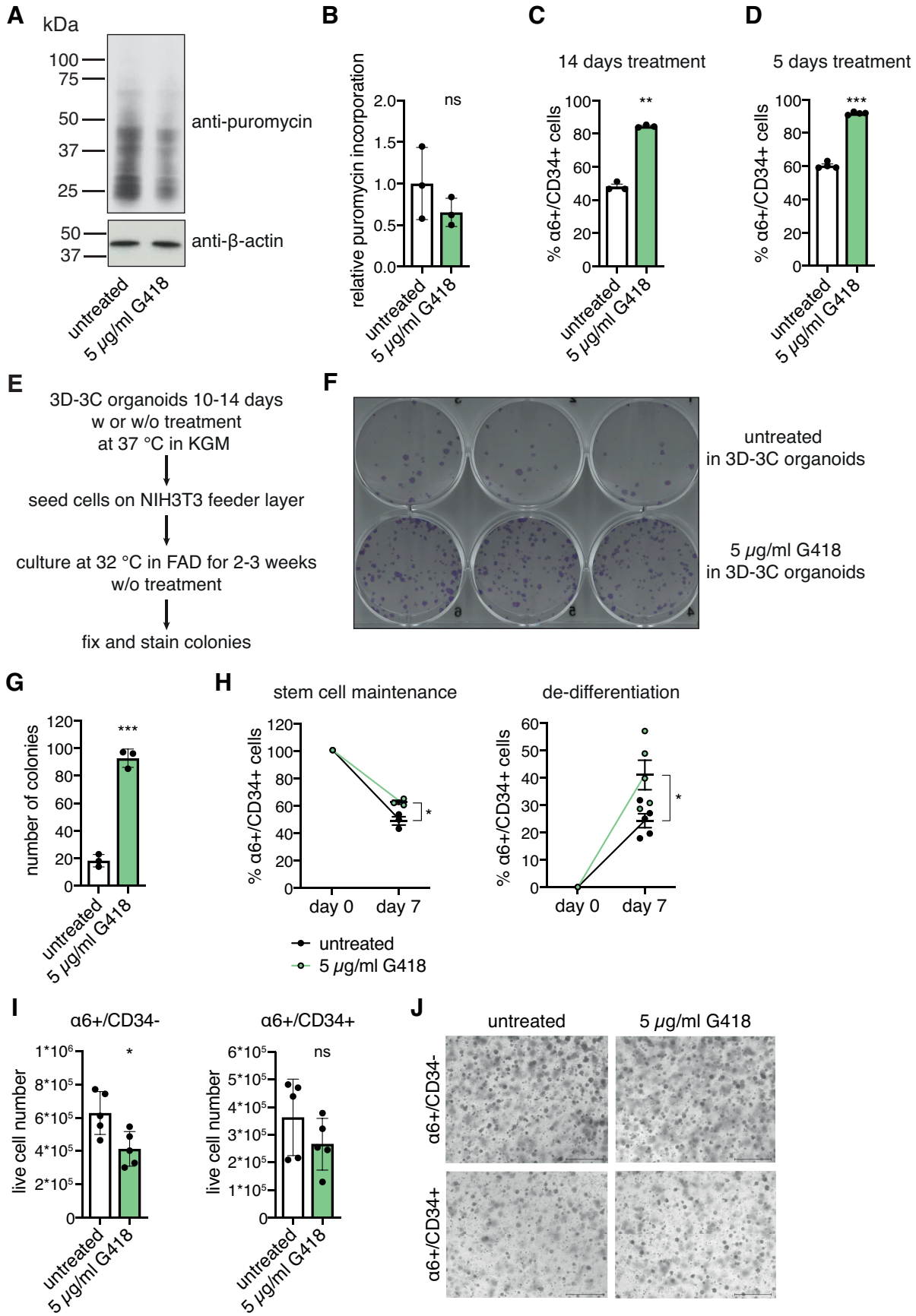

(Figure 22: legend on next page)

in the 3D-3C organoids, suggesting an increased proliferative potential, thereby confirming stem cell identity (Figure 22F-G). As mentioned above, α6+/CD34- progenitors and α6+/CD34+ HFSCs automatically form a balance in the 3D-3C organoids. This balance is influenced by self-renewal and differentiation of stem cells, but also by proliferation and de-differentiation of progenitors back to the stem cell state. To investigate which of these mechanisms was affected upon G418 treatment, I sorted the cells after two weeks of 3D-3C culture to generate pure populations of either α6+/CD34- or α6+/CD34+ cells. These pure populations were cultured for one week with or without G418 treatment for the last five days before analysis. Interestingly, G418 treatment increased both stem cell maintenance and de-differentiation, resulting in an increased number of α6+/CD34+ HFSCs on day 7 (Figure 22H). To exclude specific toxicity of G418 in one of the cell types, I determined the live cell number in the pure populations on day 7. G418 treatment reduced the live cell number in both α6+/CD34- progenitors and α6+/CD34+ HFSCs; however, the effect was slightly more pronounced in the progenitor cells. Nevertheless, this reduction of the live cell number was not strong enough to account for the increase in α6+/CD34+ HFSCs seen upon G418 treatment (Figure 22I-J). Collectively, these data suggest that reduced translation is not only a consequence of the stem cell state. Instead, a forced decrease of translation can influence cell fate decisions in the 3D-3C organoids.

Figure 22: Reduction of translation drives cell fate decisions in the 3D-3C organoids. (**A**) Representative Western blot analysis after puromycin incorporation in 3D-3C cultured cells with or without 5 µg/ml G418 treatment for 4 h. (**B**) Quantification of Western blot analysis after puromycin incorporation as shown in (**A**). Mean ± SD (n=3). (**C**) Ratio of α6+/CD34+ cells after two weeks of 3D-3C culture with or without 5 µg/ml G418 treatment for 14 days. Mean ± SEM (n=3). (**D**) Ratio of α6+/CD34+ cells after two weeks of 3D-3C culture with or without 5 µg/ml G418 treatment for the last 5 days. Mean ± SEM (n=4). (**E**) Schematic representation of the workflow for the colony formation assay using 3D-3C cultured cells. (**F**) Representative image of tissue culture plate after colony formation assay using cells with or without G418 treatment in 3D-3C organoids (n=3). (**G**) Quantification of colony number in (**F**). Mean ± SD (n=3). (**H**) Ratio of α6+/CD34+ cells on day 0 and day 7 post-sorting starting from 100 % α6+/CD34+ cells (left) or 100 % α6+/CD34- cells (right) with or without G418 treatment for the last 5 days of culture. Mean ± SEM (n≥3). (**I**) Live cell number of α6+/CD34- cells (left) and α6+/CD34+cells (right) on day 7 post-sorting. Treatment was performed for the last 5 days of culture. Mean ± SD (n=5). (**J**) Representative images of organoid cultures on day 7 post-sorting. Treatment was performed for the last 5 days of culture. (**B**-**D**, **I**) Statistical significance was calculated by paired t-test. two-tailed p-values: *** p<0.001, ** p<0.01, ns: not significant. (**G**-**H**) Statistical significance was calculated by unpaired t-test. p-values: *** p<0.001, * p<0.05.

2.3.2 Reduced translation by decreased polyamine availability and stemness do not correlate in the organoids

Having demonstrated that α6+/CD34+ HFSCs display lower translation rates and lower levels of the natural polyamines putrescine, spermidine and spermine than α6+/CD34- progenitor cells, I intended to elucidate whether polyamine availability plays a role in the regulation of protein synthesis in HFSCs. To this end, I aimed to mimic the low levels of natural polyamines found in HFSCs and study the effect on cell fate.

2.3.2.1 Depletion of the natural polyamines by DFMO treatment reduces translation without effect on stemness

To reduce polyamine levels and investigate the consequences on HFSC fate decisions in the 3D-3C organoids, I used 2-difluoromethylornithine (DFMO), which is an enzyme-activated, irreversible inhibitor of ODC (Metcalf et al. 1978), the first enzyme in the polyamine pathway (Figure 8). Andrea Annibal measured polyamine levels in the 3D-3C organoids upon DFMO treatment and found that putrescine and spermidine levels were reduced, while ornithine accumulated (Figure 23A). These results suggested successful inhibition of ODC. Of note, DFMO treatment recapitulated the low levels of natural polyamines seen in HFSCs compared to progenitors.

Depletion of the natural polyamines has been previously linked to decreased protein synthesis (Dever and Ivanov 2018). Accordingly, puromycin incorporation was decreased by around 40 % in the organoid culture upon short-term DFMO treatment (Figure 23B-C). Surprisingly, the reduction of translation was not sufficient to affect HFSC fate, as shown by the unchanged ratio of HFSCs upon DFMO treatment (Figure 23D-E). Neither stem cell maintenance, nor de-differentiation were changed when starting from pure populations (Figure 23F). DFMO treatment slightly decreased the live cell number of α6+/CD34- progenitors, without affecting the viability of α6+/CD34+ HFSCs (Figure 23G-H). Together, these data suggest that reduced mRNA translation by decreased polyamine availability does not enhance stemness in the 3D-3C organoids. This result was surprising, since I demonstrated that reduced translation can drive cell fate decisions in the 3D-3C organoids using G418 before.

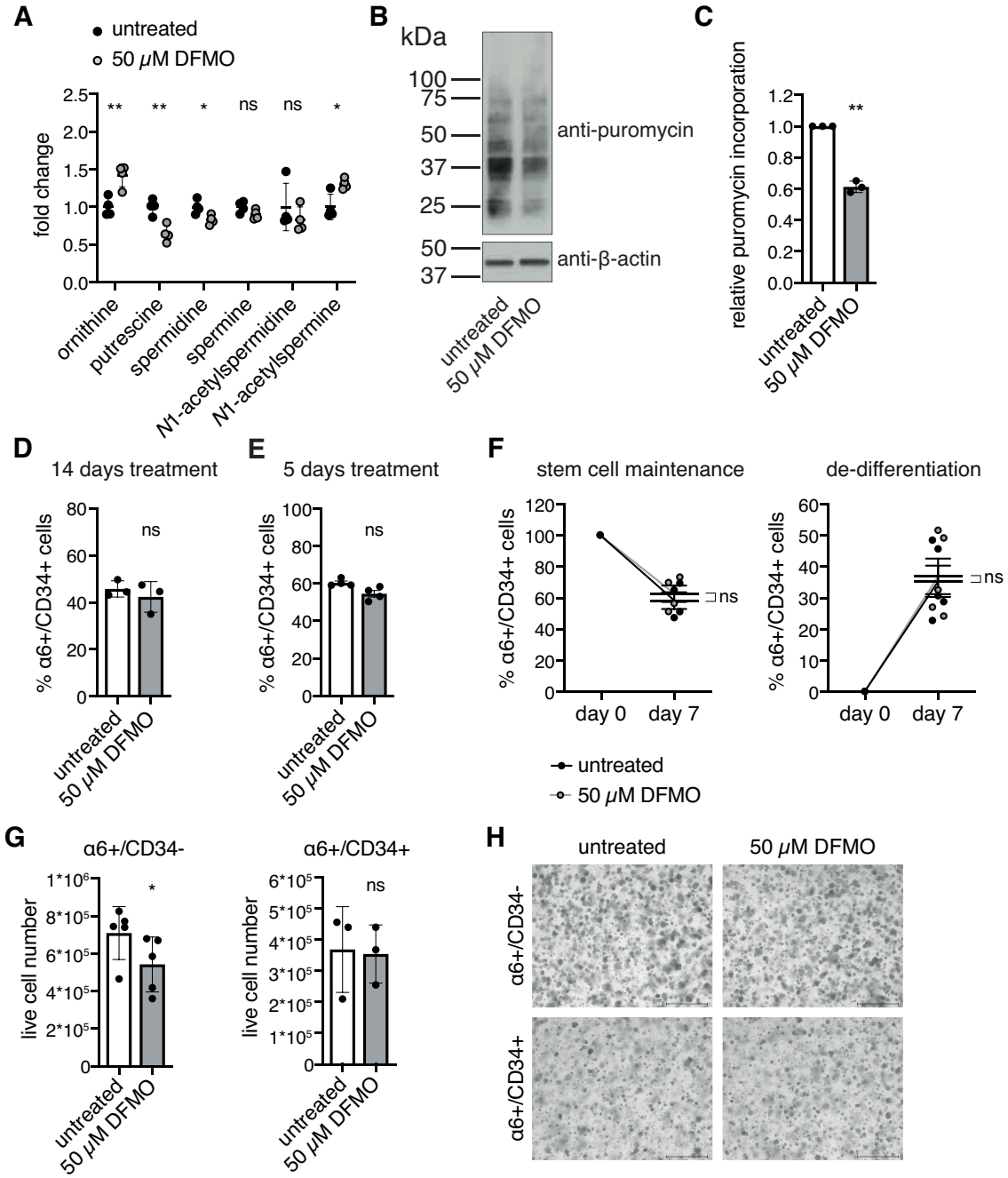

Figure 23: DFMO treatment reduces polyamine levels and translation without effect on HFSC fate. (**A**) Polyamine levels in 3D-3C cultured cells with and without 50 µM DFMO treatment. Mean ± SEM (n=4). (**B**) Representative Western blot analysis after puromycin incorporation in 3D-3C cultured cells with or without DFMO treatment for the last 72 h of culture. (**C**) Quantification of Western blot analysis after puromycin incorporation as shown in (**B**). Mean ± SD (n=3). (**D**) Ratio of α6+/CD34+ cells after two weeks of 3D-3C culture with or without 50 µM DFMO treatment for 14 days. Mean ± SEM (n=3). (**E**) Ratio of α6+/CD34+ cells after two weeks of 3D-3C culture with or without 50 µM DFMO treatment for the last 5 days. Mean ± SEM (n=4). (**F**) Ratio of α6+/CD34+ cells on day 0 and day 7 post-sorting starting from 100 % α6+/CD34+ cells (left) or 100 % α6+/CD34- cells (right) with or without DFMO treatment for the last 5 days of culture. Mean ± SEM (n≥3). (**G**) Live cell number of α6+/CD34- cells (left) and α6+/CD34+cells (right) on day 7 post-sorting. Treatment was performed for the last 5 days of culture. Mean ± SD (n≥3). (**H**) Representative images of organoid cultures on day 7 post-sorting. Treatment was performed for the last 5 days of culture. (**A**, **F**) Statistical significance was calculated by unpaired t-test. p-values: ** p<0.01, * p<0.05, ns: not significant. (**C**-**E**, **G**) Statistical significance was calculated by paired t-test. two-tailed p-values: ** p<0.01, ns: not significant.

2.3.2.2 DENSpm treatment regulates hair follicle stem cell fate decisions without reducing translation

Since G418 and DFMO supplementation reduced translation rates but differently affected stemness, I aimed to further investigate the influence of polyamine availability on HFSC fate decisions in the 3D-3C organoids. To this end, I used the spermine analog *N*1,*N*11-diethylnorspermine (DENSpm). DENSpm increases SSAT expression, mRNA stability, and enzyme activity (Coleman et al. 1995; Parry et al. 1995; Fogel-Petrovic et al. 1996) and thereby activates polyamine catabolism (Figure 8). DENSpm, like other polyamine analogs, is described to deplete natural polyamines, while the acetylated forms accumulate (Uimari et al. 2009). Andrea Annibal confirmed the described effects of DENSpm on polyamine levels in the 3D-3C organoids (Figure 24A). Remarkably, the DENSpm effect on intracellular polyamine levels resembled the one that D-mannose addition had (Figure 20D). The depletion of natural polyamines by DENSpm treatment or by SSAT OE has been shown to decrease mRNA translation in mammalian cells (Landau et al. 2010; Mandal et al. 2013). However, short-term DENSpm treatment, which did not change the HFSC ratio in the oragnoids (data not shown), did not affect puromycin incorporation in the organoid culture (Figure 24B-C). Intriguingly, treatment with 10 µM DENSpm resulted in a significant increase in α6+/CD34+ stem cells after two weeks of 3D-3C culture, although translation rates were not reduced (Figure 24D). Treatment for the last five days of the culture was sufficient to enhance stemness (Figure 24E). To investigate stem cell maintenance and de-differentiation separately, pure populations were sorted and cultured for one week with or without DENSpm treatment and the stem cell ratio was analyzed. Interestingly, DENSpm treatment increased both stem cell maintenance and de-differentiation (Figure 24F). DENSpm treatment in the 3D-3C organoids significantly increased the number of colonies in a colony formation assay, suggesting a higher proliferative potential, thereby confirming stem cell identity (Figure 24G-H). Thus, DENSpm treatment favored the HFSC state without reducing translation rates in the 3D-3C organoids.

DENSpm treatment has been shown to induce cell detachment and apoptosis in glioblastoma cells (Tian et al. 2012). Thus, I investigated apoptosis in DENSpm treated organoids. Of note, while annexin V staining was generally higher in α6+/CD34- progenitors, DENSpm treatment did not affect apoptosis in any of the cell types (Figure 24I). Since DENSpm treatment had a similar effect on intracellular polyamine levels as D-mannose addition and D-mannose supplementation reduced proliferation, I

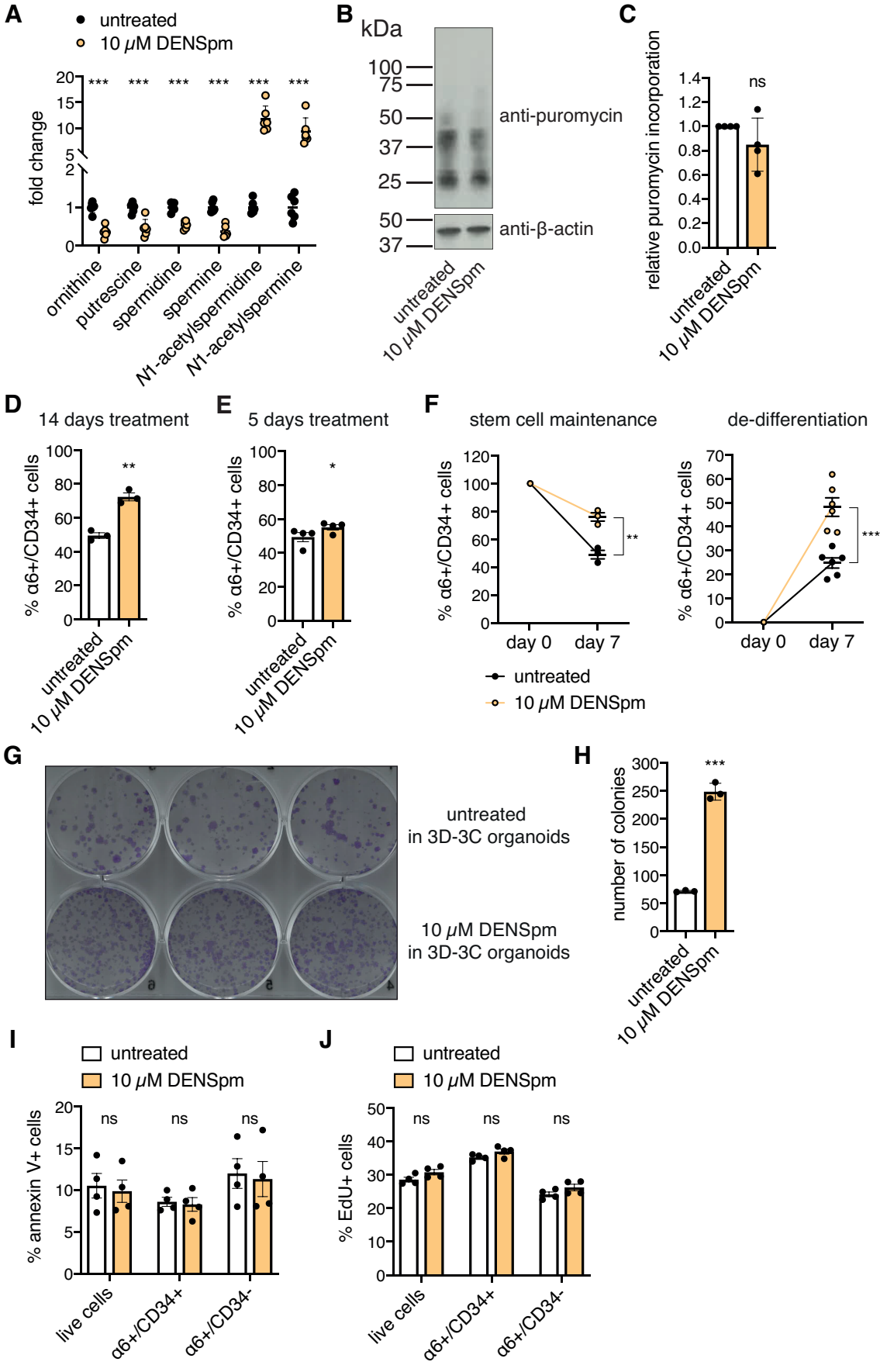

(Figure 24: legend on next page)

measured EdU incorporation in DENSpm treated organoids: EdU was incorporated comparable to untreated cells in both cell types (Figure 24J). This result indicated that stem cells actively self-renew when starting from pure populations (Figure 24F). In line with previously published data (Chacón-Martínez et al. 2017), EdU incorporation was higher in α6+/CD34+ HFSCs compared to α6+/CD34- progenitors (Figure 24J).

Overall, these results suggest that low translation rates achieved by decreased polyamine availability and stemness do not correlate in the HFSC organoids. While DFMO treatment effectively reduced translation rates without effect on stemness, DENSpm supplementation was not sufficient to affect translation rates but favored the HFSC fate in the 3D-3C organoids.

2.3.3 Polyamine availability influences hair follicle stem cell fate decisions independently of reduced translation

DENSpm treatment affected HFSC fate without reducing translation rates in the organoid culture. Thus, the changes in intracellular polyamine levels upon DENSpm addition favor the HFSC state through an independent mechanism.

DENSpm supplementation resulted in a depletion of the natural polyamines and an accumulation of the acetylated forms in the 3D-3C organoids (Figure 24A). To elucidate which of these effects was responsible for the increase in stemness, I supplemented DENSpm treated cells with putrescine to rescue the reduction of natural polyamines. When starting from pure populations the double treatment showed a partial rescue compared to

Figure 24: DENSpm treatment is not sufficient to reduce translation rates but enhances stemness in the organoids. (**A**) Polyamine levels in 3D-3C cultured cells with and without 10 µM DENSpm treatment. Mean ± SEM (n=6). (**B**) Representative Western blot analysis after puromycin incorporation in 3D-3C cultured cells with or without DENSpm treatment for the last 72 h of culture. (**C**) Quantification of Western blot analysis after puromycin incorporation as shown in (**B**). Mean ± SD (n=4). (**D**) Ratio of α6+/CD34+ cells after two weeks of 3D-3C culture with or without 10 µM DENSpm treatment for 14 days. Mean ± SEM (n=3). (**E**) Ratio of α6+/CD34+ cells after two weeks of 3D-3C culture with or without 10 µM DENSpm treatment for the last 5 days. Mean ± SEM (n=4). (**F**) Ratio of α6+/CD34+ cells on day 0 and day 7 post-sorting starting from 100 % α6+/CD34+ cells (left) or 100 % α6+/CD34- cells (right) with or without DENSpm treatment for the last 5 days of culture. Mean ± SEM (n≥3). (**G**) Representative image of tissue culture plate after colony formation assay using cells with or without DENSpm treatment in 3D-3C organoids (n=2). (**H**) Quantification of colony number in (**G**). Mean ± SD (n=3). (**I**) Ratio of annexin V+ 3D-3C cultured cells with or without DENSpm treatment for the last 24 h of culture. Mean ± SEM (n=4). (**J**) Ratio of EdU+ 3D-3C cultured cells with or without DENSpm treatment for the last 72 h of culture. EdU was incorporated for 2 h. Mean ± SEM (n=4). (**A**, **F**, **H**-**J**) Statistical significance was calculated by unpaired t-test. p-values: *** p<0.001, ** p<0.01, ns: not significant. (**C**-**E**) Statistical significance was calculated by paired t-test. two-tailed p-values: ** p<0.01, * p<0.05; ns: not significant.

DENSpm alone; stem cell maintenance and de-differentiation were decreased (Figure 25A). These data indicated that the depletion of the natural polyamines partially contributed to the observed cell fate changes. However, stem cell maintenance and de-differentiation were still significantly affected upon the double treatment compared to untreated cells (Figure 25A). This result elicits the following three hypotheses: first, the putrescine concentration was too low to replenish the natural polyamines; second, putrescine itself affects cell fate; third, DENSpm treatment determines HFSC fate by the accumulation of the acetylated polyamines.

Spermine analogs, like DENSpm, have been described to inhibit cell growth due to the depletion of the natural polyamines (Libby et al. 1989; Porter et al. 1991). Accordingly, DENSpm treatment reduced the live cell number of α6+/CD34- progenitors and α6+/CD34+ HFSCs (Figure 25B-C). Of note, additional putrescine supplementation rescued this defect in cell growth (Figure 25B-C), suggesting that the putrescine concentration used was sufficient to replenish the natural polyamines. Thus, the partial rescue of stem cell maintenance and de-differentiation upon the double treatment was not due to incomplete replenishment of the natural polyamines.

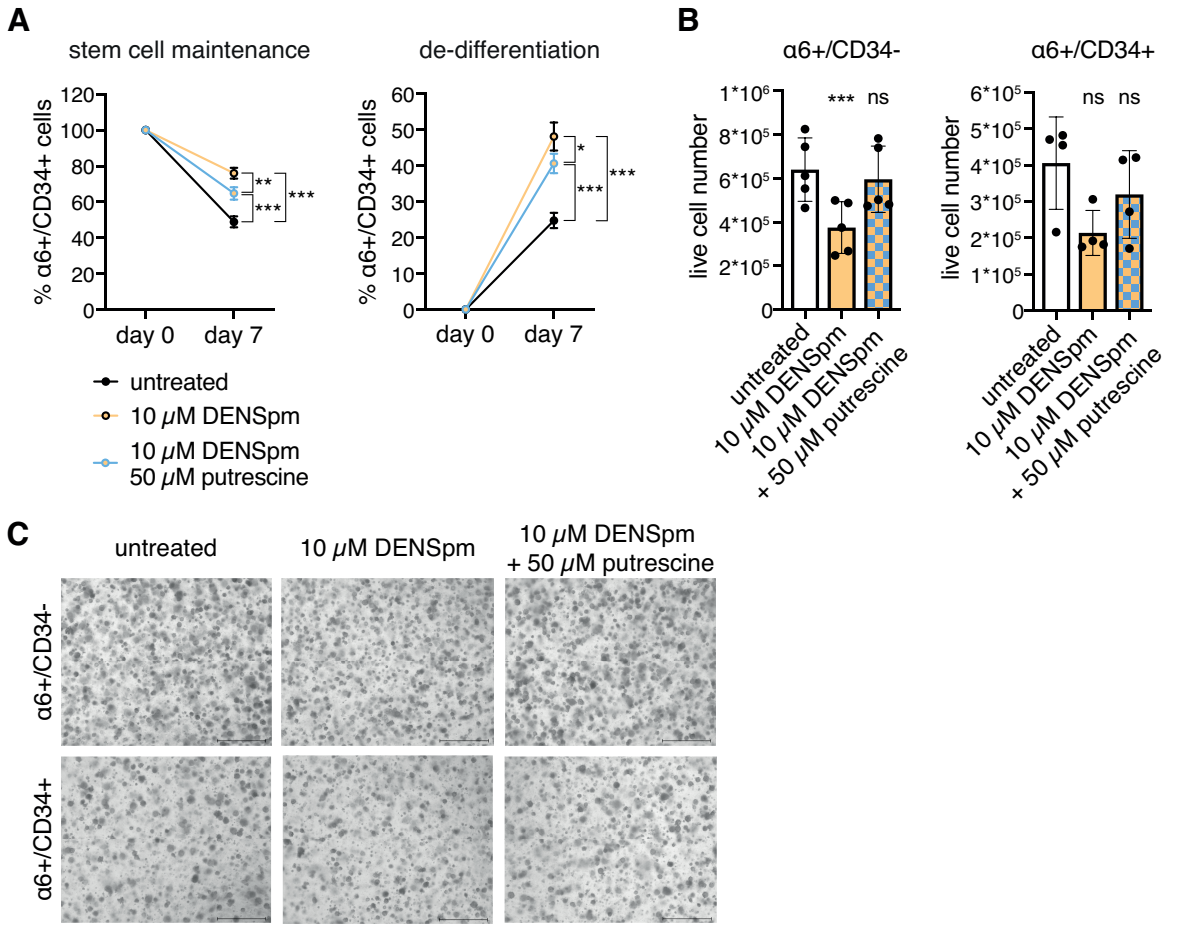

(Figure 25: legend on next page)

To exclude that additional putrescine supplementation only partially rescued the DENSpm effect on stem cell maintenance and de-differentiation (Figure 25A) because putrescine itself affects cell fate, I tested putrescine addition in the organoid culture. Remarkably, putrescine treatment increased the number of α6+/CD34+ stem cells, when supplemented for the whole duration of the culture (Figure 26A). Putrescine treatment for the last five days of culture was not sufficient to enhance stemness (Figure 26B). When starting from pure populations, putrescine supplementation specifically elevated de-differentiation of α6+/CD34- progenitor cells to α6+/CD34+ HFSCs, but did not affect stem cell maintenance (Figure 26C). However, the effect on de-differentiation was not as pronounced as with the double treatment (Figure 26A). Stem cell identity was confirmed by elevated colony number, showing increased proliferative potential (Figure 26D-E). Putrescine supplementation did not affect the live cell number of progenitors or HFSCs (Figure 26F-G). Also, puromycin incorporation was unchanged upon short-term putrescine addition (Figure 26H-I). To further investigate the effect of putrescine supplementation, Andrea Annibal measured intracellular polyamine levels in the 3D-3C organoids. Spermidine and *N*1-AcSpd levels were increased in response to putrescine supplementation (Figure 26J). The elevation of putrescine levels confirmed the effectiveness of the treatment (Figure 26J). In sum, increased polyamine availability upon putrescine addition was sufficient to elevate de-differentiation of progenitors back to the stem cell state, while stem cell maintenance was not affected. However, the putrescine-mediated effect on cell fate was not strong enough to account for the changes seen with the double treatment. Therefore, I speculated that the accumulation of the acetylated polyamines favored the stem cell state in DENSpm-treated cultures.

Figure 25: Additional putrescine supplementation partially rescues the DENSpm-mediated effect on HFSCs and live cell number. (**A**) Ratio of α6+/CD34+ cells at day 0 and day 7 post-sorting starting from 100 % α6+/CD34+ cells (left) or 100 % α6+/CD34- cells (right) with or without DENSpm or additional putrescine treatment for the last 5 days. Mean ± SEM (n≥3). Two-way ANOVA Tukey post-test. *** p<0.001, ** p<0.01, * p<0.05. (**B**) Live cell number of α6+/CD34- cells (left) and α6+/CD34+cells (right) on day 7 post-sorting. Treatment was performed for the last 5 days of culture. Mean ± SD (n≥4). Statistical significance was calculated by One-way ANOVA Dunnett post-test. p-values: *** p<0.001, ns: not significant. (**C**) Representative images of organoid cultures on day 7 post-sorting. Treatment was performed for the last 5 days of culture.

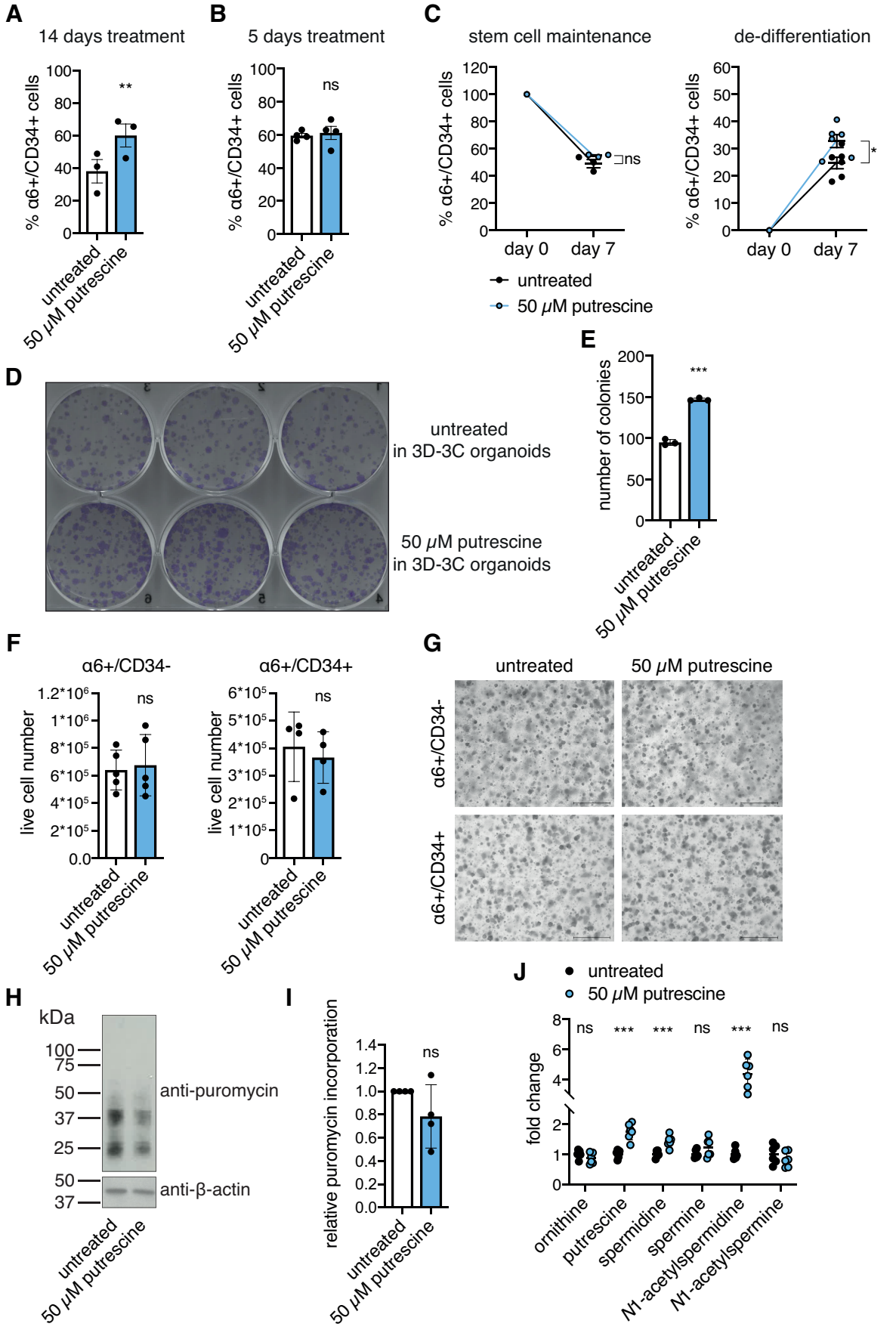

(Figure 26: legend on next page)

2.3.3.1 *N*1-acetylspermidine is a novel determinant of hair follicle stem cell fate decisions

Since both DENSpm and putrescine supplementation led to elevated *N*1-AcSpd levels (Figure 24A and Figure 26J), I hypothesized that it is not the accumulation of the acetylated polyamines in general, but that increased *N*1-AcSpd levels in particular are responsible for the observed cell fate changes. Intriguingly, *N*1-AcSpd treatment significantly increased the number of α6+/CD34+ stem cells in the 3D-3C organoids (Figure 27A). Supplementation for the last five days of culture was sufficient to enhance stemness (Figure 27B). In contrast to putrescine addition, *N*1-AcSpd treatment enhanced not only de-differentiation, but also stem cell maintenance when starting from pure populations (Figure 27C). Stemness was confirmed by enhanced proliferative potential in the colony formation assay (Figure 27D-E). Overall, these data implicate *N*1-AcSpd as a novel regulator of cell fate.

To test the *N*1-AcSpd-mediated effect on translation rates, I analyzed puromycin incorporation. Interestingly, translation rates were elevated upon short-term *N*1-AcSpd treatment (Figure 27F-G), which did not affect the ratio of HFSCs in the 3D-3C organoids (data not shown). This result strengthens the hypothesis that polyamine availability influences cell fate decisions independent of reduced protein synthesis, but through a different mechanism. To better understand the consequences of *N*1-AcSpd treatment, Andrea measured intracellular polyamine levels and found that apart from *N*1-AcSpd, also putrescine was increased (Figure 27H). Thus, the effect of *N*1-AcSpd treatment on intracellular polyamines resembled the putrescine supplementation (Figure 26J). Therefore, I aimed to discern the impact of *N*1-AcSpd from the putrescine-mediated effect.

Figure 26: Putrescine supplementation enhances de-differentiation. (**A**) Ratio of α6+/CD34+ cells after two weeks of 3D-3C culture with or without putrescine treatment for 14 days. Mean ± SEM (n=3). (**B**) Ratio of α6+/CD34+ cells after two weeks of 3D-3C culture with or without putrescine treatment for the last 5 days. Mean ± SEM (n=4). (**C**) Ratio of α6+/CD34+ cells at day 0 and day 7 post-sorting starting from 100 % α6+/CD34+ cells (left) or 100 % α6+/CD34- cells (right) with or without putrescine treatment for the last 5 days of culture. Mean ± SEM (n≥3). (**D**) Representative image of tissue culture plate after colony formation assay using cells with or without putrescine treatment in 3D-3C organoids (n=2). (**E**) Quantification of colony number of plate in (**D**). Mean ± SD (n=3). (**F**) Live cell number of α6+/CD34- cells (left) and α6+/CD34+cells (right) on day 7 post-sorting. Treatment was performed for the last 5 days of culture. Mean ± SD (n≥4). (**G**) Representative images of organoid cultures on day 7 post-sorting. Treatment was performed for the last 5 days of culture. (**H**) Representative Western blot analysis after puromycin incorporation in 3D-3C cultured cells with or without putrescine treatment for the last 72 h of culture. (**I**) Quantification of Western blot analysis after puromycin incorporation as shown in (**H**). Mean ± SD (n=4). (**J**) Polyamine levels in 3D-3C cultured cells with and without 50 µM putrescine treatment. Mean ± SEM (n=6). (**A**-**B**, **F**, **I**) Statistical significance was calculated by paired t-test. two-tailed p-values: ** p<0.01, ns: not significant. (**C**, **E**, **J**) Statistical significance was calculated by unpaired t-test. p-values: *** p<0.001, * p<0.05, ns: not significant.

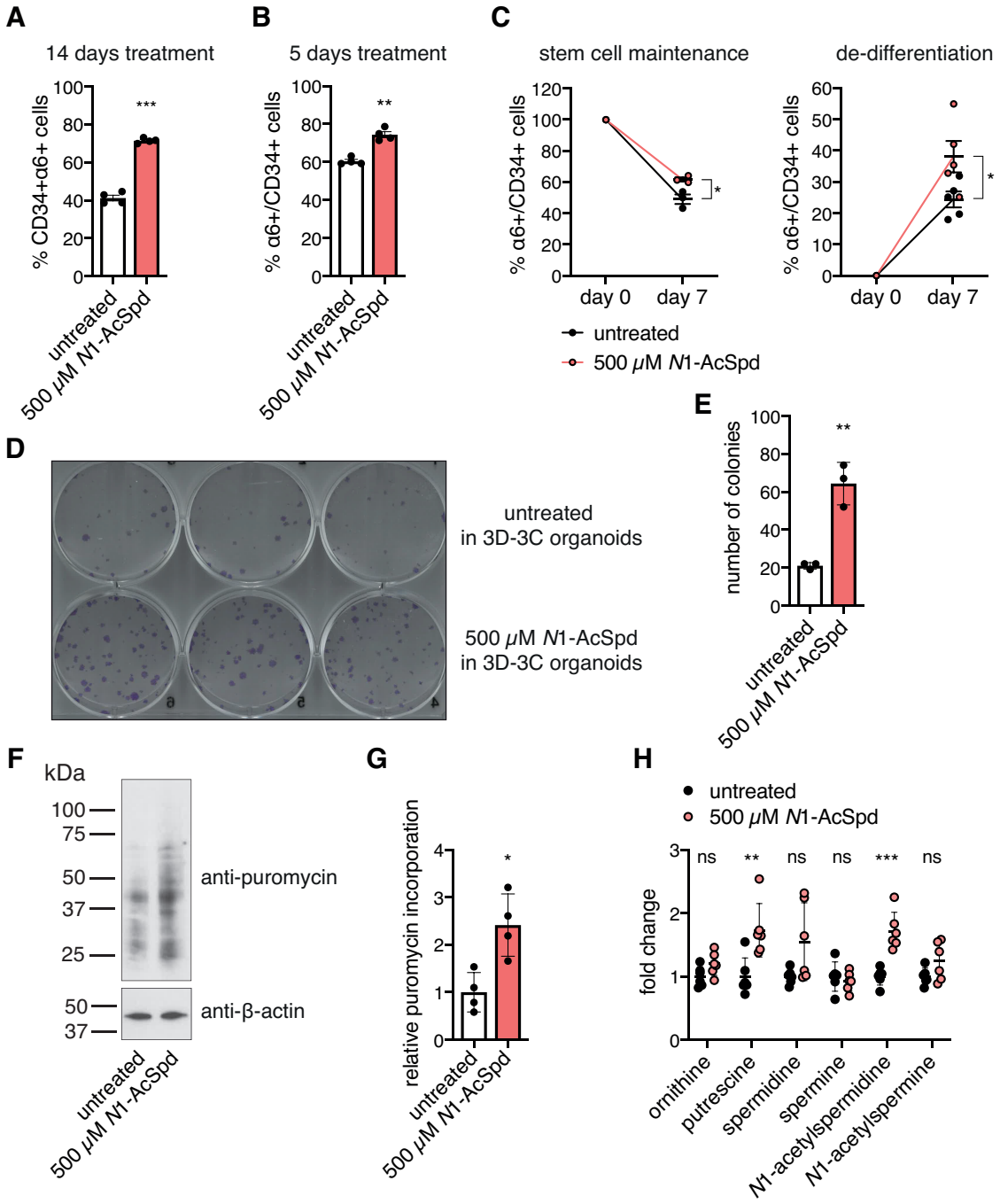

Figure 27: *N*1-acetylspermidine treatment influences cell fate decisions in the 3D-3C organoids. (**A**) Ratio of α6+/CD34+ cells after two weeks of 3D-3C culture with or without *N*1-AcSpd treatment for 14 days. Mean ± SEM (n=3). (**B**) Ratio of α6+/CD34+ cells after two weeks of 3D-3C culture with or without *N*1-AcSpd treatment for the last 5 days. Mean ± SEM (n=4). (**C**) Ratio of α6+/CD34+ cells at day 0 and day 7 post-sorting starting from 100 % α6+/CD34+ cells (left) or 100 % α6+/CD34- cells (right) with or without *N*1-AcSpd treatment for the last 5 days of culture. Mean ± SEM (n≥3). (**D**) Representative image of tissue culture plate after colony formation assay using cells with or without *N*1-AcSpd treatment in 3D-3C organoids (n=3). (**E**) Quantification of colony number of plate in (**D**). Mean ± SD (n=3). (**F**) Representative Western blot analysis after puromycin incorporation in 3D-3C cultured cells. *N*1-AcSpd treatment was performed for the last 72 h of the culture. (**G**) Quantification of the Western blot analysis after puromycin incorporation as shown in (**F**). Mean ± SD (n=4). (**H**) Polyamine levels in 3D-3C cultured cells with or without *N*1-AcSpd treatment. Mean ± SEM (n=6). (**A**-**B**, **G**) Statistical significance was calculated by paired t-test. two-tailed p-values: *** p<0.001, ** p<0.01, * p<0.05. (**C**, **E**, **H**) Statistical significance was calculated by unpaired t-test. p-values: *** p<0.001, ** p<0.01, * p<0.05, ns: not significant.

To dissect the putrescine- and *N*1-AcSpd-mediated effect, I prevented the conversion of putrescine to *N*1-AcSpd and *vice versa*: inhibition of PAOX impedes the oxidation of *N*1-AcSpd to putrescine, whereas inhibition of SSAT blocks the acetylation of spermidine to *N*1-AcSpd (Figure 8). First, I tested MDL72527, which is an irreversible inhibitor of the polyamine oxidases PAOX and SMOX (Bey et al. 1985). Importantly, SMOX inhibition by MDL72527 is less efficient than its effect on PAOX (Moriya et al. 2014). Therefore, MDL72527 addition should result in the accumulation of the acetylated polyamines *N*1-AcSpd and *N*1-AcSpm without major impact on the natural polyamines. Intriguingly, MDL72527 treatment significantly increased the number of α6+/CD34+ stem cells in the 3D-3C organoids (Figure 28A). Treatment for the last five days of the culture was sufficient to affect cell fate (Figure 28B). When starting from pure populations, MDL72527 addition elevated stem cell maintenance and de-differentiation (Figure 28C). These effects were accompanied by reduced live cell numbers of α6+/CD34- progenitors and α6+/CD34+ stem cells (Figure 28D-E). Since the viability of α6+/CD34- progenitors was reduced to a greater extend, the increase in the HFSC ratio might be partially caused by selective loss of progenitor cells. Nevertheless, de-differentiation was affected by MDL72527 treatment, suggesting a change in cell fate decisions. Overall, the MDL72527-mediated effects resembled the ones DENSpm treatment had. This finding further supports the hypothesis that the accumulation of the acetylated polyamines determines cell fate decisions in DENSpm-treated cultures.

Second, I used diminazene aceturate (DA), which inhibits SSAT (Wu et al. 1996; Neidhart et al. 2014). Thereby, DA addition should result in the reduction of the acetylated polyamines *N*1-AcSpd and *N*1-AcSpm, while the levels of putrescine should remain unchanged. Remarkably, DA treatment significantly reduced the number of α6+/CD34+ stem cells in the 3D-3C organoids (Figure 28F). Treatment for the last five days of the culture was sufficient to recapitulate this effect (Figure 28G). Both stem cell maintenance and de-differentiation were reduced by DA addition (Figure 28H). Interestingly, DA treatment decreased the live cell number of α6+/CD34- progenitors, but did not affect the viability of α6+/CD34+ stem cells (Figure 28I-J). Thus, the reduction of the HFSC ratio would be even more pronounced if the viability of the progenitor cells was not affected. Taken together, the data obtained upon inhibition of SSAT and PAOX confirm that the accumulation of the acetylated polyamines is not only required but also sufficient to enhance stemness in the HFSC organoids.

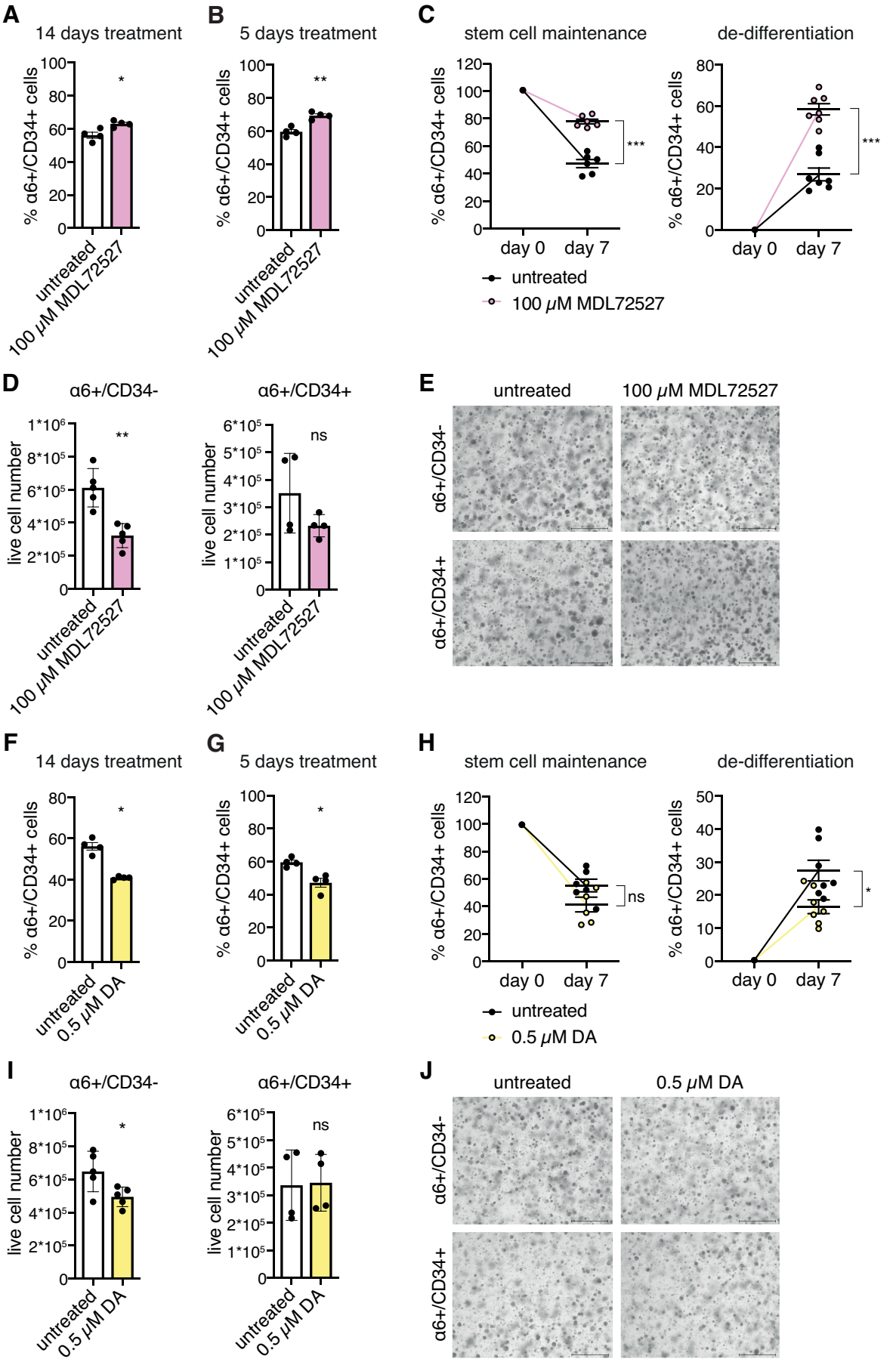

(Figure 28: legend on next page)

Since DENSpm and MDL72527 strongly increased stem cell maintenance and de-differentiation likely via increased levels of the acetylated polyamines *N*1-AcSpd and *N*1-AcSpm, I aimed to investigate the effect of *N*1-AcSpm treatment on cell fate. Surprisingly, supplementation with *N*1-AcSpm did not influence the ratio of HFSCs (Figure 29A-B). Stem cell maintenance and de-differentiation were not affected by *N*1-AcSpm treatment (Figure 29C). The live cell number tended to be decreased in α6+/CD34- progenitors and increased in α6+/CD34+ stem cells; however, this effect was not significant (Figure 29D-E). Overall, these data clearly demonstrate that elevation of the acetylated polyamines in general was not sufficient; rather, *N*1-AcSpd treatment had a specific effect on cell fate. Thus, the cell fate changes observed upon DENSpm (Figure 24F) and MDL72527 treatment (Figure 28C) are caused by increased levels of *N*1-AcSpd. Surprisingly, short-term *N*1-AcSpm treatment reduced puromycin incorporation in the organoid culture (Figure 29F-G). These data further support the finding that reducing translation rates by changes in polyamine availability does not increase stemness in the organoid culture.

Figure 28: Inhibition of PAOX and SSAT confirms the acetylated polyamines as novel regulator of cell fate decisions. (**A**) Ratio of α6+/CD34+ cells after two weeks of 3D-3C culture with or without MDL72527 treatment for 14 days. Mean ± SEM (n=4). (**B**) Ratio of α6+/CD34+ cells after two weeks of 3D-3C culture with or without MDL72527 treatment for the last 5 days. Mean ± SEM (n=4). (**C**) Ratio of α6+/CD34+ cells at day 0 and day 7 post-sorting starting from 100 % α6+/CD34+ cells (left) or 100 % α6+/CD34- cells (right) with or without MDL72527 treatment for the last 5 days of culture. Mean ± SEM (n≥6). (**D**) Live cell number of α6+/CD34- cells (left) and α6+/CD34+cells (right) on day 7 post-sorting. Treatment was performed for the last 5 days of culture. Mean ± SD (n≥4). (**E**) Representative images of organoid cultures on day 7 post-sorting. Treatment was performed for the last 5 days of culture. (**F**) Ratio of α6+/CD34+ cells after two weeks of 3D-3C culture with or without diminazene aceturate (DA) treatment for 14 days. Mean ± SEM (n=4). (**G**) Ratio of α6+/CD34+ cells after two weeks of 3D-3C culture with or without DA treatment for the last 5 days. Mean ± SEM (n=4). (**H**) Ratio of α6+/CD34+ cells at day 0 and day 7 post-sorting starting from 100 % α6+/CD34+ cells (left) or 100 % α6+/CD34- cells (right) with or without DA treatment for the last 5 days of culture. Mean ± SEM (n≥5). (**I**) Live cell number of α6+/CD34- cells (left) and α6+/CD34+cells (right) on day 7 post-sorting. Treatment was performed for the last 5 days of culture. Mean ± SD (n≥4). (**J**) Representative images of organoid cultures on day 7 post-sorting. Treatment was performed for the last 5 days of culture. (**A**-**B**, **D**, **F**-**G**, **I**) Statistical significance was calculated by paired t-test. two-tailed p-values: ** p<0.01, * p<0.05, ns: not significant. (**C**, **H**) Statistical significance was calculated by unpaired t-test. p-values: *** p<0.001, * p<0.05, ns: not significant.

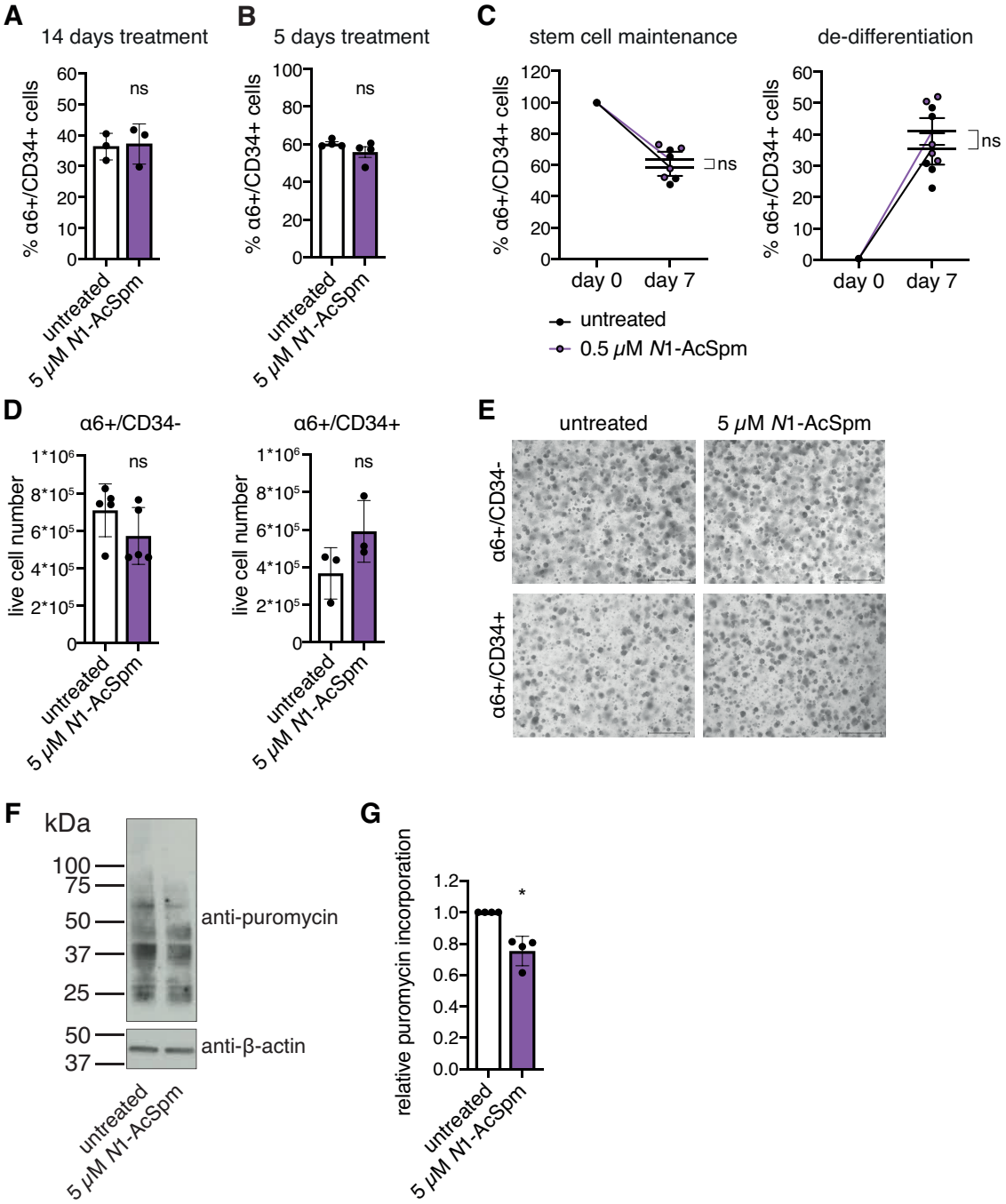

Figure 29: *N*1-acetylspermine treatment does not affect HFSC fate in the organoid culture. (**A**) Ratio of α6+/CD34+ cells after two weeks of 3D-3C culture with or without *N*1-AcSpm treatment for 14 days. Mean ± SEM (n=3). (**B**) Ratio of α6+/CD34+ cells after two weeks of 3D-3C culture with or without *N*1-AcSpm treatment for the last 5 days. Mean ± SEM (n=4). (**C**) Ratio of α6+/CD34+ cells at day 0 and day 7 post-sorting starting from 100 % α6+/CD34+ cells (left) or 100 % α6+/CD34- cells (right) with or without *N*1-AcSpm treatment for the last 5 days of culture. Mean ± SEM (n≥4). Statistical significance was calculated by unpaired t-test. p-value: ns: not significant. (**D**) Live cell number of α6+/CD34- cells (left) and α6+/CD34+cells (right) on day 7 post-sorting. Treatment was performed for the last 5 days of culture. Mean ± SD (n≥3). (**E**) Representative images of organoid cultures on day 7 post-sorting. Treatment was performed for the last 5 days of culture. (**F**) Representative Western blot analysis after puromycin incorporation in 3D-3C cultured cells with or without *N*1-AcSpm treatment for the last 72 h of culture. (**G**) Quantification of Western blot analysis after puromycin incorporation as shown in (**F**). Mean ± SD (n=4). (**A**-**B**, **D**, **G**) Statistical significance was calculated by paired t-test. two-tailed p-values: * p<0.05, ns: not significant.

2.3.3.2 *N*1-acetylspermidine treatment affects hair follicle stem cell fate decisions by increasing proliferation

To elucidate the molecular mechanism by which *N*1-AcSpd supplementation promotes stemness, I performed 3' RNA-sequencing of 3D-3C cultured cells upon short-term *N*1-AcSpd treatment. HFSCs and progenitor cells were purified and analyzed separately (Figure 30A). To identify differentially expressed genes for untreated control cells and *N*1-AcSpd treatment, α6+/CD34- progenitors were compared with α6+/CD34+ HFSCs (Figure 30B). I subjected the two groups of differentially expressed genes to further analysis. Around 2.200 genes with differential expression between cell types were not affected by *N*1-AcSpd treatment (Figure 30C). 851 genes were differentially expressed between HFSCs and progenitors only in the presence of *N*1-AcSpd, while 540 genes were differentially expressed between cell types exclusively in untreated control cells (Figure 30C).

Skin development was the most significant GO term when the around 2.200 genes not affected by *N*1-AcSpd treatment were analyzed (Figure 30D). This result suggests that *N*1-AcSpd treatment did not affect general cell identity in the 3D-3C organoids. Consistently, a comparison of the gene expression changes between cell types in a heat map showed a clear separation of α6+/CD34+ HFSCs and α6+/CD34- progenitors (Figure 30E). Although *N*1-AcSpd treated cells clustered separately of untreated control cells, their gene expression was very similar to the respective cell type in the control (Figure 30E). Analysis of the 540 genes differentially expressed between cell types only in untreated cells showed low significance for all GO terms. The most significant GO terms were intraciliary transport and cilium organization (Figure 30F).

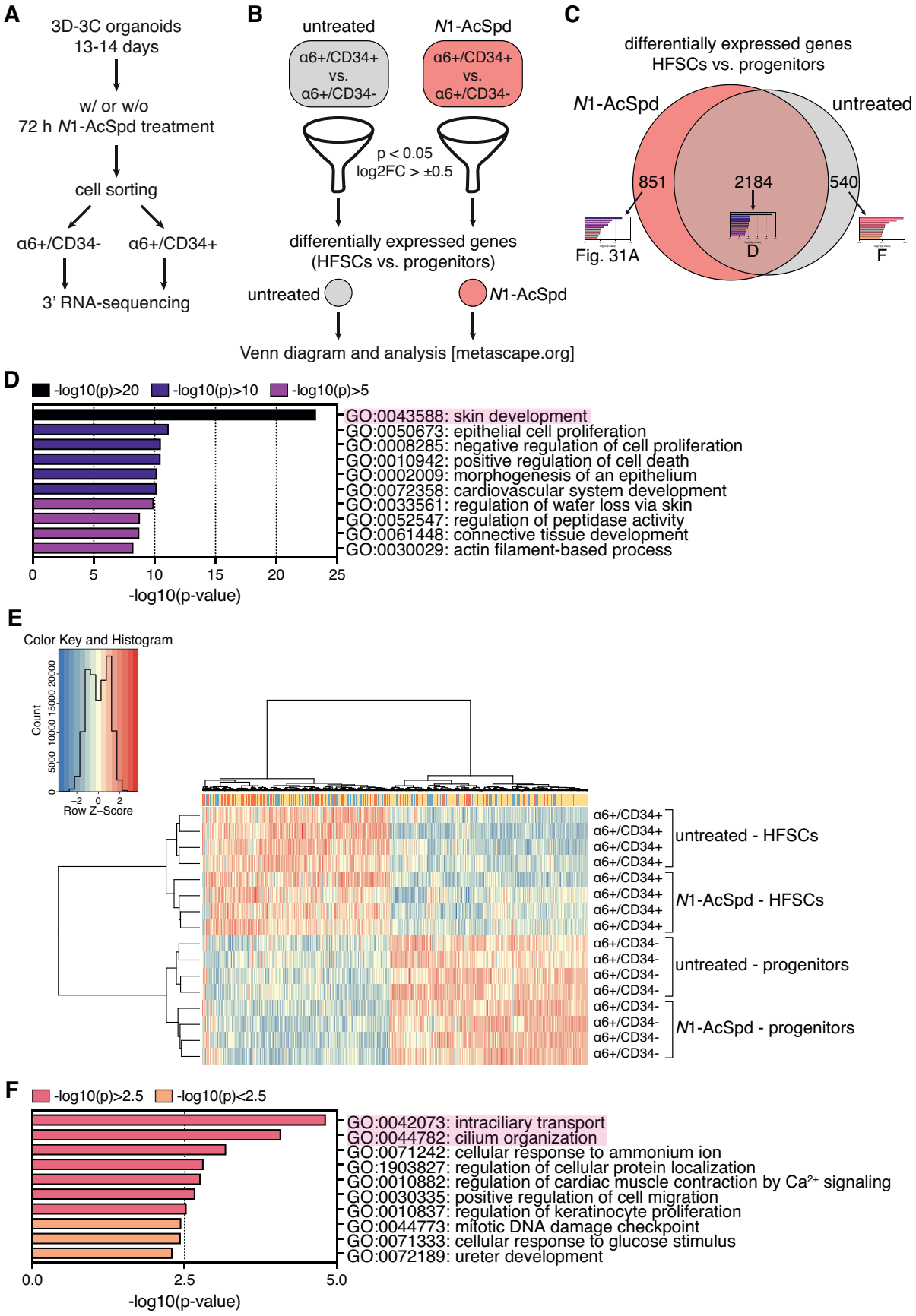

(Figure 30: legend on next page)

Strikingly, analysis of the genes differentially expressed between HFSCs and progenitors only during *N*1-AcSpd treatment revealed that most of the ten highest ranked GO terms were linked to cell cycle progression (Figure 31A). The most significantly enriched GO term upon analysis of the genes differentially expressed between HFSCs and progenitors only during *N*1-AcSpd treatment was cell division (Figure 31A). 54 genes of this GO term were present among the 851 differentially expressed genes between cell types upon *N*1-AcSpd treatment (Figure 31B). Interestingly, expression of the majority of these 54 genes was higher in α6+/CD34+ stem cells (Figure 31C). Importantly, *N*1-AcSpd treatment affected the amplitude of the fold change; the expression of these genes was higher also in the untreated α6+/CD34+ stem cells (Figure 31C). Consistently, EdU incorporation was higher in untreated α6+/CD34+ HFSCs compared to progenitor cells (Figure 31D). Together, these data suggest that *N*1-AcSpd selectively promoted self-renewal of HFSCs.

Figure 30: 3' RNA-sequencing confirms maintained cell identity upon *N*1-acetylspermidine treatment. (**A**) Schematic representation of the workflow for 3' RNA-sequencing sample collection. (**B**) Schematic representation of the bioinformatic workflow. α6+/CD34- cells and α6+/CD34+ cells were compared for untreated and *N*1-AcSpd treated conditions. Genes were filtered (p-value < 0.05, log2FC > ±0.5) and the resulting lists were used for further analysis. Untreated control is shown in gray, *N*1-AcSpd is depicted in red. (**C**) Venn diagram of the two groups from (**B**). Untreated control is shown in gray, *N*1-AcSpd is depicted in red. (**D**) GO term analysis of differentially expressed genes between cell types (p-value < 0.05, log2FC > ±0.5) from 3' RNA-sequencing experiment common in untreated and treated cells (overlap shown in (**C**), biological process, metascape.org). (**E**) Heat map showing differentially expressed genes with a p-value ≤ 0.05 (α6+/CD34- vs. α6+/CD34+; treated or untreated). (**F**) GO term analysis of differentially expressed genes between cell types (p-value < 0.05, log2FC > ±0.5) from 3' RNA-sequencing experiment only in untreated cells (gray in (**C**), biological process, metascape.org).

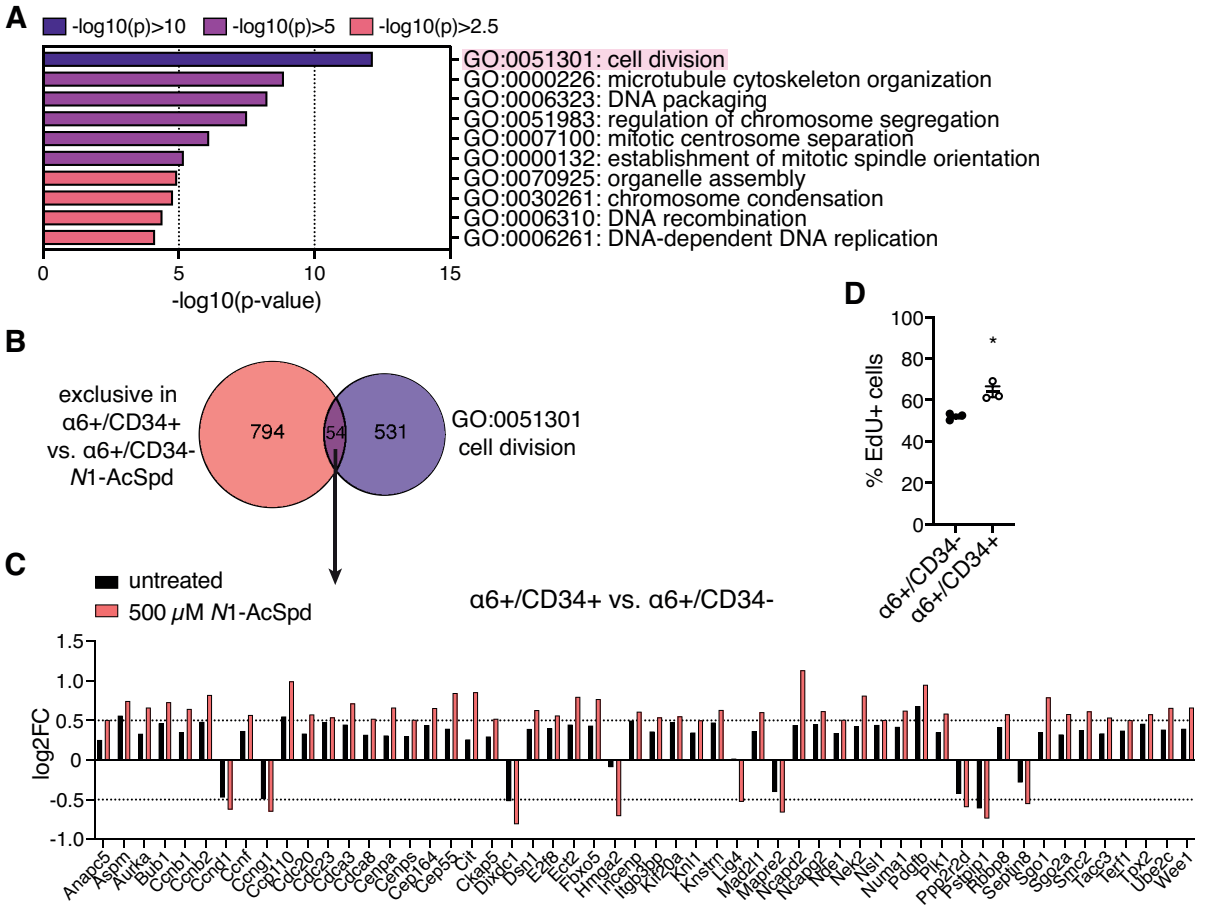

Figure 31: 3' RNA-sequencing results suggest increased cell cycle progression upon *N*1-acetylspermidine treatment. (**A**) GO term analysis of differentially regulated genes between cell types (p-value < 0.05, log2FC > ±0.5) from 3' RNA-sequencing experiment only upon *N*1-AcSpd treatment (depicted in red in Figure 30C, biological process, metascape.org). (**B**) Venn diagram of differentially expressed genes upon *N*1-AcSpd treatment (red) and genes covered by GO term cell division (purple). (**C**) log2FC of the genes associated with the GO term 'cell division' in untreated and *N*1-AcSpd treated cells. The ratio of the log2FC in α6+/CD34+ vs. α6+/CD34- cells is shown. (**D**) Ratio of EdU+ cells in α6+/CD34- progenitors and α6+/CD34+ HFSCs. EdU was incorporated for 24 h. Mean ± SEM (n=3). Statistical significance was calculated by paired t-test. Two-tailed p-value: * p<0.05.

Since the analysis of global gene expression changes clearly indicated that *N*1-AcSpd treatment would affect proliferation, I measured EdU incorporation in the 3D-3D organoids. Importantly, short-term *N*1-AcSpd supplementation increased the number of EdU+ cells (Figure 32A). The effect on α6+/CD34+ HFSCs was higher compared to α6+/CD34- progenitor cells (Figure 32A). Still, consistent with increased de-differentiation and elevated stem cell maintenance, proliferation of both populations was affected by the treatment. Furthermore, I analyzed the cell cycle phase distribution of the cells using FxCycle violet staining. Plotting of FxCycle violet intensity on the x-axis and EdU AF488 intensity on the y-axis enabled clear separation of the different cell cycle phases (Figure 32B). Consistent with increased EdU incorporation, I observed faster cell cycle

progression with fewer cells in G0/G1 phase and more cells in S phase upon short-term *N*1-AcSpd treatment (Figure 32C). The number of cells in G2/M phase was not changed. Taken together, these data suggest that the acetylated polyamine *N*1-AcSpd fulfills a functional role in cell cycle progression and that it affects cell fate by increasing proliferation. According to the enhanced cell cycle progression seen upon *N*1-AcSpd treatment, the cell number should be increased in the organoid culture. Surprisingly, the live cell number was increased in α6+/CD34+ stem cells only; viability of α6+/CD34- progenitors was not affected (Figure 32D-E). Of note, the live cell number in cultures starting from α6+/CD34- progenitors was higher compared to the cultures starting from α6+/CD34+ stem cells on day 7 post-sorting (Figure 32D-E). Thus, cell proliferation might be reduced to avoid cell crowding in α6+/CD34- progenitors.

To test whether the elevated cell proliferation seen upon *N*1-AcSpd treatment would result in premature exhaustion of the stem cells, I set up a long-term organoid culture. The cells were passaged each 11-14 days and the HFSC ratio and the live cell number were analyzed. When treated for the entire period of the culture, the number of α6+/CD34+ HFSCs was maintained at around 60% in untreated and at around 80% in treated organoids (Figure 32F), suggesting that the stem cells were not exhausted even under continuous treatment. The live cell number was slightly variable, but comparable between treated and untreated cultures during the first three passages (Figure 32G). Interestingly, the live cell number was increased in *N*1-AcSpd treated cultures on day 53 (Figure 32G). This result indicated that the treatment was still effective in the long-term culture. Furthermore, the unchanged live cell number in the first three passages might be caused by a self-regulatory mechanism to avoid crowding in the organoids, since the analysis was performed three days later compared to passage 4. Intriguingly, cell fate was also maintained in the long-term culture upon withdrawal of *N*1-AcSpd treatment after the first passage, shown by an elevated ratio of HFSCs (Figure 32H). The live cell number was not changed upon withdrawal of the treatment (Figure 32I).

In sum, these data suggest that N1-AcSpd drives HFSC fate decisions by enhancing cell cycle progression in the organoid culture. Of note, the *N*1-AcSpd-mediated effect on HFSC fate can be maintained for an extend period of time without exhaustion of the stem cells. The cells seem to memorize the treatment, since cell fate is also maintained upon withdrawal of the treatment.

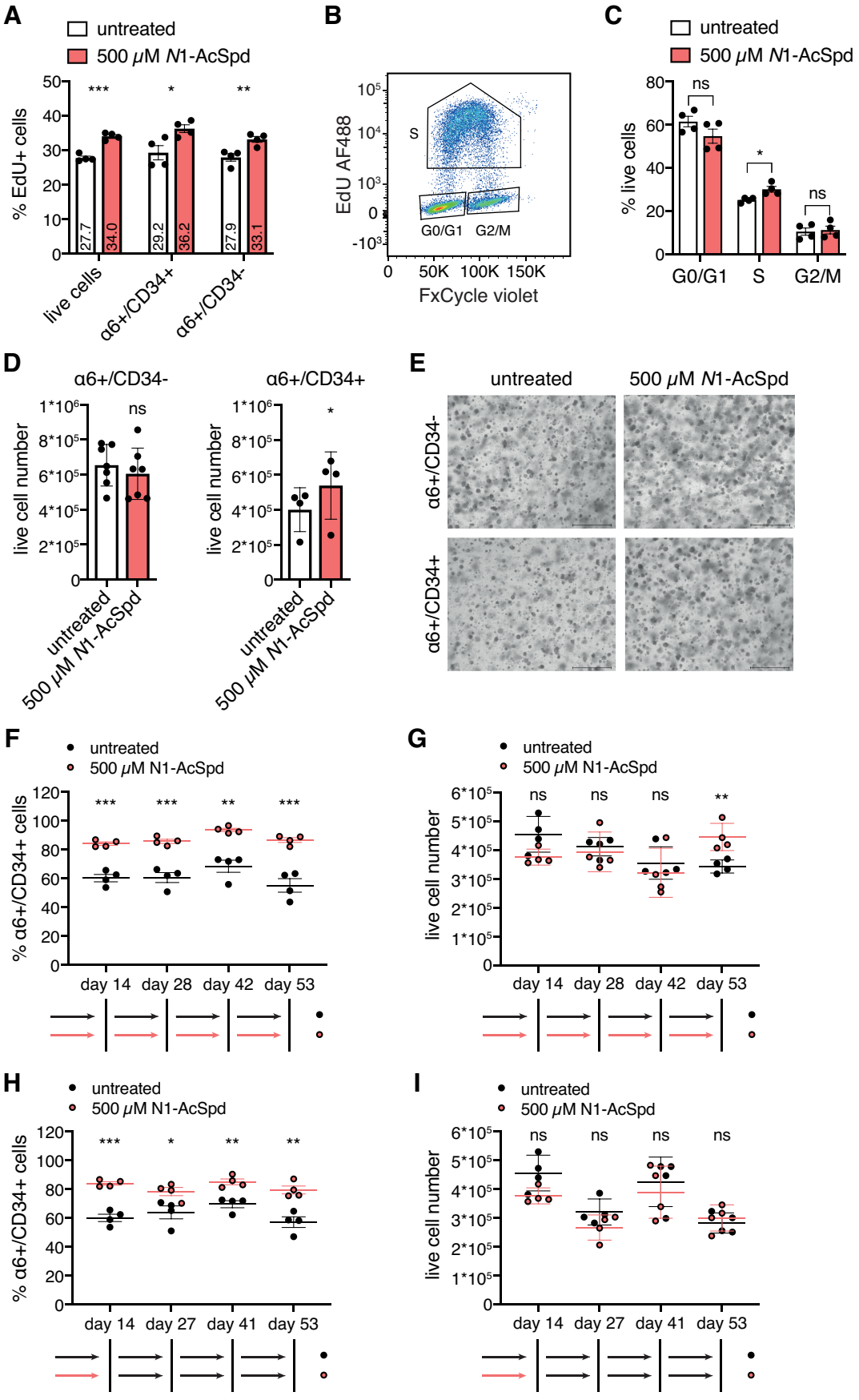

(Figure 32: legend on next page)

2.3.4 Hair follicle stem cell activation by depilation suggests a functional role of the acetylated polyamines in cell fate decisions *in vivo*

To investigate whether *N*1-AcSpd also plays a role in cell fate decisions *in vivo*, I performed a depilation experiment, comparing young and old mice. Depilation results in the removal of all hair shafts and causes a forced entry of anagen in the depilated area. Importantly, depilation also removes the keratin 6-positive inner bulge layer, which usually dampens activation of quiescent HFSCs in the outer bulge layer (Hsu et al. 2011). Because of the precise coupling of HF cycling and melanogenesis, the skin color has been reported to change from pink to black between five to eight days after depilation, indicating the transition from telogen to anagen (Slominski and Paus 1993). Consistently, in young mice, I observed a change of skin color from day 7 on (Figure 33A). However, the graying of the skin was delayed in the old mice, starting in the anterior region (neck) on day 8 (Figure 33A). Of note, aged HFSCs are described to be more difficult to activate since they are considerably more quiescent than young HFSCs (Keyes et al. 2013).

The mice were sacrificed on day 9 after depilation and tissue biopsies were collected for further analysis (Figure 33B). It has been previously described that nine days after depilation, the induced anagen HF reach their maximal length and are morphologically indistinguishable from spontaneously developing anagen follicles (Müller-Röver et al. 2001). Janis Koester and Sara Wickström confirmed that the hair follicles of the young mice were in full anagen by immunofluorescence staining for keratin 14 (Figure 33C). In contrast, the hair follicles of the old mice were still in early anagen, shown by reduced length of the hair shaft (Figure 33C). These results confirmed the delay in hair growth determined by the changes in skin color (Figure 33A). Finally, Andrea measured the

Figure 32: *N*1-acetylspermidine treatment affects cell fate by increasing proliferation. (**A**) Ratio of EdU+ cells with or without *N*1-AcSpd treatment for the last 72 h of culture. EdU was incorporated for 2 h. Mean ± SEM (n=4). (**B**) Dot plot of FxCycle violet intensity and EdU AF488 intensity, separating the phases of the cell cycle (G0/G1, S, G2/M). (**C**) Ratio of live cells with or without *N*1-AcSpd treatment for the last 72 h of culture according to their cell cycle phase distribution. Mean ± SEM (n=4). (**D**) Live cell number of α6+/CD34- cells (left) and α6+/CD34+cells (right) on day 7 post-sorting. Treatment was performed for the last 5 days of culture. Mean ± SD (n≥4). Statistical significance was calculated by paired t-test. Two-tailed p-values: * p<0.05, ns: not significant. (**E**) Representative images of organoid cultures on day 7 post-sorting. Treatment was performed for the last 5 days of culture. (**F**) Ratio of α6+/CD34+ cells in long-term 3D-3C culture with or without *N*1-AcSpd treatment. Mean ± SEM (n=4). (**G**) Live cell number in long-term 3D-3C culture shown in (**F**). Mean ± SD (n=4). (**H**) Ratio of α6+/CD34+ cells in long-term 3D-3C culture with or without *N*1-AcSpd treatment. Mean ± SEM (n=4). (**I**) Live cell number in long-term 3D-3C culture shown in (**H**). Mean ± SD (n=4). (**F**-**H**) Red arrows indicate periods of treatment, while black arrows depict periods in which the culture was left untreated. (**A**, **C, F**-**I**) Statistical significance was calculated by unpaired t-test. p-values: *** p<0.001, ** p<0.01, * p<0.05, ns: not significant.

polyamine levels in control epidermis (telogen) and depilated epidermis (anagen) in young and in old mice. Based on the results, I made three important observations: first, depilation specifically increased the levels of the acetylated polyamines *N*1-AcSpd and *N*1-AcSpm in young mice (Figure 33D); second, polyamine levels were generally lower in old mice (Figure 33E); third, although the levels of the acetylated polyamines also increased upon depilation in old mice, their levels were still lower than in young control epidermis (Figure 33E). Importantly, HFSC activation upon depilation results in their proliferation. Thus, the accumulation of *N*1-AcSpd might be required for efficient anagen onset.

In sum, the depilation experiment confirmed delayed hair growth in old mice. While the hair follicles were in full anagen and the epidermis displayed an increase in the acetylated polyamines in young mice, the old hair follicles were still in early anagen and the levels of the acetylated polyamines were lower in old epidermis compared to young epidermis. Taken together, these results suggested that the acetylated polyamines might be required for the full activation of HFSCs and an efficient onset of anagen *in vivo*.

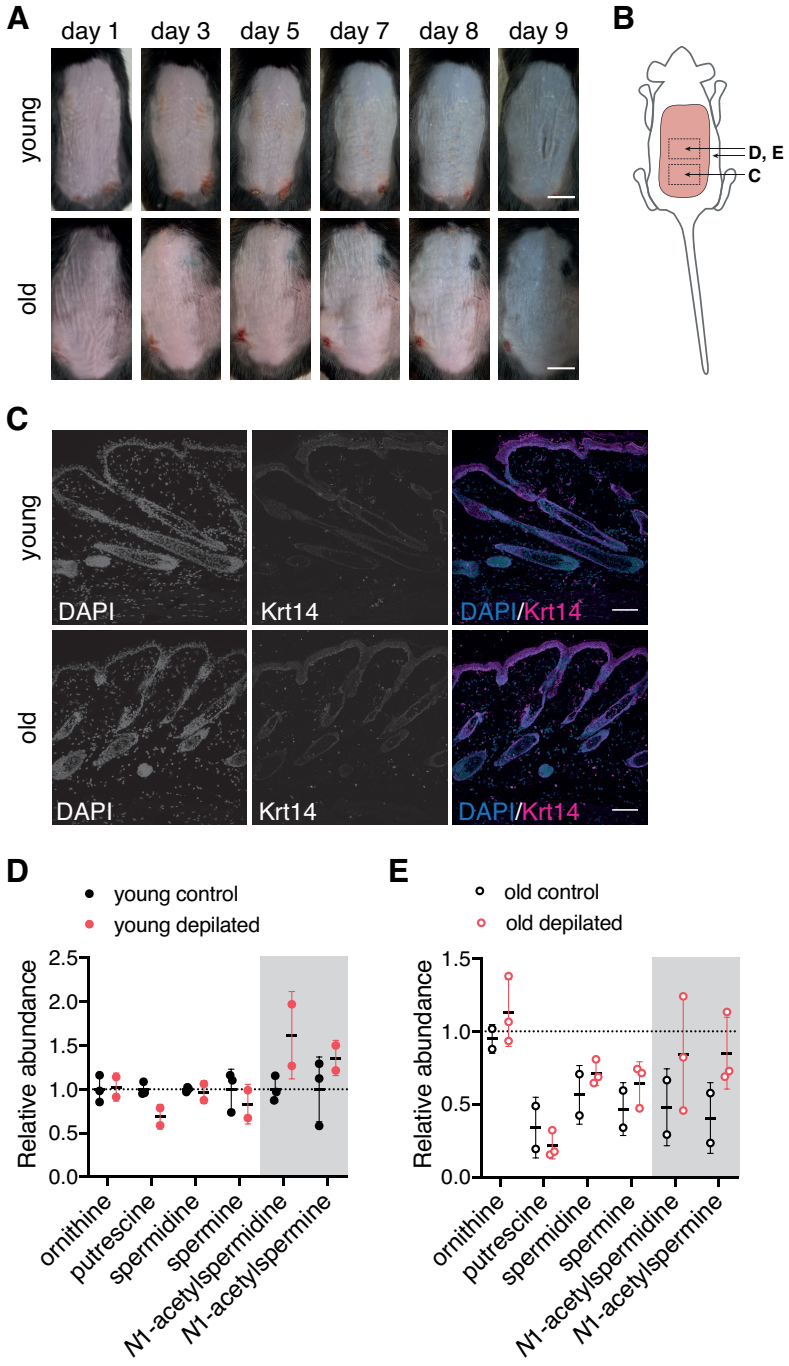

Figure 33: HFSC activation by depilation suggests a functional role of the acetylated polyamines in cell fate decisions *in vivo*. (**A**) Representative images of the depilated dorsal skin of young (top) and old (bottom) mice. n=4 for both groups. Scale bar: 1 cm (**B**) Schematic representation of the depilated area (pink) and the areas used for sample collection (squares). (**C**) Representative immunohistochemistry staining for keratin 14 (Krt14, magenta) in young (top) and old (bottom) mice. Nuclei were stained with DAPI (blue). n=4 for both groups. Scale bar: 100 µm (**D**) Polyamine levels in epidermis obtained from young mice comparing depilated epidermis (anagen) to control epidermis (telogen). Mean ± SD (n≥2). (**E**) Polyamine levels in epidermis obtained from old mice comparing depilated epidermis (anagen) to control epidermis (telogen). Values are normalized to control epidermis from young mice (dotted line). Mean ± SD (n≥2). (**D-E**) Gray boxes highlight the acetylated polyamines.

Overall, in this last part of my study I deciphered the polyamine-controlled effects on HFSC fate. I demonstrated that decreasing translation rates by changes in polyamine availability and stemness do not correlate in the organoid culture. Remarkably, I identified *N*1-acetylspermidine as novel regulator of cell fate, acting by enhancing proliferation. Going beyond the *in vitro* organoid culture, I found a correlation between efficient anagen onset and the levels of the acetylated polyamines upon depilation. These data suggest a functional role for *N*1-acetylspermidine in hair follicle stem cell fate decisions *in vivo*.

3 Discussion

In this study, I delineated the metabolic control of hair follicle stem cell fate decisions. I focused on the hexosamine pathway (HP), aerobic sugar metabolism, and the polyamine metabolism, since all three have been described to decline during the aging process and have been implicated in the regulation of stemness previously (Figure 9). To study cell fate decisions, I made use of an *in vitro* organoid culture, which allows the long-term maintenance and manipulation of hair follicle stem cells (HFSCs) and their direct progeny. First, I confirmed that the HP can be activated by GlcNAc supplementation and by genetic manipulation of its rate-limiting enzyme, GFAT1. While UDP-GlcNAc level and HA secretion were increased upon HP activation, HFSC fate was not affected. Second, I investigated the effect of sugar supplementation on cell fate decisions. A forced increase in glycolysis, achieved by D-glucose treatment, was sufficient to enhance stemness. Strikingly, D-mannose supplementation did not elevate glycolysis; instead, it resulted in a specific increase of the acetylated polyamines *N*1-acetylspermidine (*N*1-AcSpd) and *N*1-acetylspermine (*N*1-AcSpm). Third, I explored the different routes of polyamine availability-mediated effects on cell fate decisions. I confirmed that low translation rates mark the stem cell state and that a forced decrease in translation by G418 treatment was sufficient to elevate stemness. Strikingly, reducing translation by changes in polyamine availability did not correlate with increased stemness in the organoids. Remarkably, I identified *N*1-AcSpd as a novel regulator of cell fate decisions, increasing cell cycle progression in the HFSC organoids. Finally, I demonstrated that HFSC activation by depilation resulted in an elevation of the acetylated polyamines, suggesting a functional role of *N*1-AcSpd in cell fate decisions *in vivo*. Overall, my results suggest that manipulation of metabolism is an effective means to influence HFSC fate decisions.

3.1 Hexosamine pathway activation does not affect hair follicle stem cell fate decisions

The HP converts the glycolysis intermediate Frc6P to the high energy compound UDP-GlcNAc (Figure 7). The first and rate-limiting step of the HP is catalyzed by GFAT. UDP-GlcNAc can be converted to its epimer UDP-GalNAc in a reversible reaction. Both acetylated aminosugars are essential precursors for different glycosylation reactions and are required for the synthesis of glycosaminoglycans, like hyaluronic acid (HA).

HP activation has been previously described to increase protein quality control in different model organisms, likely by inducing the ISR downstream of PERK-mediated eIF2α

phosphorylation (Denzel et al. 2014; Horn et al. 2020). Further, HP activation modulates HA content by increased UDP-GlcNAc availability and *O*-GlcNAc-mediated stabilization of HAS2 (Jokela et al. 2011; Vigetti et al. 2012).

3.1.1 GlcNAc addition activates the hexosamine pathway

First, I confirmed HP activation by GlcNAc supplementation in different human cell lines. I found that GlcNAc addition increased UDP-HexNAc levels and HA secretion in HeLa, HEK293T, and HaCaT cells. Strikingly, HaCaT cells had the lowest intracellular UDP-GlcNAc concentration, while HA secretion in the medium was 5 times higher than in HeLa cells and approximately 50 times higher than in HEK293T cells. This result is confirmed by previous reports, that show that HA in the skin makes up half of the total body HA (Stern 2003). Furthermore, I showed that GlcNAc supplementation activated the HP in primary keratinocytes. Surprisingly, HA secretion was 10-fold lower in primary keratinocytes compared to HaCaT cells, whereas UDP-HexNAc levels were comparable. This difference might be due to HaCaT cells being immortalized, which has allowed them to adapt to the cultivation conditions and to readily grow on non-coated plates. In contrast, primary keratinocytes require collagen-coated plates. Thus, while HaCaT cells deposit their own ECM, as reflected by high HA secretion, primary keratinocytes are dependent on an artificial ECM. Intriguingly, GlcNAc addition was not sufficient to enhance HA secretion in primary fibroblasts, although UDP-HexNAc levels were increased 2-fold. Of note, primary fibroblasts secreted 100 times more HA than primary keratinocytes. Accordingly, fibroblasts have been described as the major source of cutaneous HA (Anderegg et al. 2014). It has been previously described that HA synthesis is controlled by substrate availability and that an increase in one UDP-sugar is sufficient to elevate HA synthesis (Vigetti et al. 2006; Jokela et al. 2008). In primary fibroblasts, however, HA secretion is so high that further increasing UDP-HexNAc levels has no effect. Nevertheless, overall, GlcNAc supplementation was sufficient to activate the HP in immortalized human cell lines as well as primary murine cells.

3.1.2 GlcNAc supplementation elevates CD34 expression

Prior to investigating the effect of HP activation on HFSC fate, I established the organoid culture as a tool. I validated that freshly isolated epidermis cells form a 50:50 balance between α6+/CD34+ HFSCs and α6+/CD34- progenitor cells after two weeks of culture. Furthermore, RNA-sequencing analysis confirmed that HFSC and progenitors represent

different cellular states. Thus, the organoid culture was proved as good model to study adult somatic stem cell fate decisions.

Importantly, I demonstrated that autophagy as well as HA deposition and intracellular signaling were partially required to maintain stemness in the 3D-3C organoids. These data suggested that HP activation would be beneficial for HFSC maintenance. However, although GlcNAc supplementation potently activated the HP as shown by increased UDP-HexNAc levels and elevated HA secretion, HFSC fate was not affected. Rather, GlcNAc treatment specifically elevated CD34 expression. Interestingly, the transcription factor Sp1 has been shown to stimulate the promoter activity of CD34 (Taranenko and Krause 2000). Importantly, the *O*-glycosylation of Sp1 has been implicated in its transcriptional activity, localization, and in the regulation of protein-protein interactions (Waby et al. 2008). Thus, I speculate that GlcNAc supplementation might influence CD34 expression by elevation of Sp1 *O*-glycosylation. Furthermore, CD34 has an extracellular domain that is highly *O*-glycosylated, and that contains additional putative *N*-glycosylation sites (Nielsen and McNagny 2008). Both types of glycosylation are required for glycoprotein function. Additionally, mucin-type *O*-glycosylation protects proteins against proteolytic cleavage and thereby increases protein stability (Kozarsky et al. 1988). Thus, GlcNAc supplementation might not only elevate CD34 expression but also enhance its stability via increased glycosylation.

3.1.3 Genetic manipulation of GFAT1 only slightly activates the hexosamine pathway

Next, I tested the effect of genetic manipulation of GFAT1 on cell fate. Importantly, genetic HP activation can influence cell fate decisions from early embryogenesis, while the GlcNAc-mediated effects are limited to the culture duration. Additionally, cell and tissue non-autonomous effects might be mediated upon genetic manipulation. GFAT1 was chosen since it is the rate-limiting enzyme of the HP and its overexpression has been previously shown to activate the HP in different model organisms (Veerababu et al. 2000; Weigert et al. 2001; Denzel et al. 2014). Further, the GFAT1 G451E substitution represents a well-understood paradigm of HP activation (Denzel et al. 2014; Horn et al. 2020; Ruegenberg et al. 2020). Western blot analysis using primary fibroblasts confirmed that the gene trap cassette worked as expected; in cells isolated from mice carrying the conditional knock-in allele ($Rosa26^{flox/wt}$) expression of the transgene was not detectable, whereas cre-mediated deletion of the transcription termination cassette resulted in strong GFAT1 overexpression ($Rosa26^{OE/wt}$). Since the *cre* gene is under transcriptional control

of the CMV promoter, it is expressed before implantation during early embryogenesis (Schwenk et al. 1995). Thus, cre-mediated deletion of the transcription termination cassette should be equally efficient in all tissues, including the hair follicle and the brain. Surprisingly, genetic manipulation of GFAT1 did not influence cell-type distribution in the epidermis. Moreover, HFSC fate was not affected in the organoid culture. Intracellular UDP-HexNAc levels and HA secretion were only slightly increased, although GFAT1 expression was potently elevated according to the Western blot analysis performed in primary fibroblasts. Moreover, the overexpression GFAT1 G451E, which displays reduced sensitivity to UDP-GlcNAc feedback inhibition (Ruegenberg et al. 2020), activated the HP to a similar extent as wildtype GFAT1 in brain tissue and 3D-3C cultured cells. Of note, homozygous overexpression was not much more efficient than the heterozygous overexpression of GFAT1.

Two factors might contribute to the poor HP activation upon GFAT1 overexpression: first, GFAT1 is feedback inhibited by its product D-glucosamine-6-phosphate (GlcN6P) and the end-product of the HP, UDP-GlcNAc (Broschat et al. 2002; Kornfeld 1967; Assrir et al. 2014). While the G451E substitution drastically reduces the sensitivity of GFAT1 to UDP-GlcNAc feedback inhibition (Ruegenberg et al. 2020), it is probably still sensitive to product inhibition by GlcN6P, which competitively interferes with Frc6P binding (Broschat et al. 2002). G451 is located in close proximity to the UDP-GlcNAc binding site; however, it is not involved in Frc6P binding: the catalytically relevant residues for Frc6P binding are K558, E561, H577, and K676 (Ruegenberg et al. 2020). Nevertheless, overexpression of huGFAT1 G451E should result in a more pronounced elevation of UDP-GlcNAc levels compared to overexpression of wildtype huGFAT1 due to loss of UDP-GlcNAc feedback inhibition. Surprisingly, analysis of brain tissue isolated from different mouse strains revealed that the level of HP activation was comparable between both transgenes, suggesting that UDP-GlcNAc feedback inhibition was negligible. However, consistent with the efficient HP activation upon GlcNAc supplementation, conversion of GlcNAc to UDP-GlcNAc is not limited by feedback inhibition since GlcNAc enters the HP downstream of the reaction catalyzed by GFAT1 (Weihofen et al. 2006). Second, the accumulation of HP intermediates activates D-glucosamine-6-phosphate deaminase (GNPDA): GlcNAc6P is an activator of both bacterial and mammalian GNPDA (Oliva et al. 1995; Arreola et al. 2003). Importantly, GNPDA has been suggested to play a significant role in the fine-tuning of UDP-GlcNAc content, since it not only converts GlcN6P to Frc6P, but also catalyzes the reverse reaction (Çayli et al. 1999; Oikari et al. 2016). The direction of the reaction seems to be controlled by substrate availability (Çayli et al. 1999; Álvarez-Añorve et al. 2011; Oikari et al. 2016). Thus, HP activation is likely to enhance the degradation of GlcN6P to

Frc6P, thereby limiting the degree of activation. Taken together, feedback inhibition of GFAT1 and activation of GNPDA might contribute to the poor HP activation upon genetic manipulation. However, genetic HP activation by the engineering of GFAT1 G451E has been previously shown to activate the HP as efficiently as GlcNAc supplementation in N2a cells (Horn et al. 2020). This finding suggests that the poor HP activation upon GFAT1 overexpression might be caused by an additional factor.

3.1.4 The N-terminal tag interferes with GFAT1 activity

Since engineering of the endogenous *Gfat1* locus demonstrated efficient genetic HP activation in N2a cells, it is likely that the poor HP activation upon huGFAT1 overexpression is due to the N-terminal tag of the transgene. Consistently, it has been previously described that an N-terminal tag interfered with GFAT1 activity: His_6-N-tagged GFAT1 does not show amidohydrolase activity, while the isomerase activity is maintained (Olchowy et al. 2006). The tag likely abolishes glutamine hydrolysis: in the wildtype enzyme, removal of the initial methionine results in a free α-amino group of cysteine 2, which is required for the catalytic reaction of the glutaminase domain (Badet et al. 1987; Isupov et al. 1996). However, the quaternary structure of GFAT1 was not affected by the His_6-N-tag (Olchowy et al. 2006). Analysis of brain tissue from transgenic mice revealed that overexpression of huGFAT1 G451E does not lead to a more pronounced elevation of UDP-GlcNAc levels compared to overexpression of wildtype huGFAT1. Additionally, UDP-HexNAc levels were only slightly increased upon homozygous overexpression of GFAT1 compared to heterozygous overexpression. The proposed loss of GFAT1 amidohydrolase activity would explain these results. Nevertheless, the transgenic mice displayed an approximate 2-fold increase in UDP-HexNAc levels. Presumably, the overexpression of huGFAT1 resulted in partial loss of feedback inhibition of the endogenous enzyme. Importantly, the tag likely does not interfere with the quaternary structure of GFAT1 (Olchowy et al. 2006). Thus, FLAG-HA tagged GFAT1 could still bind and thereby scavenge UDP-GlcNAc. Thereby, the endogenous GFAT1 might be less inhibited, resulting in elevated HP flux. Importantly, the G451E substitution does not abolish UDP-GlcNAc binding, supporting this hypothesis (Ruegenberg et al. 2020). An internal tag could overcome the loss of amidohydrolase activity since it was shown to not interfere with GFAT1 kinetic properties by independent studies (Richez et al. 2007; Ruegenberg et al. 2020). Additionally, CRISPR/Cas9-mediated engineering of the endogenous *Gfat1* locus in mice is an interesting alternative, since the introduction of the G451E substitution has already been shown to result in efficient HP activation in N2a cells:

UDP-GlcNAc levels were around 5-fold increased compared to wildtype cells; the induction was similar to treatment with 10 mM GlcNAc (Horn et al. 2020).

3.1.5 Is manipulation of GFAT2 an effective means to activate the hexosamine pathway?

Previously, Mattila et al. (2018) described that GFAT2 plays a crucial role in *Drosophila* intestinal stem cells (ISCs): GFAT2 is necessary and sufficient to promote the proliferation of ISCs. Furthermore, the authors showed that HP activity is required for a metabolic switch to glycolysis in response to nutrient signaling (Mattila et al. 2018; Beebe and Thummel 2018). In mouse and human, GFAT2 was described to be mainly expressed in the nervous system, especially in the spinal cord (Oki et al. 1999). Accordingly, GFAT2 expression is very low in HaCaT cells; however, it is strongly induced upon GNPDA1 suppression (Oikari et al. 2016). HaCaT cells, similar to normal keratinocytes, form an orderly structured and differentiated epidermal tissue with proper location of differentiation markers, when transplanted onto nude mice (Boukamp et al. 1988). This result suggests that HaCaT cells represent basal cells of the IFE. Since HaCaT are basal keratinocytes, which can differentiate to provide the cells of the upper layers of the IFE, they are not readily comparable to HFSCs. Nonetheless, the results of Oikari et al. (2016) suggest that GFAT2 expression can be modulated in keratinocytes. Overall, GFAT2 is an interesting candidate to elucidate further the role of the HP in stem cells in general and in HFSCs in particular. Its overexpression represents an additional option to activate the HP that could be tested in future experiments.

3.1.6 Does hexosamine pathway activation modulate stem cell fate?

Collectively, my data show that GlcNAc supplementation resulted in a very strong induction of HP flux. However, GlcNAc treatment in the 3D-3C organoids specifically upregulated the expression of CD34 and did not affect HFSC fate decisions. Although the overexpression of huGFAT1 slightly elevated UDP-HexNAc levels and HA secretion, the N-terminal tag likely interfered with the catalytic activity of GFAT1. The level of HP activation achieved with this construct was not sufficient to affect cell fate in the epidermis or the organoid culture. However, based on these results that inherent technical limitations, I cannot exclude genetic HP activation as a modulator of stem cell fate. In order to directly address this issue, additional experiments are required; for example, CRISPR/Cas9-mediated engineering of the endogenous *Gfat1* locus would be conceivable. Also, manipulation of GFAT2 levels would be an option. Since the effect of GlcNAc

supplementation on CD34 expression might correlate with the strong HP activation, a less drastic activation would be desirable. Given the specific effect on CD34 expression, another type of stem cells might be a required for future experiments. Of note, *O*-GlcNAcylation of pluripotency factors has been implicated in elevated stem cell maintenance before (Jang et al. 2012). Thus, ESCs might be a good model to study also other HP activation-mediated effects on stemness. However, these experiments are beyond the scope of this study.

3.2 Sugar supplementation elevates stemness in hair follicle stem cell organoids

Stem cells have unique metabolic requirements since they rely on glycolysis for energy production. However, aerobic sugar metabolism has been described to decline during the aging process (Goyal et al. 2017; Ravera et al. 2019). Thus, stem cell exhaustion might be linked to reduced glycolytic capacity, which has been shown to attenuate HSC quiescence (Takubo et al. 2013). Therefore, I tested whether sugar supplementation can improve stem cell maintenance in the HFSC organoid culture. I used different sugars, which can fuel glycolysis or are closely connected to glucose metabolism: D-glucose, D-mannose, and D-sorbitol (Figure 17).

3.2.1 Increasing lactate secretion favors the hair follicle stem cell state

It has been previously shown that elevating glycolytic flux not only improves reprogramming efficiency but also enhances stem cell capacity of HSCs (Yoshida et al. 2009; Zhu et al. 2010; Takubo et al. 2013). Consistently, I demonstrated that D-glucose supplementation elevated the number of HFSCs in the 3D-3C organoids. In contrast to GlcNAc supplementation, D-glucose addition enhanced expression of most stem cell marker genes tested 2 to 3-fold. Although the increase was not significant, gene expression was sufficiently affected to conclude that the HFSC state was promoted by D-glucose supplementation. To recover NAD^+ during aerobic glycolysis, lactate dehydrogenase (LDH) converts pyruvate to lactate using NADH (Zhang et al. 2012b; Farhana and Lappin 2020). Of note, I found increased lactate secretion upon D-glucose supplementation. Previously, Flores et al. (2017) suggested that while all cells in the epidermis use the TCA cycle extensively to generate energy, HFSCs have increased LDH expression and activity, as well as elevated glycolytic metabolism compared to total epidermis. Additionally, the authors showed that LDH activity was required for HFSC

activation, which refers to the switch from a quiescent to an actively cycling state at the onset of the anagen growth phase. Furthermore, genetic deletion of mitochondrial pyruvate carrier 1 (MPC1) or its inhibition using UK-5099, blocking pyruvate entry into the TCA cycle, increased lactate production and promoted the activation of HFSCs. Consistently, Kim et al. (2020) observed that low pO_2, which elevates anaerobic glycolytic flux, increases maintenance of HFSC in the 3D-3C organoid culture system that I also used in this study. Importantly, the activity of HFSCs varies markedly during the hair cycle (Blanpain et al. 2004; Fuchs 2009). In contrast, 3D-3C cultured HFSC are frequently dividing, suggesting that the culture conditions lead to their activation, which is comparable to the state of HFSCs at anagen onset *in vivo*. Consistent with the Flores et al. (2017) study, I demonstrated that D-glucose supplementation and the subsequent increase in lactate secretion are sufficient to promote this activated HFSC state in the 3D-3C organoids. In the future, it would be interesting to investigate proliferation upon D-glucose supplementation in the 3D-3C organoids. In addition, stem cell maintenance and de-differentiation should be analyzed separately upon D-glucose treatment. These results will ultimately help to better understand the effect of increased lactate secretion on the self-organizing plasticity of the organoid culture system.

In addition to D-glucose supplementation, I also showed that UK-5099, which blocks pyruvate entry into mitochondria by inhibiting MPC (Figure 5), increased the number of HFSCs. This effect on cell fate was likely accompanied by increased lactate production; however, measuring lactate concentration in the medium would be essential. Comparable to D-glucose supplementation, the subsequent increase in lactate secretion might be sufficient to favor the activated HFSC state in the organoid culture as shown by Flores et al. (2017) *in vivo*. Surprisingly, Kim et al. (2020) did not detect an effect of UK-5099 short-term (48 h) treatment on cell fate in the 3D-3C organoids. Therefore, a thorough investigation of stem cell maintenance, progenitor cell de-differentiation, as well as proliferation and apoptosis at different time points of UK-5099 treatment would be required. Also, the cell fate changes observed in this study have to be confirmed either by elevated colony-forming potential or through increased expression of stem cell marker genes. Additionally, genetic manipulation of MPC would be conceivable to support the findings using UK-5099.

3.2.2 Contribution of other glucose-utilizing pathways to the D-glucose-mediated effect on stemness

As mentioned above, D-glucose treatment significantly increased the amount of lactate in the medium. However, while the glucose concentration was elevated 10-fold, lactate secretion was only 2-fold increased upon D-glucose supplementation. Although the results of Flores et al. (2017) suggest that an increase in lactate production is sufficient to affect cell fate, D-glucose might also fuel other pathways besides glycolysis, which could contribute to the observed effects.

Given that UK-5099 treatment mimicked the D-glucose effect on cell fate, an increase in TCA cycle activity and OXPHOS is unlikely to be required to promote active cycling of HFSCs in the 3D-3C organoids. Rather, increased levels of OXPHOS and TCA cycle activity seem to be important upon differentiation since both processes are elevated in ORS progenitors compared to HFSCs (Kim et al. 2020a). Importantly, the de-differentiation of ORS cells back to the HFSC state requires the capability to suppress a metabolic switch from glycolysis to OXPHOS and glutamine metabolism that occurs during early HFSC lineage progression (Kim et al. 2020a). Collectively, these data suggest that increased lactate secretion promotes active cycling of HFSCs, whereas OXPHOS and glutamine metabolism seem to be important upon differentiation. Nevertheless, HFSCs might require TCA flux to provide citrate-derived acetyl-CoA, which is used for histone acetylation. Importantly, ESCs and iPSCs display higher levels of histone acetylation (Mattout et al. 2011). Consistently, inhibition of histone deacetylases (HDACs) promotes ESC self-renewal (Ware et al. 2009). Strikingly, inhibition of glycolysis in ESCs causes histone deacetylation and, subsequently, loss of pluripotency (Moussaieff et al. 2015). Thus, D-glucose supplementation might favor the HFSC state by elevating histone acetylation.

Of note, glucose is also used in the pentose phosphate pathway (PPP) and for glycogen synthesis (Rajas et al. 2019). Thus, it is interesting to investigate the effects of these pathways on HFSC fate decisions. In cardiomyocytes, high glucose inhibits maturation by promoting nucleotide biosynthesis via the PPP (Nakano et al. 2017). The authors suggest that nucleotide biosynthesis is key to balance cell proliferation and differentiation of cardiomyocytes. Again, a careful investigation of stem cell maintenance, progenitor cell de-differentiation, as well as overall proliferation upon D-glucose supplementation, would be interesting. D-glucose also fuels the polyol pathway. However, since D-sorbitol did not affect cell fate, it is unlikely that the polyol pathway plays a role in cell fate decisions. However, increasing flux through the polyol pathway upon D-glucose supplementation might have negative side-effects upon long-term treatment: activation of the polyol pathway under hyperglycemic conditions leads to the development of chronic diabetic

complications (Quattrini and La Motta 2019). Therefore, given the negative side-effects, improving stem cell maintenance by D-glucose supplementation is likely unattainable.

3.2.3 D-mannose supplementation does not elevate glycolytic flux

In addition to D-glucose, I also used D-mannose supplementation in this study, since D-mannose has been described to contribute to glycolytic flux (Slade et al. 2016). While I demonstrate that D-mannose supplementation potently increased stemness in the 3D-3C organoids, I could not confirm an increase in glycolysis. Lactate secretion was rather decreased upon D-mannose treatment, and glycolysis intermediates were not identified or not significantly changed in the untargeted metabolomics approach. Importantly, a study in tumor cells revealed that mannose administration (25 mM) leads to the accumulation of Man6P, which in turn impairs glucose metabolism, resulting in decreased lactate secretion (Gonzalez et al. 2018). These findings are in accordance with my results. In the future, it would be important to confirm Man6P accumulation in D-mannose-treated organoids.
To identify the downstream regulator upon D-mannose treatment, I performed RNA-sequencing. GO term analysis revealed that cell migration and cell adhesion were affected upon D-mannose supplementation. These processes might be regulated by receptor tyrosine kinase (RTK) signaling, which was also significantly changed. Interestingly, crosstalk of E-cadherin with RTKs, such as epidermal growth factor receptor (EGFR), for example, regulates cell adhesion and cell migration: activation of EGFR results in disassembly of the cadherin-catenin complex, reduced cell adhesion, and increased cell migration (Andl and Rustgi 2005). Remarkably, polyamines have also been described to regulate E-cadherin (Liu et al. 2009). Thus, the changed polyamine availability seen upon D-mannose supplementation might cause some of the gene expression changes observed. Moreover, GO term analysis implied reduced proliferation upon D-mannose treatment. Indeed, I found decreased live cell number and EdU incorporation upon D-mannose supplementation. Of note, RTK signaling has also been implicated in keratinocyte proliferation: inhibition of EGFR results in growth arrest (Peus et al. 1997); however, it also elevates the expression of terminal differentiation markers. Thus, further investigation of the effects of D-mannose supplementation on RTK signaling would be required to conclude which of the versatile outputs are essential for the effects of D-mannose in the organoid culture. Moreover, elucidating the role of polyamines in the gene expression changes detected upon D-mannose supplementation would be interesting in the future. Finally, GO term analysis suggested elevated apoptosis in D-mannose treated cultures. Since the increase in HFSCs might also be caused by

enhanced apoptosis of progenitor cells, it is important to perform annexin V staining upon D-mannose supplementation.

3.2.4 D-mannose supplementation influences hair follicle stem cell fate via changes in polyamine availability

To investigate the effect of D-mannose supplementation on cellular metabolism, Andrea Annibal from Adam Antebi's laboratory (Max Planck Institute for Biology of Ageing, Cologne, Germany) performed untargeted metabolomics. Of note, he found that the acetylated polyamine *N*1-acetylspermidine (*N*1-AcSpd) was 2-fold increased upon D-mannose supplementation. Targeted metabolomics confirmed the effect of D-mannose supplementation on *N*1-AcSpd levels and revealed an increase in *N*1-acetylspermine (*N*1-AcSpm) with a concomitant reduction of ornithine and putrescine levels. Overall, the effect of D-mannose supplementation on intracellular polyamine levels resembled that of DENSpm treatment. Importantly, the connection of D-mannose supplementation with intracellular polyamine levels is poorly understood. Because of the increased levels of the acetylated polyamines *N*1-AcSpm and *N*1-AcSpd, D-mannose was likely to affect SSAT expression. However, while SSAT expression was enhanced by short-term D-mannose supplementation, it was not changed after long-term D-mannose treatment. Of note, SSAT expression is highly regulated, and its level of expression is adjusted in response to alterations in polyamine content (Pegg 2008). Thus, the unchanged SSAT expression likely represents an adaptation of the cells to the changes in polyamine content upon long-term D-mannose treatment. Strikingly, ODC expression has been previously shown to be enhanced by D-mannose supplementation (Lundgren and Prokay 1988). Therefore, expression levels of the other enzymes involved in polyamine metabolism should be analyzed upon D-mannose supplementation in future experiments. Taken together, my data suggest that the changes in polyamine availability are driving the cell fate changes observed upon D-mannose supplementation.

3.2.5 Is D-mannose administration a viable option to improve stem cell maintenance?

Importantly, D-mannose supplementation has been suggested to be beneficial under different conditions. In mice, the oral administration of mannose (20% in the drinking water) did not have negative side effects on the weight or the health of the animals (Gonzalez et al. 2018). Strikingly, it enhanced the effectiveness of different chemotherapeutic agents. Additionally, oral supplementation of D-mannose via the drinking water effectively

suppressed autoimmune type 1 diabetes in mice (Zhang et al. 2017). Moreover, mannose supplementation of high-fat-diet-fed mice (2% in the drinking water) prevents weight gain, lowers adiposity, and improves glucose tolerance through effects on gut microbiota (Sharma et al. 2018). Overall, these studies suggest that D-mannose supplementation is beneficial in different settings. However, the mice were sacrificed between 10 and 16 weeks of age. Thus, possible long-term effects of D-mannose treatment cannot be excluded. In sum, DENSpm treatment is a viable option to further investigate the D-mannose-mediated effects, since the changes of intracellular polyamine levels are comparable.

3.3 The acetylated polyamine *N*1-acetylspermidine is a novel determinant of hair follicle stem cell fate

Since D-mannose supplementation clearly elevated the levels of the acetylated polyamines *N*1-AcSpd and *N*1-AcSpm, I aimed to elucidate the role of polyamine metabolism in stem cell maintenance in the last part of my work. In stark contrast to previous studies that linked high polyamine abundance to stemness, HFSCs in the organoid culture displayed lower levels of the natural polyamines, as well as *N*1-AcSpd compared to progenitor cells. These data suggest that, depending on the cellular context, not only high polyamine levels, but also low polyamine availability can be beneficial for stem cell maintenance. Do low polyamine levels endogenously reduce translation rates in stem cells? Does the reduction of polyamine levels, and translation, affect stem cell maintenance and function? Might distinct polyamine species differ in their effects on stem cells through translation or other mechanisms? Here, I delineate the polyamine-mediated regulation of HFSC maintenance and function.

3.3.1 Low polyamine levels endogenously reduce translation rates in hair follicle stem cells

Several studies demonstrated that translation is upregulated during differentiation using different types of stem cells (Sampath et al. 2008; Signer et al. 2014; Zismanov et al. 2016). HFSCs *in vivo* display low translation rates, which increase when cells become activated and differentiate (Blanco et al. 2016). Of note, I could reproduce these findings in freshly isolated and in 3D-3C cultured cells. Thus, α6+/CD34+ stem cells in the organoids recapitulate this key feature of HFSCs *in vivo*. Possibly, reduced translation

rates in HFSCs are maintained by low abundance of natural polyamines. However, this hypothesis needs to be confirmed in future experiments.

Strikingly, forced inhibition of translation by loss of NOP2/Sun RNA methyltransferase family member 2 (NSUN2) in the mouse blocks the differentiation of HFSCs to progenitor cells (Blanco et al. 2011), demonstrating that upregulation of translation is pivotal for differentiation in the HF. I confirmed the promotion of the HFSC state by reduced translation through G418 treatment. Based on the study by Blanco et al. (2011), the increase in stem cell maintenance might be caused by attenuated differentiation rather than enhanced self-renewal. However, elevated de-differentiation of progenitor cells suggested that a forced decrease of translation did not only block differentiation, but favored the HFSC state in the 3D-3C organoids. In future experiments, stem cell self-renewal upon G418 treatment could be investigated by EdU incorporation. Overall, I demonstrated that reduced translation is not only a consequence of the stem cell state but can also drive cell fate decisions in the HFSC organoid culture. Thus, these data confirmed the 3D-3C organoids as a suitable model to study the influence of translation on cell fate decisions.

3.3.2 Reduced translation rates by changes in polyamine availability do not correlate with enhanced stemness in hair follicle stem cells

To elucidate whether polyamine availability plays a role in the regulation of protein synthesis, I aimed to mimic the low levels of natural polyamines found in HFSCs and study the effect on cell fate. To this end, I used DFMO which is an enzyme-activated, irreversible inhibitor of ODC (Metcalf et al. 1978), and DENSpm, which increases SSAT expression, mRNA stability, and enzyme activity (Coleman et al. 1995; Parry et al. 1995; Fogel-Petrovic et al. 1996). Surprisingly, although DFMO treatment recapitulated the low levels of natural polyamines seen in HFSCs and reduced translation rates, it was not sufficient to enhance stemness in the organoid culture. This result suggested that the low polyamine levels seen in sorted HFSCs might endogenously reduce translation rates, but are not causal for HFSC maintenance.

DENSpm treatment had a dual effect on intracellular polyamine levels: it depleted the natural polyamines, while the acetylated forms accumulated. Of note, the depletion of natural polyamines by DENSpm treatment or by SSAT OE has been shown to decrease mRNA translation in mammalian cells (Landau et al. 2010; Mandal et al. 2013). However, DENSpm addition did not affect translation rates in the organoid culture. Surprisingly, it still favored the HFSC state. In sum, these data demonstrate that low translation rates

achieved by changes in polyamine availability and stemness do not correlate in the HFSC organoids. This conclusion is further supported by the results obtained upon *N*1-AcSpm treatment, which also decreased translation rates, but did not affect HFSC fate.

Published data clearly demonstrate a functional role of translation upregulation during differentiation (Sampath et al. 2008; Signer et al. 2014; Blanco et al. 2016; Zismanov et al. 2016). These findings are also supported by my own data, showing decreased protein synthesis in HFSCs in the organoids. Extending this notion, *N*1-AcSpd, which robustly elevated stemness in the organoid culture, increased translation rates. Thus, my results show not only that low translation rates do not correlate with stemness, but also that increased translation rates to not avoid stem cell maintenance in the organoids.

Importantly, DENSpm treatment did not only decrease the levels of the natural polyamines, but also caused an accumulation of the acetylated forms. Based on my results upon *N*1-AcSpd treatment, the expected reduction of protein synthesis due to the depletion of the natural polyamines might be masked by increased *N*1-AcSpd levels, which elevate mRNA translation in the organoids. The combination of these effects would explain why global translation rates are not changed upon DENSpm treatment. In contrast, in other cell types, *N*1-AcSpd might not exert the same effects as in HFSC, and therefore, overall translation rates are decreased. In conclusion, the depletion of the natural polyamines upon DENSpm treatment might affect translation rates, however, this effect cannot be detected by puromycin incorporation. A more precise analysis of mRNA translation would be required.

3.3.3 Is the global reduction of protein synthesis required for enhanced stemness or is post-transcriptional control of specific transcripts sufficient?

Puromycin incorporation is a useful method to monitor global changes in mRNA translation; however, a more specific post-transcriptional control will be missed using this method. Since DENSpm treatment has a dual effect on intracellular polyamine levels, the reduction of translation rates due to depletion of the natural polyamines might be masked in a global approach. Therefore, a more precise analysis of mRNA translation by ribosome footprinting, for example, should be performed in the future to elucidate the outcome of this dual effect of DENSpm treatment. This approach would also allow to investigate whether a global reduction of mRNA translation is required to enhance stemness. Furthermore, the comparison between G418 and DFMO treatment might help to explain why these treatments differently affect stemness, although global translation rates are decreased.

G418 treatment is likely to exert a global effect: Structural analysis of the 80S ribosome revealed that G418 binds to the decoding center in the small ribosomal subunit (Garreau de Loubresse et al. 2014). The decoding center forms a restricted pocket that selects the appropriate aminoacyl-tRNA according to the mRNA codon positioned in the A-site (Demeshkina et al. 2012). Accordingly, G418 is likely to exert global effects on protein synthesis. Polyamines also play a pivotal role in global protein synthesis: they are stably associated with ribosomes and with tRNAs (Cohen and Lichtenstein 1960; Cohen et al. 1969). Accordingly, the fidelity of polypeptide synthesis is increased by polyamines via enhanced binding of aminoacyl-tRNAs to the ribosome (Igarashi et al. 1982). These data suggest that manipulation of the intracellular polyamine pool is likely to affect global protein synthesis as seen with DFMO, *N*1-AcSpd, and *N*1-AcSpm treatment. However, polyamines also influence translation of specific transcripts: spermidine is converted to hypusine, which post-translationally modifies the elongation factor eIF5A (Park et al. 1981; Cooper et al. 1983). Hypusination of eIF5A is critical for translation elongation, especially for difficult substrates like polyproline stretches (Saini et al. 2009; Gutierrez et al. 2013). Thus, DENSpm treatment, which leads to the depletion of spermidine, is likely to reduce hypusination of eIF5A. Ultimately, this will affect translation of a subset of mRNAs, which is particularly dependent of eIF5A function. During OXPHOS-dependent alternative macrophage activation, for example, hypusination of eIF5A is required for efficient expression of a subset of mitochondrial genes (Puleston et al. 2019). In turn, supplementation with *N*1-AcSpd might increase hypusination, and thus, might favor translation of specific mRNAs. In sum, sequencing of the polysome-associated mRNAs or ribosome footprinting should be performed upon the different treatments. Additionally, hypusination of eIF5A should be investigated in future experiments.

3.3.4 *N*1-acetylspermidine is a novel determinant of hair follicle stem cell fate decisions

Since the elevation of *N*1-AcSpd levels was the only common change upon DENSpm and putrescine supplementation, I speculated that increased *N*1-AcSpd might affect cell fate. Intriguingly, *N*1-AcSpd treatment significantly increased the number of HFSCs in the 3D-3C organoids. Remarkably, *N*1-AcSpd treatment and putrescine addition changed intracellular polyamine levels comparably: putrescine and *N*1-AcSpd levels were increased. Therefore, it was necessary to discern whether the effect on cell fate is mediated by putrescine or *N*1-AcSpd. To this end, I prevented the conversion of putrescine to *N*1-AcSpd and *vice versa*: inhibition of PAOX by MDL72527 impedes the oxidation of

*N*1-AcSpd to putrescine, whereas inhibition of SSAT by DA blocks the acetylation of spermidine to *N*1-AcSpd. MDL72527 addition should result in the accumulation of the acetylated polyamines, while DA should reduce their levels. Importantly, the effects of the two inhibitors on intracellular polyamine levels have to be confirmed in future experiments. In sum, the data obtained upon inhibition of SSAT and PAOX confirm that the accumulation of the acetylated polyamines is not only required but also sufficient to enhance stemness in the HFSC organoids. Since putrescine levels are likely not influenced by the inhibitor treatments, these data demonstrate that *N*1-AcSpd determines HFSC fate in the organoids.

Since DENSpm and MDL72527 strongly increased stem cell maintenance and de-differentiation, likely via increased levels of the acetylated polyamines *N*1-AcSpd and *N*1-AcSpm, I aimed to investigate the effect of *N*1-AcSpm treatment on cell fate. In stark contrast to *N*1-AcSpd addition, supplementation with *N*1-AcSpm did not influence the ratio of HFSCs. Thus, I demonstrated that the elevation of the acetylated polyamines in general was not sufficient; instead, *N*1-AcSpd treatment had a specific effect on cell fate. Going beyond *in vitro* data, I demonstrated a functional role of the acetylated polyamines in cell fate decisions *in vivo*: depilation-induced HFSC activation resulted in a specific accumulation of the acetylated polyamines in the epidermis. My *in vitro* results suggest that the increase in *N*1-AcSpd levels is relevant, since *N*1-AcSpm supplementation did not influence cell fate.

3.3.5 *N*1-acetylspermidine promotes the hair follicle stem cell state by increasing cell cycle progression

Previously, the acetylated polyamines were mostly described as the major group of polyamines exported from the cell (Seiler and Dezeure 1990). Extending this notion, I find that the intracellular accumulation of *N*1-AcSpd has an effect on stemness. This occurs without reducing translation, which is consistent with previous observations that acetylated polyamines have no effect on protein synthesis *in vitro* (Kakegawa et al. 1991). Instead, 3’ RNA-sequencing of purified cell populations from the organoids revealed that *N*1-AcSpd treatment affected the expression of cell cycle-associated genes. Interestingly, the expression levels of these same genes were higher in α6+/CD34+ stem cells in the organoid culture, which also show elevated EdU incorporation compared to progenitor cells.

Intriguingly, increased proliferation and stemness have been linked before. A study in ESCs suggests that elevated CDK activity, and thus increased cell cycle progression,

contributes to stem cell maintenance (Liu et al. 2017). Strikingly, several studies have described that cells in the G1 phase are more susceptible to cell fate changes and that differentiation is associated with G1 phase lengthening (Clegg et al. 1987; Sela et al. 2012; Calder et al. 2013). Consistently, cellular reprogramming efficiency seems to be linked to the successful acceleration of the cell cycle (Guo et al. 2014; Ruiz et al. 2011). Of note, forced overexpression of AMD1 or ODC in mouse fibroblasts, resulting in the accumulation of polyamines, improves reprogramming efficiency (Zhang et al. 2012a; Zhao et al. 2012). My results suggest that this effect is caused by increased proliferation. Collectively, these data indicate that both stem cell maintenance and de-differentiation might be improved by elevated cell cycle progression in the 3D-3C organoid culture.

Remarkably, polyamines have been described to interact with DNA through electrostatic and hydrogen bonding forces, resulting in its stabilization (Flink and Pettijohn 1975; Pallan and Ganesh 1996; Tsukamoto et al. 2005). Moreover, polyamines change the conformation of the nucleosome core, thereby facilitating the replication of DNA (Morgan et al. 1987). Collectively, polyamine availability might be required for optimal rates of DNA replication during S phase (Alm and Oredsson 2009). Accordingly, *N*1-AcSpd supplementation increased the number of cells in S phase. However, putrescine supplementation in cells with low ODC activity, which display prolongation of the cell cycle phases, is sufficient to normalize cell cycle kinetics (Nasizadeh et al. 2005). Thus, increasing cell cycle progression might not be an *N*1-AcSpd-specific effect. Instead, a general increase of polyamine levels might be beneficial. Accordingly, overexpression of AMD1 or ODC, which elevates overall polyamine availability, is sufficient to increase reprogramming efficiency (Zhang et al. 2012a; Zhao et al. 2012). Furthermore, topical application of putrescine and spermidine stimulates DNA synthesis in mouse epidermis (Gange and Dequoy 1980). Therefore, cell cycle progression upon the different treatments should be investigated. Nevertheless, these published data confirm that increased cell cycle progression upon *N*1-AcSpd supplementation is sufficient to affect cell fate decisions.

3.3.6 SSAT activity might drive HFSC fate decisions

DENSpm supplementation resulted in a depletion of the natural polyamines and an accumulation of the acetylated forms in the 3D-3C organoids. To elucidate which of these effects was responsible for the increase in stemness, I supplemented DENSpm treated cells with putrescine to rescue the reduction of natural polyamines. Additional putrescine supplementation partially rescued the DENSpm-mediated effect on stem cell maintenance

and de-differentiation and fully reversed the growth defect caused by DENSpm treatment, suggesting successful replenishment of the natural polyamines. However, stem cell maintenance and de-differentiation were still significantly affected upon the double treatment compared to untreated cells. Since putrescine treatment alone was not sufficient to account for these changes, I hypothesize that the HFSCs fate changes observed upon DENSpm are connected to the accumulation of the acetylated polyamines.

Remarkably, the effect of DENSpm treatment on intracellular polyamine levels was comparable to D-mannose supplementation. Thus, since DENSpm treatment also promoted the HFSC state in the organoids, the changes in polyamine abundance detected upon D-mannose supplementation were indeed linked to the observed cell fate changes. Of note, short-term D-mannose treatment increased the expression of SSAT, which is also reported to be elevated upon DENSpm addition (Coleman et al. 1995; Parry et al. 1995; Fogel-Petrovic et al. 1996). Based on the polyamine levels, DENSpm and D-mannose treatment also increased SSAT activity. Intriguingly, both treatments elevate stemness in the HFSC organoids. These results suggest that SSAT activity and stemness correlate. Accordingly, DA treatment, which inhibits SSAT, reduces stemness in the organoids. Furthermore, depilation-induced activation of HFSCs *in vivo* also seems to induce SSAT, since both acetylated polyamines are increased. Of note, ODC and SSAT are described to be upregulated by extracellular polyamines (Dai et al. 2017), suggesting that also *N*1-AcSpd supplementation positively affects SSAT. Collectively these data suggest that SSAT activity is required and sufficient to favor the HFSC fate. However, this hypothesis needs to be confirmed in future experiments, for example by SSAT OE in the organoid culture. Also, the combination of D-mannose and DA supplementation would be conceivable to test the requirement of SSAT activity for the D-mannose-mediated effect.

3.3.7 Overexpression of SSAT or ODC causes hair loss in mice

Strikingly, mice with systemic SSAT OE under control of its own promotor display permanent hair loss starting at the age of 3 to 4 weeks, accompanied by the formation of large dermal cysts (Pietilä et al. 1997). These mice show a massive accumulation of putrescine and *N*1-AcSpd in whole skin samples. Noticeably, ODC OE specifically in the skin also results in hair loss beginning 2 to 3 weeks after birth (Soler et al. 1996). The hair loss phenotype is less pronounced or absent when SSAT or ODC is over-expressed under the control of the metallothionein I (MT) promotor (Suppola et al. 1999; Alhonen et al. 1996). MT-ODC mice display slightly, but not significantly elevated levels of the natural polyamines, while in MT-SSAT mice putrescine and *N*1-AcSpd are increased in whole skin

samples (Pietilä et al. 2001). The authors suggest that putrescine accumulation is causal for the hair loss phenotype in these mouse models since it is the only common change.
Based on the LC-MS results, SSAT was efficiently activated upon DENSpm and D-mannose treatment in the 3D-3C organoids, resulting in elevated levels of the acetylated polyamines. However, putrescine levels were reduced upon both treatments, suggesting that the effect on cell fate is independent of intracellular putrescine levels. In contrast, SSAT OE results in the accumulation of putrescine, since it activates polyamine catabolism and biosynthesis at the same time (Pietilä et al. 1997; Kee et al. 2004). Therefore, DENSpm and D-mannose treatment and SSAT OE have partially overlapping outcomes, but the overall effect on the metabolic state of the cell is difficult to compare.
The age of the mice when the hair loss occurs suggests defective entry into the second hair cycle. After the anagen phase of the first hair cycle, which is an extension of initial follicle morphogenesis, hair follicles enter the destructive phase catagen (Fuchs and Nowak 2008). During the first telogen stage at around three weeks after birth, displacement of the ORS by the club hair results in the establishment of the bulge and simultaneous upregulation of CD34 and keratin 15 expression (Liu et al. 2003; Blanpain et al. 2004; Cotsarelis 2006). However, where the adult bulge stem cells originate from and how they organize within the niche remains unknown (Nowak et al. 2008). At the onset of anagen, the bulge stem cells are activated and form the secondary hair germ, which response to signals from the dermal papilla. This sequence of events seems to be interrupted in SSAT and ODC OE mice. However, detailed investigation of the cell populations in the hair follicle at around three weeks of age would be required to conclude which of the steps goes awry. Yet, it is likely that the CD34+ bulge stem cell population is not established in these mice. Therefore, these *in vivo* data are not readily comparable to the data obtained from the organoid culture. Nevertheless, the effect of DENSpm treatment on HFSC fate has to be confirmed *in vivo* and negative side-effects have to be excluded. To this end, the topical application of DENSpm is conceivable. The treatment should be started after the first postnatal hair cycle has been completed to ensure the proper establishment of all compartments and cell populations.

3.3.8 A negative feedback loop links putrescine levels to *hairless* expression

Strikingly, SSAT and ODC OE mice phenotypically resemble mice carrying a mutation in the *hairless* (*hr*) gene, which display total alopecia at 3 to 4 weeks of age (Stoye et al. 1988; Ahmad et al. 1998). Hr functions as a nuclear receptor co-repressor and loss of *hr* expression results in the upregulation of keratinocyte differentiation markers (Zarach et

al. 2004). Investigation of the mechanistic link between putrescine abundance and *hr* expression revealed a negative regulatory network: *Odc* expression is elevated when *hr* expression is decreased, and *vice versa* (Luke et al. 2013). In summary, high putrescine levels suppress *hr* expression (Luke et al. 2013), and loss of *hr* has been implicated in keratinocyte differentiation (Zarach et al. 2004). Therefore, putrescine treatment should decrease stem cell maintenance in the 3D-3C organoids, if the effect on cell fate was mediated via reduced *hr* expression. However, I find a specific elevation of de-differentiation upon putrescine supplementation. Thus, the putrescine-mediated effect on cell fate was likely independent of *hr* expression. Consistently, *N*1-AcSpd treatment, which also resulted in increased putrescine levels, elevated stem cell maintenance. Nevertheless, the analysis of *hr* expression upon the different treatments in the 3D-3C organoids should be performed in the future. Of note, Luke et al. (2013) find that SSAT OE mice display a patchy pattern of hair loss, while it occurs wave-like in *hr* mutant mice, suggesting an additional, *hr*-independent mechanism upon SSAT OE.

3.3.9 The role of histone modifications in the polyamine-mediated effect on stemness

Microarray analysis of putrescine-treated keratinocytes revealed that genes, which are involved in protein-protein interactions, nucleotide-binding, and transcription factor regulation, were differentially regulated (Luke et al. 2013). Furthermore, the authors suggest that putrescine might affect gene expression through epigenetic changes. Accordingly, several studies have connected polyamine levels with histone modifications. Intracellular polyamines inhibit histone lysine 4 demethylase enzymes including lysine-specific demethylase 1 (LSD1), which is a homolog of polyamine oxidase (PAOX) (Tamari et al. 2018). Additionally, spermidine abundance directly affects the activity of histone acetyltransferases (HATs) (Burgio et al. 2016). Remarkably, polyamines specifically stimulate translation of HAT mRNAs and consequently increase lysine acetylation of histones H3 and H4 (Sakamoto et al. 2020). This change in histone acetylation results in enhanced transcription of genes required for cell proliferation (Sakamoto et al. 2020).

Importantly, not only the expression of HATs, but also the level of acetyl-CoA, which serves as cofactor for histone acetylation, is influenced by the polyamine pathway: activated polyamine catabolism achieved by SSAT OE in prostate carcinoma cells was previously reported to result in a marked depletion of acetyl-CoA (Kee et al. 2004), since SSAT uses acetyl-CoA to generate *N*1-AcSpd from spermidine, and *N*1-AcSpm from spermine (Figure

34). In stark contrast, *N*1-AcSpd addition likely does not diminish acetyl-CoA availability. PAOX oxidizes *N*1-AcSpd back to putrescine and generates H_2O_2 and 3-acetamidopropanal (3-AAP) during this reaction (Figure 34). 3-AAP can be converted to β-alanine (Seiler 2004), which is then degraded to acetyl-CoA (Hayaishi et al. 1961). Thus, *N*1-AcSpd treatment should rather increase intracellular acetyl-CoA levels, and thereby, might affect histone acetylation. Of note, increased histone acetylation levels might be responsible for the elevated transcription of cell proliferation-associated genes seen upon *N*1-AcSpd supplementation. Furthermore, epigenetic changes might explain the long-term effect of *N*1-AcSpd supplementation that even persist upon withdrawal of the treatment. Therefore, investigation of histone marks in future experiments might help to understand the bigger picture of the *N*1-AcSpd-mediated effects on cell fate. Importantly, quiescent HFSCs in the bulge region are marked by low levels of histone H4 acetylation (Frye et al. 2007). Since the organoid culture leads to the activation of HFSCs, which might also affect their epigenetic landscape, the *N*1-AcSpd-mediated effect on histone modification should be confirmed *in vivo*.

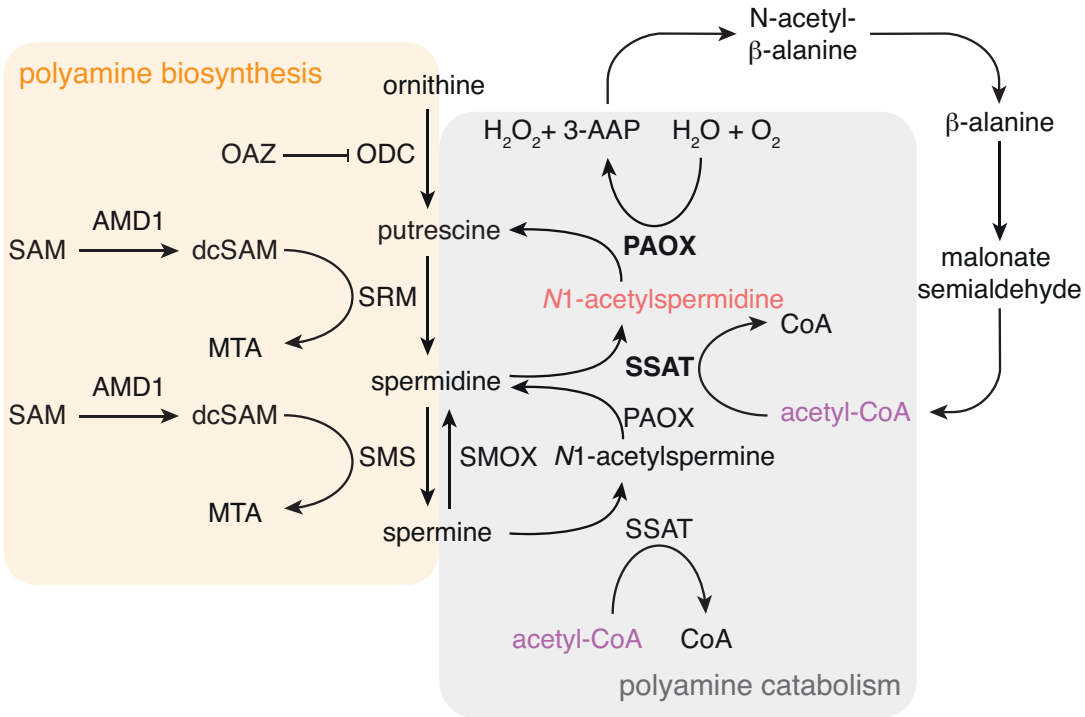

Figure 34: Polyamine biosynthesis and polyamine catabolism. During polyamine catabolism (gray) SSAT uses acetyl-CoA (displayed in violet) to acetylate spermidine and spermine to form *N*1-acetylspermidine (depicted in red) and *N*1-acetylspermine, respectively. 3-acetamidopropanal (3-AAP) can be converted to acetyl-CoA via β-alanine. dcSAM: decarboxylated SAM, MTA: 5'-methylthioadenosine, SAM: *S*-adenosylmethionine, AMD1: adenosylmethionine decarboxylase 1, OAZ: ODC antizyme, ODC: ornithine decarboxylase, PAOX: polyamine oxidase, SMS: spermine synthase, SMOX: spermine oxidase, SRM: spermidine synthase, SSAT: spermidine/spermine *N*1-acetyltransferase.

3.3.10 ODC activity links cell cycle progression and cell fate decisions in the hair follicle

Polyamines have been implicated in cell cycle progression before. Under normal growth conditions, polyamine levels are dynamically regulated during the cell cycle (Sunkara et al. 1981), which is due to cyclical changes in the activity of ODC and AMD1 (Fredlund et al. 1995). Consistently, several studies have shown that polyamine depletion results in cell cycle arrest (Ray et al. 1999; Odenlund et al. 2009; Yamashita et al. 2013). The reduction of polyamine content delays the transition from G1 to S phase (Yamashita et al. 2013). Accordingly, I found more cells in S phase upon *N*1-AcSpd treatment. Intriguingly, ODC activity was shown to be increased by *N*1-AcSpd. In contrast, *N*1-AcSpm, which did not influence cell fate in the organoid culture, does not affect ODC activity (Canellakis et al. 1989). Thus, activation of ODC might be an important step in cell fate regulation via increased cell cycle progression. Importantly, polyamines directly affect ODC levels by acting in a negative feedback loop that involves ODC antizyme (OAZ). High polyamine levels enhance synthesis and stability of OAZ, which targets ODC for ubiquitin-independent proteasomal degradation (Fong et al. 1976; Heller et al. 1976; Palanimurugan et al. 2004). Interestingly, polyamines also directly stimulate OAZ-dependent ODC degradation by the proteasome (Beenukumar et al. 2015). Intriguingly, while spermidine potently binds to OAZ, *N*1-AcSpd shows only weak interaction (Beenukumar et al. 2015), suggesting that ODC levels would be less affected by *N*1-AcSpd. In sum, ODC expression, activity, and stability should be investigated upon the different treatments in the organoid culture in future experiments.

Strikingly, the expression of ODC is dynamically regulated during the hair cycle. Nancarrow et al. (1999) showed that ODC is abundantly expressed in proliferating bulb cells of anagen follicles, while the entry of the follicle into catagen is accompanied by down-regulation of ODC. These data implicate that polyamine levels, which are controlled by ODC, might track proliferation rates in the hair follicle. Additionally, the authors revealed the expression of ODC in ORS cells in the vicinity of the follicle bulge region (Nancarrow et al. 1999). After the anagen growth phase, some ORS cells return to the bulge region, where they resume quiescence and CD34 expression. These cells become the primary stem cells for the initiation of the next hair cycle (Hsu et al. 2011). This process is comparable to the de-differentiation of α6+/CD34- progenitor cells back to the stem cell state in the 3D-3C organoids, which was enhanced by putrescine and *N*1-AcSpd supplementation. Overall, these data suggest that ODC activity, cell cycle progression, and cell fate are tightly linked. In the HF, quiescent stem cells ensure reduced translation

rates by low polyamine levels, which increase upon activation due to elevated ODC activity, resulting in accelerated cell cycle progression. My data suggest that enhanced cell cycle progression promotes stem cell self-renewal upon activation, while differentiation is decreased. At the same time, cell cycle progression might be required for successful de-differentiation of ORS cells back to HFSCs, a notion supported by elevated ODC expression in ORS cells.

Of note, HFSCs are slow-cycling, label-retaining cells *in vivo* (Cotsarelis et al. 1990; Morris and Potten 1999; Tumbar et al. 2004). Therefore, the results obtained using the organoid culture, which leads to HFSC activation, might not reflect the effects of the treatments *in vivo*. Topical application of DENSpm, putrescine, and *N*1-AcSpd is of utmost importance to confirm the observed effects on HFSC fate and ORS de-differentiation *in vivo*. To confirm the link between ODC activity, cell cycle progression, and cell fate, the influence of the different treatments on ODC expression, stability, and activity in the different cell types should be investigated.

3.3.11 Targeting the polyamine metabolism to delay stem cell exhaustion

In the final part of this study, I deciphered the polyamine-controlled effects on HFSC fate. I demonstrate that decreasing translation rates by changes in polyamine availability does not correlate with stemness. Previously, the acetylated polyamines were primarily described as the major polyamine species exported from the cell. Extending this notion, I show that *N*1-AcSpd influences cell fate decisions through enhanced cell cycle progression. My results begin to explain why elevated polyamine levels and low translation rates are not mutually exclusive in stem cell maintenance. Instead, while low mRNA translation rates favor quiescence *in vivo*, enhanced cell cycle progression ensures stem cell self-renewal upon activation. Consistently, the activation of HFSCs by depilation increases the levels of the acetylated polyamines *in vivo*. ODC activity might function as a key molecular switch to regulate polyamine availability and thus cell fate in the HF. Overall, changing polyamine availability might be a viable option to delay stem cell exhaustion. However, the outcome of the different treatments used in the final part of this study need to be validated in an *in vivo* setting and negative side-effects have to be excluded.

3.4 Metabolic control of hair follicle stem cell fate decisions

In this study, I deciphered the metabolic control of HFSC fate decisions. I focused on the hexosamine pathway, aerobic sugar metabolism, and the polyamine metabolism. While HP activation does not influence cell fate decisions, I demonstrate that sugar supplementation, as well as changes in polyamine availability are sufficient to enhance stemness in the HFSC organoids (Figure 35).

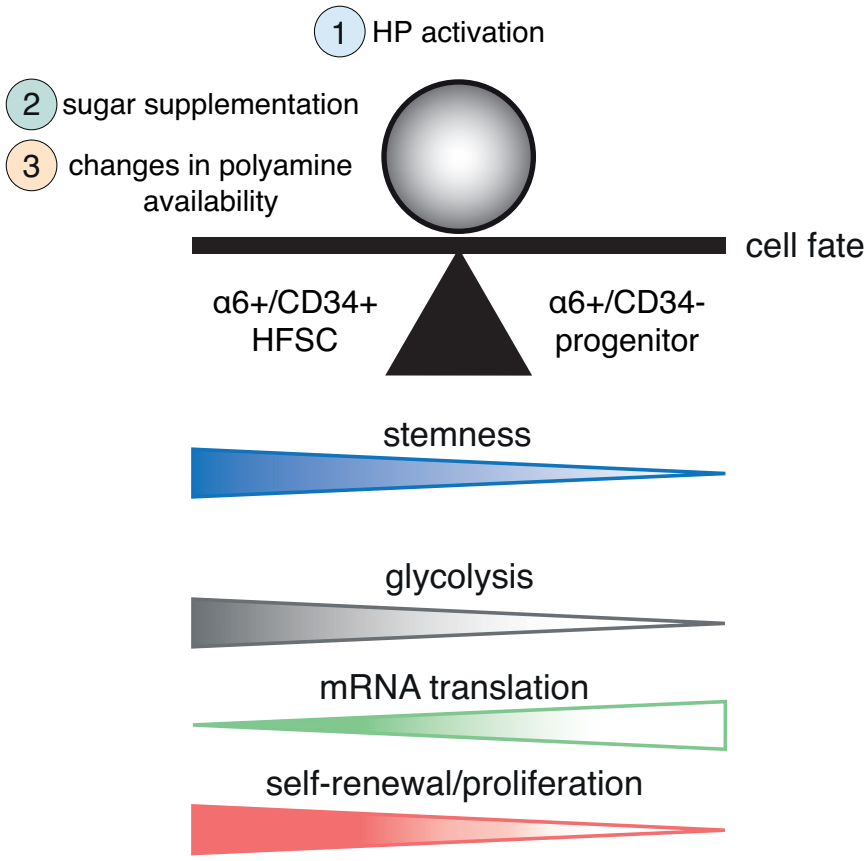

Figure 35: Model of metabolic control of cell fate decisions. Stemness (blue) correlates with high levels of glycolysis (gray) and low mRNA translation rates (green). Manipulation of aerobic sugar metabolism (2) or polyamine availability (3) elevates stemness in HFSC organoid cultures through increased aerobic glycolysis (gray) and elevated self-renewal (red), respectively. Hexosamine pathway (HP) activation (1) does not affect HFSC fate decisions in the organoids.

Unfortunately, given the negative side-effects, improving stem cell maintenance by sugar supplementation is likely unattainable. However, modulating intracellular polyamine availability might be a viable intervention to tackle age-associated diseases caused by a decline in tissue homeostasis due to stem cell exhaustion.

4 Future perspectives

My results presented in this work imply further experiments since a number of important questions remain. Although beyond the scope of this study, the answers to these questions will certainly help to better understand the polyamine-controlled effects on hair follicle stem cell fate decisions.

4.1 Does global regulation of translation affect cell fate or is post-transcriptional control of specific transcripts relevant?

I demonstrated that low translation rates mark the HFSC state and that a forced decrease in translation is sufficient to enhance stemness in the organoid culture. However, whether G418 treatment globally reduces protein synthesis or affects a specific subset of transcripts remains unclear. Further, I showed that DENSpm did not reduce global translation rates in the organoids. However, DENSpm has been reported to affect protein synthesis previously. Therefore, a change in translation of a specific subset of transcripts seems conceivable. Furthermore, *N*1-AcSpd increased global translation rates. It would be interesting to decipher the exact outcome of this change in translation. Is the global increase in translation required for the *N*1-AcSpd-mediated effect on cell fate or is translation of specific transcripts crucial? To investigate the global and specific effects on mRNA translation, sequencing of the polysome-associated mRNAs or ribosome footprinting should be performed upon the different treatments. Optimally, these approaches would be carried out in a way that allows the distinction of the two cell populations in the organoid culture. To this end, sorting of the cells prior to the experiments would be conceivable. Thereby, one might be able to identify cell type-specific effects of translational control of cell fate decisions by the treatments.

Recently, Baser et al. (2019) demonstrated that protein synthesis undergoes highly dynamic changes during the differentiation of stem cells into neurons *in* vivo. Neuronal stem cells display low translation rates, but also readily translate abundant transcripts with little discrimination. With the onset of differentiation, translation becomes progressively regulated: stem cell identity factors are translationally repressed, for example. Collectively, these data suggest that cells become increasingly dependent on post-transcriptional control as they differentiate to mature neurons (Baser et al. 2019). Whether the mechanism of post-transcriptional control also applies to HFSC differentiation still needs to be elucidated. Therefore, one could make use of the RiboTag mouse model to compare mRNA translation in HFSCs and more differentiated cells in the HF *in vivo* (Sanz et al.

2009). Further, tagging of ribosomal subunits might be useful to investigate the translational control of cell fate decisions in the organoid culture. It would allow to pull-down ribosome-bound mRNAs specifically in the population of cells that underwent de-differentiation, for example.

4.2 Does topical application of polyamines enhance stem cell function and maintenance *in vivo*?

In this study, I delineate the polyamine-controlled effects on HFSC fate. I demonstrate that accelerating cell cycle progression by *N*1-AcSpd supplementation shifts the balance towards the HFSC state in the 3D-3C organoids. However, the organoid culture leads to the activation of HFSC, which are slow cycling, label-retaining cells *in vivo* (Cotsarelis et al. 1990; Morris and Potten 1999; Tumbar et al. 2004). Therefore, it is of utmost importance to investigate the effects of the treatments *in vivo*. Although I could demonstrate an upregulation of the acetylated polyamines in the depilation experiment, it still has to be shown that polyamines in general, and *N*1-AcSpd in particular, can drive cell fate decisions *in vivo*. To this end, topical application of DENSpm, putrescine, and *N*1-AcSpd would be conceivable. *N*1-AcSpm would be the perfect control, since it did not affect cell fate in the organoid culture. Since SSAT and ODC OE results in hair loss at around 3 weeks after birth, the experiments should be started after the first postnatal hair cycle has been completed to ensure proper establishment of all compartments and cell populations.

First, one could investigate natural hair cycle progression. Importantly, the first two hair cycles occur in synchronized waves in mice; after the second cycle, hair follicles are unsynchronized (Lin et al. 2004). Entry into anagen is associated with changes in skin pigmentation due to activation of melanogenesis (Slominski and Paus 1993); thus, it can be readily monitored macroscopically. Therefore, shaving of mice in the second telogen around postnatal day (P) 50 allows for easy investigation of normal hair cycle progression. Using this method, Flores et al. (2017) demonstrated acceleration of HFSC activation and the hair cycle upon topical application of UK-5099. Thus, if topical application of DENSpm, putrescine, or *N*1-AcSpd would affect HFSC activation, anagen entry should be shifted. Since the HFSC state in the 3D-3C organoids seems to represent HFSC activation at anagen onset, the treatments used in this study are likely to accelerate hair re-growth. Especially *N*1-AcSpd should have a pronounced effect since increased proliferation is fundamental to initiate the anagen growth phase. Accordingly, application of the stable spermidine analogue α-methylspermidine (α-MeSpd) on the back of shaved mice in telogen accelerated hair growth and increased proliferation (Fashe et al. 2010).

Additionally, one could shave the mice after each round of hair cycling. This long-term hair cycle monitoring allowed Lay et al. (2016) to assess faster hair cycling with shorter resting periods in *Foxc1*-cKO mice. In these mice, entry into the second telogen occurs normally, however, precocious proliferation of *Foxc1*-cKO HFSCs results in shortened telogen phases (Lay et al. 2016). Of note, hair coats of *Foxc1*-cKO mice became sparser compared to WT counterparts and frequently greyed as they aged. Therefore, it is important to analyze the long-term effect of the treatments used here.

Second, a forced entry of anagen can be achieved by depilation-induced HFSC activation, which is a good *in vivo* model to investigate the effect of the treatments used in this study. Of note, serial depilation can accelerate the exhaustion of HFSC, since the number of hair cycles can be doubled from four to eight cycles in six months (Keyes et al. 2013). Since depilation-induced anagen is readily comparable to spontaneous anagen, topical application of DENSpm, putrescine, and *N*1-AcSpd are expected to have the same effect as upon shaving. Nevertheless, the homogeneous nature of the depilation-induced anagen might alleviate the analysis. Additionally, serial depilation can mimic the age-associated decline in stem cell function. Thus, the long-term effects of the treatments on stem cell maintenance can be easily monitored. Further, EdU injections would allow to track HFSC activation and proliferation. EdU injections can also be used to examine the kinetics of HFSC activation after depilation and topical application as shown by Keyes et al. (2013). Importantly, the effectiveness of the topical application has to be validated by quantification of polyamine levels.

5 Material and methods

5.1 Animal husbandry

5.1.1 General mouse husbandry

Animals (*Mus musculus*) were housed on a 12:12 h light:dark cycle with *ad libitum* access to food (Sniff) under pathogen-free conditions in individually ventilated cages. All animals were kept in C57BL/6J background. Animal care and experimental procedures were in accordance with the institutional and governmental guidelines.

5.1.2 Generation of transgenic mice

Generation of transgenic GFAT1 mice was performed by Taconic Biosciences (Cologne, Germany). A gene trap cassette was inserted in the *Rosa26* locus using recombination-mediated cassette exchange in embryonic stem cells. The gene trap cassette encodes a loxP-flanked transcription termination cassette upstream of the human GFAT1 (huGFAT1) open reading frame (conditional knock-in allele, $Rosa26^{flox/wt}$). Upon cre-mediated deletion of the transcription termination cassette, huGAFT1 is expressed under the control of the chicken β-actin promoter, resulting in its overexpression (constitutive knock-in allele, $Rosa26^{OE/wt}$ or $Rosa26^{G451E/wt}$). huGFAT1 is N-terminally tagged with FLAG-HA (HA: hemagglutinin; for further information, see Figure 13). Mice expressing the cre recombinase under the control of the human cytomegalovirus minimal promoter (CMV-$cre^{+/-}$) were purchased from Charles River Laboratories (Sulzfeld, Germany).

5.1.3 Breeding of transgenic mice

For breeding, $Rosa26^{flox/wt}$ males were crossed with transgenic CMV-$cre^{+/-}$ females. Homozygous overexpression of huGFAT1 was achieved by crossing double positive females ($Rosa26^{OE/wt}$, CMV-$cre^{+/-}$ or $Rosa26^{G451E/wt}$, CMV-$cre^{+/-}$) with $Rosa26^{flox/wt}$ males. Since the CMV promoter is active before implantation during early embryogenesis (Schwenk et al. 1995), animals expressing the cre recombinase and carrying the GFAT1 transgene were considered to overexpress huGFAT1 in all tissues. The offspring was genotyped as described below.

5.1.4 Tissue collection

Mice were sacrificed by cervical dislocation. Brains from 3-months old male and female mice were dissected. Cerebral hemispheres were snap frozen in liquid nitrogen and stored at -80°C until further use.

5.1.5 Depilation of dorsal skin

Animals were anesthetized with isoflurane (cp-pharma) and dorsal skin was depilated using hair removal strips. Hair re-growth was monitored daily. The mice were sacrificed on day 9 after depilation and tissue biopsies were collected for histological analysis and polyamine measurements as described below. Male mice at the age of 6 months (young) and 24 months (old) were used for the experiment.

5.2 Histological methods

5.2.1 Immunofluorescence staining

Depilated back skin was fixed using 4% PFA, embedded in paraffin and sectioned. The sections were de-paraffinized using a graded alcohol series and target retrieval was performed in Target Retrieval Solution (DAKO) pH 9 in a pressure cooker. After blocking in 5% bovine serum albumin, primary antibody (Krt14, Progen, GP-CK14, 1:500) diluted in Dako Antibody Diluent was incubated over night at 4°C. Bound primary antibody was detected by incubation with Alexa 657-conjugated secondary antibodies (Invitrogen). Nuclei were counterstained with 4′,6-diamidin-2-phenylindole (DAPI, Invitrogen). After washing, the slides were mounted in Elvanol.

5.2.2 Image acquisition and processing

All fluorescence images were collected by laser scanning confocal microscopy (SP8X; Leica) with Leica Application Suite software (LAS X version 2.0.0.14332), using a 40x immersion objective. Images were acquired using sequential scanning of frames of 1 µm thick confocal planes (pinhole 1). Afterwards, planes were projected as a maximum intensity confocal stack. Images were collected with the same settings for all samples within an experiment.

5.3 Cell biological methods

5.3.1 Cell maintenance

All cell lines and primary fibroblasts were grown in DMEM containing 4.5 g/L glucose supplemented with 10% fetal bovine serum and penicillin/streptavidin (all ThermoFisher Scientific) at 37°C in 5% CO_2 on non-coated tissue culture plates. NIH3T3 and HeLa cells were obtained from ATCC® (CRL-1658; CCL-2). HaCaT cells were a gift from Sara Wickström's laboratory (Max Planck Institute for Biology of Ageing, Cologne, Germany). HEK293T cells were a gift from Adam Antebi's laboratory (Max Planck Institute for Biology of Ageing, Cologne, Germany). Cells were passaged 2-3 times per week.

5.3.2 Isolation of primary cells from newborn mice

For keratinocyte and fibroblast isolation newborn mice (P0-P3) were sacrificed by decapitation. The corpus was incubated in 50% betaisodona/PBS (Mundipharma GmbH) for 30 min at 4°C before being washed in different solutions for 2 min each: PBS (ThermoFisher Scientific), 0.1 % octenidin in ddH2O (Serva Electrophoresis), PBS, 70% ethanol, PBS, antibiotic-antifungal-solution in PBS (ThermoFisher Scientific). Tail and legs were removed and the tail tip was used for genotyping. Complete skin was separated from the body and incubated in 2 ml dispase II solution (5 mg/ml in 50 mM HEPES/KOH pH 7.4, 150 mM NaCl; Sigma-Aldrich) over night at 4°C. The skin was placed in 500 µl FAD medium and the epidermis was separated from the dermis as a sheet. The epidermis was transferred dermal side down onto 500 µl TrypLE (ThermoFisher Scientific) and incubated for 20 min at RT. The keratinocytes were washed off the epidermis using 3 ml FAD medium. After centrifugation, the keratinocytes were resuspended in FAD medium and seeded on collagen G-coated tissue culture plates. The dermis was minced into small pieces using scalpels and transferred to a falcon tube containing collagenase (400 U/ml in 50 mM Tris base, 5 mM $CaCl_2$, pH 7.4; Sigma-Aldrich). The samples were incubated at 37°C for 1.5 h and mixed regularly. Next, the suspension was filtered through a 70 µm cell strainer, which was washed with DMEM afterwards. The cells were centrifuged for 10 min at 1000 rpm. The pellet was resuspended in DMEM (4.5 g/L glucose, 10 % FBS, P/S) and the cells were seeded on non-coated tissue culture plates. The cells were grown at 37°C in 5% CO2.

5.3.3 Culture of primary keratinocytes isolated from newborn mice

Primary keratinocytes isolated from newborn mice were cultured in DMEM/HAM's F12 (FAD) medium with low Ca^{2+} (50 µM) (Biochrom AG), supplemented with 10% fetal bovine serum (chelated, ThermoFisher Scientific), penicillin/streptavidin (ThermoFisher Scientific), L-glutamine (ThermoFisher Scientific), ascorbic acid (50 µg/ml, Sigma-Aldrich), adenine (0.18 mM, Sigma-Aldrich), insulin (5 µg/ml, Sigma-Aldrich), hydrocortisone (0.5 µg/ml, Sigma-Aldrich), EGF (10 ng/ml, Sigma-Aldrich), and cholera enterotoxin (10 ng/ml, Sigma-Aldrich) on collagen G-coated tissue culture plates (30 µg/ml in PBS, Biochrom AG). The cells were grown at 32°C in 5% CO_2.

5.3.4 Isolation of epidermal cells from adult mice

Isolation of epidermal cells from mice of both sexes in telogen stage (P21-25; P46-60) was performed as described previously (Chacón-Martínez et al. 2017). In brief, mouse skin was incubated on 0.8% trypsin (ThermoFisher Scientific) for 50 min at 37°C. The skin was transferred to 8 ml KGM medium and the epidermis was separated from the dermis. After centrifugation, keratinocytes were resuspended in ice cold KGM medium and embedded in growth factor-reduced matrigel (Corning Inc.).

5.3.5 Culture of hair follicle stem cell organoids

Hair follicle stem cell organoids were cultured in KGM medium: MEM medium (Spinner's modification, Sigma-Aldrich), supplemented with 8% fetal bovine serum (chelated, ThermoFisher Scientific), penicillin/streptavidin (ThermoFisher Scientific), L-glutamine (ThermoFisher Scientific), insulin (5 µg/ml, Sigma-Aldrich), hydrocortisone (0.36 µg/ml, Calbiochem), EGF (10 ng/ml, Sigma-Aldrich), transferrin (10 µg/ml, Sigma-Aldrich), phosphoethanolamine (10 µM, Sigma-Aldrich), ethanolamine (10 µM, Sigma-Aldrich), $CaCl_2$ (14.5 µM, Sigma-Aldrich). 5 µM Y27632, 20 ng/ml mouse recombinant VEGF, 20 ng/ml human recombinant FGF2 (all Miltenyi Biotech) were added to KGM medium. The cells were grown at 37°C in 5% CO_2 embedded in growth factor-reduced matrigel (Corning Inc.). The medium was changed 3 times per week. The following compounds were added each time the medium was changed:

2-difluoromethylornithine hydrochloride (DFMO), 2761, R&D Systems

4-methylumbelliferone (4-MU), M1381, Sigma-Aldrich

anti-CD44 antibody, clone 2C5, BBA10, R&D Systems

bafilomycin A1, B1793, Sigma-Aldrich

chloroquine diphosphate salt, C6628, Sigma-Aldrich
D-glucose, X997.2, Carl Roth
D-mannose, M8574, Sigma-Aldrich
D-sorbitol, 6213.1, Carl Roth
diminazene aceturate (DA), D7770, Sigma-Aldrich
G418 disulfate, A6798, AppliChem
hyaluronidase (HYAL) from bovine testes, H3506, Sigma-Aldrich
L-glucose, G5500, Sigma-Aldrich
MDL72527, M2949, Sigma-Aldrich
N-acetyl-D-glucosamine (GlcNAc), A8625, Sigma-Aldrich
*N*1-acetylspermidine hydrochloride (*N*1-AcSpd), 9001535, Cayman Chemical
*N*1-acetylspermine trihydrochloride (*N*1-AcSpm), 01467, Sigma-Aldrich
*N*1,*N*11-diethylnorspermine (DENSpm) tetrahydrochloride, 0468, Tocris
putrescine dihydrochloride, P5780, Sigma-Aldrich
UK-5099, PZ0160, Sigma-Aldrich
After sorting of pure populations, the cells were recovered for two days and treated for the last five days of the experiment. Before puromycin incorporation, the cells were cultured for two weeks and treated for the last 72 h, except for G418, which was only added for the last 4 h of the culture. Unless indicated otherwise, 3D-3C organoids were treated for the entire duration of the experiment. The concentrations were determined by concentration curves: the lowest concentration that had an effect on cell fate or the highest concentration without overt toxicity were chosen for further experiments.

5.3.6 Live cell number of hair follicle stem cell organoids

Sorted cells were cultured in 3D-3C organoids for 7 days and treated for the last 5 days before matrigel droplets were degraded in 0.5% trypsin, 0.5 mM EDTA in PBS for 8 min at 37°C. Trypsin was neutralized using cold KGM. The live cell number was determined using a Neubauer hemocytometer. Images of the cultures were taken on day 7 post-sorting using the EVOS FL Auto 2 Imaging System (ThermoFisher Scientific) with an 4x objective. The scale bar is 650 µm.

5.3.7 Colony formation assay

NIH3T3 fibroblasts were seeded on collagen G-coated tissue culture plates (30 µg/ml in PBS, Biochrom AG). The cells were grown at 37°C in 5% CO_2 for two days before proliferation was inhibited with mitomycin C (4 µg/ml in ddH_2O, Sigma-Aldrich).

Keratinocytes were grown in 3D-3C organodis for two weeks and analyzed by flow cytometry. 4000 cells were seeded per 6-well on the fibroblast layer in FAD medium with low Ca^{2+} (Biochrom AG), supplemented as described above. The cells were grown for 2-3 weeks at 32°C in 5% CO_2 until colonies were emerged. Remaining fibroblasts were removed using 0.25% trypsin-EDTA (ThermoFisher Scientific) for 2 min at 37°C. Trypsin was stopped using supplemented DMEM. After washing the plates with PBS, keratinocytes were fixed with 4% PFA (in PBS, Sigma-Aldrich) for 15 min at RT. The cells were washed with PBS twice and the colonies were stained using 1% crystal violet (in PBS, Sigma-Aldrich) for 1 h at RT on an orbital shaker. The wells were washed with tap water until no stain was released and air dried. The plates were scanned and the number of colonies was counted manually.

5.4 Molecular biological methods

5.4.1 Mouse genotyping

5.4.1.1 Isolation of mouse genomic DNA from ear clips

Ear clips were taken by the Comparative Biology Facility at the Max Planck Institute for Biology of Ageing (Cologne, Germany) at weaning age (3-4 weeks of age) and stored at -20°C until use. 150 µl ddH_2O and 150 µl directPCR Tail Lysis reagent (Peqlab) were mixed with 3 µl proteinase K (20 mg/ml in 25 mM Tris-HCl, 5 mM Ca_2Cl, pH 8.0, Sigma-Aldrich). This mixture was applied to the ear clips, which were then incubated at 56°C overnight (maximum 16 h) shaking at 300 rpm. Proteinase K was inactivated at 85°C for 45 min without shaking. The lysis reaction (2 µl) was used for PCR without further processing.

5.4.1.2 Genotyping PCR

For genotyping of mouse genomic DNA DreamTaq DNA polymerase (ThermoFisher Scientific) was used. PCR reactions were set up as follows:

Table 1: Composition of a DreamTaq PCR reaction mix.

Reagent	Volume (µl)	Stock concentration
Template DNA	2	
Colored buffer	2.5	10x
dNTPs	0.6-1	10 mM each nt
Primer	According to Table 3	20 µM
DreamTaq	0.125	5 U/µl
ddH_2O	ad. 25	

Table 2: Cycling and temperature profiles of a mouse genotyping PCR.

Temperature (°C)	Time (s)	Action	Number of cycles
95	120	denaturation	1
95	30	denaturation	35
60-66	30	annealing (T_A)	
72	60	elongation	
72	600	final elongation	1

Table 3: Primers used for mouse genotyping PCRs.

Trans-gene	Primer name	Sequence 5' → 3'	T_A (°C)	V (µl)	bp
Cre	Cre_fwd	GCCAGCTAAACATGCTTCATC	60	0.5	700
	Cre_rev	ATTGCCCCTGTTTCACTATCC		0.5	
	oIMR7338	CTAGGCCACAGAATTGAAAGATCT		0.5	300
	oIMR7339	GTAGGTGGAAATTCTAGCATCATCC		0.5	
hu GFAT1	huGFAT1_fwd	CGGTGGAGGTTACCCATACG	64	0.75	566
	huGFAT1_rev	CGAGCTTGGCAATTGTCTCTG		0.75	
	oIMR7338	CTAGGCCACAGAATTGAAAGATCT		0.5	300
	oIMR7339	GTAGGTGGAAATTCTAGCATCATCC		0.5	
hu GFAT1 _R26	3224_35	TTGGGTCCACTCAGTAGATGC	60	0.5	744 (tg)
	1114_1	CTCTTCCCTCGTGATCTGCAACTCC		0.25	299 (wt)
	1114_2	CTCTTCCCTCGTGATCTGCAACTCC		1.25	
hu GFAT1 _KI	2584_5	TGGCAGGCTTGAGATCTGG	66	0.75	492
	3579_152	CCCAAGGCACACAAAAAACC		0.75	
	oIMR7338	CTAGGCCACAGAATTGAAAGATCT		0.5	300
	oIMR7339	GTAGGTGGAAATTCTAGCATCATCC		0.5	

The product amplified using oIMR7338 and oIMR7339 served as internal control. The primer targeting huGFAT1 detected presence of the transgene without distinction of

zygosity. Using the huGFAT1_R26 PCR, the wildtype *Rosa26* locus and the targeted *Rosa26* locus could be distinguished. However, this reaction did not separate the conditional and constitutive knock-in alleles. The product of the huGFAT1_KI PCR is specific for the conditional knock-in allele before cre recombination, since the binding side for primer 3569_152 is in the transcription termination cassette (for further information, see Figure 13).

5.4.1.3 Agarose gel electrophoresis

DNA fragments were separated in agarose gels (1.5% agarose in 1x TAE buffer: 40 mM Tris Base, 1 mM EDTA, 1.1 ml acetic acid, pH 8.0) using horizontal gel electrophoresis at 120 V and visualized with Roti®-GelStain (Carl Roth). The Quick-Load® 100 bp DNA Ladder (New England Biolabs) was used as a marker.

5.4.2 RNA isolation

After two weeks of 3D-3C organoid culture, matrigel droplets were degraded in 0.5% trypsin, 0.5 mM EDTA in PBS for 8 min at 37°C. Trypsin was neutralized using cold KGM. After centrifugation for 5 min at 2000 rpm cells were washed with PBS. The pellet was resuspended in QIAzol (Qiagen) and frozen in liquid nitrogen. Sorted keratinocytes were collected in QIAzol and frozen in liquid nitrogen.
The samples were subjected to four freeze/thaw cycles (liquid nitrogen/37°C water bath). Half the volume of QIAZol was added and the samples were incubated for 5 min at RT. Next, 200 µl chloroform per 1 ml QIAzol were added, the samples were vortexed and incubated for 2 min at RT. After centrifugation for 15 min at 10.000 rpm and 4°C the aqueous phase was collected. An equal volume of 70% ethanol was slowly added. The mixture was transferred to a RNeasy spin column (Qiagen) and total RNA was isolated with the RNeasy Mini Kit (Qiagen) according to manufacturer's instructions.

5.4.2.1 Quantitative RT-PCR

cDNA was generated using the iScript cDNA Synthesis Kit (Bio-Rad Laboratories). Quantitative RT-PCR was performed using Power SYBR Green master mix (Applied Biosystems) on a ViiA 7 Real-Time PCR System (Applied Biosystems). Primer sequences are listed below.

Table 4: Primer sequences for quantitative RT-PCR.

Primer/gene name	Sequence (5'→ 3')
msβ-actin_fwd	TCAAGATCATTGCTCCTCCTG
msβ-actin_rev	TACTTCTGCTTGCTGATCCAC
msGAPDH_fwd	GGTGTGAACGGATTTGGCCGTATTG
msGAPDH_rev	CCGTTGAATTTGCCGTGAGTGGAGT
msCD34_fwd	TGAGATGACATCACCCACCG
msCD34_rev	GCCAACCTCACTTCTCGGAT
msSox9_fwd	AGGAAGCTGGCAGACCAGTA
msSox9_rev	TCCACGAAGGGTCTCTTCTC
msTcf3_fwd	CTCAGCAGCAAATCCAAGAGGCAGAG
msTcf3_rev	TGGGAAGACGCAGGGCTATCACAAG
msLhx2_fwd	ATCGACGAGATGGACCGCA
msLhx2_rev	TCACTGCTGATGGACGGC
msNfatc1_fwd	GGTGCTGTCTGGCCATAACT
msNfatc1_rev	CCAGGGAATTTGGCTTGCAC
msId2_fwd	ATCCCCCAGAACAAGAAGGT
msId2_rev	TGTCCAGGTCTCTGGTGATG
msDkk3_fwd	ATGCTATGCACCCGAGACAG
msDkk3_rev	GAACAGCAGGCCTCTTTGGA
msSSAT_fwd	GAGAACACCCCTTCTACCACT
msSSAT_rev	GCCTCTGTAATCACTCATCACGA

5.4.3 RNA-sequencing

5.4.3.1 Library preparation and sequencing

Total RNA was isolated as described above. Libraries were prepared at the Cologne Center for Genomics (Cologne, Germany). Sequencing was carried out on an Illumina HiSeq2000.

5.4.3.2 Bioinformatic analysis of RNA-sequencing data

Reads were mapped to the mouse reference genome GRCm38 (release 91) using HISAT2 v2.0.4 (Pertea et al. 2016). Guided transcript assembly was performed with StringTie v1.3.3 (Pertea et al. 2016) and respective assemblies were merged with Cuffmerge v.2.2.1 (Trapnell et al. 2012). After feature quantification with Cuffquant v.2.2.1, differential gene

expression was analyzed with Cuffdiff v.2.2.1 (Trapnell et al. 2012). Venn diagrams were generated using the R package VennDiagram. Functional enrichment analysis was performed using the Metascape tool [http://metascape.org] (Zhou et al. 2019). Only genes with a p-value < 0.01 and a log2FC > ±0.5 (untreated vs. treated) were defined as differentially expressed and included in the functional enrichment analysis.

5.4.4 3' RNA-sequencing

5.4.4.1 Preparation of 3' RNA-sequencing libraries

Sorted cells were collected in QIAzol and frozen in liquid nitrogen. Total RNA was isolated as described above. 50 ng RNA per sample were used for cDNA synthesis with Maxima H Minus reverse transcriptase (ThermoFisher Scientific). During reverse transcription, unique barcodes including unique molecular identifiers (UMI) were attached to each sample. After cDNA synthesis, all samples were pooled and processed in one single tube. DNA was purified using AmpureXP beads (Beckman Coulter) and the eluted cDNA was subjected to Exonuclease I treatment (New England Biolabs). cDNA was PCR-amplified for 12 cycles and subsequently purified. After purification, cDNA was tagmented in 5 technical replicates of 1 ng cDNA each using the Nextera XT Kit (Illumina), according to manufacturer's instructions. The final library was purified and concentration and size were validated by Qubit and High Sensitivity TapeStation D1000 analyses. Sequencing was carried out on an Illumina NovaSeq system.

5.4.4.2 Bioinformatic analysis of 3' RNA-sequencing data

The raw reads were demultiplexed and the UMI-tag was added to each read name using FLEXBAR (Dodt et al. 2012). The second end of the read-pairs were mapped using Kallisto creating pseudo-alignments to the mouse reference genome mm10 (Bray et al. 2016). UMI-tags were assigned using BEDTools intersect and bash re-formatting (Quinlan and Hall 2010). An R script was used to count the unique UMI-tags per gene. Differential gene expression was calculated using the R package Deseq2 (Love et al. 2014). Only genes with an average of more or equal to 5 reads over all samples were used for the analysis. Only genes with an adjusted p-value ≤ 0.05 (α6+/CD34- vs. α6+/CD34+; untreated or treated) are shown in the heatmap. Venn diagrams were generated using the R package VennDiagram. Functional enrichment analysis was performed using the Metascape tool [http://metascape.org] (Zhou et al. 2019). Only genes with a p-value < 0.05 and a

log2FC > ±0.5 (α6+/CD34- vs. α6+/CD34+; untreated or treated) were defined as differentially expressed and included in the functional enrichment analysis.

5.5 Protein biochemical methods

5.5.1 Puromycin incorporation

HaCaT cells were incubated with 10 µg/ml puromycin (Sigma-Aldrich) in the medium for exactly 10 min at 37°C. The cells were washed with PBS and collected in RIPA buffer (50 mM TrisHCl, 120 mM NaCl, 0.1% SDS, 1% NP40, 0.5% sodium deoxycholate) with proteinase and phosphatase inhibitors (Roche Diagnostics GmbH).
For 3D-3C cultured cells, matrigel droplets were degraded in 0.5% trypsin, 0.5 mM EDTA in PBS for 8 min at 37°C. Trypsin was neutralized using KGM containing puromycin (final concentration 10 µg/ml). Puromycin was incubated for exactly 10 min at 37°C. The cells were collected, washed with PBS, and collected in RIPA buffer.
After sorting, cells were allowed to recover for 30 min at 37°C before puromycin was added to the medium.

5.5.2 Western blot analysis

The protein concentration of cell lysates was determined using the Pierce™ BCA protein assay kit according to manufacturer's instructions (ThermoFisher Scientific). Samples were subsequently subjected to SDS-PAGE using 4-15% Mini-PROTEAN® TGX™ Precast Protein Gels (Bio-Rad Laboratories) and blotted on a nitrocellulose membrane using a Trans-Blot Turbo Transfer System (Bio-Rad Laboratories). The Precision Plus Protein Dual Color Standard (Bio-Rad Laboratories) was used as a marker. The following antibodies were used in 5% low-fat milk (Carl Roth) or 1% bovine serum albumin (BSA; Carl Roth) in TBS-Tween buffer (25 mM Tris base, 150 mM NaCl, 2 mM KCl, pH 7.4; 0.05% Tween-20 (w/v)) over night at 4°C: GFPT1 (rabbit, Abcam, EPR4854, 1:1.000 in BSA), hemagglutinin (HA; rat, Roche Diagnostics GmbH, 3F10, 1:1.000 in milk), puromycin (mouse, Millipore, 12D10, 1:10.000 in milk), β-actin (mouse, Cell Signaling Technologies, 8H10D10, 1:25.000 in milk), β-actin (rabbit, Cell Signaling Technologies, 4967, 1:50.000 in milk). After incubation with HRP-conjugated secondary antibody (goat anti-mouse, goat anti-rabbit, goat anti-rat, Invitrogen, 1:5000), the blot was developed with ECL solution (Merck Millipore). Films (Amersham Biosciences) were used for detection upon puromycin incorporation. Following antibody staining of GFAT1/HA bands were

detected on a ChemiDoc MP Imaging System (Bio-Rad Laboratories). The intensity of the bands was quantified using Fiji (Schindelin et al. 2012).

5.5.3 Glycosaminoglycan analysis

5.5.3.1 Hyaluronic acid ELISA

The cells were cultured for 48 h and treatment with 10 mM GlcNAc was performed for the last 24 h. The cells were grown in 10 ml serum-free DMEM for the last 8 h. The supernatant was collected and stored at -20°C until further analysis. The cells were washed with PBS and collected in RIPA buffer (50 mM TrisHCl, 120 mM NaCl, 0.1% SDS, 1% NP40, 0.5% sodium deoxycholate). 3D-3C cultured cells were grown in 500 µl serum-free KGM for the last 8 h. The supernatant was collected and stored at -20°C until further analysis. Matrigel droplets were degraded in 0.5% trypsin, 0.5 mM EDTA in PBS for 8 min at 37°C. Trypsin was neutralized using cold KGM. After centrifugation for 5 min at 2000 rpm cells were washed with PBS and collected in RIPA buffer. The protein concentration was determined using the Pierce™ BCA protein assay kit (ThermoFisher Scientific).

The hyaluronic acid concentration in the medium was analyzed using the Hyaluronan Quantikine® ELISA Kit (R&D systems) according to manufacturer's instructions. In brief, the cell culture supernatant was centrifuged and diluted 1:2 with calibrator diluent. Standard, samples, and controls were added to the microplate and incubated at RT for 2 h on an orbital shaker. The wells were washed 5 times before hyaluronan conjugate was added. After 2 h incubation at RT, the wells were washed again. Substrate solution was added to each well and incubated for 30 min in the dark. The colorimetric reaction was stopped by addition of stop solution. The optical density was measured using a microplate reader set to 450 nm with wavelength correction set to 540 nm. The results were normalized using the protein concentration measured using the Pierce™ BCA protein assay kit (ThermoFisher Scientific).

5.5.3.2 Fluorophore-Assisted Carbohydrate Electrophoresis

Cells were cultured for 48 h and treatment with 10 mM GlcNAc was performed for the last 24 h. Next, the medium was aspirated and the cells were washed 2 times with PBS. Proteinase K (Fisher BioReagents) was solved in 100 mM ammonium acetate (10x stock: 1 mg/ml). 6.9 ml 1x proteinase K were added per 10 cm plate and incubated for 2 h at

60°C. The cell layer was collected with a cell scraper and aliquots were stored at -20°C until further analysis.
Glycosaminoglycans in the cell layer were quantified using Fluorophore-Assisted Carbohydrate Electrophoresis (FACE) performed at the Cleveland Clinic (Cleveland, Ohio). In brief, upon ethanol precipitation chondroitin sulfate and hyaluronan were digested using chondroitinase and hyaluronidase, respectively. After the second ethanol precipitation the lyophilized samples were labeled with 2-amino-acridone and incubated at 37°C for 18 h in the dark. The labelled samples were analyzed using FACE. The intensity of the bands was quantified and normalized to a standard and the DNA content of the respective sample. The measurements and subsequent analysis were performed by Valbona Cali, Ronald Midura, and Vincent Hascall from the Cleveland Clinic as previously described (Calabro et al. 2000).

5.6 Flow cytometry-based methods

5.6.1 Fluorescence-activated cell sorting and analysis

Matrigel droplets were degraded in 0.5% trypsin, 0.5 mM EDTA in PBS for 8 min at 37°C. Trypsin was neutralized using cold KGM. After centrifugation for 5 min at 2000 rpm cells were washed with FACS buffer (2% FBS, 2 mM EDTA in PBS). Surface marker staining was performed for 30 min on ice with the following antibodies: CD34-eFluor 660 (eBioscience, clone RAM34, 1:100) and ITGA6-PE/Cy7 (Biolegend, clone GoH3, 1:1000) for sorting or CD34-eFluor 660 (eBioscience, clone RAM34, 1:100) and ITGA6-pacific blue (Biolegend, clone GoH3, 1:200) for analysis. Freshly isolated keratinocytes were stained additionally with Sca1-pacific blue (Biolegend, clone D7, 1:400). 7-aminoactinomycin D (7AAD, 1 µg/ml in DSMO; ThermoFisher Scientific) or propidium iodide (PI, 0.5 µg/ml in H_2O; Sigma-Aldrich) was used to exclude dead cells. Cells were analyzed on FACSCantoII (BD Biosciences) or sorted on FACSAria IIIu Svea and FACSAria Fusion sorters (BD Biosciences). Sorted cells were collected in 15 ml tubes containing KGM at 4°C.
Cell sorting was performed by Kat Folz-Donahue and Lena Schumacher from the FACS and Imaging Core Facility (Max Planck Institute for Biology of Ageing, Cologne, Germany).

5.6.2 EdU incorporation and detection

Cell proliferation was assessed using the Click-iT™ Plus EdU Alexa Fluor™ 488 Flow Cytometry Assay Kit (ThermoFisher Scientific) following the manufacturer's instructions. Cells were grown for 9-14 days in 3D-3C culture before 10 µM EdU was added to the

medium and incubated for 24 h. Alternatively, cells were grown for 14 days in 3D-3C culture before 10 µM EdU was added to the medium and incubated for 2 h. Matrigel droplets were degraded, the cells were washed with PBS and subsequently stained with fixable LIVE/DEAD-violet (ThermoFisher Scientific, 1:500) for 20 min at RT. The cells were washed with FACS buffer and surface marker staining was performed for 30 min on ice using CD34-eFluor 660 (eBioscience, clone RAM34, 1:100) and ITGA6-PE/Cy7 (Biolegend, clone GoH3, 1:1000). The cells were washed with 1% BSA in PBS, fixed with 4% PFA for 10 min at RT and permeabilized using Click-iT saponin-based permeabilization buffer for 15 min at RT. The EdU reaction cocktail was prepared following the manufacturer's instructions and incubated for 30 min at RT in the dark after washing the cells. The cells were analyzed on FACSCantoII (BD Biosciences).

5.6.3 Cell cycle analysis

Cell proliferation was assessed using the Click-iT™ Plus EdU Alexa Fluor™ 488 Flow Cytometry Assay Kit (ThermoFisher Scientific) as described above. Cells were grown for two weeks in 3D-3C culture before 10 µM EdU was added to the medium and incubated for 2 h. Matrigel droplets were degraded, the cells were washed with PBS and stained with fixable Zombie NIR dye (Biolegend, 1:500) for 20 min at RT. The cells were washed, fixed, and permeabilized and the EdU reaction cocktail was incubated as described above. Subsequently, the cells were permeabilized using 0.1% triton X-100 in PBS for 15 min at RT and stained with FxCycle violet (ThermoFisher Scientific, 1:500) for 30 min at RT. The cells were analyzed on FACSCantoII (BD Biosciences) without further washing.

5.6.4 Annexin V staining

Matrigel droplets were degraded in 0.5% trypsin, 0.5 mM EDTA in PBS for 8 min at 37°C. Trypsin was neutralized using cold KGM. After centrifugation for 5 min at 2000 rpm cells were washed with FACS buffer. Surface marker staining was performed for 30 min on ice using CD34-eFluor 660 (eBioscience, clone RAM34, 1:100) and ITGA6-pacific blue (Biolegend, clone GoH3, 1:200). Cells were washed with PBS and stained with annexin V-AF488 (1:20 in 100 µl annexin-binding buffer per sample; ThermoFisher Scientific) for 15 min at RT. 100 µl annexin-binding buffer containing PI (0.5 µg/ml in H_2O; Sigma-Aldrich) were added per sample. The supernatant of the matrigel droplets was collected and stained together with the embedded cells. The samples were analyzed on FACSCantoII (BD Biosciences).

5.7 Metabolomic approaches

5.7.1 Metabolomic analysis of acetylated aminosugars

Two different methods were applied for the analysis of UDP-HexNAc levels (5.7.1.1) or UDP-GlcNAc and UDP-GalNAc levels (5.7.1.2).

5.7.1.1 Determination of UDP-HexNAc levels

Cells were trypsinized and collected. The pellet was washed once with PBS and snap frozen in liquid nitrogen. 250 µl ddH2O were added to the pellet and the samples were vortexed for 30 s. The samples were subjected to four freeze/ thaw cycles (liquid nitrogen/ 37°C water bath). Next, the protein concentration was measured using the Pierce™ BCA protein assay kit (ThermoFisher Scientific). 200 µl with a protein concentration of 1 µg/µl were mixed with 1 ml chloroform:methanol (1:2) and incubated on a nutator mixer for 1 h at RT. After centrifugation for 5 min at full speed, the supernatant was transferred to a glass vial. The liquid was evaporated in an EZ-2 Plus Genevac centrifuge evaporator (SP Scientific) with the following settings: time to final stage 15 min, final stage time 4 h, low boiling point mixture. After evaporation, the samples were stored at -20°C until further use. Absolute UDP-HexNAc levels were determined using an Acquity UPLC connected to a Xevo TQ Mass Spectrometer (both Waters) and normalized to total protein content. The measurements and subsequent analysis were performed by Yvonne Hinze from the Metabolomics Core Facility at the Max Planck Institute for Biology of Ageing (Cologne, Germany) as previously described (Denzel et al. 2014).

5.7.1.2 Determination of UDP-GlcNAc and UDP-GalNAc levels

Matrigel droplets were degraded in 0.5% trypsin, 0.5 mM EDTA in PBS for 8 min at 37°C. Trypsin was neutralized using cold KGM. After centrifugation for 5 min at 2000 rpm cells were washed with PBS and the pellet was snap frozen in liquid nitrogen.
Brains were collected from 3 months old mice, cut in half, and snap frozen in liquid nitrogen. Tissue was disrupted using a TissueLyser II (Qiagen) at 20-25 Hz. The powder was transferred to a fresh tube and subjected to metabolite extraction.
Metabolite extraction was performed using 80% methanol. After vortexing, the samples were incubated at -20°C for 30 min. Afterwards, samples were incubated on an orbital mixer at 5°C for 30 min. The samples were centrifuged for 5 min at full speed and 4°C. The supernatant was transferred to a fresh tube and the pellet was used for protein

extraction with 0.5% SDS. The supernatant was evaporated in a SpeedVac concentrator at 25°C.

The metabolite analysis was conducted using a Dionex ICS-5000 anion exchange chromatography (ThermoFisher Scientific). Separation was performed with a Dionex Ionpac AS11-HC column (2 mm x 250 mm, 4 µm particle size, Thermo Fisher) at 30°C. A guard column, Dionex Ionpac AG11-HC b (2 mm x 50 mm, 4 µm particle size, ThermoFisher Scientific), was placed before the separation column. The eluent (KOH) was generated by a KOH cartridge using ddH_2O. A gradient was used for the separation at a flow rate of 0.380 ml/min: 0-8 min 30 mM KOH, 8-12 min 35-100 mM KOH, 12-15 min 100 mM KOH, 15-19 min 30 mM KOH. A Dionex suppressor AERS 500 (2 mm) was used for the exchange of KOH and operated with 95 mA at 17°C. The suppressor pump flow was set to 0.6 ml/min. Samples were diluted in ddH_2O and injected from a tempered autosampler (8°C) using full loop mode (10 µl). The Dionex ICS-5000 was connected to a XevoTM TQ mass spectrometer (Waters) and operated in negative ESI MRM (multi reaction monitoring) mode. The source temperature was set to 150°C, the desolvation temperature was set to 350°C and desolvation gas was set to 650 l/h, while cone gas was set to 50 l/h. The MRM transition 606.10 $\rightarrow$ 158.80 was used for quantification of UDP-GlcNAc and UDP-GalNAc. An external standard calibration curve was prepared from 50 to 1000 ng/ml UDP-GlcNAc and UDP-GalNAc. Data were analyzed using the MassLynx and TargetLynx software (Waters). Metabolite extraction, measurements, and subsequent analysis were performed by Silvina Perin from the Metabolomics Core Facility at the Max Planck Institute for Biology of Ageing (Cologne, Germany).

5.7.2 Untargeted metabolomics

Metabolite extraction, measurements and subsequent analysis were performed by Andrea Annibal from Adam Antebi's laboratory at the Max Planck Institute for Biology of Ageing (Cologne, Germany) with the help of Christina Latza.

5.7.2.1 Metabolite extraction for untargeted metabolomics

Cells were collected and washed with PBS. The pellet was frozen in liquid nitrogen. The cells were lysed in ddH_2O by freeze/thaw cycles and the protein concentration was determined using the Pierce™ BCA protein assay kit (ThermoFisher Scientific).

Metabolites were extracted by Bligh and Dyer extraction (Noga et al. 2012; Pieragostino et al. 2015). In brief, a methanol:chloroform mixture 2:1 (v/v) was added to a volume of cell lysate, which corresponded to 150 µg of protein and incubated for 1 h at 4°C. Samples

were centrifuged for 5 min at 3000 rcf at 4°C and the liquid phase was transferred to a fresh tube and dried in a SpeedVac Vacuum Concentrator (Genevac). Before LC injections, samples were reconstituted in 10% aqueous acetonitrile. Samples were analyzed using an untargeted method for total metabolomics.

5.7.2.2 Untargeted analysis of metabolites

Analytes were separated using an UHPLC system (Vanquish, ThermoFisher Scientific) coupled to an HRAM mass spectrometer (Q-Exactive Plus, ThermoFischer Scientific) using a modified RP-MS method from Wang et al. (2019). Briefly, 2 µl of the sample were injected into a X Select HSS T3 XP column, 100 Å, 2.5 µm, 2.1 mm x 100 mm (Waters), using a binary system (A: water with 0.1% formic acid, B: acetonitrile with 0.1% formic acid) with a flowrate of 0.1 ml/min. The column temperature was kept at 30°C. Gradient elution was conducted as follows: isocratic step at 0.1% eluent B for 0.3 min, gradient increase up to 2% eluent B in 2 min, then increase up to 30% eluent B in 6 min and to 95% eluent B in 7 min, isocratic step at 95% eluent B for 2 min. Gradient decreases to 0.1% eluent B in 3 min and held at 0.1% eluent B for 5 min. Mass spectra were recorded from 100-800 m/z at a mass resolution of 70.000 at m/z 400 in both positive and negative ion modes using data dependent acquisition (Top 3, dynamic exclusion list 10 s). Tandem mass spectra were acquired by performing CID (isolation 1.5 a.u., stepped collision energy 20 and 80 NCE). The m/z of leucine enkephaline was used as lock mass. Sample injection order was randomized to minimize the effect of instrumental signal drift. MS data analysis was performed using Xcalibur software 4.0.

5.7.2.3 Compound identification and quantification

Metabolite search was performed using Compound discoverer 2.0 and m/z Cloud as online databases, considering precursor ions with a deviation > 5 ppm, 0.3 min maximum retention time shift, minimum peak intensity 100.000, intensity tolerance 10, FT fragment mass tolerance 0.0025 Da, group covariance [%] < 30, p-value < 0.05 and area Max ≥ 10.000. Metabolites are correctly identified when at least two specific fragments were found in the MS2 spectra. Because of the high mass accuracy > 3 ppm, predicted elemental compositions of the unknown features were submitted to other online databases such as Chemspider (http://www.chemspider.com/), HMDB (http://www.hmdb.org/), KEGG (http://www.genome.jp/kegg/), and METLIN (http://metlin.scripps.edu/).
Quantification was performed using Trace finder 4.1, using genesis detection algorithm, nearest RT, S/N threshold 8, min peak height (S/N) equal to 3, peak S/N cutoff 2.00, valley

rise 2%, valley S/N 1.10. Relative quantification was obtained by dividing the area of individual metabolites to spiked internal standards (leucine enkephaline, myrystic acid and cysteamine sodium salt).

5.7.3 Targeted analysis of polyamines

The measurements and subsequent analysis were performed by Andrea Annibal from Adam Antebi's laboratory at the Max Planck Institute for Biology of Ageing (Cologne, Germany) with the help of Christina Latza.

5.7.3.1 Sample preparation for polyamine extraction from cells

Matrigel droplets were degraded in 0.5% trypsin, 0.5 mM EDTA in PBS for 8 min at 37°C. Trypsin was neutralized using cold KGM. After centrifugation for 5 min at 2000 rpm cells were washed with PBS. Sorted cells were centrifuged and washed with PBS. The pellet was flash frozen in liquid nitrogen. The cells were lysed in ddH_2O by freeze/thaw cycles and the protein concentration was determined using the Pierce™ BCA protein assay kit (ThermoFisher Scientific).

5.7.3.2 Sample preparation for polyamine extraction from epidermis

Depilated skin (anagen) and control skin (telogen) was collected and incubated on collagenase (400 U/ml in 50 mM Tris base, 5 mM $CaCl_2$, pH 7.4; Sigma-Aldrich) at 37°C for 45 min with the dermal side down. The dermis was separated from the epidermis using a scalpel and the epidermis was frozen in liquid nitrogen. Tissue was disrupted using a TissueLyser II (Qiagen) at 20-25 Hz. The powder was transferred to a fresh tube and solved in ddH_2O. After four freeze/thaw cycles, the protein concentration was determined using the Pierce™ BCA protein assay kit (ThermoFisher Scientific).

5.7.3.3 Polyamine extraction

Polyamines were extracted by Bligh and Dyer extraction (Noga et al. 2012; Pieragostino et al. 2015). In brief, a methanol:chloroform mixture 2:1 (v/v) was added to a volume of cell lysate, which corresponded to 100 µg of protein and incubated 1 h at 4°C. Samples were centrifuged for 5 min at 3000 rcf at 4°C and the liquid phase was transferred to a fresh tube and dried in a SpeedVac Vacuum Concentrator (Genevac). Samples were

reconstituted with 15 µL aqueous acetonitrile 2:3 (v/v) and 10 µl were injected into the LC-MS system.

5.7.3.4 Targeted analysis of polyamines by LC-MS

The identification of polyamines was performed on a triple stage quadrupole (TSQ Altis, ThermoFisher Scientific GmbH) coupled with a binary pump system (Vanquish, ThermoFisher Scientific GmbH). Polyamine species were separated using a reverse column (Xselect column, 2.1x100mm, 2,5 µm) using solvent A (water with 0.1% formic acid) and B (acetonitrile with 0.1% formic acid) as previously reported (Sanchez-Lopez et al. 2009; Hakkinen et al. 2008; Hakkinen et al. 2013).

The gradient started from 0.1% eluent B and ramped to 0.3% eluent B in 0.5 min. It ramped further to 0.5% eluent B in 0.5 min and to 1% B in the next 0.5 min. The gradient increased to 2% eluent B in the next minute, then it ramped to 5% eluent B in 1 min. In the following 3 min it went to 95% eluent B and stayed constant for 3 min. Afterwards the gradient decreased to 0.1% eluent B in 2 min and stayed constant for 3 min adding up to a total time of 15 min. The column was heated to 30°C using a flow rate of 100 µl/min. The LC system was flushed in between runs with isopropanol:water 75:25 (v/v) with 0.1% FA.

Polyamines were detected using heated electrospray ionization (HESI) with the following parameters: 10 (a.u.) sheath gas, 5 (a.u.) auxiliary, 200°C transfer ion capillary and 3 kV for spray voltage.

Relative quantification was performed using selected ion monitoring chromatogram mode (SIM-Q1) in positive ion mode using a scan rate of 1000 Da/sec, Q1 resolution was set to 0.7 *m/z* and calibrated RF lenses were used. The following ions were monitored: arginine $\rightarrow$ 175.2, ornithine $\rightarrow$ 133.17, putrescine $\rightarrow$ 89.17, spermidine $\rightarrow$ 146.23, spermine $\rightarrow$ 203.32, *N*1-acetylspermidine $\rightarrow$ 188.25, *N*1-acetylspermine $\rightarrow$ 245.34, *N*1,*N*11-diethylnorspermine $\rightarrow$ 245.39. The relative response for each polyamine was calculated using Spermidine-(butyl-d8) as internal standard.

Table 5: Detailed description of the detected metabolites.

Name	Elemental composition	retention time (min)	Mass (amu)	$[M+H]^+$ *(m/z)*
Arginine	$C_6H_{14}N_4O_2$	2.38	174.111	175.118
Ornithine	$C_5H_{12}N_2O_2$	2.73	132.089	133.097
Putrescine	$C_4H_{12}N_2$	2.41	88.099	89.107
Spermidine	$C_7H_{19}N_3$	2.22	145.157	146.165
Spermine	$C_{10}H_{26}N_4$	2.46	202.215	203.223
*N*1-acetylspermidine	$C_9H_{21}N_3O$	3.14	187.167	188.175
*N*1-acetylspermine	$C_{12}H_{28}N_4O$	3.05	244.225	245.233
*N*1,*N*11-diethylnorspermine	$C_{13}H_{32}N_4$	2.30	244.262	245.269

5.7.4 Lactate assay

Medium was collected after 24 h of culture. Lactate concentration was determined using the Lactate Assay Kit (Sigma-Aldrich) according to manufacturer's instructions. In brief, a standard curve was prepared using the 1 nmol/µl lactate standard provided. The samples were diluted 1:200 in lactate assay buffer and lactate enzyme mix was added to each well. After incubation for 30 min at RT on an orbital shaker protected from light, absorbance was measured at 570 nm. The results were multiplied by the molecular weight of lactate (89.07 g/mol) and normalized to protein concentration measured by BCA assay.

5.8 Statistical analysis

Data are presented as mean ± SEM, mean ± SD or as mean + SEM. Biological replicates represent different passages of the cells that were seeded on independent days, independent donors for 3D-3C organoids, or independent mice. Statistical significance was calculated using GraphPad Prism 8 (GraphPad Software). The statistical test used is indicated in the respective figure legend. Significance levels are * $p<0.05$, ** $p<0.01$, *** $p<0.001$ versus the respective control.

5.9 Software

Most graphs were generated using GraphPad Prism 8 (GraphPad Software). For Western blot analysis, the intensity of the bands was quantified using Fiji (Schindelin et al. 2012). Flow profiles were recorded and exported with the FACSDiva™ software (BD Biosciences). FlowJo™ Software v.10.0.8 (FlowJo LLC) was used for the analysis of flow cytometry data and for the generation of dot plots. Functional enrichment analysis was performed using the Metascape tool [http://metascape.org] (Zhou et al. 2019).

References

Abbruzzese, A., Park, M. H., and Folk, J. E. 1986. 'Deoxyhypusine hydroxylase from rat testis. Partial purification and characterization', *J Biol Chem*, 261: 3085-9.

Abdel Rahman, A. M., Ryczko, M., Pawling, J., and Dennis, J. W. 2013. 'Probing the hexosamine biosynthetic pathway in human tumor cells by multitargeted tandem mass spectrometry', *ACS Chem Biol*, 8: 2053-62.

Abeloff, M. D., Slavik, M., Luk, G. D., Griffin, C. A., Hermann, J., Blanc, O., Sjoerdsma, A., and Baylin, S. B. 1984. 'Phase I trial and pharmacokinetic studies of alpha-difluoromethylornithine--an inhibitor of polyamine biosynthesis', *J Clin Oncol*, 2: 124-30.

Ahmad, W., Panteleyev, A. A., Sundberg, J. P., and Christiano, A. M. 1998. 'Molecular basis for the rhino (hrrh-8J) phenotype: a nonsense mutation in the mouse hairless gene', *Genomics*, 53: 383-6.

Alhonen, L., Heikkinen, S., Sinervirta, R., Halmekytö, M., Alakuijala, P., and Jänne, J. 1996. 'Transgenic mice expressing the human ornithine decarboxylase gene under the control of mouse metallothionein I promoter', *Biochem J*, 314 (Pt 2): 405-8.

Alm, K., and Oredsson, S. 2009. 'Cells and polyamines do it cyclically', *Essays Biochem*, 46: 63-76.

Alonso, L., and Fuchs, E. 2003. 'Stem cells of the skin epithelium', *Proc Natl Acad Sci U S A*, 100 Suppl 1: 11830-5.

Alonso, L., and Fuchs, E. 2006. 'The hair cycle', *J Cell Sci*, 119: 391-3.

Álvarez-Añorve, L. I., Alonzo, D. A., Mora-Lugo, R., Lara-González, S., Bustos-Jaimes, I., Plumbridge, J., and Calcagno, M. L. 2011. 'Allosteric kinetics of the isoform 1 of human glucosamine-6-phosphate deaminase', *Biochim Biophys Acta*, 1814: 1846-53.

Anderegg, U., Simon, J. C., and Averbeck, M. 2014. 'More than just a filler - the role of hyaluronan for skin homeostasis', *Exp Dermatol*, 23: 295-303.

Andl, C. D., and Rustgi, A. K. 2005. 'No one-way street: cross-talk between e-cadherin and receptor tyrosine kinase (RTK) signaling: a mechanism to regulate RTK activity', *Cancer Biol Ther*, 4: 28-31.

Andreotti, G., Pedone, E., Giordano, A., and Cubellis, M. V. 2013. 'Biochemical phenotype of a common disease-causing mutation and a possible therapeutic approach for the phosphomannomutase 2-associated disorder of glycosylation', *Mol Genet Genomic Med*, 1: 32-44.

Andres, L. M., Blong, I. W., Evans, A. C., Rumachik, N. G., Yamaguchi, T., Pham, N. D., Thompson, P., Kohler, J. J., and Bertozzi, C. R. 2017. 'Chemical Modulation of Protein O-GlcNAcylation via OGT Inhibition Promotes Human Neural Cell Differentiation', *ACS Chem Biol*, 12: 2030-39.

Arreola, R., Valderrama, B., Morante, M. L., and Horjales, E. 2003. 'Two mammalian glucosamine-6-phosphate deaminases: a structural and genetic study', *FEBS Lett*, 551: 63-70.

Aruffo, A., Stamenkovic, I., Melnick, M., Underhill, C. B., and Seed, B. 1990. 'CD44 is the principal cell surface receptor for hyaluronate', *Cell*, 61: 1303-13.

Ashapkin, V. V., Kutueva, L. I., Kurchashova, S. Y., and Kireev, II. 2019. 'Are There Common Mechanisms Between the Hutchinson-Gilford Progeria Syndrome and Natural Aging?', *Front Genet*, 10: 455.

Assrir, N., Richez, C., Durand, P., Guittet, E., Badet, B., Lescop, E., and Badet-Denisot, M. A. 2014. 'Mapping the UDP-N-acetylglucosamine regulatory site of human glucosamine-6P synthase by saturation-transfer difference NMR and site-directed mutagenesis', *Biochimie*, 97: 39-48.

Aunan, J. R., Watson, M. M., Hagland, H. R., and Soreide, K. 2016. 'Molecular and biological hallmarks of ageing', *Br J Surg*, 103: e29-46.

Aviner, R. 2020. 'The science of puromycin: From studies of ribosome function to applications in biotechnology', *Comput Struct Biotechnol J*, 18: 1074-83.

Badet, B., Vermoote, P., Haumont, P. Y., Lederer, F., and LeGoffic, F. 1987. 'Glucosamine synthetase from Escherichia coli: purification, properties, and glutamine-utilizing site location', *Biochemistry*, 26: 1940-8.

Bar-Nun, S., Shneyour, Y., and Beckmann, J. S. 1983. 'G-418, an elongation inhibitor of 80 S ribosomes', *Biochim Biophys Acta*, 741: 123-7.

Barna, M., Pusic, A., Zollo, O., Costa, M., Kondrashov, N., Rego, E., Rao, P. H., and Ruggero, D. 2008. 'Suppression of Myc oncogenic activity by ribosomal protein haploinsufficiency', *Nature*, 456: 971-5.

Baser, A., Skabkin, M., Kleber, S., Dang, Y., Gülcüler Balta, G. S., Kalamakis, G., Göpferich, M., Ibañez, D. C., Schefzik, R., Lopez, A. S., Bobadilla, E. L., Schultz, C., Fischer, B., and Martin-Villalba, A. 2019. 'Onset of differentiation is post-transcriptionally controlled in adult neural stem cells', *Nature*, 566: 100-04.

Beebe, K., and Thummel, C. S. 2018. 'For Intestinal Homeostasis, You Are What You Eat', *Dev Cell*, 47: 1-2.

Beenukumar, R. R., Gödderz, D., Palanimurugan, R., and Dohmen, R. J. 2015. 'Polyamines directly promote antizyme-mediated degradation of ornithine decarboxylase by the proteasome', *Microb Cell*, 2: 197-207.

Bello-Fernandez, C., Packham, G., and Cleveland, J. L. 1993. 'The ornithine decarboxylase gene is a transcriptional target of c-Myc', *Proc Natl Acad Sci U S A*, 90: 7804-8.

Bernstein, E. F., Underhill, C. B., Hahn, P. J., Brown, D. B., and Uitto, J. 1996. 'Chronic sun exposure alters both the content and distribution of dermal glycosaminoglycans', *Br J Dermatol*, 135: 255-62.

Bey, P., Bolkenius, F. N., Seiler, N., and Casara, P. 1985. 'N-2,3-Butadienyl-1,4-butanediamine derivatives: potent irreversible inactivators of mammalian polyamine oxidase', *J Med Chem*, 28: 1-2.

Bickel, T., Lehle, L., Schwarz, M., Aebi, M., and Jakob, C. A. 2005. 'Biosynthesis of lipid-linked oligosaccharides in Saccharomyces cerevisiae: Alg13p and Alg14p form a complex required for the formation of GlcNAc(2)-PP-dolichol', *J Biol Chem*, 280: 34500-6.

Biteau, B., Karpac, J., Supoyo, S., Degennaro, M., Lehmann, R., and Jasper, H. 2010. 'Lifespan extension by preserving proliferative homeostasis in Drosophila', *PLoS Genet*, 6: e1001159.

Blanco, S., Bandiera, R., Popis, M., Hussain, S., Lombard, P., Aleksic, J., Sajini, A., Tanna, H., Cortes-Garrido, R., Gkatza, N., Dietmann, S., and Frye, M. 2016. 'Stem cell function and stress response are controlled by protein synthesis', *Nature*, 534: 335-40.

Blanco, S., Kurowski, A., Nichols, J., Watt, F. M., Benitah, S. A., and Frye, M. 2011. 'The RNA-methyltransferase Misu (NSun2) poises epidermal stem cells to differentiate', *PLoS Genet*, 7: e1002403.

Blanpain, C., and Fuchs, E. 2009. 'Epidermal homeostasis: a balancing act of stem cells in the skin', *Nat Rev Mol Cell Biol*, 10: 207-17.

Blanpain, C., Lowry, W. E., Geoghegan, A., Polak, L., and Fuchs, E. 2004. 'Self-renewal, multipotency, and the existence of two cell populations within an epithelial stem cell niche', *Cell*, 118: 635-48.

Bonnans, C., Chou, J., and Werb, Z. 2014. 'Remodelling the extracellular matrix in development and disease', *Nat Rev Mol Cell Biol*, 15: 786-801.

Boukamp, P., Petrussevska, R. T., Breitkreutz, D., Hornung, J., Markham, A., and Fusenig, N. E. 1988. 'Normal keratinization in a spontaneously immortalized aneuploid human keratinocyte cell line', *J Cell Biol*, 106: 761-71.

Bourguignon, L. Y. 2014. 'Matrix hyaluronan-activated CD44 signaling promotes keratinocyte activities and improves abnormal epidermal functions', *Am J Pathol*, 184: 1912-9.

Boyce, M., Carrico, I. S., Ganguli, A. S., Yu, S. H., Hangauer, M. J., Hubbard, S. C., Kohler, J. J., and Bertozzi, C. R. 2011. 'Metabolic cross-talk allows labeling of O-linked beta-N-acetylglucosamine-modified proteins via the N-acetylgalactosamine salvage pathway', *Proc Natl Acad Sci U S A*, 108: 3141-6.

Bradley, E., Bieberich, E., Mivechi, N. F., Tangpisuthipongsa, D., and Wang, G. 2012. 'Regulation of embryonic stem cell pluripotency by heat shock protein 90', *Stem Cells*, 30: 1624-33.

Bray, N. L., Pimentel, H., Melsted, P., and Pachter, L. 2016. 'Erratum: Near-optimal probabilistic RNA-seq quantification', *Nat Biotechnol*, 34: 888.

Broschat, K. O., Gorka, C., Page, J. D., Martin-Berger, C. L., Davies, M. S., Huang Hc, H. C., Gulve, E. A., Salsgiver, W. J., and Kasten, T. P. 2002. 'Kinetic characterization of human glutamine-fructose-6-phosphate amidotransferase I: potent feedback inhibition by glucosamine 6-phosphate', *J Biol Chem*, 277: 14764-70.

Brunton, V. G., MacPherson, I. R., and Frame, M. C. 2004. 'Cell adhesion receptors, tyrosine kinases and actin modulators: a complex three-way circuitry', *Biochim Biophys Acta*, 1692: 121-44.

Buckley, S. M., Aranda-Orgilles, B., Strikoudis, A., Apostolou, E., Loizou, E., Moran-Crusio, K., Farnsworth, C. L., Koller, A. A., Dasgupta, R., Silva, J. C., Stadtfeld, M., Hochedlinger, K., Chen, E. I., and Aifantis, I. 2012. 'Regulation of pluripotency and cellular reprogramming by the ubiquitin-proteasome system', *Cell Stem Cell*, 11: 783-98.

Budenholzer, L., Cheng, C. L., Li, Y., and Hochstrasser, M. 2017. 'Proteasome Structure and Assembly', *J Mol Biol*, 429: 3500-24.

Bueb, J. L., Da Silva, A., Mousli, M., and Landry, Y. 1992. 'Natural polyamines stimulate G-proteins', *Biochem J*, 282 (Pt 2): 545-50.

Buhren, B. A., Schrumpf, H., Hoff, N. P., Bolke, E., Hilton, S., and Gerber, P. A. 2016. 'Hyaluronidase: from clinical applications to molecular and cellular mechanisms', *Eur J Med Res*, 21: 5.

Burda, P., and Aebi, M. 1999. 'The dolichol pathway of N-linked glycosylation', *Biochim Biophys Acta*, 1426: 239-57.

Burgio, G., Corona, D. F., Nicotra, C. M., Carruba, G., and Taibi, G. 2016. 'P/CAF-mediated spermidine acetylation regulates histone acetyltransferase activity', *J Enzyme Inhib Med Chem*, 31: 75-82.

Calabro, A., Benavides, M., Tammi, M., Hascall, V. C., and Midura, R. J. 2000. 'Microanalysis of enzyme digests of hyaluronan and chondroitin/dermatan sulfate by fluorophore-assisted carbohydrate electrophoresis (FACE)', *Glycobiology*, 10: 273-81.

Calder, A., Roth-Albin, I., Bhatia, S., Pilquil, C., Lee, J. H., Bhatia, M., Levadoux-Martin, M., McNicol, J., Russell, J., Collins, T., and Draper, J. S. 2013. 'Lengthened G1 phase indicates differentiation status in human embryonic stem cells', *Stem Cells Dev*, 22: 279-95.

Canellakis, Z. N., Marsh, L. L., and Bondy, P. K. 1989. 'Polyamines and their derivatives as modulators in growth and differentiation', *Yale J Biol Med*, 62: 481-91.

Çayli, A., Hirschmann, F., Wirth, M., Hauser, H., and Wagner, R. 1999. 'Cell lines with reduced UDP-N-acetylhexosamine pool in the presence of ammonium', *Biotechnol Bioeng*, 65: 192-200.

Chacón-Martínez, C. A., Klose, M., Niemann, C., Glauche, I., and Wickström, S. A. 2017. 'Hair follicle stem cell cultures reveal self-organizing plasticity of stem cells and their progeny', *EMBO J*, 36: 151-64.

Chacón-Martínez, C. A., Koester, J., and Wickström, S. A. 2018. 'Signaling in the stem cell niche: regulating cell fate, function and plasticity', *Development*, 145.

Chandel, N. S., Jasper, H., Ho, T. T., and Passegué, E. 2016. 'Metabolic regulation of stem cell function in tissue homeostasis and organismal ageing', *Nat Cell Biol*, 18: 823-32.

Chang, N. C. 2020. 'Autophagy and Stem Cells: Self-Eating for Self-Renewal', *Front Cell Dev Biol*, 8: 138.

Chang, Q., Su, K., Baker, J. R., Yang, X., Paterson, A. J., and Kudlow, J. E. 2000. 'Phosphorylation of human glutamine:fructose-6-phosphate amidotransferase by cAMP-dependent protein kinase at serine 205 blocks the enzyme activity', *J Biol Chem*, 275: 21981-7.

Chen, C. T., Shih, Y. R., Kuo, T. K., Lee, O. K., and Wei, Y. H. 2008. 'Coordinated changes of mitochondrial biogenesis and antioxidant enzymes during osteogenic differentiation of human mesenchymal stem cells', *Stem Cells*, 26: 960-8.

Chen, J., Rao, J. N., Zou, T., Liu, L., Marasa, B. S., Xiao, L., Zeng, X., Turner, D. J., and Wang, J. Y. 2007. 'Polyamines are required for expression of Toll-like receptor 2 modulating intestinal epithelial barrier integrity', *Am J Physiol Gastrointest Liver Physiol*, 293: G568-76.

Cheng, T., Rodrigues, N., Shen, H., Yang, Y., Dombkowski, D., Sykes, M., and Scadden, D. T. 2000. 'Hematopoietic stem cell quiescence maintained by p21cip1/waf1', *Science*, 287: 1804-8.

Cherepanova, N., Shrimal, S., and Gilmore, R. 2016. 'N-linked glycosylation and homeostasis of the endoplasmic reticulum', *Curr Opin Cell Biol*, 41: 57-65.

Chermnykh, E., Kalabusheva, E., and Vorotelyak, E. 2018. 'Extracellular Matrix as a Regulator of Epidermal Stem Cell Fate', *Int J Mol Sci*, 19.

Cho, Y. M., Kwon, S., Pak, Y. K., Seol, H. W., Choi, Y. M., Park, D. J., Park, K. S., and Lee, H. K. 2006. 'Dynamic changes in mitochondrial biogenesis and antioxidant enzymes during the spontaneous differentiation of human embryonic stem cells', *Biochem Biophys Res Commun*, 348: 1472-8.

Choi, E. H. 2019. 'Aging of the skin barrier', *Clin Dermatol*, 37: 336-45.

Chung, S., Dzeja, P. P., Faustino, R. S., Perez-Terzic, C., Behfar, A., and Terzic, A. 2007. 'Mitochondrial oxidative metabolism is required for the cardiac differentiation of stem cells', *Nat Clin Pract Cardiovasc Med*, 4 Suppl 1: S60-7.

Chung, S. S., Ho, E. C., Lam, K. S., and Chung, S. K. 2003. 'Contribution of polyol pathway to diabetes-induced oxidative stress', *J Am Soc Nephrol*, 14: S233-6.

Clegg, C. H., Linkhart, T. A., Olwin, B. B., and Hauschka, S. D. 1987. 'Growth factor control of skeletal muscle differentiation: commitment to terminal differentiation occurs in G1 phase and is repressed by fibroblast growth factor', *J Cell Biol*, 105: 949-56.

Cohen, S. S., and Lichtenstein, J. 1960. 'Polyamines and ribosome structure', *J Biol Chem*, 235: 2112-6.

Cohen, S. S., Morgan, S., and Streibel, E. 1969. 'The polyamine content of the tRNA of E. coli', *Proc Natl Acad Sci U S A*, 64: 669-76.

Coleman, C. S., Huang, H., and Pegg, A. E. 1995. 'Role of the carboxyl terminal MATEE sequence of spermidine/spermine N1-acetyltransferase in the activity and stabilization by the polyamine analog N1,N12-bis(ethyl)spermine', *Biochemistry*, 34: 13423-30.

Conboy, I. M., Conboy, M. J., Wagers, A. J., Girma, E. R., Weissman, I. L., and Rando, T. A. 2005. 'Rejuvenation of aged progenitor cells by exposure to a young systemic environment', *Nature*, 433: 760-4.

Cooper, H. L., Park, M. H., Folk, J. E., Safer, B., and Braverman, R. 1983. 'Identification of the hypusine-containing protein hy+ as translation initiation factor eIF-4D', *Proc Natl Acad Sci U S A*, 80: 1854-7.

Cotsarelis, G. 2006. 'Epithelial stem cells: a folliculocentric view', *J Invest Dermatol*, 126: 1459-68.

Cotsarelis, G., Sun, T. T., and Lavker, R. M. 1990. 'Label-retaining cells reside in the bulge area of pilosebaceous unit: implications for follicular stem cells, hair cycle, and skin carcinogenesis', *Cell*, 61: 1329-37.

Courtois, M., Loussouarn, G., Hourseau, C., and Grollier, J. F. 1995. 'Ageing and hair cycles', *Br J Dermatol*, 132: 86-93.

Crook, E. D., Crenshaw, G., Veerababu, G., and Singh, L. P. 2000. 'Overexpression of glutamine:fructose-6-phosphate amidotransferase in rat-1 fibroblasts enhances glucose-mediated glycogen accumulation via suppression of glycogen phosphorylase activity', *Endocrinology*, 141: 1962-70.

d'Angelo, M., Benedetti, E., Tupone, M. G., Catanesi, M., Castelli, V., Antonosante, A., and Cimini, A. 2019. 'The Role of Stiffness in Cell Reprogramming: A Potential Role for Biomaterials in Inducing Tissue Regeneration', *Cells*, 8.

Dai, F., Yu, W., Song, J., Li, Q., Wang, C., and Xie, S. 2017. 'Extracellular polyamines-induced proliferation and migration of cancer cells by ODC, SSAT, and Akt1-mediated pathway', *Anticancer Drugs*, 28: 457-64.

Damiani, E., and Wallace, H. M. 2018. 'Polyamines and Cancer', *Methods Mol Biol*, 1694: 469-88.

Day, A. J., and Prestwich, G. D. 2002. 'Hyaluronan-binding proteins: tying up the giant', *J Biol Chem*, 277: 4585-8.

DeHaven, J. E., Robinson, K. A., Nelson, B. A., and Buse, M. G. 2001. 'A novel variant of glutamine: fructose-6-phosphate amidotransferase-1 (GFAT1) mRNA is selectively expressed in striated muscle', *Diabetes*, 50: 2419-24.

Demeshkina, N., Jenner, L., Westhof, E., Yusupov, M., and Yusupova, G. 2012. 'A new understanding of the decoding principle on the ribosome', *Nature*, 484: 256-9.

Denisot, M. A., Le Goffic, F., and Badet, B. 1991. 'Glucosamine-6-phosphate synthase from Escherichia coli yields two proteins upon limited proteolysis: identification of the glutamine amidohydrolase and 2R ketose/aldose isomerase-bearing domains based on their biochemical properties', *Arch Biochem Biophys*, 288: 225-30.

Denzel, M. S., Storm, N. J., Gutschmidt, A., Baddi, R., Hinze, Y., Jarosch, E., Sommer, T., Hoppe, T., and Antebi, A. 2014. 'Hexosamine pathway metabolites enhance protein quality control and prolong life', *Cell*, 156: 1167-78.

Desforges, B., Curmi, P. A., Bounedjah, O., Nakib, S., Hamon, L., De Bandt, J. P., and Pastré, D. 2013. 'An intercellular polyamine transfer via gap junctions regulates proliferation and response to stress in epithelial cells', *Mol Biol Cell*, 24: 1529-43.

Dever, T. E., Dinman, J. D., and Green, R. 2018. 'Translation Elongation and Recoding in Eukaryotes', *Cold Spring Harb Perspect Biol*, 10.

Dever, T. E., and Ivanov, I. P. 2018. 'Roles of polyamines in translation', *J Biol Chem*, 293: 18719-29.

Dobashi, Y., Watanabe, Y., Miwa, C., Suzuki, S., and Koyama, S. 2011. 'Mammalian target of rapamycin: a central node of complex signaling cascades', *Int J Clin Exp Pathol*, 4: 476-95.

Dodt, M., Roehr, J. T., Ahmed, R., and Dieterich, C. 2012. 'FLEXBAR-Flexible Barcode and Adapter Processing for Next-Generation Sequencing Platforms', *Biology (Basel)*, 1: 895-905.

Dong, D. L., and Hart, G. W. 1994. 'Purification and characterization of an O-GlcNAc selective N-acetyl-beta-D-glucosaminidase from rat spleen cytosol', *J Biol Chem*, 269: 19321-30.

Dong, X., Milholland, B., and Vijg, J. 2016. 'Evidence for a limit to human lifespan', *Nature*, 538: 257-59.

Driskell, I., Oeztuerk-Winder, F., Humphreys, P., and Frye, M. 2015. 'Genetically induced cell death in bulge stem cells reveals their redundancy for hair and epidermal regeneration', *Stem Cells*, 33: 988-98.

Echandi, G., and Algranati, I. D. 1975. 'Defective 30S ribosomal particles in a polyamine auxotroph of Escherichia coli', *Biochem Biophys Res Commun*, 67: 1185-91.

Eguchi, S., Oshiro, N., Miyamoto, T., Yoshino, K., Okamoto, S., Ono, T., Kikkawa, U., and Yonezawa, K. 2009. 'AMP-activated protein kinase phosphorylates glutamine : fructose-6-phosphate amidotransferase 1 at Ser243 to modulate its enzymatic activity', *Genes Cells*, 14: 179-89.

Eisenberg, T., Knauer, H., Schauer, A., Buttner, S., Ruckenstuhl, C., Carmona-Gutierrez, D., Ring, J., Schroeder, S., Magnes, C., Antonacci, L., Fussi, H., Deszcz, L., Hartl, R., Schraml, E., Criollo, A., Megalou, E., Weiskopf, D., Laun, P., Heeren, G., Breitenbach, M., Grubeck-Loebenstein, B., Herker, E., Fahrenkrog, B., Frohlich, K. U., Sinner, F., Tavernarakis, N., Minois, N., Kroemer, G., and Madeo, F. 2009. 'Induction of autophagy by spermidine promotes longevity', *Nat Cell Biol*, 11: 1305-14.

El-Domyati, M., Attia, S., Saleh, F., Brown, D., Birk, D. E., Gasparro, F., Ahmad, H., and Uitto, J. 2002. 'Intrinsic aging vs. photoaging: a comparative histopathological, immunohistochemical, and ultrastructural study of skin', *Exp Dermatol*, 11: 398-405.

Elias, P. M., and Ghadially, R. 2002. 'The aged epidermal permeability barrier: basis for functional abnormalities', *Clin Geriatr Med*, 18: 103-20, vii.

Engler, A. J., Sen, S., Sweeney, H. L., and Discher, D. E. 2006. 'Matrix elasticity directs stem cell lineage specification', *Cell*, 126: 677-89.

Ezashi, T., Das, P., and Roberts, R. M. 2005. 'Low O2 tensions and the prevention of differentiation of hES cells', *Proc Natl Acad Sci U S A*, 102: 4783-8.

Farhana, A., and Lappin, S. L. 2020. 'Biochemistry, Lactate Dehydrogenase (LDH).' in, *StatPearls* (Treasure Island (FL)).

Fashe, T. M., Keinänen, T. A., Grigorenko, N. A., Khomutov, A. R., Jänne, J., Alhonen, L., and Pietilä, M. 2010. 'Cutaneous application of alpha-methylspermidine activates the growth of resting hair follicles in mice', *Amino Acids*, 38: 583-90.

Fenelon, J. C., and Murphy, B. D. 2017. 'Inhibition of polyamine synthesis causes entry of the mouse blastocyst into embryonic diapause', *Biol Reprod*, 97: 119-32.

Fernandez-Flores, A., Saeb-Lima, M., and Cassarino, D. S. 2019. 'Histopathology of aging of the hair follicle', *J Cutan Pathol*, 46: 508-19.

Ferraro, F., Celso, C. L., and Scadden, D. 2010. 'Adult stem cels and their niches', *Adv Exp Med Biol*, 695: 155-68.

Ficker, E., Taglialatela, M., Wible, B. A., Henley, C. M., and Brown, A. M. 1994. 'Spermine and spermidine as gating molecules for inward rectifier K+ channels', *Science*, 266: 1068-72.

Flink, I., and Pettijohn, D. E. 1975. 'Polyamines stabilise DNA folds', *Nature*, 253: 62-3.

Flores, A., Schell, J., Krall, A. S., Jelinek, D., Miranda, M., Grigorian, M., Braas, D., White, A. C., Zhou, J. L., Graham, N. A., Graeber, T., Seth, P., Evseenko, D., Coller, H. A., Rutter, J., Christofk, H. R., and Lowry, W. E. 2017. 'Lactate dehydrogenase activity drives hair follicle stem cell activation', *Nat Cell Biol*, 19: 1017-26.

Flores, I., Cayuela, M. L., and Blasco, M. A. 2005. 'Effects of telomerase and telomere length on epidermal stem cell behavior', *Science*, 309: 1253-6.

Fogel-Petrovic, M., Vujcic, S., Brown, P. J., Haddox, M. K., and Porter, C. W. 1996. 'Effects of polyamines, polyamine analogs, and inhibitors of protein synthesis on spermidine-spermine N1-acetyltransferase gene expression', *Biochemistry*, 35: 14436-44.

Foitzik, K., Lindner, G., Mueller-Roever, S., Maurer, M., Botchkareva, N., Botchkarev, V., Handjiski, B., Metz, M., Hibino, T., Soma, T., Dotto, G. P., and Paus, R. 2000. 'Control of murine hair follicle regression (catagen) by TGF-beta1 in vivo', *FASEB J*, 14: 752-60.

Folmes, C. D., Dzeja, P. P., Nelson, T. J., and Terzic, A. 2012. 'Metabolic plasticity in stem cell homeostasis and differentiation', *Cell Stem Cell*, 11: 596-606.

Folmes, C. D., Nelson, T. J., Martinez-Fernandez, A., Arrell, D. K., Lindor, J. Z., Dzeja, P. P., Ikeda, Y., Perez-Terzic, C., and Terzic, A. 2011. 'Somatic oxidative bioenergetics transitions into pluripotency-dependent glycolysis to facilitate nuclear reprogramming', *Cell Metab*, 14: 264-71.

Fong, W. F., Heller, J. S., and Canellakis, E. S. 1976. 'The appearance of an ornithine decarboxylase inhibitory protein upon the addition of putrescine to cell cultures', *Biochim Biophys Acta*, 428: 456-65.

Foo, M. X. R., Ong, P. F., and Dreesen, O. 2019. 'Premature aging syndromes: From patients to mechanism', *J Dermatol Sci*, 96: 58-65.

Fredlund, J. O., Johansson, M. C., Dahlberg, E., and Oredsson, S. M. 1995. 'Ornithine decarboxylase and S-adenosylmethionine decarboxylase expression during the cell cycle of Chinese hamster ovary cells', *Exp Cell Res*, 216: 86-92.

Frydman, J., Nimmesgern, E., Ohtsuka, K., and Hartl, F. U. 1994. 'Folding of nascent polypeptide chains in a high molecular mass assembly with molecular chaperones', *Nature*, 370: 111-7.

Frye, M., Fisher, A. G., and Watt, F. M. 2007. 'Epidermal stem cells are defined by global histone modifications that are altered by Myc-induced differentiation', *PLoS One*, 2: e763.

Fuchs, E. 2007. 'Scratching the surface of skin development', *Nature*, 445: 834-42.

Fuchs, E. 2009. 'The tortoise and the hair: slow-cycling cells in the stem cell race', *Cell*, 137: 811-9.

Fuchs, E., Merrill, B. J., Jamora, C., and DasGupta, R. 2001. 'At the roots of a never-ending cycle', *Dev Cell*, 1: 13-25.

Fuchs, E., and Nowak, J. A. 2008. 'Building epithelial tissues from skin stem cells', *Cold Spring Harb Symp Quant Biol*, 73: 333-50.

Fuchs, E., Tumbar, T., and Guasch, G. 2004. 'Socializing with the neighbors: stem cells and their niche', *Cell*, 116: 769-78.

Funakoshi-Tago, M., Sumi, K., Kasahara, T., and Tago, K. 2013. 'Critical roles of Myc-ODC axis in the cellular transformation induced by myeloproliferative neoplasm-associated JAK2 V617F mutant', *PLoS One*, 8: e52844.

Funderburgh, J. L. 2002. 'Keratan sulfate biosynthesis', *IUBMB Life*, 54: 187-94.

Gange, R. W., and Dequoy, P. R. 1980. 'Topical spermine and putrescine stimulated DNA synthesis in the hairless mouse epidermis', *Br J Dermatol*, 103: 27-32.

García-Prat, L., Sousa-Victor, P., and Muñoz-Cánoves, P. 2017. 'Proteostatic and Metabolic Control of Stemness', *Cell Stem Cell*, 20: 593-608.

Gardner, B. M., Pincus, D., Gotthardt, K., Gallagher, C. M., and Walter, P. 2013. 'Endoplasmic reticulum stress sensing in the unfolded protein response', *Cold Spring Harb Perspect Biol*, 5: a013169.

Garreau de Loubresse, N., Prokhorova, I., Holtkamp, W., Rodnina, M. V., Yusupova, G., and Yusupov, M. 2014. 'Structural basis for the inhibition of the eukaryotic ribosome', *Nature*, 513: 517-22.

Garza, L. A., Yang, C. C., Zhao, T., Blatt, H. B., Lee, M., He, H., Stanton, D. C., Carrasco, L., Spiegel, J. H., Tobias, J. W., and Cotsarelis, G. 2011. 'Bald scalp in men with androgenetic alopecia retains hair follicle stem cells but lacks CD200-rich and CD34-positive hair follicle progenitor cells', *J Clin Invest*, 121: 613-22.

Ge, Y., Miao, Y., Gur-Cohen, S., Gomez, N., Yang, H., Nikolova, M., Polak, L., Hu, Y., Verma, A., Elemento, O., Krueger, J. G., and Fuchs, E. 2020. 'The aging skin microenvironment dictates stem cell behavior', *Proc Natl Acad Sci U S A*.

Gebauer, F., and Hentze, M. W. 2004. 'Molecular mechanisms of translational control', *Nat Rev Mol Cell Biol*, 5: 827-35.

Gems, D., and Partridge, L. 2013. 'Genetics of longevity in model organisms: debates and paradigm shifts', *Annu Rev Physiol*, 75: 621-44.

Genander, M., Cook, P. J., Ramskold, D., Keyes, B. E., Mertz, A. F., Sandberg, R., and Fuchs, E. 2014. 'BMP signaling and its pSMAD1/5 target genes differentially regulate hair follicle stem cell lineages', *Cell Stem Cell*, 15: 619-33.

Ghosh, S., Blumenthal, H. J., Davidson, E., and Roseman, S. 1960. 'Glucosamine metabolism. V. Enzymatic synthesis of glucosamine 6-phosphate', *J Biol Chem*, 235: 1265-73.

Gloster, T. M., Zandberg, W. F., Heinonen, J. E., Shen, D. L., Deng, L., and Vocadlo, D. J. 2011. 'Hijacking a biosynthetic pathway yields a glycosyltransferase inhibitor within cells', *Nat Chem Biol*, 7: 174-81.

Gonzalez, P. S., O'Prey, J., Cardaci, S., Barthet, V. J. A., Sakamaki, J. I., Beaumatin, F., Roseweir, A., Gay, D. M., Mackay, G., Malviya, G., Kania, E., Ritchie, S., Baudot, A. D., Zunino, B., Mrowinska, A., Nixon, C., Ennis, D., Hoyle, A., Millan, D., McNeish, I. A., Sansom, O. J., Edwards, J., and Ryan, K. M. 2018. 'Mannose impairs tumour growth and enhances chemotherapy', *Nature*, 563: 719-23.

Goodier, M., and Hordinsky, M. 2015. 'Normal and aging hair biology and structure 'aging and hair'', *Curr Probl Dermatol*, 47: 1-9.

Gordon, M. K., and Hahn, R. A. 2010. 'Collagens', *Cell Tissue Res*, 339: 247-57.

Goyal, M. S., Vlassenko, A. G., Blazey, T. M., Su, Y., Couture, L. E., Durbin, T. J., Bateman, R. J., Benzinger, T. L., Morris, J. C., and Raichle, M. E. 2017. 'Loss of Brain Aerobic Glycolysis in Normal Human Aging', *Cell Metab*, 26: 353-60 e3.

Gracy, R. W., and Noltmann, E. A. 1968. 'Studies on phosphomannose isomerase. I. Isolation, homogeneity measurements, and determination of some physical properties', *J Biol Chem*, 243: 3161-8.

Greco, V., Chen, T., Rendl, M., Schober, M., Pasolli, H. A., Stokes, N., Dela Cruz-Racelis, J., and Fuchs, E. 2009. 'A two-step mechanism for stem cell activation during hair regeneration', *Cell Stem Cell*, 4: 155-69.

Grigorian, A., Lee, S. U., Tian, W., Chen, I. J., Gao, G., Mendelsohn, R., Dennis, J. W., and Demetriou, M. 2007. 'Control of T Cell-mediated autoimmunity by metabolite flux to N-glycan biosynthesis', *J Biol Chem*, 282: 20027-35.

Gruber, R., Koch, H., Doll, B. A., Tegtmeier, F., Einhorn, T. A., and Hollinger, J. O. 2006. 'Fracture healing in the elderly patient', *Exp Gerontol*, 41: 1080-93.

Guo, S., Zi, X., Schulz, V. P., Cheng, J., Zhong, M., Koochaki, S. H., Megyola, C. M., Pan, X., Heydari, K., Weissman, S. M., Gallagher, P. G., Krause, D. S., Fan, R., and Lu, J. 2014. 'Nonstochastic reprogramming from a privileged somatic cell state', *Cell*, 156: 649-62.

Gutierrez, E., Shin, B. S., Woolstenhulme, C. J., Kim, J. R., Saini, P., Buskirk, A. R., and Dever, T. E. 2013. 'eIF5A promotes translation of polyproline motifs', *Mol Cell*, 51: 35-45.

Hahm, H. A., Ettinger, D. S., Bowling, K., Hoker, B., Chen, T. L., Zabelina, Y., and Casero, R. A., Jr. 2002. 'Phase I study of N(1),N(11)-diethylnorspermine in patients with non-small cell lung cancer', *Clin Cancer Res*, 8: 684-90.

Hakkinen, M. R., Keinanen, T. A., Vepsalainen, J., Khomutov, A. R., Alhonen, L., Janne, J., and Auriola, S. 2008. 'Quantitative determination of underivatized polyamines by using isotope dilution RP-LC-ESI-MS/MS', *J Pharm Biomed Anal*, 48: 414-21.

Hakkinen, M. R., Roine, A., Auriola, S., Tuokko, A., Veskimae, E., Keinanen, T. A., Lehtimaki, T., Oksala, N., and Vepsalainen, J. 2013. 'Analysis of free, mono- and diacetylated polyamines from human urine by LC-MS/MS', *J Chromatogr B Analyt Technol Biomed Life Sci*, 941: 81-9.

Haltiwanger, R. S., Blomberg, M. A., and Hart, G. W. 1992. 'Glycosylation of nuclear and cytoplasmic proteins. Purification and characterization of a uridine diphospho-N-acetylglucosamine:polypeptide beta-N-acetylglucosaminyltransferase', *J Biol Chem*, 267: 9005-13.

Hamon, L., Savarin, P., and Pastre, D. 2016. 'Polyamine signal through gap junctions: A key regulator of proliferation and gap-junction organization in mammalian tissues?', *Bioessays*, 38: 498-507.

Hanisch, F. G. 2001. 'O-glycosylation of the mucin type', *Biol Chem*, 382: 143-9.

Hansen, L. A., Alexander, N., Hogan, M. E., Sundberg, J. P., Dlugosz, A., Threadgill, D. W., Magnuson, T., and Yuspa, S. H. 1997. 'Genetically null mice reveal a central role for epidermal growth factor receptor in the differentiation of the hair follicle and normal hair development', *Am J Pathol*, 150: 1959-75.

Harding, H. P., Novoa, I., Zhang, Y., Zeng, H., Wek, R., Schapira, M., and Ron, D. 2000. 'Regulated translation initiation controls stress-induced gene expression in mammalian cells', *Mol Cell*, 6: 1099-108.

Harding, H. P., Zhang, Y., and Ron, D. 1999. 'Protein translation and folding are coupled by an endoplasmic-reticulum-resident kinase', *Nature*, 397: 271-4.

Harding, H. P., Zhang, Y., Zeng, H., Novoa, I., Lu, P. D., Calfon, M., Sadri, N., Yun, C., Popko, B., Paules, R., Stojdl, D. F., Bell, J. C., Hettmann, T., Leiden, J. M., and Ron, D. 2003. 'An integrated stress response regulates amino acid metabolism and resistance to oxidative stress', *Mol Cell*, 11: 619-33.

Hardingham, T. E., and Fosang, A. J. 1992. 'Proteoglycans: many forms and many functions', *FASEB J*, 6: 861-70.

Hartl, F. U., Bracher, A., and Hayer-Hartl, M. 2011. 'Molecular chaperones in protein folding and proteostasis', *Nature*, 475: 324-32.

Hartl, F. U., and Hayer-Hartl, M. 2009. 'Converging concepts of protein folding in vitro and in vivo', *Nat Struct Mol Biol*, 16: 574-81.

Hayaishi, O., Nishizuka, Y., Tatibana, M., Takeshita, M., and Kuno, S. 1961. 'Enzymatic studies on the metabolism of beta-alanine', *J Biol Chem*, 236: 781-90.

Hebert, J. M., Rosenquist, T., Gotz, J., and Martin, G. R. 1994. 'FGF5 as a regulator of the hair growth cycle: evidence from targeted and spontaneous mutations', *Cell*, 78: 1017-25.

Hebert, L. F., Jr., Daniels, M. C., Zhou, J., Crook, E. D., Turner, R. L., Simmons, S. T., Neidigh, J. L., Zhu, J. S., Baron, A. D., and McClain, D. A. 1996. 'Overexpression of glutamine:fructose-6-phosphate amidotransferase in transgenic mice leads to insulin resistance', *J Clin Invest*, 98: 930-6.

Helenius, A., and Aebi, M. 2004. 'Roles of N-linked glycans in the endoplasmic reticulum', *Annu Rev Biochem*, 73: 1019-49.

Hellen, C. U. T. 2018. 'Translation Termination and Ribosome Recycling in Eukaryotes', *Cold Spring Harb Perspect Biol*, 10.

Heller, J. S., Fong, W. F., and Canellakis, E. S. 1976. 'Induction of a protein inhibitor to ornithine decarboxylase by the end products of its reaction', *Proc Natl Acad Sci U S A*, 73: 1858-62.

Hershey, J. W. B., Sonenberg, N., and Mathews, M. B. 2019. 'Principles of Translational Control', *Cold Spring Harb Perspect Biol*, 11.

Hetz, C., Martinon, F., Rodriguez, D., and Glimcher, L. H. 2011. 'The unfolded protein response: integrating stress signals through the stress sensor IRE1alpha', *Physiol Rev*, 91: 1219-43.

Hidalgo San Jose, L., Sunshine, M. J., Dillingham, C. H., Chua, B. A., Kruta, M., Hong, Y., Hatters, D. M., and Signer, R. A. J. 2020. 'Modest Declines in Proteome Quality Impair Hematopoietic Stem Cell Self-Renewal', *Cell Rep*, 30: 69-80 e6.

Hinnebusch, A. G. 1993. 'Gene-specific translational control of the yeast GCN4 gene by phosphorylation of eukaryotic initiation factor 2', *Mol Microbiol*, 10: 215-23.

Ho, T. T., Warr, M. R., Adelman, E. R., Lansinger, O. M., Flach, J., Verovskaya, E. V., Figueroa, M. E., and Passegué, E. 2017. 'Autophagy maintains the metabolism and function of young and old stem cells', *Nature*, 543: 205-10.

Horn, M., Denzel, S. I., Srinivasan, B., Allmeroth, K., Schiffer, I., Karthikaisamy, V., Miethe, S., Breuer, P., Antebi, A., and Denzel, M. S. 2020. 'Hexosamine Pathway Activation Improves Protein Homeostasis through the Integrated Stress Response', *iScience*, 23: 100887.

Horn, Y., Schechter, P. J., and Marton, L. J. 1987. 'Phase I-II clinical trial with alpha-difluoromethylornithine--an inhibitor of polyamine biosynthesis', *Eur J Cancer Clin Oncol*, 23: 1103-7.

Hsu, Y. C., Li, L., and Fuchs, E. 2014a. 'Emerging interactions between skin stem cells and their niches', *Nat Med*, 20: 847-56.

Hsu, Y. C., Li, L., and Fuchs, E. 2014b. 'Transit-amplifying cells orchestrate stem cell activity and tissue regeneration', *Cell*, 157: 935-49.

Hsu, Y. C., Pasolli, H. A., and Fuchs, E. 2011. 'Dynamics between stem cells, niche, and progeny in the hair follicle', *Cell*, 144: 92-105.

Huelsken, J., Vogel, R., Erdmann, B., Cotsarelis, G., and Birchmeier, W. 2001. 'beta-Catenin controls hair follicle morphogenesis and stem cell differentiation in the skin', *Cell*, 105: 533-45.

Hynes, R. O. 2009. 'The extracellular matrix: not just pretty fibrils', *Science*, 326: 1216-9.

Hynes, R. O., and Naba, A. 2012. 'Overview of the matrisome--an inventory of extracellular matrix constituents and functions', *Cold Spring Harb Perspect Biol*, 4: a004903.

Igarashi, K., Hashimoto, S., Miyake, A., Kashiwagi, K., and Hirose, S. 1982. 'Increase of fidelity of polypeptide synthesis by spermidine in eukaryotic cell-free systems', *Eur J Biochem*, 128: 597-604.

Igarashi, K., and Kashiwagi, K. 2010. 'Modulation of cellular function by polyamines', *Int J Biochem Cell Biol*, 42: 39-51.

Igarashi, K., Kishida, K., and Hirose, S. 1980. 'Stimulation by polyamines of enzymatic methylation of two adjacent adenines near the 3' and end of 16S ribosomal RNA of Escherichia coli', *Biochem Biophys Res Commun*, 96: 678-84.

Ingolia, N. T., Lareau, L. F., and Weissman, J. S. 2011. 'Ribosome profiling of mouse embryonic stem cells reveals the complexity and dynamics of mammalian proteomes', *Cell*, 147: 789-802.

Ishida, T., Nakao, S., Ueyama, T., Harada, Y., and Kawamura, T. 2020. 'Metabolic remodeling during somatic cell reprogramming to induced pluripotent stem cells: involvement of hypoxia-inducible factor 1', *Inflamm Regen*, 40: 8.

Issop, Y., Hathazi, D., Khan, M. M., Rudolf, R., Weis, J., Spendiff, S., Slater, C. R., Roos, A., and Lochmüller, H. 2018. 'GFPT1 deficiency in muscle leads to myasthenia and myopathy in mice', *Hum Mol Genet*, 27: 3218-32.

Isupov, M. N., Obmolova, G., Butterworth, S., Badet-Denisot, M. A., Badet, B., Polikarpov, I., Littlechild, J. A., and Teplyakov, A. 1996. 'Substrate binding is required for assembly of the active conformation of the catalytic site in Ntn amidotransferases: evidence from the 1.8 A crystal structure of the glutaminase domain of glucosamine 6-phosphate synthase', *Structure*, 4: 801-10.

Itano, N., and Kimata, K. 2002. 'Mammalian hyaluronan synthases', *IUBMB Life*, 54: 195-9.

Ito, K., Carracedo, A., Weiss, D., Arai, F., Ala, U., Avigan, D. E., Schafer, Z. T., Evans, R. M., Suda, T., Lee, C. H., and Pandolfi, P. P. 2012. 'A PML-PPAR-delta pathway for fatty acid oxidation regulates hematopoietic stem cell maintenance', *Nat Med*, 18: 1350-8.

Ito, K., and Ito, K. 2016. 'Metabolism and the Control of Cell Fate Decisions and Stem Cell Renewal', *Annu Rev Cell Dev Biol*, 32: 399-409.

James, C., Zhao, T. Y., Rahim, A., Saxena, P., Muthalif, N. A., Uemura, T., Tsuneyoshi, N., Ong, S., Igarashi, K., Lim, C. Y., Dunn, N. R., and Vardy, L. A. 2018. 'MINDY1 Is a Downstream Target of the Polyamines and Promotes Embryonic Stem Cell Self-Renewal', *Stem Cells*, 36: 1170-78.

Jang, H., Kim, T. W., Yoon, S., Choi, S. Y., Kang, T. W., Kim, S. Y., Kwon, Y. W., Cho, E. J., and Youn, H. D. 2012. 'O-GlcNAc regulates pluripotency and reprogramming by directly acting on core components of the pluripotency network', *Cell Stem Cell*, 11: 62-74.

Janzen, V., Forkert, R., Fleming, H. E., Saito, Y., Waring, M. T., Dombkowski, D. M., Cheng, T., DePinho, R. A., Sharpless, N. E., and Scadden, D. T. 2006. 'Stem-cell ageing modified by the cyclin-dependent kinase inhibitor p16INK4a', *Nature*, 443: 421-6.

Jasper, H., and Jones, D. L. 2010. 'Metabolic regulation of stem cell behavior and implications for aging', *Cell Metab*, 12: 561-5.

Jensen, K. B., Collins, C. A., Nascimento, E., Tan, D. W., Frye, M., Itami, S., and Watt, F. M. 2009. 'Lrig1 expression defines a distinct multipotent stem cell population in mammalian epidermis', *Cell Stem Cell*, 4: 427-39.

Jensen, U. B., Yan, X., Triel, C., Woo, S. H., Christensen, R., and Owens, D. M. 2008. 'A distinct population of clonogenic and multipotent murine follicular keratinocytes residing in the upper isthmus', *J Cell Sci*, 121: 609-17.

Jeon, J. H., Suh, H. N., Kim, M. O., Ryu, J. M., and Han, H. J. 2014. 'Glucosamine-induced OGT activation mediates glucose production through cleaved Notch1 and FoxO1, which coordinately contributed to the regulation of maintenance of self-renewal in mouse embryonic stem cells', *Stem Cells Dev*, 23: 2067-79.

Ji, J., Ho, B. S., Qian, G., Xie, X. M., Bigliardi, P. L., and Bigliardi-Qi, M. 2017. 'Aging in hair follicle stem cells and niche microenvironment', *J Dermatol*, 44: 1097-104.

Jokela, T. A., Jauhiainen, M., Auriola, S., Kauhanen, M., Tiihonen, R., Tammi, M. I., and Tammi, R. H. 2008. 'Mannose inhibits hyaluronan synthesis by down-regulation of the cellular pool of UDP-N-acetylhexosamines', *J Biol Chem*, 283: 7666-73.

Jokela, T. A., Makkonen, K. M., Oikari, S., Kärnä, R., Koli, E., Hart, G. W., Tammi, R. H., Carlberg, C., and Tammi, M. I. 2011. 'Cellular content of UDP-N-acetylhexosamines controls hyaluronan synthase 2 expression and correlates with O-linked N-acetylglucosamine modification of transcription factors YY1 and SP1', *J Biol Chem*, 286: 33632-40.

Julenius, K., Molgaard, A., Gupta, R., and Brunak, S. 2005. 'Prediction, conservation analysis, and structural characterization of mammalian mucin-type O-glycosylation sites', *Glycobiology*, 15: 153-64.

Kakegawa, T., Guo, Y., Chiba, Y., Miyazaki, T., Nakamura, M., Hirose, S., Canellakis, Z. N., and Igarashi, K. 1991. 'Effect of acetylpolyamines on in vitro protein synthesis and on the growth of a polyamine-requiring mutant of Escherichia coli', *J Biochem*, 109: 627-31.

Kakizaki, I., Kojima, K., Takagaki, K., Endo, M., Kannagi, R., Ito, M., Maruo, Y., Sato, H., Yasuda, T., Mita, S., Kimata, K., and Itano, N. 2004. 'A novel mechanism for the inhibition of hyaluronan biosynthesis by 4-methylumbelliferone', *J Biol Chem*, 279: 33281-9.

Kanitakis, J. 2002. 'Anatomy, histology and immunohistochemistry of normal human skin', *Eur J Dermatol*, 12: 390-9; quiz 400-1.

Kapetanou, M., Chondrogianni, N., Petrakis, S., Koliakos, G., and Gonos, E. S. 2017. 'Proteasome activation enhances stemness and lifespan of human mesenchymal stem cells', *Free Radic Biol Med*, 103: 226-35.

Katajisto, P., Dohla, J., Chaffer, C. L., Pentinmikko, N., Marjanovic, N., Iqbal, S., Zoncu, R., Chen, W., Weinberg, R. A., and Sabatini, D. M. 2015. 'Stem cells. Asymmetric apportioning of aged mitochondria between daughter cells is required for stemness', *Science*, 348: 340-3.

Kee, K., Vujcic, S., Merali, S., Diegelman, P., Kisiel, N., Powell, C. T., Kramer, D. L., and Porter, C. W. 2004. 'Metabolic and antiproliferative consequences of activated polyamine catabolism in LNCaP prostate carcinoma cells', *J Biol Chem*, 279: 27050-8.

Kenyon, C. 2005. 'The plasticity of aging: insights from long-lived mutants', *Cell*, 120: 449-60.

Keyes, B. E., Segal, J. P., Heller, E., Lien, W. H., Chang, C. Y., Guo, X., Oristian, D. S., Zheng, D., and Fuchs, E. 2013. 'Nfatc1 orchestrates aging in hair follicle stem cells', *Proc Natl Acad Sci U S A*, 110: E4950-9.

Kim, C. S., Ding, X., Allmeroth, K., Biggs, L. C., Kolenc, O. I., L'Hoest, N., Chacon-Martinez, C. A., Edlich-Muth, C., Giavalisco, P., Quinn, K. P., Denzel, M. S., Eming, S. A., and Wickstrom, S. A. 2020a. 'Glutamine Metabolism Controls Stem Cell Fate Reversibility and Long-Term Maintenance in the Hair Follicle', *Cell Metab*, 32: 629-42 e8.

Kim, H. S., Park, S. Y., Choi, Y. R., Kang, J. G., Joo, H. J., Moon, W. K., and Cho, J. W. 2009. 'Excessive O-GlcNAcylation of proteins suppresses spontaneous cardiogenesis in ES cells', *FEBS Lett*, 583: 2474-8.

Kippin, T. E., Martens, D. J., and van der Kooy, D. 2005. 'p21 loss compromises the relative quiescence of forebrain stem cell proliferation leading to exhaustion of their proliferation capacity', *Genes Dev*, 19: 756-67.

Kondoh, H., Lleonart, M. E., Nakashima, Y., Yokode, M., Tanaka, M., Bernard, D., Gil, J., and Beach, D. 2007. 'A high glycolytic flux supports the proliferative potential of murine embryonic stem cells', *Antioxid Redox Signal*, 9: 293-9.

Kontis, V., Bennett, J. E., Mathers, C. D., Li, G., Foreman, K., and Ezzati, M. 2017. 'Future life expectancy in 35 industrialised countries: projections with a Bayesian model ensemble', *Lancet*, 389: 1323-35.

Koomoa, D. L., Geerts, D., Lange, I., Koster, J., Pegg, A. E., Feith, D. J., and Bachmann, A. S. 2013. 'DFMO/eflornithine inhibits migration and invasion downstream of MYCN and involves p27Kip1 activity in neuroblastoma', *Int J Oncol*, 42: 1219-28.

Kornfeld, R. 1967. 'Studies on L-glutamine D-fructose 6-phosphate amidotransferase. I. Feedback inhibition by uridine diphosphate-N-acetylglucosamine', *J Biol Chem*, 242: 3135-41.

Kozarsky, K., Kingsley, D., and Krieger, M. 1988. 'Use of a mutant cell line to study the kinetics and function of O-linked glycosylation of low density lipoprotein receptors', *Proc Natl Acad Sci U S A*, 85: 4335-9.

Kristensen, A. R., Gsponer, J., and Foster, L. J. 2013. 'Protein synthesis rate is the predominant regulator of protein expression during differentiation', *Mol Syst Biol*, 9: 689.

Kuhn, H. G., Dickinson-Anson, H., and Gage, F. H. 1996. 'Neurogenesis in the dentate gyrus of the adult rat: age-related decrease of neuronal progenitor proliferation', *J Neurosci*, 16: 2027-33.

Kultti, A., Pasonen-Seppänen, S., Jauhiainen, M., Rilla, K. J., Kärnä, R., Pyöriä, E., Tammi, R. H., and Tammi, M. I. 2009. '4-Methylumbelliferone inhibits hyaluronan synthesis by depletion of cellular UDP-glucuronic acid and downregulation of hyaluronan synthase 2 and 3', *Exp Cell Res*, 315: 1914-23.

Landau, G., Bercovich, Z., Park, M. H., and Kahana, C. 2010. 'The role of polyamines in supporting growth of mammalian cells is mediated through their requirement for translation initiation and elongation', *J Biol Chem*, 285: 12474-81.

Langer, T., Lu, C., Echols, H., Flanagan, J., Hayer, M. K., and Hartl, F. U. 1992. 'Successive action of DnaK, DnaJ and GroEL along the pathway of chaperone-mediated protein folding', *Nature*, 356: 683-9.

Latham, K. E., Garrels, J. I., Chang, C., and Solter, D. 1991. 'Quantitative analysis of protein synthesis in mouse embryos. I. Extensive reprogramming at the one- and two-cell stages', *Development*, 112: 921-32.

Lay, K., Kume, T., and Fuchs, E. 2016. 'FOXC1 maintains the hair follicle stem cell niche and governs stem cell quiescence to preserve long-term tissue-regenerating potential', *Proc Natl Acad Sci U S A*, 113: E1506-15.

Lee, D. H., Oh, J. H., and Chung, J. H. 2016. 'Glycosaminoglycan and proteoglycan in skin aging', *J Dermatol Sci*, 83: 174-81.

Lemmon, M. A., and Schlessinger, J. 2010. 'Cell signaling by receptor tyrosine kinases', *Cell*, 141: 1117-34.

Li, A., Simmons, P. J., and Kaur, P. 1998. 'Identification and isolation of candidate human keratinocyte stem cells based on cell surface phenotype', *Proc Natl Acad Sci U S A*, 95: 3902-7.

Li, Y., Roux, C., Lazereg, S., LeCaer, J. P., Laprevote, O., Badet, B., and Badet-Denisot, M. A. 2007. 'Identification of a novel serine phosphorylation site in human glutamine:fructose-6-phosphate amidotransferase isoform 1', *Biochemistry*, 46: 13163-9.

Libby, P. R., Henderson, M., Bergeron, R. J., and Porter, C. W. 1989. 'Major increases in spermidine/spermine-N1-acetyltransferase activity by spermine analogues and their relationship to polyamine depletion and growth inhibition in L1210 cells', *Cancer Res*, 49: 6226-31.

Lin, K. K., Chudova, D., Hatfield, G. W., Smyth, P., and Andersen, B. 2004. 'Identification of hair cycle-associated genes from time-course gene expression profile data by using replicate variance', *Proc Natl Acad Sci U S A*, 101: 15955-60.

Lindner, G., Botchkarev, V. A., Botchkareva, N. V., Ling, G., van der Veen, C., and Paus, R. 1997. 'Analysis of apoptosis during hair follicle regression (catagen)', *Am J Pathol*, 151: 1601-17.

Liu, L., Guo, X., Rao, J. N., Zou, T., Xiao, L., Yu, T., Timmons, J. A., Turner, D. J., and Wang, J. Y. 2009. 'Polyamines regulate E-cadherin transcription through c-Myc modulating intestinal epithelial barrier function', *Am J Physiol Cell Physiol*, 296: C801-10.

Liu, L., Michowski, W., Inuzuka, H., Shimizu, K., Nihira, N. T., Chick, J. M., Li, N., Geng, Y., Meng, A. Y., Ordureau, A., Kolodziejczyk, A., Ligon, K. L., Bronson, R. T., Polyak, K., Harper, J. W., Gygi, S. P., Wei, W., and Sicinski, P. 2017. 'G1 cyclins link proliferation, pluripotency and differentiation of embryonic stem cells', *Nat Cell Biol*, 19: 177-88.

Liu, N., Matsumura, H., Kato, T., Ichinose, S., Takada, A., Namiki, T., Asakawa, K., Morinaga, H., Mohri, Y., De Arcangelis, A., Geroges-Labouesse, E., Nanba, D., and Nishimura, E. K. 2019. 'Stem cell competition orchestrates skin homeostasis and ageing', *Nature*, 568: 344-50.

Liu, Y., Lyle, S., Yang, Z., and Cotsarelis, G. 2003. 'Keratin 15 promoter targets putative epithelial stem cells in the hair follicle bulge', *J Invest Dermatol*, 121: 963-8.

Livesey, G., and Brown, J. C. 1995. 'Whole body metabolism is not restricted to D-sugars because energy metabolism of L-sugars fits a computational model in rats', *J Nutr*, 125: 3020-9.

López-Otín, C., Blasco, M. A., Partridge, L., Serrano, M., and Kroemer, G. 2013. 'The hallmarks of aging', *Cell*, 153: 1194-217.

Love, D. C., and Hanover, J. A. 2005. 'The hexosamine signaling pathway: deciphering the "O-GlcNAc code"', *Sci STKE*, 2005: re13.

Love, M. I., Huber, W., and Anders, S. 2014. 'Moderated estimation of fold change and dispersion for RNA-seq data with DESeq2', *Genome Biol*, 15: 550.

Lu, R., Markowetz, F., Unwin, R. D., Leek, J. T., Airoldi, E. M., MacArthur, B. D., Lachmann, A., Rozov, R., Ma'ayan, A., Boyer, L. A., Troyanskaya, O. G., Whetton, A. D., and Lemischka, I. R. 2009. 'Systems-level dynamic analyses of fate change in murine embryonic stem cells', *Nature*, 462: 358-62.

Luke, C. T., Casta, A., Kim, H., and Christiano, A. M. 2013. 'Hairless and the polyamine putrescine form a negative regulatory loop in the epidermis', *Exp Dermatol*, 22: 644-9.

Lundgren, D. W., and Prokay, S. L. 1988. 'Glucose elevates ornithine decarboxylase expression in Vero cells', *J Cell Physiol*, 137: 469-75.

Mäkitie, L. T., Kanerva, K., and Andersson, L. C. 2009. 'Ornithine decarboxylase regulates the activity and localization of rhoA via polyamination', *Exp Cell Res*, 315: 1008-14.

Mandal, S., Mandal, A., Johansson, H. E., Orjalo, A. V., and Park, M. H. 2013. 'Depletion of cellular polyamines, spermidine and spermine, causes a total arrest in translation and growth in mammalian cells', *Proc Natl Acad Sci U S A*, 110: 2169-74.

Marshall, S., Bacote, V., and Traxinger, R. R. 1991. 'Discovery of a metabolic pathway mediating glucose-induced desensitization of the glucose transport system. Role of hexosamine biosynthesis in the induction of insulin resistance', *J Biol Chem*, 266: 4706-12.

Marshall, S., Nadeau, O., and Yamasaki, K. 2004. 'Dynamic actions of glucose and glucosamine on hexosamine biosynthesis in isolated adipocytes: differential effects on glucosamine 6-phosphate, UDP-N-acetylglucosamine, and ATP levels', *J Biol Chem*, 279: 35313-9.

Martel, J. L., Miao, J. H., and Badri, T. 2020. 'Anatomy, Hair Follicle.' in, *StatPearls* (Treasure Island (FL)).

Matsumura, H., Mohri, Y., Binh, N. T., Morinaga, H., Fukuda, M., Ito, M., Kurata, S., Hoeijmakers, J., and Nishimura, E. K. 2016. 'Hair follicle aging is driven by transepidermal elimination of stem cells via COL17A1 proteolysis', *Science*, 351: aad4395.

Mattila, J., Kokki, K., Hietakangas, V., and Boutros, M. 2018. 'Stem Cell Intrinsic Hexosamine Metabolism Regulates Intestinal Adaptation to Nutrient Content', *Dev Cell*, 47: 112-21 e3.

Mattout, A., Biran, A., and Meshorer, E. 2011. 'Global epigenetic changes during somatic cell reprogramming to iPS cells', *J Mol Cell Biol*, 3: 341-50.

Mauthe, M., Orhon, I., Rocchi, C., Zhou, X., Luhr, M., Hijlkema, K. J., Coppes, R. P., Engedal, N., Mari, M., and Reggiori, F. 2018. 'Chloroquine inhibits autophagic flux by decreasing autophagosome-lysosome fusion', *Autophagy*, 14: 1435-55.

Mechulam, A., Chernov, K. G., Mucher, E., Hamon, L., Curmi, P. A., and Pastre, D. 2009. 'Polyamine sharing between tubulin dimers favours microtubule nucleation and elongation via facilitated diffusion', *PLoS Comput Biol*, 5: e1000255.

Melkonian, E. A., and Schury, M. P. 2020. 'Biochemistry, Anaerobic Glycolysis.' in, *StatPearls* (Treasure Island (FL)).

Melzer, D., Pilling, L. C., and Ferrucci, L. 2020. 'The genetics of human ageing', *Nat Rev Genet*, 21: 88-101.

Merida-de-Barros, D. A., Chaves, S. P., Belmiro, C. L. R., and Wanderley, J. L. M. 2018. 'Leishmaniasis and glycosaminoglycans: a future therapeutic strategy?', *Parasit Vectors*, 11: 536.

Mesa, K. R., Kawaguchi, K., Cockburn, K., Gonzalez, D., Boucher, J., Xin, T., Klein, A. M., and Greco, V. 2018. 'Homeostatic Epidermal Stem Cell Self-Renewal Is Driven by Local Differentiation', *Cell Stem Cell*, 23: 677-86 e4.

Metcalf, B. W., Bey, P., Danzin, C., Jung, M. J., Casara, P., and Vevert, J. P. 1978. 'Catalytic irreversible inhibition of mammalian ornithine decarboxylase (E.C.4.1.1.17) by substrate and product analogs', *Journal of the American Chemical Society*, 100: 2551-53.

Mio, T., Yabe, T., Arisawa, M., and Yamada-Okabe, H. 1998. 'The eukaryotic UDP-N-acetylglucosamine pyrophosphorylases. Gene cloning, protein expression, and catalytic mechanism', *J Biol Chem*, 273: 14392-7.

Mitrečić, D., Petrović, D. J., Stančin, P., Isaković, J., Zavan, B., Tricarico, G., Kujundžić Tiljak, M., and Di Luca, M. 2020. 'How to face the aging world - lessons from dementia research', *Croat Med J*, 61: 139-46.

Montoya, J., López-Gallardo, E., Herrero-Martín, M. D., Martínez-Romero, I., Gómez-Durán, A., Pacheu, D., Carreras, M., Díez-Sánchez, C., López-Pérez, M. J., and Ruiz-Pesini, E. 2009. 'Diseases of the human mitochondrial oxidative phosphorylation system', *Adv Exp Med Biol*, 652: 47-67.

Moore, D. L., Pilz, G. A., Arauzo-Bravo, M. J., Barral, Y., and Jessberger, S. 2015. 'A mechanism for the segregation of age in mammalian neural stem cells', *Science*, 349: 1334-38.

Morgan, J. E., Blankenship, J. W., and Matthews, H. R. 1987. 'Polyamines and acetylpolyamines increase the stability and alter the conformation of nucleosome core particles', *Biochemistry*, 26: 3643-9.

Moriya, S. S., Miura, T., Takao, K., Sugita, Y., Samejima, K., Hiramatsu, K., and Kawakita, M. 2014. 'Development of irreversible inactivators of spermine oxidase and N1-acetylpolyamine oxidase', *Biol Pharm Bull*, 37: 475-80.

Morris, R. J., Liu, Y., Marles, L., Yang, Z., Trempus, C., Li, S., Lin, J. S., Sawicki, J. A., and Cotsarelis, G. 2004. 'Capturing and profiling adult hair follicle stem cells', *Nat Biotechnol*, 22: 411-7.

Morris, R. J., and Potten, C. S. 1999. 'Highly persistent label-retaining cells in the hair follicles of mice and their fate following induction of anagen', *J Invest Dermatol*, 112: 470-5.

Morrison, S. J., Wandycz, A. M., Akashi, K., Globerson, A., and Weissman, I. L. 1996. 'The aging of hematopoietic stem cells', *Nat Med*, 2: 1011-6.

Morselli, E., Galluzzi, L., Kepp, O., Criollo, A., Maiuri, M. C., Tavernarakis, N., Madeo, F., and Kroemer, G. 2009. 'Autophagy mediates pharmacological lifespan extension by spermidine and resveratrol', *Aging (Albany NY)*, 1: 961-70.

Mouilleron, S., Badet-Denisot, M. A., and Golinelli-Pimpaneau, B. 2006. 'Glutamine binding opens the ammonia channel and activates glucosamine-6P synthase', *J Biol Chem*, 281: 4404-12.

Moussaieff, A., Rouleau, M., Kitsberg, D., Cohen, M., Levy, G., Barasch, D., Nemirovski, A., Shen-Orr, S., Laevsky, I., Amit, M., Bomze, D., Elena-Herrmann, B., Scherf, T., Nissim-Rafinia, M., Kempa, S., Itskovitz-Eldor, J., Meshorer, E., Aberdam, D., and Nahmias, Y. 2015. 'Glycolysis-mediated changes in acetyl-CoA and histone acetylation control the early differentiation of embryonic stem cells', *Cell Metab*, 21: 392-402.

Moyle, L. A., Cheng, R. Y., Liu, H., Davoudi, S., Ferreira, S. A., Nissar, A. A., Sun, Y., Gentleman, E., Simmons, C. A., and Gilbert, P. M. 2020. 'Three-dimensional niche stiffness synergizes with Wnt7a to modulate the extent of satellite cell symmetric self-renewal divisions', *Mol Biol Cell*: mbcE20010078.

Müller-Röver, S., Handjiski, B., van der Veen, C., Eichmüller, S., Foitzik, K., McKay, I. A., Stenn, K. S., and Paus, R. 2001. 'A comprehensive guide for the accurate classification of murine hair follicles in distinct hair cycle stages', *J Invest Dermatol*, 117: 3-15.

Naba, A., Clauser, K. R., Hoersch, S., Liu, H., Carr, S. A., and Hynes, R. O. 2012. 'The matrisome: in silico definition and in vivo characterization by proteomics of normal and tumor extracellular matrices', *Mol Cell Proteomics*, 11: M111 014647.

Nagy, N., Kuipers, H. F., Frymoyer, A. R., Ishak, H. D., Bollyky, J. B., Wight, T. N., and Bollyky, P. L. 2015. '4-methylumbelliferone treatment and hyaluronan inhibition as a therapeutic strategy in inflammation, autoimmunity, and cancer', *Front Immunol*, 6: 123.

Naifeh, J., Jiang, J., and Varacallo, M. 2020. 'Biochemistry, Aerobic Glycolysis.' in, *StatPearls* (Treasure Island (FL)).

Nakajima, K., Kitazume, S., Angata, T., Fujinawa, R., Ohtsubo, K., Miyoshi, E., and Taniguchi, N. 2010. 'Simultaneous determination of nucleotide sugars with ion-pair reversed-phase HPLC', *Glycobiology*, 20: 865-71.

Nakamura, T., Takagaki, K., Shibata, S., Tanaka, K., Higuchi, T., and Endo, M. 1995. 'Hyaluronic-acid-deficient extracellular matrix induced by addition of 4-methylumbelliferone to the medium of cultured human skin fibroblasts', *Biochem Biophys Res Commun*, 208: 470-5.

Nakano, H., Minami, I., Braas, D., Pappoe, H., Wu, X., Sagadevan, A., Vergnes, L., Fu, K., Morselli, M., Dunham, C., Ding, X., Stieg, A. Z., Gimzewski, J. K., Pellegrini, M., Clark, P. M., Reue, K., Lusis, A. J., Ribalet, B., Kurdistani, S. K., Christofk, H., Nakatsuji, N., and Nakano, A. 2017. 'Glucose inhibits cardiac muscle maturation through nucleotide biosynthesis', *Elife*, 6.

Nancarrow, M. J., Nesci, A., Hynd, P. I., and Powell, B. C. 1999. 'Dynamic expression of ornithine decarboxylase in hair growth', *Mech Dev*, 84: 161-4.

Nasizadeh, S., Myhre, L., Thiman, L., Alm, K., Oredsson, S., and Persson, L. 2005. 'Importance of polyamines in cell cycle kinetics as studied in a transgenic system', *Exp Cell Res*, 308: 254-64.

Neidhart, M., Karouzakis, E., Jüngel, A., Gay, R. E., and Gay, S. 2014. 'Inhibition of spermidine/spermine N1-acetyltransferase activity: a new therapeutic concept in rheumatoid arthritis', *Arthritis Rheumatol*, 66: 1723-33.

Nielsen, J. S., and McNagny, K. M. 2008. 'Novel functions of the CD34 family', *J Cell Sci*, 121: 3683-92.

Niemann, C., and Watt, F. M. 2002. 'Designer skin: lineage commitment in postnatal epidermis', *Trends Cell Biol*, 12: 185-92.

Niimi, M., Ogawara, T., Yamashita, T., Yamamoto, Y., Ueyama, A., Kambe, T., Okamoto, T., Ban, T., Tamanoi, H., Ozaki, K., Fujiwara, T., Fukui, H., Takahashi, E. I., Kyushiki, H., and Tanigami, A. 2001. 'Identification of GFAT1-L, a novel splice variant of human glutamine: fructose-6-phosphate amidotransferase (GFAT1) that is expressed abundantly in skeletal muscle', *J Hum Genet*, 46: 566-71.

Nikolakis, G., Makrantonaki, E., and Zouboulis, C. C. 2013. 'Skin mirrors human aging', *Horm Mol Biol Clin Investig*, 16: 13-28.

Nishimura, E. K., Granter, S. R., and Fisher, D. E. 2005. 'Mechanisms of hair graying: incomplete melanocyte stem cell maintenance in the niche', *Science*, 307: 720-4.

Nishimura, K., Shiina, R., Kashiwagi, K., and Igarashi, K. 2006. 'Decrease in polyamines with aging and their ingestion from food and drink', *J Biochem*, 139: 81-90.

Noga, M. J., Dane, A., Shi, S., Attali, A., van Aken, H., Suidgeest, E., Tuinstra, T., Muilwijk, B., Coulier, L., Luider, T., Reijmers, T. H., Vreeken, R. J., and Hankemeier, T. 2012. 'Metabolomics of cerebrospinal fluid reveals changes in the central nervous system metabolism in a rat model of multiple sclerosis', *Metabolomics*, 8: 253-63.

Nomura, T., Kawae, T., Kataoka, H., and Ikeda, Y. 2018. 'Assessment of lower extremity muscle mass, muscle strength, and exercise therapy in elderly patients with diabetes mellitus', *Environ Health Prev Med*, 23: 20.

Nowak, J. A., Polak, L., Pasolli, H. A., and Fuchs, E. 2008. 'Hair follicle stem cells are specified and function in early skin morphogenesis', *Cell Stem Cell*, 3: 33-43.

Odenlund, M., Holmqvist, B., Baldetorp, B., Hellstrand, P., and Nilsson, B. O. 2009. 'Polyamine synthesis inhibition induces S phase cell cycle arrest in vascular smooth muscle cells', *Amino Acids*, 36: 273-82.

Oeppen, J., and Vaupel, J. W. 2002. 'Demography. Broken limits to life expectancy', *Science*, 296: 1029-31.

Oikari, S., Makkonen, K., Deen, A. J., Tyni, I., Kärnä, R., Tammi, R. H., and Tammi, M. I. 2016. 'Hexosamine biosynthesis in keratinocytes: roles of GFAT and GNPDA enzymes in the maintenance of UDP-GlcNAc content and hyaluronan synthesis', *Glycobiology*, 26: 710-22.

Oki, T., Yamazaki, K., Kuromitsu, J., Okada, M., and Tanaka, I. 1999. 'cDNA cloning and mapping of a novel subtype of glutamine:fructose-6-phosphate amidotransferase (GFAT2) in human and mouse', *Genomics*, 57: 227-34.

Olchowy, J., Kur, K., Sachadyn, P., and Milewski, S. 2006. 'Construction, purification, and functional characterization of His-tagged Candida albicans glucosamine-6-phosphate synthase expressed in Escherichia coli', *Protein Expr Purif*, 46: 309-15.

Oliva, G., Fontes, M. R., Garratt, R. C., Altamirano, M. M., Calcagno, M. L., and Horjales, E. 1995. 'Structure and catalytic mechanism of glucosamine 6-phosphate deaminase from Escherichia coli at 2.1 A resolution', *Structure*, 3: 1323-32.

Ozfiliz, P., Kizilboga, T., Demir, S., Alkurt, G., Palavan-Unsal, N., Arisan, E. D., and Dinler-Doganay, G. 2015. 'Bag-1 promotes cell survival through c-Myc-mediated ODC upregulation that is not preferred under apoptotic stimuli in MCF-7 cells', *Cell Biochem Funct*, 33: 293-307.

Pakos-Zebrucka, K., Koryga, I., Mnich, K., Ljujic, M., Samali, A., and Gorman, A. M. 2016. 'The integrated stress response', *EMBO Rep*, 17: 1374-95.

Palanimurugan, R., Scheel, H., Hofmann, K., and Dohmen, R. J. 2004. 'Polyamines regulate their synthesis by inducing expression and blocking degradation of ODC antizyme', *EMBO J*, 23: 4857-67.

Pallan, P. S., and Ganesh, K. N. 1996. 'DNA triple helix stabilization by bisguanidinyl analogues of biogenic polyamines', *Biochem Biophys Res Commun*, 222: 416-20.

Park, M. H., Cooper, H. L., and Folk, J. E. 1981. 'Identification of hypusine, an unusual amino acid, in a protein from human lymphocytes and of spermidine as its biosynthetic precursor', *Proc Natl Acad Sci U S A*, 78: 2869-73.

Park, M. H., Cooper, H. L., and Folk, J. E. 1982. 'The biosynthesis of protein-bound hypusine (N epsilon -(4-amino-2-hydroxybutyl)lysine). Lysine as the amino acid precursor and the intermediate role of deoxyhypusine (N epsilon -(4-aminobutyl)lysine)', *J Biol Chem*, 257: 7217-22.

Parry, L., Balana Fouce, R., and Pegg, A. E. 1995. 'Post-transcriptional regulation of the content of spermidine/spermine N1-acetyltransferase by N1N12-bis(ethyl)spermine', *Biochem J*, 305 (Pt 2): 451-8.

Partridge, L., Deelen, J., and Slagboom, P. E. 2018. 'Facing up to the global challenges of ageing', *Nature*, 561: 45-56.

Pause, A., Belsham, G. J., Gingras, A. C., Donze, O., Lin, T. A., Lawrence, J. C., Jr., and Sonenberg, N. 1994. 'Insulin-dependent stimulation of protein synthesis by phosphorylation of a regulator of 5'-cap function', *Nature*, 371: 762-7.

PDQ, Adult Treatment Editorial Board. 2020. 'Schematic representation of normal skin', *PDQ Cancer Information Summaries [Internet], National Cancer Institute*.

Pegg, A. E. 2008. 'Spermidine/spermine-N(1)-acetyltransferase: a key metabolic regulator', *Am J Physiol Endocrinol Metab*, 294: E995-1010.

Pegg, A. E. 2016. 'Functions of Polyamines in Mammals', *J Biol Chem*, 291: 14904-12.

Pertea, M., Kim, D., Pertea, G. M., Leek, J. T., and Salzberg, S. L. 2016. 'Transcript-level expression analysis of RNA-seq experiments with HISAT, StringTie and Ballgown', *Nat Protoc*, 11: 1650-67.

Peters, F., Tellkamp, F., Brodesser, S., Wachsmuth, E., Tosetti, B., Karow, U., Bloch, W., Utermohlen, O., Kronke, M., and Niessen, C. M. 2020. 'Murine Epidermal Ceramide Synthase 4 Is a Key Regulator of Skin Barrier Homeostasis', *J Invest Dermatol*.

Peus, D., Hamacher, L., and Pittelkow, M. R. 1997. 'EGF-receptor tyrosine kinase inhibition induces keratinocyte growth arrest and terminal differentiation', *J Invest Dermatol*, 109: 751-6.

Piccoli, C., Ria, R., Scrima, R., Cela, O., D'Aprile, A., Boffoli, D., Falzetti, F., Tabilio, A., and Capitanio, N. 2005. 'Characterization of mitochondrial and extra-mitochondrial oxygen consuming reactions in human hematopoietic stem cells. Novel evidence of the occurrence of NAD(P)H oxidase activity', *J Biol Chem*, 280: 26467-76.

Pieragostino, D., D'Alessandro, M., di Ioia, M., Rossi, C., Zucchelli, M., Urbani, A., Di Ilio, C., Lugaresi, A., Sacchetta, P., and Del Boccio, P. 2015. 'An integrated metabolomics approach for the research of new cerebrospinal fluid biomarkers of multiple sclerosis', *Mol Biosyst*, 11: 1563-72.

Pietilä, M., Alhonen, L., Halmekytö, M., Kanter, P., Jänne, J., and Porter, C. W. 1997. 'Activation of polyamine catabolism profoundly alters tissue polyamine pools and affects hair growth and female fertility in transgenic mice overexpressing spermidine/spermine N1-acetyltransferase', *J Biol Chem*, 272: 18746-51.

Pietilä, M., Parkkinen, J. J., Alhonen, L., and Jänne, J. 2001. 'Relation of skin polyamines to the hairless phenotype in transgenic mice overexpressing spermidine/spermine N-acetyltransferase', *J Invest Dermatol*, 116: 801-5.

Plikus, M. V., Baker, R. E., Chen, C. C., Fare, C., de la Cruz, D., Andl, T., Maini, P. K., Millar, S. E., Widelitz, R., and Chuong, C. M. 2011. 'Self-organizing and stochastic behaviors during the regeneration of hair stem cells', *Science*, 332: 586-9.

Plikus, M. V., Mayer, J. A., de la Cruz, D., Baker, R. E., Maini, P. K., Maxson, R., and Chuong, C. M. 2008. 'Cyclic dermal BMP signalling regulates stem cell activation during hair regeneration', *Nature*, 451: 340-4.

Porter, C. W., Ganis, B., Libby, P. R., and Bergeron, R. J. 1991. 'Correlations between polyamine analogue-induced increases in spermidine/spermine N1-acetyltransferase activity, polyamine pool depletion, and growth inhibition in human melanoma cell lines', *Cancer Res*, 51: 3715-20.

Preiss, T., and Hentze, M. W. 2003. 'Starting the protein synthesis machine: eukaryotic translation initiation', *Bioessays*, 25: 1201-11.

Prydz, K., and Dalen, K. T. 2000. 'Synthesis and sorting of proteoglycans', *J Cell Sci*, 113 Pt 2: 193-205.

Puleston, D. J., Buck, M. D., Klein Geltink, R. I., Kyle, R. L., Caputa, G., O'Sullivan, D., Cameron, A. M., Castoldi, A., Musa, Y., Kabat, A. M., Zhang, Y., Flachsmann, L. J., Field, C. S., Patterson, A. E., Scherer, S., Alfei, F., Baixauli, F., Austin, S. K., Kelly, B., Matsushita, M., Curtis, J. D., Grzes, K. M., Villa, M., Corrado, M., Sanin, D. E., Qiu, J., Pällman, N., Paz, K., Maccari, M. E., Blazar, B. R., Mittler, G., Buescher, J. M., Zehn, D., Rospert, S., Pearce, E. J., Balabanov, S., and Pearce, E. L. 2019. 'Polyamines and eIF5A Hypusination Modulate Mitochondrial Respiration and Macrophage Activation', *Cell Metab*, 30: 352-63 e8.

Quattrini, L., and La Motta, C. 2019. 'Aldose reductase inhibitors: 2013-present', *Expert Opin Ther Pat*, 29: 199-213.

Quinlan, A. R., and Hall, I. M. 2010. 'BEDTools: a flexible suite of utilities for comparing genomic features', *Bioinformatics*, 26: 841-2.

Rajas, F., Gautier-Stein, A., and Mithieux, G. 2019. 'Glucose-6 Phosphate, A Central Hub for Liver Carbohydrate Metabolism', *Metabolites*, 9.

Rando, T. A., and Chang, H. Y. 2012. 'Aging, rejuvenation, and epigenetic reprogramming: resetting the aging clock', *Cell*, 148: 46-57.

Ravera, S., Podestà, M., Sabatini, F., Dagnino, M., Cilloni, D., Fiorini, S., Barla, A., and Frassoni, F. 2019. 'Discrete Changes in Glucose Metabolism Define Aging', *Sci Rep*, 9: 10347.

Ray, R. M., McCormack, S. A., Covington, C., Viar, M. J., Zheng, Y., and Johnson, L. R. 2003. 'The requirement for polyamines for intestinal epithelial cell migration is mediated through Rac1', *J Biol Chem*, 278: 13039-46.

Ray, R. M., Zimmerman, B. J., McCormack, S. A., Patel, T. B., and Johnson, L. R. 1999. 'Polyamine depletion arrests cell cycle and induces inhibitors p21(Waf1/Cip1), p27(Kip1), and p53 in IEC-6 cells', *Am J Physiol*, 276: C684-91.

Rera, M., Bahadorani, S., Cho, J., Koehler, C. L., Ulgherait, M., Hur, J. H., Ansari, W. S., Lo, T., Jr., Jones, D. L., and Walker, D. W. 2011. 'Modulation of longevity and tissue homeostasis by the Drosophila PGC-1 homolog', *Cell Metab*, 14: 623-34.

Ricciardiello, F., Votta, G., Palorini, R., Raccagni, I., Brunelli, L., Paiotta, A., Tinelli, F., D'Orazio, G., Valtorta, S., De Gioia, L., Pastorelli, R., Moresco, R. M., La Ferla, B., and Chiaradonna, F. 2018. 'Inhibition of the Hexosamine Biosynthetic Pathway by targeting PGM3 causes breast cancer growth arrest and apoptosis', *Cell Death Dis*, 9: 377.

Richez, C., Boetzel, J., Floquet, N., Koteshwar, K., Stevens, J., Badet, B., and Badet-Denisot, M. A. 2007. 'Expression and purification of active human internal His(6)-tagged L-glutamine: D-Fructose-6P amidotransferase I', *Protein Expr Purif*, 54: 45-53.

Rinnerthaler, M., Duschl, J., Steinbacher, P., Salzmann, M., Bischof, J., Schuller, M., Wimmer, H., Peer, T., Bauer, J. W., and Richter, K. 2013. 'Age-related changes in the composition of the cornified envelope in human skin', *Exp Dermatol*, 22: 329-35.

Rinnerthaler, M., Streubel, M. K., Bischof, J., and Richter, K. 2015. 'Skin aging, gene expression and calcium', *Exp Gerontol*, 68: 59-65.

Rojas-Ríos, P., and González-Reyes, A. 2014. 'Concise review: The plasticity of stem cell niches: a general property behind tissue homeostasis and repair', *Stem Cells*, 32: 852-9.

Rompolas, P., Mesa, K. R., and Greco, V. 2013. 'Spatial organization within a niche as a determinant of stem-cell fate', *Nature*, 502: 513-8.

Rossi, D. J., Bryder, D., Seita, J., Nussenzweig, A., Hoeijmakers, J., and Weissman, I. L. 2007. 'Deficiencies in DNA damage repair limit the function of haematopoietic stem cells with age', *Nature*, 447: 725-9.

Roux, P. P., and Topisirovic, I. 2018. 'Signaling Pathways Involved in the Regulation of mRNA Translation', *Mol Cell Biol*, 38.

Rowlands, A. G., Panniers, R., and Henshaw, E. C. 1988. 'The catalytic mechanism of guanine nucleotide exchange factor action and competitive inhibition by phosphorylated eukaryotic initiation factor 2', *J Biol Chem*, 263: 5526-33.

Ruegenberg, S., Horn, M., Pichlo, C., Allmeroth, K., Baumann, U., and Denzel, M. S. 2020. 'Loss of GFAT-1 feedback regulation activates the hexosamine pathway that modulates protein homeostasis', *Nat Commun*, 11: 687.

Ruiz, S., Panopoulos, A. D., Herrerias, A., Bissig, K. D., Lutz, M., Berggren, W. T., Verma, I. M., and Izpisua Belmonte, J. C. 2011. 'A high proliferation rate is required for cell reprogramming and maintenance of human embryonic stem cell identity', *Curr Biol*, 21: 45-52.

Ryczko, M. C., Pawling, J., Chen, R., Abdel Rahman, A. M., Yau, K., Copeland, J. K., Zhang, C., Surendra, A., Guttman, D. S., Figeys, D., and Dennis, J. W. 2016. 'Metabolic Reprogramming by Hexosamine Biosynthetic and Golgi N-Glycan Branching Pathways', *Sci Rep*, 6: 23043.

Saini, P., Eyler, D. E., Green, R., and Dever, T. E. 2009. 'Hypusine-containing protein eIF5A promotes translation elongation', *Nature*, 459: 118-21.

Sakamoto, A., Terui, Y., Uemura, T., Igarashi, K., and Kashiwagi, K. 2020. 'Polyamines regulate gene expression by stimulating translation of histone acetyltransferase mRNAs', *J Biol Chem*, 295: 8736-45.

Salemi, S., Yousefi, S., Constantinescu, M. A., Fey, M. F., and Simon, H. U. 2012. 'Autophagy is required for self-renewal and differentiation of adult human stem cells', *Cell Res*, 22: 432-5.

Sampath, P., Pritchard, D. K., Pabon, L., Reinecke, H., Schwartz, S. M., Morris, D. R., and Murry, C. E. 2008. 'A hierarchical network controls protein translation during murine embryonic stem cell self-renewal and differentiation', *Cell Stem Cell*, 2: 448-60.

Sanchez-Lopez, J., Camanes, G., Flors, V., Vicent, C., Pastor, V., Vicedo, B., Cerezo, M., and Garcia-Agustin, P. 2009. 'Underivatized polyamine analysis in plant samples by ion pair LC coupled with electrospray tandem mass spectrometry', *Plant Physiol Biochem*, 47: 592-8.

Sanz, E., Yang, L., Su, T., Morris, D. R., McKnight, G. S., and Amieux, P. S. 2009. 'Cell-type-specific isolation of ribosome-associated mRNA from complex tissues', *Proc Natl Acad Sci U S A*, 106: 13939-44.

Saretzki, G., Armstrong, L., Leake, A., Lako, M., and von Zglinicki, T. 2004. 'Stress defense in murine embryonic stem cells is superior to that of various differentiated murine cells', *Stem Cells*, 22: 962-71.

Saretzki, G., Walter, T., Atkinson, S., Passos, J. F., Bareth, B., Keith, W. N., Stewart, R., Hoare, S., Stojkovic, M., Armstrong, L., von Zglinicki, T., and Lako, M. 2008. 'Downregulation of multiple stress defense mechanisms during differentiation of human embryonic stem cells', *Stem Cells*, 26: 455-64.

Sasai, K., Ikeda, Y., Fujii, T., Tsuda, T., and Taniguchi, N. 2002. 'UDP-GlcNAc concentration is an important factor in the biosynthesis of beta1,6-branched oligosaccharides: regulation based on the kinetic properties of N-acetylglucosaminyltransferase V', *Glycobiology*, 12: 119-27.

Schaefer, L., and Schaefer, R. M. 2010. 'Proteoglycans: from structural compounds to signaling molecules', *Cell Tissue Res*, 339: 237-46.

Schell, J. C., Wisidagama, D. R., Bensard, C., Zhao, H., Wei, P., Tanner, J., Flores, A., Mohlman, J., Sorensen, L. K., Earl, C. S., Olson, K. A., Miao, R., Waller, T. C., Delker, D., Kanth, P., Jiang, L., DeBerardinis, R. J., Bronner, M. P., Li, D. Y., Cox, J. E., Christofk, H. R., Lowry, W. E., Thummel, C. S., and Rutter, J. 2017. 'Control of intestinal stem cell function and proliferation by mitochondrial pyruvate metabolism', *Nat Cell Biol*, 19: 1027-36.

Schindelin, J., Arganda-Carreras, I., Frise, E., Kaynig, V., Longair, M., Pietzsch, T., Preibisch, S., Rueden, C., Saalfeld, S., Schmid, B., Tinevez, J. Y., White, D. J., Hartenstein, V., Eliceiri, K., Tomancak, P., and Cardona, A. 2012. 'Fiji: an open-source platform for biological-image analysis', *Nat Methods*, 9: 676-82.

Schmidt, E. K., Clavarino, G., Ceppi, M., and Pierre, P. 2009. 'SUnSET, a nonradioactive method to monitor protein synthesis', *Nat Methods*, 6: 275-7.

Schofield, R. 1978. 'The relationship between the spleen colony-forming cell and the haemopoietic stem cell', *Blood Cells*, 4: 7-25.

Schröder, M., and Kaufman, R. J. 2005. 'The mammalian unfolded protein response', *Annu Rev Biochem*, 74: 739-89.

Schultz, M. B., and Sinclair, D. A. 2016. 'When stem cells grow old: phenotypes and mechanisms of stem cell aging', *Development*, 143: 3-14.

Schulz, J. M., Watson, A. L., Sanders, R., Ross, K. L., Thoden, J. B., Holden, H. M., and Fridovich-Keil, J. L. 2004. 'Determinants of function and substrate specificity in human UDP-galactose 4'-epimerase', *J Biol Chem*, 279: 32796-803.

Schwenk, F., Baron, U., and Rajewsky, K. 1995. 'A cre-transgenic mouse strain for the ubiquitous deletion of loxP-flanked gene segments including deletion in germ cells', *Nucleic Acids Res*, 23: 5080-1.

Seiler, N. 2004. 'Catabolism of polyamines', *Amino Acids*, 26: 217-33.

Seiler, N., and Dezeure, F. 1990. 'Polyamine transport in mammalian cells', *Int J Biochem*, 22: 211-8.

Sela, Y., Molotski, N., Golan, S., Itskovitz-Eldor, J., and Soen, Y. 2012. 'Human embryonic stem cells exhibit increased propensity to differentiate during the G1 phase prior to phosphorylation of retinoblastoma protein', *Stem Cells*, 30: 1097-108.

Shah, A. R., and Kennedy, P. M. 2018. 'The Aging Face', *Med Clin North Am*, 102: 1041-54.

Sharma, V., Ichikawa, M., and Freeze, H. H. 2014. 'Mannose metabolism: more than meets the eye', *Biochem Biophys Res Commun*, 453: 220-8.

Sharma, V., Smolin, J., Nayak, J., Ayala, J. E., Scott, D. A., Peterson, S. N., and Freeze, H. H. 2018. 'Mannose Alters Gut Microbiome, Prevents Diet-Induced Obesity, and Improves Host Metabolism', *Cell Rep*, 24: 3087-98.

Shtraizent, N., DeRossi, C., Nayar, S., Sachidanandam, R., Katz, L. S., Prince, A., Koh, A. P., Vincek, A., Hadas, Y., Hoshida, Y., Scott, D. K., Eliyahu, E., Freeze, H. H., Sadler, K. C., and Chu, J. 2017. 'MPI depletion enhances O-GlcNAcylation of p53 and suppresses the Warburg effect', *Elife*, 6.

Signer, R. A., Magee, J. A., Salic, A., and Morrison, S. J. 2014. 'Haematopoietic stem cells require a highly regulated protein synthesis rate', *Nature*, 509: 49-54.

Signer, R. A., and Morrison, S. J. 2013. 'Mechanisms that regulate stem cell aging and life span', *Cell Stem Cell*, 12: 152-65.

Simsek, T., Kocabas, F., Zheng, J., Deberardinis, R. J., Mahmoud, A. I., Olson, E. N., Schneider, J. W., Zhang, C. C., and Sadek, H. A. 2010. 'The distinct metabolic profile of hematopoietic stem cells reflects their location in a hypoxic niche', *Cell Stem Cell*, 7: 380-90.

Slade, P. G., Caspary, R. G., Nargund, S., and Huang, C. J. 2016. 'Mannose metabolism in recombinant CHO cells and its effect on IgG glycosylation', *Biotechnol Bioeng*, 113: 1468-80.

Slominski, A., and Paus, R. 1993. 'Melanogenesis is coupled to murine anagen: toward new concepts for the role of melanocytes and the regulation of melanogenesis in hair growth', *J Invest Dermatol*, 101: 90S-97S.

Smith, M. H., Ploegh, H. L., and Weissman, J. S. 2011. 'Road to ruin: targeting proteins for degradation in the endoplasmic reticulum', *Science*, 334: 1086-90.

Solanas, G., and Benitah, S. A. 2013. 'Regenerating the skin: a task for the heterogeneous stem cell pool and surrounding niche', *Nat Rev Mol Cell Biol*, 14: 737-48.

Soler, A. P., Gilliard, G., Megosh, L. C., and O'Brien, T. G. 1996. 'Modulation of murine hair follicle function by alterations in ornithine decarboxylase activity', *J Invest Dermatol*, 106: 1108-13.

Sonenberg, N., and Hinnebusch, A. G. 2009. 'Regulation of translation initiation in eukaryotes: mechanisms and biological targets', *Cell*, 136: 731-45.

Sonnenberg, A., Calafat, J., Janssen, H., Daams, H., van der Raaij-Helmer, L. M., Falcioni, R., Kennel, S. J., Aplin, J. D., Baker, J., Loizidou, M., and et al. 1991. 'Integrin alpha 6/beta 4 complex is located in hemidesmosomes, suggesting a major role in epidermal cell-basement membrane adhesion', *J Cell Biol*, 113: 907-17.

Speakman, C. M., Domke, T. C., Wongpaiboonwattana, W., Sanders, K., Mudaliar, M., van Aalten, D. M., Barton, G. J., and Stavridis, M. P. 2014. 'Elevated O-GlcNAc levels activate epigenetically repressed genes and delay mouse ESC differentiation without affecting naive to primed cell transition', *Stem Cells*, 32: 2605-15.

St-Jacques, B., Dassule, H. R., Karavanova, I., Botchkarev, V. A., Li, J., Danielian, P. S., McMahon, J. A., Lewis, P. M., Paus, R., and McMahon, A. P. 1998. 'Sonic hedgehog signaling is essential for hair development', *Curr Biol*, 8: 1058-68.

Stern, R. 2003. 'Devising a pathway for hyaluronan catabolism: are we there yet?', *Glycobiology*, 13: 105R-15R.

Stoye, J. P., Fenner, S., Greenoak, G. E., Moran, C., and Coffin, J. M. 1988. 'Role of endogenous retroviruses as mutagens: the hairless mutation of mice', *Cell*, 54: 383-91.

Sun, C., Shang, J., Yao, Y., Yin, X., Liu, M., Liu, H., and Zhou, Y. 2016. 'O-GlcNAcylation: a bridge between glucose and cell differentiation', *J Cell Mol Med*, 20: 769-81.

Sunkara, P. S., Ramakrishna, S., Nishioka, K., and Rao, P. N. 1981. 'The relationship between levels and rates of synthesis of polyamines during mammalian cell cycle', *Life Sci*, 28: 1497-506.

Suppola, S., Pietilä, M., Parkkinen, J. J., Korhonen, V. P., Alhonen, L., Halmekytö, M., Porter, C. W., and Jänne, J. 1999. 'Overexpression of spermidine/spermine N1-acetyltransferase under the control of mouse metallothionein I promoter in transgenic mice: evidence for a

striking post-transcriptional regulation of transgene expression by a polyamine analogue', *Biochem J*, 338 (Pt 2): 311-6.

Tahmasebi, S., Khoutorsky, A., Mathews, M. B., and Sonenberg, N. 2018. 'Translation deregulation in human disease', *Nat Rev Mol Cell Biol*, 19: 791-807.

Tain, L. S., Jain, C., Nespital, T., Froehlich, J., Hinze, Y., Gronke, S., and Partridge, L. 2019. 'Longevity in response to lowered insulin signaling requires glycine N-methyltransferase-dependent spermidine production', *Aging Cell*: e13043.

Takubo, K., Nagamatsu, G., Kobayashi, C. I., Nakamura-Ishizu, A., Kobayashi, H., Ikeda, E., Goda, N., Rahimi, Y., Johnson, R. S., Soga, T., Hirao, A., Suematsu, M., and Suda, T. 2013. 'Regulation of glycolysis by Pdk functions as a metabolic checkpoint for cell cycle quiescence in hematopoietic stem cells', *Cell Stem Cell*, 12: 49-61.

Tamari, K., Konno, M., Asai, A., Koseki, J., Hayashi, K., Kawamoto, K., Murai, N., Matsufuji, S., Isohashi, F., Satoh, T., Goto, N., Tanaka, S., Doki, Y., Mori, M., Ogawa, K., and Ishii, H. 2018. 'Polyamine flux suppresses histone lysine demethylases and enhances ID1 expression in cancer stem cells', *Cell Death Discov*, 4: 104.

Taniuchi, S., Miyake, M., Tsugawa, K., Oyadomari, M., and Oyadomari, S. 2016. 'Integrated stress response of vertebrates is regulated by four eIF2alpha kinases', *Sci Rep*, 6: 32886.

Taranenko, N., and Krause, D. S. 2000. 'Regulation of CD34 transcription by Sp1 requires sites upstream and downstream of the transcription start site', *Exp Hematol*, 28: 974-84.

Taylor, G., Lehrer, M. S., Jensen, P. J., Sun, T. T., and Lavker, R. M. 2000. 'Involvement of follicular stem cells in forming not only the follicle but also the epidermis', *Cell*, 102: 451-61.

Thoden, J. B., Wohlers, T. M., Fridovich-Keil, J. L., and Holden, H. M. 2001. 'Human UDP-galactose 4-epimerase. Accommodation of UDP-N-acetylglucosamine within the active site', *J Biol Chem*, 276: 15131-6.

Tian, Y., Wang, S., Wang, B., Zhang, J., Jiang, R., and Zhang, W. 2012. 'Overexpression of SSAT by DENSPM treatment induces cell detachment and apoptosis in glioblastoma', *Oncol Rep*, 27: 1227-32.

Toole, B. P. 2004. 'Hyaluronan: from extracellular glue to pericellular cue', *Nat Rev Cancer*, 4: 528-39.

Tra, T., Gong, L., Kao, L. P., Li, X. L., Grandela, C., Devenish, R. J., Wolvetang, E., and Prescott, M. 2011. 'Autophagy in human embryonic stem cells', *PLoS One*, 6: e27485.

Tran, D. H., May, H. I., Li, Q., Luo, X., Huang, J., Zhang, G., Niewold, E., Wang, X., Gillette, T. G., Deng, Y., and Wang, Z. V. 2020. 'Chronic activation of hexosamine biosynthesis in the heart triggers pathological cardiac remodeling', *Nat Commun*, 11: 1771.

Trapnell, C., Roberts, A., Goff, L., Pertea, G., Kim, D., Kelley, D. R., Pimentel, H., Salzberg, S. L., Rinn, J. L., and Pachter, L. 2012. 'Differential gene and transcript expression analysis of RNA-seq experiments with TopHat and Cufflinks', *Nat Protoc*, 7: 562-78.

Trempus, C. S., Morris, R. J., Bortner, C. D., Cotsarelis, G., Faircloth, R. S., Reece, J. M., and Tennant, R. W. 2003. 'Enrichment for living murine keratinocytes from the hair follicle bulge with the cell surface marker CD34', *J Invest Dermatol*, 120: 501-11.

Tsai, Y. H., Lin, K. L., Huang, Y. P., Hsu, Y. C., Chen, C. H., Chen, Y., Sie, M. H., Wang, G. J., and Lee, M. J. 2015. 'Suppression of ornithine decarboxylase promotes osteogenic

differentiation of human bone marrow-derived mesenchymal stem cells', *FEBS Lett*, 589: 2058-65.

Tsukamoto, K., Odoko, M., Ohishi, H., Hiyama, Y., Maezaki, N., Okabe, N., Tanaka, T., and Ishida, T. 2005. 'Stabilization of the left-handed Z-DNA with monoamines and polyamines', *Nucleic Acids Symp Ser (Oxf)*: 251-2.

Tumbar, T., Guasch, G., Greco, V., Blanpain, C., Lowry, W. E., Rendl, M., and Fuchs, E. 2004. 'Defining the epithelial stem cell niche in skin', *Science*, 303: 359-63.

Turner, W. S., Seagle, C., Galanko, J. A., Favorov, O., Prestwich, G. D., Macdonald, J. M., and Reid, L. M. 2008. 'Nuclear magnetic resonance metabolomic footprinting of human hepatic stem cells and hepatoblasts cultured in hyaluronan-matrix hydrogels', *Stem Cells*, 26: 1547-55.

Uimari, A., Keinänen, T. A., Karppinen, A., Woster, P., Uimari, P., Jänne, J., and Alhonen, L. 2009. 'Spermine analogue-regulated expression of spermidine/spermine N1-acetyltransferase and its effects on depletion of intracellular polyamine pools in mouse fetal fibroblasts', *Biochem J*, 422: 101-9.

Uitto, J. 1989. 'Connective tissue biochemistry of the aging dermis. Age-associated alterations in collagen and elastin', *Clin Geriatr Med*, 5: 127-47.

van der Laarse, S. A. M., Leney, A. C., and Heck, A. J. R. 2018. 'Crosstalk between phosphorylation and O-GlcNAcylation: friend or foe', *FEBS J*, 285: 3152-67.

Van Mater, D., Kolligs, F. T., Dlugosz, A. A., and Fearon, E. R. 2003. 'Transient activation of beta -catenin signaling in cutaneous keratinocytes is sufficient to trigger the active growth phase of the hair cycle in mice', *Genes Dev*, 17: 1219-24.

Vander Heiden, M. G., Cantley, L. C., and Thompson, C. B. 2009. 'Understanding the Warburg effect: the metabolic requirements of cell proliferation', *Science*, 324: 1029-33.

Varum, S., Momcilovic, O., Castro, C., Ben-Yehudah, A., Ramalho-Santos, J., and Navara, C. S. 2009. 'Enhancement of human embryonic stem cell pluripotency through inhibition of the mitochondrial respiratory chain', *Stem Cell Res*, 3: 142-56.

Veerababu, G., Tang, J., Hoffman, R. T., Daniels, M. C., Hebert, L. F., Jr., Crook, E. D., Cooksey, R. C., and McClain, D. A. 2000. 'Overexpression of glutamine: fructose-6-phosphate amidotransferase in the liver of transgenic mice results in enhanced glycogen storage, hyperlipidemia, obesity, and impaired glucose tolerance', *Diabetes*, 49: 2070-8.

Vigetti, D., Deleonibus, S., Moretto, P., Karousou, E., Viola, M., Bartolini, B., Hascall, V. C., Tammi, M., De Luca, G., and Passi, A. 2012. 'Role of UDP-N-acetylglucosamine (GlcNAc) and O-GlcNAcylation of hyaluronan synthase 2 in the control of chondroitin sulfate and hyaluronan synthesis', *J Biol Chem*, 287: 35544-55.

Vigetti, D., Ori, M., Viola, M., Genasetti, A., Karousou, E., Rizzi, M., Pallotti, F., Nardi, I., Hascall, V. C., De Luca, G., and Passi, A. 2006. 'Molecular cloning and characterization of UDP-glucose dehydrogenase from the amphibian Xenopus laevis and its involvement in hyaluronan synthesis', *J Biol Chem*, 281: 8254-63.

Vijg, J., and Campisi, J. 2008. 'Puzzles, promises and a cure for ageing', *Nature*, 454: 1065-71.

Vilchez, D., Boyer, L., Morantte, I., Lutz, M., Merkwirth, C., Joyce, D., Spencer, B., Page, L., Masliah, E., Berggren, W. T., Gage, F. H., and Dillin, A. 2012. 'Increased proteasome activity in human embryonic stem cells is regulated by PSMD11', *Nature*, 489: 304-8.

Vilchez, D., Saez, I., and Dillin, A. 2014a. 'The role of protein clearance mechanisms in organismal ageing and age-related diseases', *Nat Commun*, 5: 5659.

Vilchez, D., Simic, M. S., and Dillin, A. 2014b. 'Proteostasis and aging of stem cells', *Trends Cell Biol*, 24: 161-70.

Vinod, V., Padmakrishnan, C. J., Vijayan, B., and Gopala, S. 2014. "How can I halt thee?' The puzzles involved in autophagic inhibition', *Pharmacol Res*, 82: 1-8.

Vivó, M., de Vera, N., Cortés, R., Mengod, G., Camón, L., and Martínez, E. 2001. 'Polyamines in the basal ganglia of human brain. Influence of aging and degenerative movement disorders', *Neurosci Lett*, 304: 107-11.

Waby, J. S., Bingle, C. D., and Corfe, B. M. 2008. 'Post-translational control of sp-family transcription factors', *Curr Genomics*, 9: 301-11.

Wallace, H. M., Fraser, A. V., and Hughes, A. 2003. 'A perspective of polyamine metabolism', *Biochem J*, 376: 1-14.

Waller, J. M., and Maibach, H. I. 2005. 'Age and skin structure and function, a quantitative approach (I): blood flow, pH, thickness, and ultrasound echogenicity', *Skin Res Technol*, 11: 221-35.

Walter, P., and Ron, D. 2011. 'The unfolded protein response: from stress pathway to homeostatic regulation', *Science*, 334: 1081-6.

Wang, J., Li, S., Wang, J., Wu, F., Chen, Y., Zhang, H., Guo, Y., Lin, Y., Li, L., Yu, X., Liu, T., and Zhao, Y. 2020. 'Spermidine alleviates cardiac aging by improving mitochondrial biogenesis and function', *Aging (Albany NY)*, 11.

Wang, J., Liu, X., Liang, Y. H., Li, L. F., and Su, X. D. 2008. 'Acceptor substrate binding revealed by crystal structure of human glucosamine-6-phosphate N-acetyltransferase 1', *FEBS Lett*, 582: 2973-8.

Wang, L., Naser, F. J., Spalding, J. L., and Patti, G. J. 2019. 'A Protocol to Compare Methods for Untargeted Metabolomics', *Methods Mol Biol*, 1862: 1-15.

Wang, L., Wang, X., and Proud, C. G. 2000. 'Activation of mRNA translation in rat cardiac myocytes by insulin involves multiple rapamycin-sensitive steps', *Am J Physiol Heart Circ Physiol*, 278: H1056-68.

Wang, Z. V., Deng, Y., Gao, N., Pedrozo, Z., Li, D. L., Morales, C. R., Criollo, A., Luo, X., Tan, W., Jiang, N., Lehrman, M. A., Rothermel, B. A., Lee, A. H., Lavandero, S., Mammen, P. P. A., Ferdous, A., Gillette, T. G., Scherer, P. E., and Hill, J. A. 2014. 'Spliced X-box binding protein 1 couples the unfolded protein response to hexosamine biosynthetic pathway', *Cell*, 156: 1179-92.

Warburg, O. 1956. 'On the origin of cancer cells', *Science*, 123: 309-14.

Ware, C. B., Wang, L., Mecham, B. H., Shen, L., Nelson, A. M., Bar, M., Lamba, D. A., Dauphin, D. S., Buckingham, B., Askari, B., Lim, R., Tewari, M., Gartler, S. M., Issa, J. P., Pavlidis, P., Duan, Z., and Blau, C. A. 2009. 'Histone deacetylase inhibition elicits an

evolutionarily conserved self-renewal program in embryonic stem cells', *Cell Stem Cell*, 4: 359-69.

Waters, J. M., Richardson, G. D., and Jahoda, C. A. 2007. 'Hair follicle stem cells', *Semin Cell Dev Biol*, 18: 245-54.

Watt, F. M., and Jensen, K. B. 2009. 'Epidermal stem cell diversity and quiescence', *EMBO Mol Med*, 1: 260-7.

Wei, P., Dove, K. K., Bensard, C., Schell, J. C., and Rutter, J. 2018. 'The Force Is Strong with This One: Metabolism (Over)powers Stem Cell Fate', *Trends Cell Biol*, 28: 551-59.

Weigert, C., Brodbeck, K., Lehmann, R., Haring, H. U., and Schleicher, E. D. 2001. 'Overexpression of glutamine:fructose-6-phosphate-amidotransferase induces transforming growth factor-beta1 synthesis in NIH-3T3 fibroblasts', *FEBS Lett*, 488: 95-9.

Weihofen, W. A., Berger, M., Chen, H., Saenger, W., and Hinderlich, S. 2006. 'Structures of human N-Acetylglucosamine kinase in two complexes with N-Acetylglucosamine and with ADP/glucose: insights into substrate specificity and regulation', *J Mol Biol*, 364: 388-99.

Weimer, S., Priebs, J., Kuhlow, D., Groth, M., Priebe, S., Mansfeld, J., Merry, T. L., Dubuis, S., Laube, B., Pfeiffer, A. F., Schulz, T. J., Guthke, R., Platzer, M., Zamboni, N., Zarse, K., and Ristow, M. 2014. 'D-Glucosamine supplementation extends life span of nematodes and of ageing mice', *Nat Commun*, 5: 3563.

Wells, L., Vosseller, K., and Hart, G. W. 2003. 'A role for N-acetylglucosamine as a nutrient sensor and mediator of insulin resistance', *Cell Mol Life Sci*, 60: 222-8.

Williams, K. 1997. 'Interactions of polyamines with ion channels', *Biochem J*, 325 (Pt 2): 289-97.

Wolff, A. C., Armstrong, D. K., Fetting, J. H., Carducci, M. K., Riley, C. D., Bender, J. F., Casero, R. A., Jr., and Davidson, N. E. 2003. 'A Phase II study of the polyamine analog N1,N11-diethylnorspermine (DENSpm) daily for five days every 21 days in patients with previously treated metastatic breast cancer', *Clin Cancer Res*, 9: 5922-8.

Wu, R., Saab, N. H., Huang, H., Wiest, L., Pegg, A. E., Casero, R. A., Jr., and Woster, P. M. 1996. 'Synthesis and evaluation of a polyamine phosphinate and phosphonamidate as transition-state analogue inhibitors of spermidine/spermine-N1-acetyltransferase', *Bioorg Med Chem*, 4: 825-36.

Yamashita, T., Nishimura, K., Saiki, R., Okudaira, H., Tome, M., Higashi, K., Nakamura, M., Terui, Y., Fujiwara, K., Kashiwagi, K., and Igarashi, K. 2013. 'Role of polyamines at the G1/S boundary and G2/M phase of the cell cycle', *Int J Biochem Cell Biol*, 45: 1042-50.

Yoo, J., Mashalidis, E. H., Kuk, A. C. Y., Yamamoto, K., Kaeser, B., Ichikawa, S., and Lee, S. Y. 2018. 'GlcNAc-1-P-transferase-tunicamycin complex structure reveals basis for inhibition of N-glycosylation', *Nat Struct Mol Biol*, 25: 217-24.

Yoshida, Y., Takahashi, K., Okita, K., Ichisaka, T., and Yamanaka, S. 2009. 'Hypoxia enhances the generation of induced pluripotent stem cells', *Cell Stem Cell*, 5: 237-41.

Zarach, J. M., Beaudoin, G. M., 3rd, Coulombe, P. A., and Thompson, C. C. 2004. 'The co-repressor hairless has a role in epithelial cell differentiation in the skin', *Development*, 131: 4189-200.

Zhang, D., Chia, C., Jiao, X., Jin, W., Kasagi, S., Wu, R., Konkel, J. E., Nakatsukasa, H., Zanvit, P., Goldberg, N., Chen, Q., Sun, L., Chen, Z. J., and Chen, W. 2017. 'D-mannose induces regulatory T cells and suppresses immunopathology', *Nat Med*, 23: 1036-45.

Zhang, D., Zhao, T., Ang, H. S., Chong, P., Saiki, R., Igarashi, K., Yang, H., and Vardy, L. A. 2012a. 'AMD1 is essential for ESC self-renewal and is translationally down-regulated on differentiation to neural precursor cells', *Genes Dev*, 26: 461-73.

Zhang, H., Alsaleh, G., Feltham, J., Sun, Y., Napolitano, G., Riffelmacher, T., Charles, P., Frau, L., Hublitz, P., Yu, Z., Mohammed, S., Ballabio, A., Balabanov, S., Mellor, J., and Simon, A. K. 2019. 'Polyamines Control eIF5A Hypusination, TFEB Translation, and Autophagy to Reverse B Cell Senescence', *Mol Cell*, 76: 110-25 e9.

Zhang, J., Nuebel, E., Daley, G. Q., Koehler, C. M., and Teitell, M. A. 2012b. 'Metabolic regulation in pluripotent stem cells during reprogramming and self-renewal', *Cell Stem Cell*, 11: 589-95.

Zhang, S., and Duan, E. 2018. 'Fighting against Skin Aging: The Way from Bench to Bedside', *Cell Transplant*, 27: 729-38.

Zhao, T., Goh, K. J., Ng, H. H., and Vardy, L. A. 2012. 'A role for polyamine regulators in ESC self-renewal', *Cell Cycle*, 11: 4517-23.

Zhong, Y., Li, X., Yu, D., Li, X., Li, Y., Long, Y., Yuan, Y., Ji, Z., Zhang, M., Wen, J. G., Nesland, J. M., and Suo, Z. 2015. 'Application of mitochondrial pyruvate carrier blocker UK5099 creates metabolic reprogram and greater stem-like properties in LnCap prostate cancer cells in vitro', *Oncotarget*, 6: 37758-69.

Zhou, J., Huynh, Q. K., Hoffman, R. T., Crook, E. D., Daniels, M. C., Gulve, E. A., and McClain, D. A. 1998. 'Regulation of glutamine:fructose-6-phosphate amidotransferase by cAMP-dependent protein kinase', *Diabetes*, 47: 1836-40.

Zhou, Y., Zhou, B., Pache, L., Chang, M., Khodabakhshi, A. H., Tanaseichuk, O., Benner, C., and Chanda, S. K. 2019. 'Metascape provides a biologist-oriented resource for the analysis of systems-level datasets', *Nat Commun*, 10: 1523.

Zhu, S., Li, W., Zhou, H., Wei, W., Ambasudhan, R., Lin, T., Kim, J., Zhang, K., and Ding, S. 2010. 'Reprogramming of human primary somatic cells by OCT4 and chemical compounds', *Cell Stem Cell*, 7: 651-5.

Zismanov, V., Chichkov, V., Colangelo, V., Jamet, S., Wang, S., Syme, A., Koromilas, A. E., and Crist, C. 2016. 'Phosphorylation of eIF2alpha Is a Translational Control Mechanism Regulating Muscle Stem Cell Quiescence and Self-Renewal', *Cell Stem Cell*, 18: 79-90.

Appendix

Supplementary material

Supplementary Table 1: Differentially expressed genes upon 24 h D-mannose treatment that belong to the GO term 'mitotic cell cycle progression' (GO:1903047). The gene name, the FPKM value, the log2FC, and the p-value are shown.

gene name	untreated	D-mannose 24 h	log2(FC)	p-value
Anapc11	57,5999	38,0561	-0,597941	0,00005
Anln	0,225284	0,720993	1,67824	0,0003
Atad5	3,71663	2,05894	-0,852089	0,00005
Aurka	23,2675	11,2729	-1,04546	0,00005
Aurkb	27,1192	10,558	-1,36097	0,00005
Bach1	22,6074	14,6627	-0,624649	0,00005
Birc5	66,8906	24,7201	-1,43612	0,00005
Blm	8,02615	3,9375	-1,02743	0,00005
Bora	10,5243	7,1635	-0,554985	0,00025
Brca1	5,95757	2,92999	-1,02383	0,00005
Brca2	4,46797	2,43798	-0,873931	0,00195
Bub1	10,0712	3,26455	-1,62528	0,00005
Bub1b	21,9136	8,74286	-1,32565	0,00005
Cables1	2,42735	1,60781	-0,594292	0,0011
Camk2b	0,872965	0,131117	-2,73507	0,00005
Camk2d	34,5466	24,2921	-0,508055	0,00095
Casp2	19,5893	13,4831	-0,538909	0,0003
Ccna2	46,2666	15,5375	-1,57422	0,00005
Ccnb1	67,9272	24,5655	-1,46736	0,00005
Ccnb2	36,4452	10,8906	-1,74265	0,00005
Ccnd3	36,2724	24,1824	-0,584918	0,00065
Ccne1	10,6172	6,07413	-0,805656	0,00005
Ccne2	8,91923	3,80781	-1,22796	0,0025
Ccnf	13,2303	5,63034	-1,23256	0,00005
Ccng1	63,3897	122,366	0,948882	0,00005
Ccng2	15,0575	29,4612	0,968332	0,00005
Cdc20	62,1478	26,2449	-1,24366	0,00005
Cdc25a	11,5728	7,8312	-0,563438	0,00005
Cdc25b	50,1853	18,8753	-1,41077	0,00005
Cdc25c	7,51421	2,18662	-1,78092	0,00005
Cdc45	10,7077	6,00454	-0,834526	0,00025

gene name	untreated	D-mannose 24 h	log2(FC)	p-value
Cdc6	5,61743	2,94959	-0,929397	0,00005
Cdc7	5,32619	2,48456	-1,10011	0,00005
Cdca5	9,51724	4,55183	-1,0641	0,00005
Cdca8	49,8892	24,3356	-1,03566	0,00005
Cdk1	115,745	46,925	-1,30252	0,00005
Cdk2	22,3944	13,8859	-0,689517	0,00015
Cdk5rap3	21,2063	14,8884	-0,510306	0,00665
Cdkn1a	162,272	357,265	1,13858	0,00005
Cdkn2a	2,90062	1,26421	-1,19813	0,00005
Cdkn2c	6,5993	2,53341	-1,38123	0,00005
Cdkn2d	7,47694	2,79428	-1,41997	0,00005
Cenpa	63,3936	24,1423	-1,39277	0,00005
Cenpe	11,3558	4,60743	-1,30139	0,00005
Cenpf	7,89495	2,95287	-1,41881	0,00005
Cenph	12,6409	5,24744	-1,26841	0,00005
Cenpk	7,7158	3,2576	-1,244	0,00175
Cep126	1,29984	3,68396	1,50292	0,00005
Cep192	9,19041	6,20372	-0,566996	0,0002
Cep55	15,1569	7,19318	-1,07527	0,00005
Chek1	11,2152	6,90236	-0,700296	0,0023
Chmp4c	7,19076	10,2907	0,517124	0,00005
Cit	4,73277	1,94823	-1,28052	0,00005
Ckap2	21,9133	12,6168	-0,79646	0,00005
Ckap5	24,5379	17,0483	-0,525386	0,00005
Cks1b	88,247	52,0596	-0,761383	0,00005
Cks2	90,111	52,724	-0,773244	0,00005
Clspn	10,7245	4,32987	-1,30851	0,00005
Dna2	4,25522	2,79645	-0,60564	0,00115
Dscc1	3,73762	1,4655	-1,35072	0,00005
Dsn1	9,42292	5,50259	-0,776065	0,0001
Dtl	9,73106	5,17144	-0,912031	0,00005
E2f1	6,80342	3,87333	-0,812688	0,00005
E2f7	2,66367	1,05638	-1,33428	0,00025
Ect2	21,7695	9,98824	-1,12401	0,00005
Edn1	0,551462	4,66781	3,08141	0,00005
Efhc1	0,766433	0,141365	-2,43873	0,0007
Epgn	72,8659	116,537	0,677472	0,00005
Espl1	5,90481	2,13914	-1,46486	0,00005
Fancd2	4,33717	1,56881	-1,46708	0,00005
Fbxo5	12,1391	4,71305	-1,36493	0,00005
Fgfr3	26,2514	9,96986	-1,39675	0,00005
Foxm1	21,7129	11,9023	-0,867312	0,00005

gene name	untreated	D-mannose 24 h	log2(FC)	p-value
Gen1	4,67875	1,75294	-1,41635	0,00005
Gins1	11,6739	5,45818	-1,09679	0,00005
Gja1	160,417	65,6279	-1,28945	0,00005
Gnai1	34,4786	21,3952	-0,688416	0,00005
Gpnmb	113,839	39,2425	-1,5365	0,00005
Haspin	4,56442	2,14876	-1,08692	0,00005
Il1a	12,3478	19,3724	0,649747	0,00005
Incenp	33,7536	17,4295	-0,953507	0,00005
Inhba	9,06692	27,0219	1,57544	0,00005
Iqgap3	10,7448	5,64669	-0,928166	0,00005
Kank2	1,73472	2,94951	0,765775	0,00005
Kif14	5,06372	1,5862	-1,67462	0,00005
Kif18a	5,90355	3,12378	-0,918291	0,00005
Kif20a	27,417	12,8583	-1,09237	0,00005
Kif20b	9,50652	4,77474	-0,993494	0,00005
Kif22	26,4647	11,1899	-1,24187	0,00005
Kif23	25,4087	11,4227	-1,15342	0,00005
Kif2c	15,1819	5,15969	-1,557	0,00005
Kif4	10,7758	4,58706	-1,23216	0,00005
Kifc1	22,1754	15,2282	-0,542217	0,00005
Kifc5b	5,20133	3,59519	-0,532814	0,00035
Klf11	3,7798	7,97573	1,07731	0,00005
Klhl22	6,71764	12,5145	0,897571	0,00005
Knstrn	26,9131	9,00656	-1,57926	0,00005
Kntc1	7,70965	3,32117	-1,21497	0,0007
Lig1	40,6974	17,7573	-1,19652	0,00005
Lmnb1	28,3947	12,2482	-1,21306	0,00005
Mad2l1	27,6994	14,6466	-0,919289	0,00005
Map10	0,47541	0,279692	-0,765335	0,00415
Map9	0,430747	0,777935	0,852807	0,0025
Mastl	7,15942	2,53219	-1,49946	0,00005
Mcm2	38,136	22,0681	-0,789191	0,00005
Mcm3	43,0332	23,2479	-0,888352	0,00005
Mcm4	48,9509	30,7491	-0,670793	0,00005
Mcm6	59,988	30,1521	-0,992414	0,00005
Mdm2	31,6569	58,9639	0,897314	0,00005
Mepce	21,2732	32,1439	0,595507	0,00045
Miip	20,2171	10,8194	-0,901953	0,00005
Mki67	49,2376	17,7567	-1,4714	0,00005
Mybl2	18,6954	10,5081	-0,831187	0,00005
Nasp	68,4006	45,1329	-0,59983	0,00005
Ncapd2	39,0647	18,5042	-1,07801	0,00005

gene name	untreated	D-mannose 24 h	log2(FC)	p-value
Ncapd3	12,1945	8,33796	-0,548468	0,00005
Ncapg	12,6442	4,40847	-1,52013	0,00005
Ncaph	19,6985	9,60783	-1,0358	0,00005
Ncaph2	57,8767	36,7271	-0,656139	0,00005
Ndc80	12,2452	5,61457	-1,12497	0,00005
Nsl1	3,80825	1,87248	-1,02418	0,0006
Nuf2	15,1547	6,05222	-1,32423	0,00005
Nusap1	15,3111	5,87413	-1,38213	0,00005
Orc1	6,57418	3,95559	-0,732919	0,0001
Pbx1	18,2501	7,3259	-1,31683	0,00005
Pcna	158,203	106,448	-0,571635	0,00005
Pim2	2,77597	4,07491	0,553772	0,0032
Pkd2	10,474	16,2752	0,635862	0,00005
Plk1	34,0348	13,3254	-1,35284	0,00005
Plk2	88,8017	175,635	0,983925	0,00005
Plk5	0,095363	0,365864	1,93981	0,00165
Poc1a	11,9863	6,08171	-0,978839	0,00005
Pola1	9,6604	4,88561	-0,983544	0,00005
Pole	11,7421	5,77532	-1,02371	0,00005
Ppp1r10	18,4764	37,036	1,00324	0,00005
Prmt2	5,006	7,41033	0,565878	0,0007
Racgap1	39,8899	16,797	-1,24782	0,00005
Rad51	16,2284	7,7774	-1,06116	0,00005
Rad51b	1,82366	1,17502	-0,634149	0,00485
Rad51c	1,10585	0,496713	-1,15466	0,00005
Rbm38	2,39303	5,06457	1,0816	0,00005
Rgcc	0,561858	0,196925	-1,51256	0,00525
Rhoc	13,9021	27,7092	0,995062	0,00005
Rpa2	20,1385	13,6086	-0,565432	0,00005
Sapcd2	3,7196	1,03571	-1,84453	0,00005
Sgo1	9,21159	3,92821	-1,22958	0,00005
Smc2	20,3414	11,3979	-0,835649	0,00005
Smc4	49,2913	24,5768	-1,00404	0,00005
Sox4	20,8327	57,0237	1,45271	0,00005
Spag5	16,7493	8,34434	-1,00523	0,00005
Spc25	19,428	10,358	-0,9074	0,00005
Spdl1	10,6351	6,55746	-0,697627	0,00005
Spry1	3,71362	1,46232	-1,34456	0,00005
Stil	6,74836	4,52492	-0,576644	0,0014
Stmn1	150,073	100,764	-0,574677	0,00005
Tacc1	1,12731	1,88971	0,745283	0,0018
Tacc3	42,96	20,7809	-1,04774	0,00005

gene name	untreated	D-mannose 24 h	log2(FC)	p-value
Tcf19	15,9864	7,19551	-1,15168	0,00005
Tert	0,832124	1,47555	0,826381	0,0058
Tfap4	10,6446	7,47476	-0,510022	0,00015
Tgfb1	14,253	9,18602	-0,633757	0,00005
Ticrr	5,30498	2,35512	-1,17155	0,00005
Tipin	44,9252	23,6261	-0,927143	0,00005
Top2a	76,616	27,8854	-1,45814	0,00005
Topbp1	50,0638	34,6698	-0,53009	0,00025
Tpx2	32,1368	14,3331	-1,16487	0,00005
Trim39	10,2157	15,1208	0,565748	0,00005
Trip13	13,8542	9,66271	-0,519826	0,0002
Trp53	107,786	155,24	0,526336	0,00005
Ttk	9,55809	3,65119	-1,38836	0,00005
Tubg1	27,7299	17,8327	-0,636923	0,00005
Ube2c	84,1613	27,0825	-1,6358	0,00005
Unc119	3,40649	4,93109	0,533618	0,0084
Wee1	11,8879	4,92334	-1,27178	0,0049
Wnt9a	1,20195	2,70209	1,1687	0,00005
Zfp365	4,5824	11,7709	1,36105	0,00005
Zwilch	17,8378	7,50165	-1,24966	0,00005

Supplementary Table 2: Metabolites identified by untargeted metabolomics. The metabolite, the mean values for untreated and D-mannose treated cells, the fold change (FC), and the p-value are shown.

metabolites	untreated	D-mannose	FC	p-value
N-Acetylspermidine	20082967	45563724	2,26877	0,00093
N-Formyl-L-methionine	3457392	763650	0,22087	0,00811
L-Acetylcarnitine	22311992	10653664	0,47749	0,01103
Uridine diphosphate glucose	3973004	7297788	1,83684	0,01263
Inosinic acid	40906840	16109380	0,39381	0,01638
UDP	5485539	10098231	1,84088	0,03697
Homocysteine	709024	1452124	2,04806	0,04069
Phosphoenolpyruvic acid	463876	1046085	2,25510	0,05718
Uracil	13155098	25037527	1,90326	0,06242
Glycocholic acid	121831	171310	1,40612	0,06518
L-Aspartic acid	105716558	53139359	0,50266	0,06913
Hexose phosphate	8298277	15330373	1,84742	0,07502
Glutathione	3210308649	2157583343	0,67208	0,08066
L-Carnitine	104581541	75307751	0,72009	0,08347
Oxidized glutathione	753790439	504081261	0,66873	0,08678

metabolites	untreated	D-mannose	FC	p-value
Adenine	89383650	57338151	0,64148	0,08723
Cysteinylglycine	25880053	17349918	0,67040	0,10013
Gluconic acid	5080260	7429618	1,46245	0,10234
Arginyl-Glutamine	4044193	7209982	1,78280	0,11512
Biotin	1298839	2523519	1,94290	0,12407
1-Deoxy-D-xylulose 5-phosphate	201334	296770	1,47401	0,12615
Xanthosine 5 phosphate	2023766	912483	0,45088	0,15024
Cytidine	16259928	27983930	1,72104	0,15071
Aminoadipic acid	15373604	11471514	0,74618	0,15544
Heme cofactor	20064927	14413519	0,71834	0,16113
5-Methylthioadenosine	24043383	19785363	0,82290	0,17564
Methionine sulfoxide	5529638	7011728	1,26803	0,18329
Cytosine	35530332	49728841	1,39962	0,20238
Hypoxanthine	997723890	738299730	0,73998	0,21222
L-Arginine	140617190	115863616	0,82396	0,21895
2-oxoglutarate	8173	4832	0,59122	0,22017
Choline	2088913984	1731729138	0,82901	0,26228
Citicholine	10112290	12584096	1,24444	0,26390
4-(Glutamylamino) butanoate	9907368	11458869	1,15660	0,27146
LysoPS(18:0/0:0)	7101150	10684802	1,50466	0,27233
Cytidine monophosphate	7780861	10264550	1,31920	0,28740
Taurine	60347334	48670579	0,80651	0,29713
Uridine diphosphate-N-acetylglucosamine	8817571	4586598	0,52017	0,29778
L-Lysine	86182831	74676485	0,86649	0,29780
Inosine	425917188	309307670	0,72622	0,29805
Lipoic acid	1951012	1688208	0,86530	0,32496
Spermidine	657709145	557340604	0,84740	0,32879
Gamma-glutamyl-L-putrescine	361422	27492	0,07607	0,32895
L-Glutamic acid	972460018	736009156	0,75685	0,33018
O-Acetyl serine	972407931	735944439	0,75683	0,33027
Indole	8708580	10112763	1,16124	0,33347
CDP-Ethanolamine	1478420	1892495	1,28008	0,34124
N-Acetyl-glucosamine 1-phosphate	706636	475641	0,67311	0,34359
L-Tryptophan	368941640	483940615	1,31170	0,37030
Creatinine	41793429	37324098	0,89306	0,37278
S-Adenosylmethionine	71527398	59691155	0,83452	0,38130
L-Kynurenine	3612021	4378233	1,21213	0,38235
Prostaglandin E2	58594166	71954864	1,22802	0,38378
Methyladenosine	1433671	1259962	0,87884	0,42352
Citric acid	36058726	27321147	0,75768	0,42609
Thiamine	625965	785888	1,25548	0,42616

metabolites	untreated	D-mannose	FC	p-value
Serotonine	19726856	14568808	0,73853	0,44267
Phosphoserine	10669403	8379753	0,78540	0,44569
Adenosine monophosphate	842774813	734526870	0,87156	0,47998
N-Acetyl ornithine	5794945	6417535	1,10744	0,48605
LysoPC(18:1(11Z))	316274533	381441934	1,20605	0,49072
Dimethylmalonic acid	838506	934478	1,11446	0,49486
L-Threonine	158080957	180265887	1,14034	0,49626
L-Isoleucine	975373591	1094574482	1,12221	0,50133
ADP	15859633	22435519	1,41463	0,53522
L-Proline	504325046	550118809	1,09080	0,53662
Adenyl succinic acid	23913	19167	0,80152	0,54410
Pantetheine 4'-phosphate	2218942	1932073	0,87072	0,54672
Dihydroxyacetone phosphate	736398	892214	1,21159	0,55492
L-Methionine	240794182	261407184	1,08560	0,56672
L-Cystathionine	24583	19365	0,78775	0,56942
Pantothenic acid	18411970	21242742	1,15375	0,58692
Guanosine monophosphate	124767157	118264851	0,94788	0,58771
L-Valine	329104661	356687899	1,08381	0,61668
Sphinganine	28465770	24831403	0,87232	0,61737
Propionylcarnitine	7210996	6412642	0,88929	0,62308
Allantoin	319298	244518	0,76580	0,63324
Asymmetric dimethylarginine	14434854	12957679	0,89767	0,63841
Hydroxy deoxy guanosine	68312249	56354094	0,82495	0,66088
Dopaquinone	610151	696247	1,14111	0,67051
Guanine	36463401	30715301	0,84236	0,68249
Dodecanedioylcarnitine	12928	15993	1,23713	0,68798
Betaine	585220416	612946184	1,04738	0,69679
L-Leucine	638778401	680160897	1,06478	0,71360
Nicotinamide	168782874	157698139	0,93433	0,71550
Erythronic acid	11189860	10424110	0,93157	0,72434
5,6-Dihydrouridine	1011609	1074417	1,06209	0,73260
Guanosine	5311166	6067018	1,14231	0,74789
L-Tyrosine	554372057	582909744	1,05148	0,76137
L-Dopa	9504862	9967430	1,04867	0,76977
L-Phenylalanine	2292139137	2432444474	1,06121	0,77153
Sphingosine	234592032	214838053	0,91579	0,77387
L-Glutamine	71760661	74240726	1,03456	0,79369
N-Acetyl-D-glucosamine	8720163	8335943	0,95594	0,81505
Xanthine	49061334	45448593	0,92636	0,82408
Gamma-glutamyl-Cysteine	10093221	9648128	0,95590	0,83697
NAD+	19629450	18707484	0,95303	0,85321
Carnosine	31473	32902	1,04541	0,92736

metabolites	untreated	D-mannose	FC	p-value
6-Methylquinoline	8489483	8263013	0,97332	0,93098
5-Methyl tetrahydrofolic acid	122038	116312	0,95308	0,95939
Pyroglutamic acid	110746504	109868016	0,99207	0,97295
Ascorbic acid	6380695	6201008	0,97184	0,97318
Spermine	56789497	56493885	0,99479	0,97661
Glycerol 3 phosphate	2351670	2356930	1,00224	0,98477
Xylulose phosphate	12608128	12662536	1,00432	0,98513
L-Histidine	41512444	41605677	1,00225	0,98659
L-Palmitoylcarnitine	6306175	6309991	1,00061	0,99861

Supplementary Table 3: Raw data of targeted analysis of polyamines. The peak area for the different metabolites and the internal standard, as well as the protein concentration are shown.

	[Area]								
treatment/ cell type	**L-arginine**	**ornithine**	**putrescine**	**spermidine**	**spermine**	***N*1-AcSpd**	***N*1-AcSpm**	**internal standard [Area]**	**protein conc. [mg/ml]**
untreated	12904018	6021103	5326573	1036862148	7137990	2012994	2977580	39394907	1,002
untreated	16352950	7928900	6216904	946967125	7660604	1829712	1622610	35716089	1,002
untreated	16431492	7668382	7116032	904984375	6796574	1787566	2615367	37922465	1,002
untreated	18607745	9036285	6009626	874852809	6416679	2700460	1347596	38926198	1,002
untreated	14396709	7236863	7120108	711015790	6236085	1634127	1846039	36363078	1,003
untreated	16929638	7090301	6127276	792096085	7769351	1998869	2819385	34246433	1,000
DENSpm	16363072	3583811	1099531	454853772	1932649	17596369	14187594	30028333	1,000
DENSpm	17587686	2007148	1565508	376639130	3302484	19495941	16560888	32964720	0,862
DENSpm	12416176	2616135	2685384	340950777	2111436	19041298	15212244	35661187	1,017
DENSpm	13230527	1148019	2652942	364111326	1690120	17369644	16762121	37294437	0,912
DENSpm	11111375	2650340	2732719	420562130	1481126	19575718	16945374	32902850	1,003
DENSpm	11549726	1247606	3035578	317456522	1940232	18022009	17629706	34035939	0,606
putresceine	12804579	5509460	10451637	1026625723	6247991	7256514	2612713	38652173	1,000
putresceine	13033223	5812637	9642466	1263904808	8329373	8180923	1014807	31263473	1,001
putresceine	19080052	6403054	10651154	1060410898	9422890	9113535	1017360	30203973	1,001
putresceine	18349609	5240671	8843357	1260778567	7504113	6424555	2633330	39720634	1,000
putresceine	12425284	7353753	11375181	1101586055	6380869	7658883	1645146	33715324	1,002
putresceine	12772236	4768646	9317535	1105773845	8240577	8304955	1451430	31404827	1,001
D-mannose	15315208	5900663	2120007	997812185	8483237	9718101	9366215	36634239	1,0003
D-mannose	17440126	4254496	3428607	718825222	6744556	10748684	8369599	31315196	1,0015
D-mannose	11646921	3864521	2846168	830542685	5757335	12290023	4489525	36293345	1,0021

	[Area]								
treatment/ cell type	**L-arginine**	**ornithine**	**putrescine**	**spermidine**	**spermine**	***N*1-AcSpd**	***N*1-AcSpm**	**internal standard [Area]**	**protein conc. [mg/ml]**
D-mannose	10243308	3883470	2957409	992837015	5911648	8652242	7498077	33061643	1,0018
D-mannose	10687392	5185379	3762404	825102177	6430119	7461887	5065440	32598908	1,0001
D-mannose	11774897	4819032	2789928	752174620	7798264	8133542	6512877	30451138	1,0012
untreated	50724343	66263675	1215445	178074766	4281526	21904079	1020263	203339987	1,000
untreated	46323420	95780051	1235023	215000000	4457186	24843614	1318297	205813183	1,000
untreated	43729548	73973436	2270521	227869299	4058347	22162075	1220567	212521117	1,000
untreated	57152879	81784985	1641547	254983263	5587886	20720553	1958348	262971855	1,000
untreated	60873204	95600750	1809671	264132949	3190392	25994102	1394405	239531504	1,000
untreated	87303039	86629271	1047401	260944664	5949319	20827485	1310905	210021491	1,000
*N*1AcSpd	63361474	109573037	3494320	229503543	4650967	46282585	1327794	199165173	1,000
*N*1AcSpd	45721491	88605877	2374912	259275863	5349188	36712524	1353637	249686192	1,000
*N*1AcSpd	56077443	97798528	2351026	254347992	4069894	38659193	1401810	238265783	1,000
*N*1AcSpd	64682857	104113654	2666028	405125371	4555275	37135271	2273111	234875063	1,000
*N*1AcSpd	62870782	102886600	2332357	479554702	3921417	35371569	1734322	203574582	1,000
*N*1AcSpd	64028732	103534358	2738738	556998882	3317066	43280407	2162712	228871049	1,000
α6+/CD34-	44320461	29262019	738633	241991360	348937	4912186	526497	38505101	1,000
α6+/CD34-	57764359	39802858	822279	276798676	463234	4899961	888088	35614662	1,000
α6+/CD34-	55684476	38539738	706845	283286713	877893	5046721	1827085	36544303	1,000
α6+/CD34-	37176079	26675480	744831	271573916	630790	4767082	1025270	32292454	1,000
α6+/CD34-	59447334	39699622	885841	271109560	410567	6334926	792995	35507982	1,000
α6+/CD34-	62261042	36674931	772120	298449401	1152903	5524953	1116650	36353593	1,000
α6+/CD34+	69792389	46893917	678622	139641091	191225	3998758	1275896	37135001	1,000
α6+/CD34+	68379008	43652359	561803	101000000	174386	2168249	1607748	35919469	1,000
α6+/CD34+	26613509	20699131	503564	179218681	121073	3470147	1190545	35409493	1,000

	[Area]								
treatment/ cell type	**L-arginine**	**ornithine**	**putrescine**	**spermidine**	**spermine**	***N*1-AcSpd**	***N*1-AcSpm**	**internal standard [Area]**	**protein conc. [mg/ml]**
α6+/CD34+	35621462	24479860	530220	187445682	102813	3736078	1216116	30615025	1,000
α6+/CD34+	41046805	28865887	423651	100953347	138799	3788929	976349	34045430	1,000
α6+/CD34+	46913327	29838854	393572	109638582	171407	5632880	1195561	36879363	1,000
untreated	59347119	36631850	274743	168588631	2153945	74123375	9900773	79880743	1,000
untreated	55014516	30343264	281929	141599389	1150902	74734362	6639454	75150191	1,000
untreated	55796338	37812145	212690	133573234	1161732	62458557	6544792	72723144	1,000
untreated	57443775	31183130	263538	130239415	1151407	78210201	7231213	76869416	1,000
DFMO	53030155	47667344	123998	119767361	1374904	65076503	8827850	70181350	1,000
DFMO	51972889	42302439	166199	120162772	1048999	69140878	10373158	79046011	1,000
DFMO	56929559	45784891	189647	100375233	1074477	56394417	9754542	70627309	1,000
DFMO	59916156	47428483	151912	111491614	904232	57045560	8618793	70318776	1,000

List of figures

List of tables

Work contributions

I performed all experiments described in this work independently, except for:

Cell sorting was performed by Kat Folz-Donahue and Lena Schumacher from the FACS and Imaging Core Facility (Max Planck Institute for Biology of Ageing, Cologne, Germany).

UDP-HexNAc levels were analyzed by Yvonne Hinze from the Metabolomics Core Facility (Max Planck Institute for Biology of Ageing, Cologne, Germany).

UDP-GlcNAc and UPD-GalNAc levels were determined by Silvina Perin from the Metabolomics Core Facility (Max Planck Institute for Biology of Ageing, Cologne, Germany).

FACE analysis was performed by Valbona Cali, Ronald Midura, and Vincent Hascall from the Cleveland Clinic (Cleveland, Ohio).

Untargeted metabolomics and targeted analysis of polyamines were performed by Andrea Annibal from Adam Antebi's laboratory (Max Planck Institute for Biology of Ageing, Cologne, Germany) with the help of Christian Latza.

Andromachi Pouikli from Peter Tessarz' laboratory (Max Planck Institute for Biology of Ageing, Cologne, Germany) prepared the library for the 3' RNA-sequening.

Franziska Metge from the Bioinformatics Core Facility (Max Planck Institute for Biology of Ageing, Cologne, Germany) analyzed the 3' RNA-sequencing data.

Rafael Cuadrat from the Bioinformatics Core Facility (Max Planck Institute for Biology of Ageing, Cologne, Germany) analyzed the RNA-sequencing data.

Janis Koester from Sara Wickström's laboratory (Max Planck Institute for Biology of Ageing, Cologne, Germany) performed the image acquisition of depilated mice. Janis Koester and Sara Wickström (Helsinki Institute for Life Science, Helsinki, Finland) performed embedding, sectioning, staining, and imaging of depilated dorsal skin.

I thank these people for their important contributions.

Curriculum vitae

Persönliche Informationen

Kira Allmeroth
wohnhaft in Köln

geboren am 13.05.1989 in Aachen
Nationalität: deutsch

Ausbildung

10/2014 – 02/2021	**Promotion in Genetik** Max-Planck-Institut für Biologie des Alterns, Köln, Deutschland Arbeitsgruppe von Dr. Martin Denzel Titel der Dissertation: Metabolic control of hair follicle stem cell fate decisions
10/2011 – 08/2014	**Master of Science in Molekularer Biomedizin** Westfälische Wilhelms-Universität Münster Masterarbeit in der Arbeitsgruppe von Dr. Erik Storkebaum am Max-Planck-Institut für Molekulare Biomedizin, Münster, Deutschland
10/2008 – 09/2011	**Bachelor of Science in Molekularer Biotechnologie** Universität Bielefeld Bachelorarbeit in der Arbeitsgruppe von Dr. Bernd Stratmann am Herz- und Diabeteszentrum NRW, Bad Oeynhausen, Deutschland
06/2008	**Allgemeine Hochschulreife** Bettina-von-Arnim Gymnasium, Dormagen, Deutschland

Relevante Publikationen

Allmeroth, K., Kim, C. S., Annibal, A., Pouikli, A., Koester, J., Derisbourg, M. J., Chacon-Martinez, C., Latza, C., Antebi, A., Tessarz, P., Wickström, S. A., and Denzel, M. S. 2021. 'N1-acetylspermidine is a determinant of hair follicle stem cell fate', *J Cell Sci*, 134

Allmeroth, K., Horn, M., Kroef, V., Miethe, S., Muller, R. U., and Denzel, M. S. 2020. 'Bortezomib resistance mutations in PSMB5 determine response to second-generation proteasome inhibitors in multiple myeloma', *Leukemia*.

Horn, M., Denzel, S. I., Srinivasan, B., Allmeroth, K., Schiffer, I., Karthikaisamy, V., Miethe, S., Breuer, P., Antebi, A., and Denzel, M. S. 2020. 'Hexosamine Pathway Activation Improves Protein Homeostasis through the Integrated Stress Response', *iScience*, 23: 100887.

Kim, C. S., Ding, X., Allmeroth, K., Biggs, L. C., Kolenc, O. I., L'Hoest, N., Chacon-Martinez, C. A., Edlich-Muth, C., Giavalisco, P., Quinn, K. P., Denzel, M. S., Eming, S. A., and Wickström, S. A. 2020. 'Glutamine Metabolism Controls Stem Cell Fate Reversibility and Long-Term Maintenance in the Hair Follicle', *Cell Metab*, 32: 629-42 e8.

Ruegenberg, S., Horn, M., Pichlo, C., Allmeroth, K., Baumann, U., and Denzel, M. S. 2020. 'Loss of GFAT-1 feedback regulation activates the hexosamine pathway that modulates protein homeostasis', *Nat Commun*, 11: 687.

Horn, M., Kroef, V., Allmeroth, K., Schuller, N., Miethe, S., Peifer, M., Penninger, J. M., Elling, U., and Denzel, M. S. 2018. 'Unbiased compound-protein interface mapping and prediction of chemoresistance loci through forward genetics in haploid stem cells', *Oncotarget*, 9: 9838-51.

Erklärung

Ich versichere, dass ich die von mir vorgelegte Dissertation selbständig angefertigt, die benutzten Quellen und Hilfsmittel vollständig angegeben und die Stellen der Arbeit − einschließlich Tabellen, Karten und Abbildungen −, die anderen Werken im Wortlaut oder dem Sinn nach entnommen sind, in jedem Einzelfall als Entlehnung kenntlich gemacht habe; dass diese Dissertation noch keiner anderen Fakultät oder Universität zur Prüfung vorgelegen hat; dass sie − abgesehen von unten angegebenen Teilpublikationen − noch nicht veröffentlicht worden ist, sowie, dass ich eine solche Veröffentlichung vor Abschluss des Promotionsverfahrens nicht vornehmen werde.
Die Bestimmungen der Promotionsordnung sind mir bekannt. Die von mir vorgelegte Dissertation ist von Dr. Martin Denzel betreut worden.

Teilpublikationen:

Horn, M., Denzel, S. I., Srinivasan, B., Allmeroth, K., Schiffer, I., Karthikaisamy, V., Miethe, S., Breuer, P., Antebi, A., and Denzel, M. S. 2020. 'Hexosamine Pathway Activation Improves Protein Homeostasis through the Integrated Stress Response', *iScience*, 23: 100887.

Allmeroth, K., Kim, C. S., Annibal, A., Pouikli, A., Koester, J., Derisbourg, M. J., Chacon-Martinez, C., Latza, C., Antebi, A., Tessarz, P., Wickström, S. A., and Denzel, M. S. 2021. 'N1-acetylspermidine is a determinant of hair follicle stem cell fate', *J Cell Sci*, 134

Datum Unterschrift